Construction and Behavior of Precast Bridge Deck Panel Systems

Sean Sullivan

Dissertation submitted to the faculty of the Virginia Polytechnic Institute and State University in partial fulfillment of the requirements for the degree of

Doctor of Philosophy
In
Civil and Environmental Engineering

Dr. Carin Roberts-Wollmann, Committee Chair
Dr. Thomas Cousins
Dr. Rodney Davis
Dr. Kamal Rojiani
Dr. Elisa Sotelino
Dr. Surot Thangjitham

April 27, 2007
Blacksburg, Virginia

Keywords: Bridge Deck, Shear Connectors, Deck Panels, Post-Tensioning

Construction and Behavior of Precast Bridge Deck Panel Systems

Sean Sullivan

ABSTRACT

A bridge with precast bridge deck panels was built at the Virginia Tech Structures Laboratory to examine constructability issues, creep and shrinkage behavior, and strength and fatigue performance of transverse joints, different types of shear connectors, and different shear pocket spacings. The bridge consisted of two AASHTO type II girders, 40 ft long and simply supported, and five precast bridge deck panels. Two of the transverse joints were epoxied male-female joints and the other two transverse joints were grouted female-female joints. Two different pocket spacings were studied: 4 ft pocket spacing and 2 ft pocket spacing. Two different shear connector types were studied: hooked reinforcing bars and a new shear stud detail that can be used with concrete girders.

The construction process was well documented. The change in strain in the girders and deck was examined and compared to a finite element model to examine the effects of differential creep and shrinkage. After the finite element model verification study, the model was used to predict the long term stresses in the deck and determine if the initial level of post-tensioning was adequate to keep the transverse joints in compression throughout the estimated service life of the bridge. Cyclic loading tests and shear and flexural strength tests were performed to examine performance of the different pocket spacings, shear connector types and transverse joint configurations. A finite element study examined the accuracy of the AASHTO LRFD shear friction equation for the design of the horizontal shear connectors.

The initial level of post-tensioning in the bridge was adequate to keep the transverse joints in compression throughout the service life of the bridge. Both types of pocket spacings and shear connectors performed exceptionally well. The AASHTO LRFD shear friction equation was shown to be applicable to deck panel systems and was conservative for determining the number of shear connectors required in each pocket. A

recommended design and detailing procedure was provided for the shear connectors and shear pockets.

Acknowledgments

First of all, I would like to thank my advisor, Dr. Carin Roberts-Wollmann, for serving as my advisor and awarding me with this excellent research project. I would also like to thank Dr. Thomas Cousins for his help with this research project. It has been a very enjoyable experience working with the two of you the past three years. I appreciate you both giving me this wonderful opportunity at Virginia Tech. I would also like to thank Dr. Rodney Davis, Dr. Elisa Sotelino, Dr. Kamal Rojiani, and Dr. Surot Thangjitham for serving on my research committee and providing me with guidance during this project. Thank you, Dr. Finley Charney, for teaching me a great deal about matrix analysis of structures though the courses I had taken from you and the diagonal knee connection project we worked on together.

The completion of the experimental component of this research project at the Structures and Materials Laboratory would not have been possible without the help of Brett Farmer and Dennis Huffmann. Thank you for the many hours you helped with the construction of the bridge and helping prepare the bridge for the live load tests. I would also like to thank everyone else who had helped me at the Structures and Materials Laboratory: Don Scholz, Devin Harris, Joe Wallenfelsz, Susan Bowers, Matt Swenty, Chris Carroll, Hunter Hodges, Zihong Liu, Daniel Axson, Justin Marshall, and Chuck Newhouse. I apologize if I missed someone.

I want to give a very special thank you to my girls: my wonderful wife, Jacquelyn, and my daughter, Mailey. Jacquelyn, you have provided me with so much motivation and support! Likewise, our little "Mailey Moo" has changed our lives for the better forever. Thank you, Mom and Dad, or should I say "Grammy" and "Grampy". I can't even think of where to begin to thank you for everything you have done over the past three decades! But I hope you know how much I love you both. I would also like to thank my brother, Kevin, and sister, Kristin.

Table of Contents

List of Tables

List of Figures

Chapter 1
Introduction

1.1 Introduction to Precast Bridge Deck Panel Systems

Precast bridge deck panels can be used in place of a cast-in-place concrete deck in order to reduce bridge closure times for deck replacements. The panels are prefabricated at a precasting plant providing optimal casting and curing conditions. The panels can be transported to the bridge site for immediate erection. Precast panels can be either full depth or partial depth. Partial depth panels act as a stay-in-place form for a cast-in-place concrete topping. This research program only investigates the behavior of full depth precast panels.

Figure 1.1.1 shows a representation of a bridge with precast deck panels and prestressed concrete girders. The construction process consists of first placing the panels on top of the girders. The self weight of the panels is transferred to the girders through leveling bolts. Leveling bolts are threaded through the depth of the panels and protrude through the bottom of the panels. The protrusion can be adjusted depending on the desired haunch height or desired top-of-deck elevation. The transverse joints are grouted next. If the deck is to be post-tensioned, this operation can then be performed. After the post-tensioning operation is complete, the post-tensioning ducts are typically grouted. The haunch is poured after the post-tensioning operation. Once the grout in the haunch has cured, the leveling bolts can be removed and the panels and girders act as a composite system. Barrier rails can be cast and a wearing surface is placed.

The most common type of joint between adjacent panels is a grouted female-female joint. Epoxied male-female shear keys have been used in precast pavements. The mechanical interlock provides continuity between the panels. The panels are typically post-tensioned together to help add strength to the joint, act as distribution reinforcement, reduce the chance for water leakage at the joint, and improve the durability of the deck. However, if post-tensioning is not applied, mild reinforcing steel is often placed across the joint in order to properly reinforce the joint. The mild reinforcing steel must be properly developed on each side of the joint.

Composite action between the deck and girders is provided by shear connectors that extend out of the girder and into the shear pockets of the panels. The connectors typically consist of either hooked reinforcing bars or shear studs. The girders are typically either precast, prestressed girders or steel girders. Precast, prestressed girders were used in this research program.

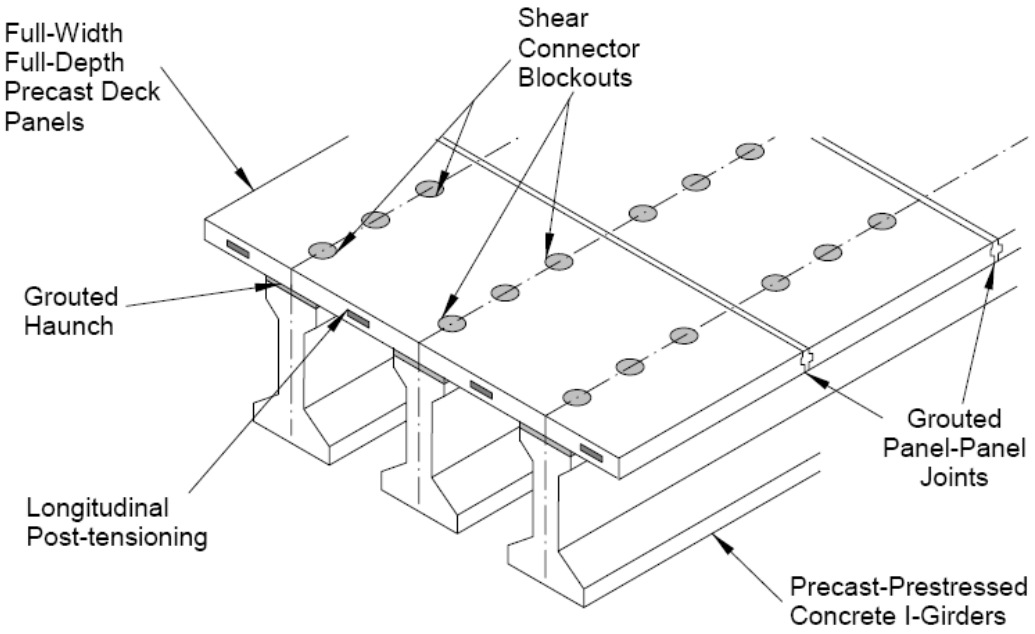

Figure 1.1.1 Representation of Bridge Deck Panel System[1]

1.2 Summary of Challenges Associated with Precast Bridge Deck Panel Systems

1.2.1 Horizontal Shear Connectors

Composite action between the panels and girders is provided by the haunch and shear connectors which are clustered together at the shear pockets instead of having a more uniform shear connector spacing found with cast-in-place concrete decks. The discrete locations of the shear connectors raises questions about the proper way to design for horizontal shear transfer. The pocket spacing is typically 2 ft. Larger pocket spacing is desirable because it results in less grout that has to be poured during the bridge closure, and fewer blockout forms that have to be placed during fabrication. This also allows for shorter construction delays. Larger pocket spacing may cause cracking to occur along the interface between the shear pockets where there is no reinforcement present. Current

design provisions do not address the design of shear connectors for precast bridge deck panel systems.

There are a variety of shear connectors that can be used with precast bridge deck panel systems. Hooked reinforcing bars are the most common type for panels installed on prestressed concrete girders. Shear studs are the most common type for panels installed on steel girders. Prior performance and applicable code provisions for hooked reinforcing bars and shear studs are discussed in Chapter 2.

This research program investigated the performance of shear studs and hooked reinforcing bars with precast, prestressed girders. The hooked reinforcing bars were cast with a girder. A portion of the hooked reinforcing bar then protruded from the top flange of the girder into the shear pocket. The shear connector detail with the shear studs was fabricated by casting a steel plate in the top flange of a prestressed girder. Shear studs were located on the bottom of the steel plate. This is shown in Figure 1.2.1. Additional shear studs were then be shot directly on to the top of the steel plate after the girder was erected and the panels were placed. No prior use or testing of this detail was found in the literature review presented in Chapter 2.

Post-installed hooked reinforcing bars have also been proposed in deck replacement projects. Shear connectors that are post-installed reduce the tripping hazard associated with shear connectors during early construction phases. They also ensure that all the shear connectors fit in the shear pockets when casting tolerances are exceeded. Preinstalled hooked reinforcing bars are also used in this research.

Figure 1.2.1 New Detail For Horizontal Shear Reinforcement

1.2.2 Prestress Losses in Post-Tensioning Ducts

Long term prestress losses may be significant enough to decrease the pre-compressive stress across a transverse joint to a point where the bottom surface of a transverse joint goes into tension under service load. Prestress losses due to creep, shrinkage, and relaxation of the prestressing strands are long term losses. The research program investigated the use of standard equations provided by current code provisions to estimate the loss of prestress in the panels and whether they produce accurate results, particularly when considering the shrinkage and creep losses. The research program also looks at whether current creep and shrinkage models accurately predict creep and shrinkage induced strains. Several key factors are taken in to account when considering prestress loss from differential creep and shrinkage:

1. Secondary moments due to prestress loss in continuous spans,
2. The amount of mild reinforcing steel in the panels and girders,
3. Girder spacing which effects the axial stiffness of the deck to axial stiffness of the girder ratio,
4. Span lengths,
5. Concrete composition discussed in most code provisions regarding creep and shrinkage,
6. Differential creep and shrinkage due to substantial differences

in casting dates and the concrete age at the time of prestressing between the panels and girders,

7. Creep deformation associated with the post-tensioning force on the composite system,
8. Creep associated with the prestressing force from the girder on the composite system,
9. Stiffness of the girder compared to the stiffness of the deck,
10. Time at which the system is made composite relative to the casting date of the girders (if applicable) and panels,
11. Time at which the post-tensioning is applied relative to the casting date of the panels,
12. Steel girders vs. prestressed concrete girders,
13. Partial composite action.

The above factors cause force and moment redistribution in the system which are not taken into account in standard code provisions. Doing so requires a rigorous, time consuming analysis and prior knowledge of the actual construction schedule, environmental conditions, and material properties.

Many states have reported problems with leaking at the transverse joints[2,3]. This can often be attributed to a lack of post-tensioning or poor construction practices such as bowing of the formwork. There has been much speculation as to which type of transverse joint is the best to use in terms of strength, durability, ease of construction, and cost. The transverse joints are often thought of as one of the "weak links" of the system and special consideration needs to be given to these joints. Recommended levels of post-tensioning have been given to keep the joint in compression under live loads[4,5]. Attention also has to be given to the decrease in this compressive force across the joint from the long term post-tensioning losses, loss of composite action between the girder and panels that may result over time, and stress redistributions within the composite girder.

1.3 Objectives of Research Program

The research program described herein was developed to address the challenges and problems discussed in the previous section. By doing so, current design provisions

and practices can be improved and modifications to code provisions can be made, if necessary.

The first objective was to conduct a literature review to develop a thorough understanding of the precast deck panel system. The performance of the precast deck panel systems used currently and in the past was investigated. In addition, the structural behavior of components in the system was studied. Current code provisions were reviewed that pertain to design issues encountered in precast deck panel systems.

The second objective was to examine the constructability of the system. A bridge consisting of precast deck panels and precast, prestressed concrete girders was built in the Virginia Tech Structures and Materials Laboratory. This bridge was referred to as the lab mockup. The construction process was well documented. Particular attention was given to the transverse joint details, the types of shear connectors, and the construction process. Some details may result in more relaxed casting tolerances and/or reduce construction time.

The third objective was to study the composite action of the system. The hooked reinforcing bars and the new detail with shear studs were both considered in the testing program. Both cyclic and overload tests were performed. The cracking patterns at the interface between the haunch and girder, the strains in the shear connectors and the vertical deflections of the system were used as the primary indicators for the level of composite action. The shear pocket spacing was also examined to see if 4 ft pocket spacing performed adequately compared to 2 ft pocket spacing. Finite element studies were also conducted to aid in making more general conclusions about the composite action of the system by modeling push-off specimens and the lab mockup. The push-off specimen consisted of a thin layer of grout cast between the two "L-shaped" concrete blocks. Reinforcement was provided across the interfaces between the grout and concrete blocks. The specimen was loaded in pure shear to measure the horizontal shear strength of the interfaces. Modifications to current code provisions were suggested as necessary.

The fourth objective was to investigate to what extent creep and shrinkage effects the long term post-tensioning losses and deck stresses in the lab mockup. Forces in the post-tensioning strands in the lab mockup were monitored along with the longitudinal

strains in the deck and girders. The experimental results were used to verify the results of the finite element models. The results were used to recommend an initial level of post-tensioning.

The fifth objective was to study the structural behavior of the transverse joints and evaluate constructability issues associated with the transverse joints used in the lab mockup. Epoxied male-female joints and grouted female-female joints were used. Both cyclic and overload tests were performed and relative displacements and crack patterns were compared to see if one joint performed better than the other. Water was also ponded at selected intervals during the testing program to determine if the joints leaked.

The results were used to recommend guidelines for precast deck panel systems. Guidelines were recommended for

1. Fabrication practices,
2. The types of shear connectors to use,
3. Design methods for horizontal shear transfer,
4. Spacing of shear pockets,
5. Transverse joint configuration(s),
6. Transverse joint formwork (for grouted female-female joints),
7. Required initial levels of post-tensioning,
8. Panel leveling screws,
9. Haunch formwork,
10. Grout specifications.

Chapter 2
Literature Review

This chapter presents a review of literature concerned with precast deck panel systems. Previous investigations on the behavior of bridge deck panels systems are covered first. Previous studies dealing with prestress loss, horizontal shear, panel joints, as well as general issues such as constructability and durability are covered. Current code provisions are discussed next. Code provisions on creep and shrinkage of concrete, prestress loss, and horizontal shear design are covered.

2.1 Previous Studies

2.1.1 Prestress Losses

2.1.1.1 NCHRP Report 496

NCHRP (National Cooperative Highway Research Program) Report 496[6] , Prestress Losses in Pretensioned High-Strength Concrete Bridge Girders," identified limitations for current methods for estimating prestress losses and proposed new methods for estimating prestress losses in high strength bridge girders. The report investigated many of the factors influencing long term losses. The recommendations presented by this report were adopted in to the AASHTO LRFD 2006 Interims[7]. The creep and shrinkage models and the method for determining prestress losses are presented in Section 2.2.1.3 and 2.2.2.1.

The report proposed new models for predicting creep coefficients and shrinkage strains. Multipliers were developed for non-standard relative humidities, V/S (volume-to-surface) ratios, loading age, and concrete strength. In other models for predicting creep coefficients and shrinkage strains, the standard relative humidity, V/S ratio, loading age, and concrete strength were not representative of the findings presented by NCHRP Report 496. These include the volume-to-surface ratio and the variation of the creep coefficient and shrinkage strain with time.

The report pointed out that the effects of composite action between the deck slab and precast girders must be taken in to account to accurately estimate prestress loss in high strength girders. NCHRP Report 496 proposed what was referred to as the "detailed

method" for determining the prestress losses in composite systems. In this method, the report suggested taking in to account any elastic gains in prestress such as the addition of the deck dead load.

The method consisted of using strain compatibility equations and constitutive relationships to determine the prestress loss at various stages of construction. The change in strain in the concrete at the location of the centroid of the strands was set equal to the change in strain in the prestressing strands. The gradual change in stress was taken into account by using an aging coefficient instead of using a time stepping approach. This method was used to determine the creep and shrinkage losses between the time of transfer and deck placement.

The relaxation loss was small during the entire time period for the analysis. An average value of 2.4 ksi was reported and it was decided to split it evenly between two distinct stages: up until deck placement and after deck placement.

The elastic gain in prestress due to the deck placement was calculated next. The report stresses this was not necessary if the transformed section properties were being used, since it will automatically be taken into account. The long term loss from the time the deck was placed until the final time was also calculated using a strain compatibility approach at the centroid of the strands.

The losses and gains due to the different effects on the composite section were calculated separately; such as the shrinkage of the girder concrete in the composite section, creep of girder concrete in the composite section caused by the initial prestress force and self weight, creep of girder concrete in the composite section caused by deck weight and superimposed dead loads, relaxation of strands in the composite section, shrinkage of the deck in the composite section. The resulting expressions for prestress loss and gain were added together to determine the total loss of prestress from prestress transfer up until the specified final time.

The "detailed method" was examined and altered to produce an "approximate method" that was easier and much quicker to use. The following assumptions were used to develop the "approximate method":

1. Prestress losses were calculated at the maximum positive moment section,

2. No mild steel reinforcement existed at that section,
3. Elastic losses and gains from external loads were not considered,
4. Prestress was transferred to the concrete at 1 day in accelerated plant curing conditions,
5. The cast-in-place deck weight was applied to the precast girder without any shortening after at least 28 days from the time of prestress transfer,
6. V/S ratio for the girder was between 3 in. and 4 in.

The proposed correction factors, "detailed method", and "approximate method" were verified by comparing predicted prestress loss values to values inferred from strain measurements in seven bridges in four states. The bridges were instrumented with vibrating wire gages at the centroid of the prestressing strands, mid-depth of the girder, and at the center of gravity of the top flange. The proposed "approximate method" gives almost as accurate an estimate as the "detailed method."

The approach above does indeed prove to be robust. However, the proposed formulas are not general enough to take in to account post-tensioned bridge decks.

2.1.1.2 Wollmann et al.

Wollmann et al.[8] examined the age-adjusted effective modulus approach and applied it to a project in Salt Lake City, Utah. Particular attention was given to creep and shrinkage effects on the composite system. Spliced precast and post-tensioned concrete girders were used on the project. Because the girders were very deep, the long term effects of creep and shrinkage had to be taken in to account. The girders were pretensioned as well as post-tensioned. The post-tensioning was applied at a minimum concrete age of 50 days in order to minimize prestress loss and other creep and shrinkage effects, such as larger long term deflections.

The aging coefficient was used to approximate the gradual development of stresses over time in a larger time interval compared to using a time stepping approach without an aging coefficient, where the time intervals must be small enough to eliminate any error. The error is due to the nonlinear nature of the problem. By using small time steps, the increment of the increase (or decrease) in strain is small enough that the

difference between the exact change in strain and estimated change in strain is small. This requires a great number of time steps in order to produce an answer that is close to the exact solution. This often calls for a computer program or elaborate spreadsheet to carry out the calculations. The aging coefficient, originally developed by Trost[9], mentioned above was expressed as

$$\mu = \frac{E_o}{(\sigma_t - \sigma_o)\upsilon_{t,t_o}} \int_{t_o}^{t} \frac{1}{E(\tau)} \frac{d\sigma(\tau)}{d\tau} [1 + \upsilon(t,\tau)] - \frac{1}{\upsilon_{t,t_o}} d\tau \qquad [2.1]$$

where,

E_o = modulus of elasticity at time t_o.

$E(\tau)$ = modulus of elasticity at time τ.

σ_o = stress at time t_o.

σ_t = stress at time t.

$\sigma(\tau)$ = stress at time τ.

v_{t,t_o} = creep coefficient at time t due to a load applied at time t_o.

$v(t,\tau)$ = creep coefficient at time t due to a load applied at time τ.

As shown in the above equation, the aging coefficient depends on the loading history and variation of concrete properties over time. The aging coefficient usually varies from 0.5 to 1.0. Typical values of μ, depending on the age of loading, are tabulated in ACI-209[10]. If a constant value is used for the aging coefficient, then the expression for the strain at any time can be given in the following form

$$\varepsilon_t = \frac{\sigma_o}{E_o}(1 + v_{t,t_o}) + \frac{\sigma_t - \sigma_o}{E_o}(1 + \mu v_{t,t_o}) + \varepsilon_{s,t} \qquad [2.2]$$

where $\varepsilon_{s,i}$ = shrinkage strain at time t. This concept was applied to the creep and shrinkage analysis of the I-15 Reconstruction project in Salt Lake City, Utah.

Wollmann et al. proposed a method consisting of stain compatibility equations, equilibrium equations, and material constitutive relationships to solve for the changes in forces, moments, strains, and curvatures in the system. The initial forces and moments acting on the composite systems are broken down into forces acting on the girder and deck by using axial rigidity ratios and flexural rigidity ratios, respectively. Expressions for change in strain at the centroid of the deck and change in strain at the centroid of the

girder are considered along with the change in curvature in the deck and change in curvature in the girder. Compatibility equations are written to establish the relationship between the strains and relationship between the curvatures. The change in axial forces in the longitudinal direction of the bridge are considered in an equilibrium equation. The changes in moments are summed about an arbitrary point. If the system is indeterminate, then the equilibrium equations must account for time-dependent redundant forces. The deflections can be found by using the principle of virtual work,

$$\Delta(d) = \int_L \kappa(x)\overline{M}(x,d)dx \qquad [2.3]$$

where,

Δ(d) = deflection at location, d, along the span

κ(x) = curvatures due to long-tem effects

$\overline{M}$ (x,d) = moments due to a virtual force applied at location, d.

In order to handle the loss in prestress on the composite section, the approach used by Wollmann et al. was to assume a change in strain at the centroid of the prestressing steel. The corresponding change in force, with a strand relaxation increment, can be broken down into individual components acting on the deck and girder using the axial rigidity ratio discussed above. The resulting change in axial forces can be incorporated in to the expressions for strain. After a solution is determined, the initial assumption for the prestress loss can be checked. If the initial assumption is incorrect, another iteration can be run. This is the approach discussed by Wollmann et al.

Another approach to handling the prestress loss is to treat the loss in prestress force and change in strain at the level of prestressing as additional unknown variables. This requires writing an additional equation for the strain at the level of the prestressing, writing an additional strain compatibility equation, incorporating the change in force into the equilibrium equation, and incorporating the moment induced on the composite system by the change in prestress in to the expression for the change in curvature.

Because there were large blockouts in the girder for the post-tensioning ducts in the Salt Lake City project, the system of equations was refined, using the net section properties of the girder and grouted ducts. The results of the analysis showed that the time dependent stress changes due to differential creep and shrinkage were quite small.

This was accomplished with the use of partial depth precast deck panels. The long term deflection of the system was found to be in the downward direction. The detailed analysis presented by Wollmann allows designers to take advantage of high early concrete strengths resulting in lower creep and shrinkage strains and lower prestress loss. Wollmann et al. recommended an aging coefficient of 0.8 for spliced precast concrete bridges.

2.1.1.3 Harrison and LeBlanc

Harrison and LeBlanc[5] carried out a time-dependent analysis on the West Sandusky Street Bridge over I-75 in Findlay, OH. This was done to determine the required level of prestress in the precast deck panel system with hybrid steel plate girders. This included an investigation of the long term creep effects on the system and the restraint provided by the steel girders. The authors also commented on the fabrication of the deck panels and construction of the bridge.

The 10 ½ in. thick panels used in this project were post-tensioned in both the transverse and longitudinal direction. Post-tensioning in the transverse direction was shown to be more feasible to accommodate the crown in the roadway. Before the panels were shipped to the job site, the entire deck was assembled to verify all the deck panels were constructed in compliance with the plan requirements. Shear studs were used in the shear pockets in order to obtain composite action with the steel girders. A grouted female-female shear key was used between the panels in order provide continuity between the deck panels. Dimmerling et al.[11] did a study on the transverse joints in this bridge, looking at the long term behavior of these joints.

The commercial software SAP2000[12] was used to determine the required level of prestressing in the bridge deck. The bridge was modeled with plate elements and beam elements. In addition to the dead and live loads, temperature and shrinkage effects were included. A temperature range of 60 °F was incorporated into the loading cases. The results determined a maximum tensile stress in the deck of 400 psi. Therefore, a post-tensioning level of 400 psi was suggested. Since the girders were simply supported, causing the deck to be in compression for most of the load cases, the governing load case was found to be the shrinkage of the concrete deck.

The commercial software Bridge Designer II[13] was used to determine the stress redistribution over time in the deck and girders, due to creep and shrinkage effects, and determine resulting prestress losses. The different stages of construction were taken in to consideration, since they have a large impact on the behavior of the system. The stages used by Harrison and LeBlanc were

1. Casting and curing of the deck panels,
2. Placement of the panels on the girders,
3. Stressing of the tendons in the post-tensioning ducts,
4. Grouting of the haunch to obtain composite action,
5. Removal of ½ in. sacrificial layer of the deck,
6. Application of wearing surface and other superimposed dead loads,
7. 10 year evaluation.

Each of these phases was evaluated over a specified time period to include creep and shrinkage. Two different scenarios were run. The first scenario assumed the deck was cast 45 days before stressing the longitudinal tendons. The second scenario assumed the deck was cast 7 days before the stressing of the longitudinal tendons. This was done to look at the effects of the age of the deck at the time of post-tensioning, and incorporate this into the design of both the panels and girders. The CEB-FIP[14] Model Code 1990 was used to determine the time-dependent concrete properties.

Results showed that a compressive stress increase of 11.5 ksi and 12.8 ksi occurred in the top flange of the steel girder for the 45 day tensioning time lapse and 7 day tensioning time lapse, respectively. The compressive stress in the deck decreased from 435 psi to 405 psi for the 45 day tensioning time lapse and from 435 psi to 400 psi for the 7 day tensioning time lapse.

The results of Harrison and LeBlanc's study should not be used as a recommended level of post-tensioning in precast deck panel systems. The results are based on the analysis of one bridge. In addition, if prestressed concrete girders were used, additional stress redistribution would occur from the creep associated with the prestressing of the girders on the composite section and shrinkage of the girder.

2.1.1.4 Dimmerling et al.

Dimmerling et al.[11] also looked at the behavior of the Sandusky Street Bridge over I-75 in Findlay, OH, addressing the leaking of the shear keys, a common problem with this type of deck system. Vibrating wire gages were placed in the grouted shear keys and the post-tensioning process was monitored for the effects of creep, shrinkage, and temperature. The vibrating wire gages were suspended from segments of plastic that span the width of the transverse joint. The gages were placed at the joints at midspan, at the quarter points, and at the end joints.

A non-shrink grout was used in the joints. Variations in the way the grout was mixed from batch to batch caused a variation in the response of the joints. Dimmerling pointed out that this has been a problem with other projects as well.

Dimmerling reported the elastic strain increments in each joint for each tendon that was stressed. The results indicated that the tensioning was successful and the joint stresses were kept around 400 psi.

The strains were monitored for the next eight months. During this time, several observations were made. The grouting of the shear pockets did not significantly change the strains in the joints. The heat of hydration reaction that occurred during the grouting of the shear pockets created a temperature gradient in the system that may or may not have produced significant residual strains. The compressive strain during the first 2 ½ months decreased steadily. This was reported to be contraction associated with the effects of creep and shrinkage instead of compressive stress. After the first 2 ½ months, the changes in strain were believed to be caused only by daily temperature effects.

A load test was performed approximately 5 months after the post-tensioning operation. The purpose of this test was to see if close to full composite action between the girders and panels is present. The strains in the vibrating wire gages were compared to hand calculations assuming full composite action. There was good agreement between the hand calculations and field data.

2.1.1.5 Peterson and Ramirez

Peterson and Ramirez[15,16] investigated the behavior of precast, prestressed concrete form panels with a CIP (cast-in-place) topping. One issue addressed was the

restraint moment developed at interior piers[15]. While the precast panels have undergone a substantial amount of shrinkage, a fresh CIP topping has not undergone any shrinkage. The precast panels restrain the shrinkage producing compressive stresses in the panels and tensile stresses develop in the CIP topping.

In a continuous span, this causes negative restraint moments to develop at the interior supports and positive restraint moments to develop at midspan for each span. Additionally, the reactions at the interior supports increase and the reactions at the end supports decrease. The creep associated with the prestress force in the panels acting on the composite section causes the opposite effect. In a continuous span, this causes positive restraint moments to develop at the interior supports and negative restraint moments to develop at midspan for each span. This assumes the direction of the prestressing strands is oriented in the longitudinal direction. The creep of the panels and CIP topping under the self weight of the system will also produce restraint moments. The restraint moments caused by this effect are similar to the moments caused by the differential shrinkage between the panels and CIP topping.

To investigate this issue, two bridges were constructed and tested at Purdue University. Each bridge had two spans consisting of prestressed concrete form panels and a CIP topping. The bridges were continuous over the interior support. The interior support of each bridge was pinned and the exterior supports were roller supports. Two loads were applied near the interior support to create a large negative moment at the interior support. One load was placed on each span. During casting of the CIP topping and throughout the testing of the bridges, the end reactions were monitored using load cells. These end reactions, along with the applied loads, were used to calculate the moment at the interior support. The restraint moments can also be calculated by multiplying the change in the end reaction by the span length.

During the first few days of observation, the change in the end reactions was believed to be due to the thermal bowing effect. The panels and CIP topping cambered upward in each span, causing the end reactions to increase. Another large change in the behavior of the system occurred when cracking was observed in the CIP topping at the center support. This caused the restraint moment to decrease. The experimental values for the restraint moments were compared to analytical methods for calculating the

restraint moments. However, these methods were based on continuous spans for prestressed girders with a CIP topping. The CIP topping only accounted for a small portion of the composite depth. Therefore, Peterson and Ramirez proposed a new method for calculating the restraint moment at the center pier for a two span, symmetric bridge

$$M_r = (\frac{3}{2}\alpha M_p - \alpha(M_d)_{precast})(\Delta(1-e^{-\phi_1})) - \alpha(M_d)_{CIP}(1-e^{-\phi_2})$$
$$-\frac{3}{2}\alpha M_s(\frac{1-e^{-\phi_2}}{\phi_2}) \quad [2.4]$$

where,

α = factor accounting for the relative stiffness of the diaphragm region and the main spans.

$$= \frac{\frac{2I_d}{L_d}}{\frac{2I_d}{L_d} + \frac{3I_m}{L_m}} \quad [2.5]$$

I_d = moment of inertia of diaphragm region (area between support points at center pier)

L_d = length of diaphragm region

I_m = moment of inertia of main spans

L_m = length of main spans

M_p = moment caused by prestressing force about the centroid of the composite member

M_s = differential shrinkage moment, adjusted for restraint of precast panels and steel reinforcement

$(M_d)_{precast}$ = midspan moment due to dead load of precast panels

$(M_d)_{CIP}$ = midspan moment due to dead load of CIP topping

ϕ_1 = creep coefficient for creep effects initiated when prestress force is transferred to the precast panels

ϕ_2 = creep coefficient for creep effects initiated when CIP topping is cast

$\Delta(1-e^{-\phi_1})$ = change in expression $(1-e^{-\phi_1})$ occurring from time CIP

topping was cast to time corresponding with restraint moment calculation

Peterson and Ramirez stated that if the restraint moment exceeded the cracking moment, the restraint moment should be recalculated using a new α that accounts for the reduced stiffness using cracked section properties.

The PCA (Portland Cement Association)[17] proposed a method for calculating the differential shrinkage moment in a composite section, M_s, required for the calculation of the restraint moment in Equation 2.4. The method was originally produced for the design of continuity connections between adjacent precast, prestressed girders in multi-span bridges. Peterson and Ramirez modified the equation with a factor, which will be referred to as 'p', to account for the restraint by the precast panels and reinforcement in the CIP topping

$$M_s = p\varepsilon_s E_d A_d (e_c + \frac{h}{2}) \qquad [2.6]$$

where,

p = modification factor proposed by Perterson and Ramirez

$$= \left(\frac{1}{1 + \frac{E_p A_p}{E_d A_d}} \right) \left(\frac{1}{1 + \frac{E_s A_s}{E_d A_d}} \right) \qquad [2.7]$$

E_p = modulus of elasticity of the precast panels

A_p = area of precast panels

E_s = modulus of elasticity of steel reinforcement in CIP deck

A_s = area of steel reinforcement in CIP topping

E_d = modulus of elasticity of CIP topping

A_d = area of CIP topping

ε_s = differential shrinkage strain

h = CIP topping thickness

e_c = distance between the top of the precast member and the centroid of the composite section

In addition to monitoring the two bridges over the curing period, a static test was also conducted on each bridge. Each bridge was loaded up to 20 kips. The cracks which had developed during the curing period propagated and additional cracking formed. The moments at the interior supports were tracked with increasing load. The proposed method for calculating the restraint moment with cracked section properties showed very good correlation with the experimental data.

The restraint moments developed from differential creep and shrinkage between the CIP topping and precast panels is analogous to the same phenomena developed between full depth precast panels and prestressed concrete girders. However, the change in support reactions from thermal bowing of the panels during curing from the heat of hydration reaction obviously would not pertain to full depth panel construction. This is because the girders and panels would cure separately before being made composite. However, casting the haunch may cause enough of a temperature gradient to create a thermal bowing effect.

Perterson and Ramirez also conducted a study on the two bridges to examine the behavior and strength when exposed to repeated service loadings[16]. Five million cycles were applied to each bridge. The applied loads were based on producing a stress range in the reinforcement of 120% of the maximum allowable design stress range. After the first 2 million cycles of loading, the stiffness of the system did not change significantly. A durability study was conducted after 2 million cycles which consisted of ponding water for prescribed time increments. This was done for 48 weeks. There appeared to be a significant change in stiffness after the durability study was done. This was believed to be caused by positive restraint moments at the interior support which caused some of the cracks to close. This positive restraint moment was developed when the surface of the CIP topping swelled due to re-wetting the surface. During the last 3 million cycles of loading, the stiffness of the system did not change significantly.

The bridges were then loaded to failure. The capacity of each system was compared to the calculated capacity using virtual work. The calculated failure load was within 1.3% of the actual failure load. The calculated failure load did not take into account the restraint moments at the center pier. Cracking of the concrete and yielding of the steel prior to failure relieved the stresses producing the restraint moment. Based on

this information, it was noted that the restraint moments developed do not affect the ultimate strength of the structure.

2.1.1.6 Issa et al.

Much work on full-depth deck panels had been done at the University of Illinois at Chicago by Issa et al.[2-4,18-19]. Issa pointed out that every DOT (department of transportation) has their own method of design and construction. The purpose of the studies was to formulate an optimum full depth precast bridge deck to be used on steel girders. Some of the work included the following:

1. An extensive survey sent to state DOT's to gather information of the current details used and performance of their deck panel systems,
2. Field inspection of selected bridges across the country using precast deck panels,
3. An analytical study on the required level of post-tensioning,
4. Laboratory testing to look at the effects of post-tensioning, behavior of the transverse joints, and measure of composite action.

Issa's work on required levels of post-tensioning is discussed in this section. The remaining studies conducted by Issa are discussed in Section 2.1.2.6 and Section 2.1.4.2.

Issa[4] performed finite element analyses to investigate the required level of post-tensioning to keep the transverse joints in compression. Several bridges were modeled. Two of the bridges modeled were the Culpeper bridge in Virginia and the Welland River bridge in the Niagara Falls, Ontario. These two bridges were the focus of the study. The Culpeper bridge was a 54.5 ft simply supported span supported by steel rolled beams spaced at 6.25 ft. The joints between the adjacent panels are the female-female configuration. The 18 span Welland River bridge had 3 spans rehabilitated with precast panels, spanning 48 ft and supported by steel girders.

The finite element software ALGOR[20] was used along with the program PCBRIDGE[21] to perform the analyses. Symmetry of the bridges was considered and only a portion of each bridge was modeled in ALGOR. This reduced the number of degrees of freedom and analysis run time. PCBRIDGE was used to determine the resulting shears and moments to apply to the boundaries of the model in ALGOR. The precast panels,

transverse joints, shear pockets, parapets, and closure pours were modeled with six and eight node brick elements. Four layers of brick elements were used in the deck panels. The mild reinforcement for the precast panels and closure pours and the post-tensioning tendons were modeled with truss elements. The post-tensioning was applied by imposing a temperature change in the truss elements for the post-tensioning tendons. The steel stringers and diaphragms were modeled with four node plate elements. Beam elements were used to model the shear studs.

Three different levels of post-tensioning were examined in this study; 200 psi, 300 psi and 400 psi. These were the stresses in the deck caused by the post-tensioning force applied. The joints that were studied in each of the bridges were the ones with high tensile stresses. A number of analyses were run for each bridge modeled to account for the different levels of post-tensioning and live load positioning to create maximum shear or live load positioning to create maximum moment.

For the Culpeper bridge, the maximum tensile stress at the transverse joints was only 100 psi from the worse-case live load wheel positions. A post-tensioning level of 200 psi was recommended to keep the joints in compression. For the Welland River bridge, the critical location for high tensile stresses was in the top surface of the deck in the vicinity of the supports. Issa found that a level of 400 psi of post-tensioning was not enough to eliminate the tensile stresses near the supports in this case. Issa analyzed several more continuous bridges using a post-tensioning level of 600 psi. This proved to be more than enough to keep the joints in compression. The results were interpolated to find the minimum level of post-tensioning that created a tensile stress of zero was 450 psi. In all other regions of the continuous bridges, 200 psi was acceptable.

Issa recommends a post-tensioning level of 200 psi for simply supported bridges. For continuous bridges, a post-tensioning level of 200 psi in positive moment regions and a post-tensioning level of 450 psi in negative moment regions was recommended. Long term creep and shrinkage effects were briefly mentioned. Issa arbitrarily increased his recommendation for initial post-tensioning levels by 100 psi to "account for all residual stresses in the concrete including the effect of creep and shrinkage."[4] Creep and shrinkage can have a substantial effect on the loss of post-tensioning force and deserves more consideration. The levels of post-tensioning recommended in this report may or

may not work well for keeping the joints in compression for panels supported on prestressed concrete girders. In addition, full composite action was assumed between the panels and girders. Partial composite action caused by relative slip between the deck and girders causes a tensile stress increment in the deck in positive moment regions.

An experimental study was done by Issa[18] to investigate the transverse joints, shear pocket connection, and amount of post-tensioning required in the deck. Three bridges, modeled from a four-span continuous prototype bridge in Virginia, were built in a laboratory setting at a scale factor of ¼. Shear connectors used were specially fabricated to meet the designed model requirements. Headed shear studs were used for the shear connectors. The headed shear studs were ¼ in. in diameter and 1 ¾ in. long. The ultimate strength of the shear studs was 75.8 ksi and the yield strength was 65.2 ksi. The corners of the shear pockets that housed the shear studs were beveled to eliminate stress concentrations.

The difference between the bridge models was the level of post-tensioning. One model had no post-tensioning, another had a post-tensioning level of 208 psi, and the last model had a post-tensioning level of 380 psi. Grouted female-female joints were used as the transverse joint configuration between adjacent panels. The panels were cast and cured for 60 days under controlled humidity and moisture room. The panels were supported on two steel beams. Each span was 9.5 ft. with a girder spacing of 18 in.

The three bridges were tested under both static and fatigue loading. The truck loadings for the static tests were positioned to create a maximum positive moment in the system. The loading scheme for the fatigue tests were the same as the static tests. The first two models were subjected to 2 million cycles of simulated HS20 AASHTO truck loading[22] at a frequency of 3 Hz. The last model, post-tensioned to 380 psi, was subjected to 1.3 million cycles. Additionally, an ultimate load test was performed on each model.

The bridges were instrumented at maximum negative moment regions, maximum positive moment regions, and maximum horizontal shear regions to monitor the applied load, deflections, rotations, changes in strain, crack patterns, and relative slip. Surface strain gages, LVDTs, vibrating wire gages, and crack displacement transducers were the instrumentation devices used.

The model with no post-tensioning initially cracked in the transverse joints near the central support. This ultimately led to the failure of the system. The models with post-tensioning also experienced cracking at the center support. However, more cracking occurred away from the central support as the load was increased. Issa's results indicated that higher levels of post-tensioning delay the onset of cracking at the central support. No relative slip occurred between the panels and girders until high static load levels were reached or high stress ranges were introduced during the fatigue test.

2.1.1.7 Markowski

Components of Markowski's[23] work at the University of Wisconsin at Madison on precast deck panels relevant to this study included the required level of post-tensioning across the transverse joints and composite action between steel girders and precast panels with different shear stud layouts. Other aspects of the deck panel system investigated by Markowski included the required level of post-tensioning across longitudinal joints and panel edge strength. This study was the first of three phases for this particular research project at the University of Wisconsin at Madison.

Markowski's work on the required level of post-tensioning across the transverse joints is covered in this section. Section 2.1.2.7 covers Markowski's work on the composite behavior of the steel girders and precast panels.

The transverse joints were tested in flexure to see when the bottom of the joint would open up under different levels of post-tensioning. The size of the panels used for this test was 4 ft x 8 ft x 8 in. The panels were prestressed in the transverse direction. Two lab specimens were placed end to end in a 8 ft -10 in. simply supported condition with a grouted female-female joint between them. The panels did not rest on steel girders. The panels were prestressed in the transverse direction and were post-tensioned to a level of 154 psi across the joint. The setup was instrumented with LVDTs, strain potentiometers, and strain gages. The longitudinal separation of the transverse joint on the bottom face of the panels, the relative vertical movement on the top face of the panels, and the strain adjacent to the joint were measured. The panels were "preconditioned" with 100 cycles of loading and then an ultimate load test was conducted.

During the testing of the transverse joints, significant nonlinear behavior was observed. The joint opening exceeded 0.18 in. on the bottom surface of the panels. Markowski noted that cracking occurred at the bottom of the joint in a gradual manner. Unloading and reloading showed that large residual relative displacements and relative slip occurred.

Using the results from the LVDTs for both the transverse joints and longitudinal joints, moment vs. curvature plots were developed to establish the rotational spring constants that could be used in computer modeling of the joints. Constitutive relationships and the geometry of the cross section were used with the strain distribution to calculate the axial force and moment acting on the cross section. If the assumed neutral axis location did not result in a net horizontal force equal to zero for the flexural strain distribution, then another neutral axis location was assumed and the process was continued.

In his modeling approach, Markowski offset the axial force with the total effective post-tensioning force. An initial prestress force was then backed out by taking into account creep, shrinkage, and elastic losses. However, it does not appear that the losses reported by Markowski were based on a composite section with a steel girder. The losses seem to only be based on the test setup consisting of only the panels. There was no mention about seating losses or friction and wobble losses. Based on the results of the analytical models and experimental results, the level of post-tensioning of 250 psi across the transverse joint was deemed adequate.

2.1.2 Horizontal Shear Transfer

2.1.2.1 Seracino

Using partial-interaction theory to model the composite action of a bridge more accurately models the behavior of a bridge. Loss of full composite action between the deck slab and girder results in a tensile stress increment in positive moment regions. Seracino[24] formed the concept of partial interaction focal points to present the linear elastic partial interaction theory. His work was based on composite steel beams only.

There are two extreme bounds that measure the degree of composite action. One bound being no composite action and the other bound being full composite action. For full composite action, the curvature can be calculated as

$$\phi_{fi}(x) = \frac{M(x)}{E_c I_{fi}} \qquad [2.8]$$

where,

I_{fi} = the moment of inertia transformed to concrete with full interaction of the concrete slab with the beam.

E_c = modulus of elasticity of the concrete

Assuming a pure flexural state, the strain is zero at the centroid of the composite section. For no composite action, the curvature can be calculated as

$$\phi_{ni}(x) = \frac{M(x)}{(EI)_c + (EI)_s} \qquad [2.9]$$

where,

$(EI)_c$ = flexural rigidity of the concrete component

$(EI)_s$ = flexural rigidity of the steel component

The steel section and the concrete section have the same curvature under the no composite action state assuming there is no vertical separation between the concrete section and steel section. The strain distribution is zero at the concrete section's centroid and zero at the steel section's centroid. Note that there must be a discontinuity in strain at the steel and concrete interface when there is partial composite action or no composite action.

The two PIFPs (partial interaction focal points) can now be found. The PIFPs are shown in Figure 2.1.1. One PIFP occurs at the intersection of the full interaction strain distribution and the no interaction strain distribution for the concrete section. This is referred to as $PIFP_c$. The other PIFP occurs at the intersection of the full interaction strain distribution and the no interaction strain distribution for the steel section. This is referred to as the $PIFP_s$. The strain distribution in a partial composite action state must pass through both the $PIFP_c$ and $PIFP_s$. The only unknown remaining is the curvature in the partial interaction state.

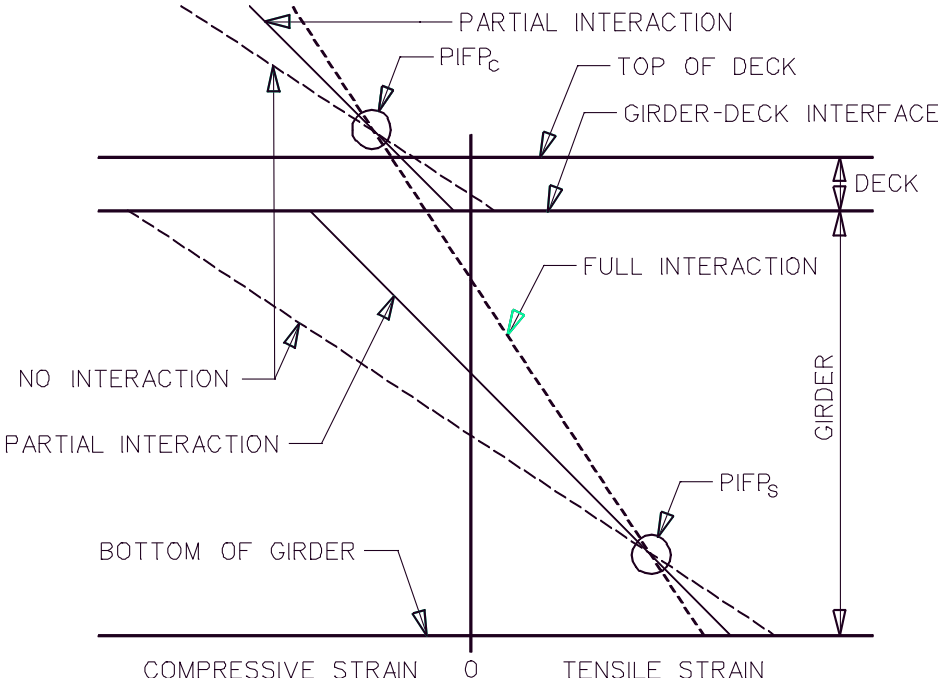

Figure 2.1.1 Strain Distributions for Variable Degrees of Composite Action

A magnification factor (MF_ϕ) can be applied to the full composite interaction state to get the curvature in the partial composite action state. The magnification factor is

$$MF_\phi = (-d_c{}^2 A'+1)^{-1}(d_c{}^2 A'(\frac{L}{\alpha x(L-x)}(\cosh(\alpha x)- \coth(\alpha L)\sinh(\alpha x))\sinh(\alpha x)-1)+1) \quad [2.10]$$

where,

$$\alpha = \sqrt{\frac{k}{pE_s I_o A'}} \quad [2.11]$$

$$I_o = I_s + \frac{I_c}{n} \quad [2.12]$$

$$\frac{1}{A_o} = \frac{n}{A_c} + \frac{1}{A_s} \quad [2.13]$$

$$\frac{1}{A'} = d_c{}^2 + \frac{I_o}{A_o} \quad [2.14]$$

$$n = \frac{E_s}{E_c} \quad [2.15]$$

k = connector stiffness

p = connector spacing

E_s = modulus of elasticity of the steel component

d_c = distance between the centroid of the steel section and centroid of the concrete section

x = distance from the end of the span

L = length of the span

$MF_\phi = 1$ implies full composite action. Although the calculation for the magnification factor is not too complicated, it may not be very practical for design use. Therefore, Seracino looked at the magnification factors at the supports, midspan, and quarter points and made some observations to simplify the expressions. The magnification factor at the supports can be expressed as

$$(MF_\phi)_s = \frac{1}{-d_c{}^2 A' + 1} \quad [2.16]$$

The magnification factor at midspan is

$$(MF_\phi)_m = \frac{1}{d_c{}^2 A' + 1}\left(d_c{}^2 A'\left(\frac{2}{\alpha L} - 1\right) + 1\right) \quad [2.17]$$

The magnification factor at the quarter points is

$$(MF_\phi)_q = \frac{1}{d_c{}^2 A' + 1}\left(d_c{}^2 A'\left(\frac{8}{3\alpha L} - 1\right) + 1\right) \quad [2.18]$$

The magnification factors between the supports, midspan and quarter points can be linearly interpolated without introducing much error compared to the "exact" solution presented in Equation 2.10. The curvature for partial composite action can be found by multiplying the curvature for full composite action by the magnification factor. The curvature for partial composite action can be used with the PIFPs to find the strain distribution at any section.

2.1.2.2 Tadros et al.

Tadros et al.[25] proposed a debonded shear key system to be used with concrete girders. Design criteria and specifications were also cited. This system can be used with cast-in-place concrete decks and partial and full depth precast panel decks. The purpose of this new system is to facilitate deck removal. The girders are cast with blockouts so shear keys are present in the top flange of the girder along the entire length. Hooked reinforcing bars are used as the shear connectors. A sealant is applied to the top of the girder that will break the bond between the girder and the deck concrete. Therefore, the shear resistance is provided by the mechanical interlock between the deck and girder via the shear key and the shear reinforcement.

The shear keys must be properly sized so they don't fail prematurely. Tadros claimed the shear keys can fail in one of two ways. The shear key can fail by bearing on the side of the shear key. The factored horizontal shear force can be compared to the factored horizontal shear capacity

$$v_{uh}(b_v S_{sk}) \le \phi(0.85 f_c' t_{sk}(b_{sk} - t_{sk})) \quad [2.19]$$

where,

v_{uh} = factored horizontal shear stress (psi)

b_v = width of the top flange (in.)

S_{sk} = shear key spacing (in.)

ϕ = 0.7 for bearing design

f_c' = smaller of the compressive strength of the beam and compressive strength of the concrete (psi)

t_{sk} = depth of the shear key (in.)

b_{sk} = width of the shear key (in.)

The shear key can also fail by shearing of the base of the shear key. The factored horizontal shear force can be compared to the factored horizontal shear capacity

$$v_{uh}(b_v S_{sk}) \le \phi(cA_{sk} + \mu A_{vf} f_y) \quad [2.20]$$

where,

c = cohesion stress (psi)

$A_{sk} = w_{sk} b_{sk}$ = area of shear key at base (in^2)

ϕ = 0.9 for shear design

μ = coefficient of friction

A_{vf} = area of horizontal shear reinforcement (in^2)

f_y = yield strength of the shear reinforcement (psi)

AASHTO LRFD[22] and the ACI 318, Building Code for Structural Concrete[26] give values for 'c' and 'μ', depending on whether the deck is cast monolithically, the surface preparation, and the material of the bonding surface. This will be discussed in subsequent sections. In this application, the cohesion stress, 'c', is zero since there is no bond between the deck and girder. Tadros recommends $\mu = 1$ for this application.

Tadros recommended the following equation in the calculation of the horizontal shear stress

$$v_{uh} = \frac{V_u}{b_v d_v} \qquad [2.21]$$

where d_v = distance between the tension and compression resultant forces in the section. Tadros argued that only the composite loads on the system be used when calculating v_{uh}. Tadros went on to claim the shear connectors and shear keys don't resist the deck self weight or the girder self weight since they are introduced prior to composite action being achieved. This will reduce the number of connectors that are required. Tadros does not address the issue of load redistribution in the system after significant cracking occurs.

The design of the shear key system can be accomplished by utilizing Equations 2.19 and 2.20. The unknown variables are t_{sk}, b_{sk}, w_{sk}, f'_c, and A_{vf}. Three of the variables can be chosen in advance by the designer and the remaining variables can be solved for. Tadros recommended using the following equation to establish a maximum for the amount of shear reinforcement:

$$A_{vf} f_y \leq 0.25 f_c' b_v S_{sk} \qquad [2.22]$$

This debonded shear key system was used in a bridge in Nebraska. The southbound structure had the debonded shear key system and the northbound structure had the conventional roughened, bonded interface. Tests were performed with a three axle truck. Deflections of the southbound structure were compared to deflections of the northbound structure. Deflections on the southbound structure were almost the same as the deflections on the northbound structure, indicating there was no increase in flexibility or loss of strength at the interface associated with the debonded shear key system. The

bridge was also inspected three months after completion and so signs of distress were noticed.

2.1.2.3 Push-off Tests at Virginia Polytechnic Institute and State University

There have been extensive studies done on the horizontal composite action between precast concrete panels and precast concrete girders via push-off tests. Two "L-shaped" blocks are cast to simulate a precast panel and a precast girder. A haunch is then cast between the panel and girder. Such parameters as haunch heights, grout types, amount of shear reinforcement, type of shear reinforcement, and surface preparation were investigated to determine their impact on the strength and behavior of the interface between the panels and girders. Load-slip plots were used to examine the overall behavior of the interface between the panel and girder. Load-strain plots were used to examine the behavior of the shear connectors. Push-off tests are discussed further in Chapters 3 and 5.

Menkulasi[27] performed a total of 36 push off tests. The bottom surface of the panels had a rough, exposed aggregate finish. This was accomplished by placing a cloth soaked in a retarder mix on the formwork. The surface was later hosed down to remove the unhydrated grout. The top surface of the girder was given a raked finish. The compressive strength of the concrete for the panel and girder was 5 ksi. The casting orientation for the grout in the haunch was with the girder and panel on their sides. There was no mention of the age of the grout at the time of testing.

The grouts tested were a latex modified mix that was created in the lab and Set® 45 Hot Weather grout. The shear connectors used in the parametric studies included hooked reinforcing bars, post-installed hooked reinforcing bars, post-installed, epoxied Dayton Richmond anchors, and no shear connectors. The post-installed shear connectors are advantageous because they make deck removal easier, allow for larger casting tolerances during a deck replacement project, and don't pose a tripping hazard. Two of the tests had shear keys present in the girder. This was similar to the detail proposed by Tadros[25], except that no debonding agent was applied to the girder.

A force normal to the surface of the panel was applied to the top surface of the panel to simulate the self weight of a tributary area of the deck. This was accomplished

with a force of 2.5 k. A load was applied to the side of the test specimen, passing through the centerline of the haunch in an attempt to load the specimen in pure shear. The specimen was instrumented with two potentiometers to measure the relative displacement between the panel and girder. Electrical resistance strain gages were placed on the shear reinforcement to measure the strain in the reinforcement.

The tests exposed several key aspects about the behavior of the system. First, the strength of the specimen does not vary significantly with the haunch height. However, Menkulasi found that improperly developed shear connectors caused the failure of the specimen to be a pull-out failure of the shear connector. This occurred in a specimen with a 3 in. haunch. The Dayton Richmond connectors showed very brittle behavior. They were very convenient to install though. The Set® 45 Hot Weather mix performed better than the latex modified mix. However, Menkulasi proposed that more grout types be tested in the future. The shear keys on the top surface of the girders increased the capacity of the specimen. Based on the limited tests on this detail, the shear key appeared to increase the capacity anywhere from 15-67%. Most of the failures occurred at the interface between the haunch and girder or haunch and panel.

Menkulasi proposed two equations to be used in design to predict the capacity of the interface between precast concrete panels and precast concrete girders. The equations that he proposed were lower-bound capacities derived from his data. For an uncracked interface,

$$v_{nh} = 0.06 + \frac{0.51(A_{vh} f_y + P_n)}{b_v s} \qquad [2.23]$$

where,

v_{nh} = nominal horizontal shear stress resistance (ksi)

A_{vh} = area of shear reinforcement (in^2)

f_y = yield strength of the shear reinforcement (ksi)

b_v = width of the interface (in.)

s = length of the interface (in.)

P_n = sustained compressive force, normal to the interface (kips)

For a cracked interface,

$$v_{nh} = \frac{0.86(A_{vh} f_y + P_n)}{b_v s} \quad [2.24]$$

Equations 2.23 and 2.24 were compared to code provisions for calculating the horizontal shear resistance, such as ACI 318[26], AASHTO LRFD[22], and AASHTO Standard Specifications[28]. The AASHTO LRFD provisions showed the best correlation with Menkulasi's data and ACI 318 and AASTHO Standard Specifications were deemed unconservative.

Scholz[1] performed push-off tests similar to Menkulasi's push-off tests. Six push-off tests were done, two for each grout examined. The grouts used were a Five Star® Highway Patch, Set® 45 Hot Weather Mix, and Set® 45 Hot Weather mix with a pea gravel extension. The same surface preparation used in the previous study by Menkulasi was used in this study. The casting orientation of the grout for the haunch differed from Menkulasi's specimen in that the grout was cast with the girder and panel upright instead of on their side. No shear connectors were used in these tests. A constant haunch height of 1 ½ in. was used. The specimens were tested two days after the casting of the haunch.

Results showed that the Set® 45 Hot Weather extended mix performed the best. Scholz's data compared favorably with Menkulasi's proposed equations for predicting the shear capacity of the interface (see Equations 2.23 and 2.24). Scholz recognized that in many of Menkulasi's tests, the shear reinforcement did not yield, meaning that using the yield strength in Equations 2.23 and 2.24 may not be valid. Using the strain in the shear connector at the time the interface cracks, ε_s, times the modulus of elasticity of the steel, E_s, was proposed by Scholz to replace the yield strength of the shear connectors. For Menkulasi's push off specimen with the Set® 45 Hot Weather extended grout mix, a new equation was developed using the strain in the shear connector at the time the interface cracked,

$$v = 115 + 1.45\frac{A_{vh}\varepsilon_s E_s + P_n}{b_v s} \quad [2.25]$$

In addition to push-off tests, Scholz also completed tests to measure the cube compressive strength, tensile strength via split cylinder tests, shrinkage characteristics, flow and workability, and bond strength of different grouts. The tests were carried out in strict accordance with ASTM standards. These material properties are critical when

selecting a grout to be used for the haunch between the precast panels and girders. The grouts tested were ThoRoc® 10-60 Rapid Mortar, SikaQuick® 2500, Five Star® Highway Patch, Set® 45 Hot Weather with and without pea gravel aggregate extensions.

The ThoRoc® 10-60 grout had the highest 7 day compressive strength. The grouts with the extended pea gravel did not gain as much strength as the grouts without the extensions. All of the grouts without the pea gravel extension had comparable compressive strengths at 2 hrs. The Five Star® grout had the best tensile strength.

Shrinkage bars for each mix were used to establish the relationship of the shrinkage strains with time. This was done over a 28 day period. Because of the different size bars used and the need to compare these shrinkage values with ones from other tests, the shrinkage strains were multiplied by the volume-to-surface ratio correction factor found in ACI 209[10]. The Five Star® Highway Patch and Set® 45 Hot Weather had the lowest shrinkage strains for the shrinkage bar tests.

In addition to the shrinkage bar tests, a small mockup of the shear pocket was created to test the durability of the detail. After the grout was poured into the blockout and cured for a substantial amount of time, water was ponded on the top of the specimen to look for any leaks that may occur in cracks resulting from large shrinkage strains in the grout. The Five Star® Highway Patch and Set® 45 Hot Weather had the lowest shrinkage strains for the mockup. No water leakage was present in any of the specimens after approximately 60 days.

The flow and workability of the grouts were examined with drop tests on a flow table with a truncated flow cone. A haunch flow mockup was also constructed to test the flow and workability. The mockup was built to mimic the flow of grout between two shear pockets spaced at 2 ft. The grout was poured in one end and the flow was monitored to determine if it flowed completely to the other pocket and see if the entire haunch was filled. The Set® 45 and SikaQuick® performed the best for the haunch flow mockup and Five Star® Highway Patch and Set® 45 performed the best for the drop tests.

Slant shear cylinder tests were used to examine the bond strength. The bottom portion of the cylinders were given different surface preparations: exposed aggregate finish, raked finish, raked and sand blasted finish. Scholz's data shows that the exposed aggregate finish definitely increases the capacity of the interface. The Five Star®

Highway Patch and SikaQuick® performed the best. ThoRoc® 10-60 also performed favorably. There was an attempt to find a correlation between the slant shear cylinder tests and the push off tests. However, no correlation was found. Scholz suggests performing more slant cylinder tests using different angles for the cylinder component for each test.

Wallenfelsz[29] performed 29 push off tests. Like Scholz's[1] tests Wallenfelsz's tests were very similar to Menkulasi's[27] tests. Five Star® Highway Patch, Set 45 Hot Weather, and Set 45® Hot Weather with a pea gravel extension were the grouts used. The girders were given a raked finish and the panels were given either an exposed aggregate finish or a smooth finish. All of the tests were performed within 24 hours of the grouting operation. In addition to testing specimens with hooked reinforcing bars, specimens in which a steel plate was cast with the girder were also tested. Post-installed shear studs were shot to the top and bottom of the plate. This eliminates tripping hazards during construction and allows for easier panel placement during construction.

Another series of Wallenfelsz's tests examined a hidden pocket detail. This detail provided a reduced pocket diameter at the top of the panel, improving the appearance and performance of the riding surface. With this detail, the grout was pumped in at one location and the air was allowed to escape through a predetermined vent location.

During most of Wallenfelsz's tests, failure of the interface occurred between the slab and the haunch for the specimen with hooked reinforcing bars. This may be attributed to air getting trapped during the casting operation. For specimens with the steel plate detail and shear connectors, the failure of the interface occurred between the girder and haunch.

The behavior of the system was broken down into three different categories. The first category was characterized by the shear capacity of the shear connectors being less than the shear capacity provided by cohesion at the interfaces. For this case, the load-slip plot was linear up until cracking. After cracking, there was a sudden drop in the load carried. There was still a considerable post-crack capacity, maintained at a fairly constant magnitude. In general, the shear connectors did not yield at the time the peak capacity was reached. Yielding occured sometime after the peak load was reached.

The second category was characterized by the shear capacity of the shear connectors being greater than the shear capacity provided by the cohesion at the interfaces. The load-slip plot did not show a significant decrease in strength as the slip increased in the post-peak load region. In general, the shear connectors did yield by the time the peak capacity was reached. The specimens with the steel plate embedded in the girder with shear connectors fell in this category.

The third category was characterized by the shear capacity of the shear connectors being approximately equal to the shear capacity provided by cohesion at the interfaces. Here, there was a slight drop in the load carried when the interface cracks. The specimen then continued to carry additional load after cracking.

Based on Wallenfelsz's data, the majority of the shear connectors have not yielded at the time the peak strength was reached. The equations for the capacity the interface provided by many code provisions assume the shear connectors have yielded. The peak shear stresses provided in this study were compared to those obtained by AASHTO LRFD[22]. The AASHTO LRFD equation that used a coefficient of friction and cohesion value that correspond with an unintentionally roughened surface showed the best correlation with the push-off test data. Wallenfelsz proposed a change to the current AASHTO LRFD equation to predict the horizontal shear strength, which was more consistent with his results when the amount of steel was increased

$$v_n = \max[cA_{cv}, \mu(A_s f_y + P_n)] \qquad [2.26]$$

where,

c = cohesion stress

A_{cv} = area of interface

μ = coefficient of friction

= 0.9 for grout/concrete interface

= 0.6 for grout/steel interface

A_s = area of shear connectors

f_y = yield strength of shear connectors

P_n = sustained compressive force, normal to the interface

The hidden pocket detail provided no noticeable increase or decrease in capacity. However, forming the pocket for the hidden detail can prove to be difficult. The strength

of the specimen was not affected by the surface preparation on the bottom of the panel. Additionally, an exposed aggregate finish may promote the formation of additional air bubbles during the casting of the haunch. Therefore, it was recommended to use a smooth finish on the bottom of the panels. Another point worth noting from Wallenfelsz's work was that the specimen with the embedded steel plate and shear studs performed similarly to the detail with the hooked reinforcing bars. This indicated that this detail may be a suitable alternative to the hooked reinforcing bar.

2.1.2.4 Badie et al.

Badie et al.[30] proposed the use of large diameter shear studs in composite bridge construction. The advantages of the system include less installation time, ease in deck removal, and safer working conditions during construction. The diameter of the studs used in this study were 1 ¼ in. An emphasis on quality control during the welding process is mentioned. Push-off tests were done to investigate the ultimate strength of the large diameter shear connectors using a rolled steel section as the girder. Control groups of $\frac{7}{8}$ in. studs were tested as a basis of comparison. Both headed and headless studs were tested. Confinement ties were provided in the deck for some of the specimens to see if there was an influence on the capacity. The specimens were tested for ultimate strength and some of the specimens were also subjected to 2 million cycles of fatigue loading.

The same mode of failure was observed in most of the specimens. The failure occurred by shear at the base of the weld. Other failure modes observed were a base plate failure for two specimens and concrete failure for three of the specimens. After observing the failure of the base plate, a minimum top flange thickness of ½ in. was recommended. The concrete failure occurred at the unloaded end of the push-off specimen. This was believed to be a local effect, specific to this type of test, and would not be typical in most bridges since the majority of the studs are well confined.

In addition to the insight of the failure mode of 1 ¼ in. diameter studs, other key aspects of the behavior of these large diameter connectors was noticed. The use of confinement steel greatly increased the capacity of the push off specimen. Most bridge decks do have a high level of confinement from the top and bottom transverse and

longitudinal reinforcement. Using headless studs decreased the capacity of the specimen. However, Badie suggested further studies are needed in this area. Based on the data, fatigue loading did not have an effect on the capacity of 1 ¼ in. diameter studs. The large diameter shear studs showed 30% less slippage at failure than the smaller diameter studs. However, the large diameter studs did show larger slip values after the fatigue loading was applied. The tests showed that the AASHTO LRFD specifications are conservative for estimating the number of studs needed, based on fatigue requirements, but may overestimate the amount of studs needed by as much as 30%. A stud spacing of 6 in. or more was recommended.

Based on the observations and design recommendations, a full-scale beam was tested to further evaluate the 1 ¼ in. diameter stud's performance. The beam was a 40 ft long, W36x160 with an 8 in. thick concrete deck. The beam was tested to 4.8 million cycles of HS-25 vehicle loading, as specified in AASHTO LRFD[22]. The fatigue test showed no loss of composite action between the concrete deck and beam. No distress was noted in the concrete deck due to the use of the large diameter studs.

2.1.2.5 Kahn and Slapkus

Kahn and Slapkus[31] tested six composite concrete T-beams to investigate the interface shear strength for sections made with high strength concrete. The flange was cast against a precast web that had cured for 4 weeks. The precast webs had a nominal compressive strength of 12 ksi. For the cast-in-place flanges, three of the specimens had a nominal compressive strength of 7 ksi and the other three specimens had a nominal compressive strength of 11 ksi. The surface between the web and flange was not intentionally roughened. The ratio of reinforcement crossing the interface ranged from 0.0019 to 0.0037. The transverse reinforcement consisted of 5, 7, or 9 No. 3 U-shaped stirrups.

The specimens were loaded to failure under a 4-point bending test. The specimens were instrumented with electrical resistance strain gages and LVDTs. The specimens with the 11 ksi flanges failed in flexure with the concrete crushing between the load points in the top flanges. The specimens with the 7 ksi flanges failed by cracking at the interface between the web and flange. Push-off tests were also performed using a

wide range of concrete strengths. There was a good correlation between the results for the push-off tests and composite beam tests.

The experimental shear stresses from the composite beam tests were compared to the predicted peak shear stress values proposed in previous research and current code provisions. AASHTO LRFD[22], AASHTO Standard Specifications[28], and ACI 318[26] were found to be conservative for predicting the strength of the interface for high strength concrete specimens. In some cases when the experimental shear strength was compared to the AASHTO Standard Specifications, the experimental shear strength was six times greater. Kahn and Slapkus compared the shear strength from their tests to an equation proposed by Kahn and Mitchell[32]

$$v_n = 0.05 f_c' + 1.4 \rho_v f_y \leq 0.2 f_c' \qquad [2.27]$$

where,

f_c' = compressive strength of the weaker of the flange or web concrete (psi)

$\rho_v = \frac{A_v}{b_v s}$ = transverse reinforcement ratio

f_y = yield stress of the transverse reinforcement (psi)

Equation 2.27 showed a reasonably good correlation with the experimental data. Kahn and Slapkus' results were also compared to an equation proposed by Loov and Patnaik[33]

$$v_n = k\lambda\sqrt{(15 + \rho_v f_y) f_c'} \leq 0.25 f_c' \qquad [2.28]$$

where,

k = "roughness" constant

= 0.6 for rough surfaces

= 0.5 for smooth surfaces

λ = correction factor related to the concrete density

Equation 2.28 predicted the shear strength more accurately than all the other methods for calculating the shear strength that were studied by Kahn and Slapkus.

2.1.2.6 Issa et. al.

Issa[19] carried out further lab studies to investigate composite action between the precast deck panels and supporting steel girders. This was done by testing 28 push-off specimens. Fourteen of the specimens were ¼ scale and 14 of the specimens were full scale. Each specimen consisted of a steel beam and two precast panels. Two of the full scale specimens did not have any studs so the friction contribution of the interface to the total capacity could be evaluated. The number of pockets and the number of shear studs in each pocket were the two main parameters examined by Issa. One, two, three and four stud specimen were examined. All the studs were placed in a line perpendicular to the longitudinal axis the of the steel girder specimen.

Part of the specimen preparation consisted of saturating the shear pockets with water so that there would not be any exchange of water between the grout and concrete panels during the grout pour. LVDTs were installed to measure the relative slip and uplift between the panels are steel girders. Crack initiation and crack propagation were also monitored throughout the test.

Finite element models were created in ANSYS[34] to simulate the push-off tests. Nonlinear behavior such as cracking and crushing of the concrete and grout, slip via contact and target elements were incorporated in the analysis. Whether or not the plasticity of the steel was modeled was not mentioned. Shear transfer coefficients of 0.6 and 0.75 were used for open cracks and closed cracks, respectively, as part of the concrete material model. There was no mention about whether the models were run under force control or displacement control.

During the testing, the failure of the first stud was characterized by a sudden drop in load. The dominate failure mode of the studs was a shear failure; although, some studs were subjected to bending. A critical slip level of 0.02 in. was established based on the results of the push-off specimen. Issa defined the critical slip as the level where there was a slight increase in load with a larger increase in slip. Here, the shear stud was engaged and a clamping stress was imposed on the specimen. At higher loads, the stud started to yield and was accompanied by local cracking and crushing of the concrete. The stud would then typically fail through the weld.

Issa shows that the two, three, and four stud specimen, with the same number of pockets, experienced ultimate loads at the same relative slip point. It was also shown that as the number of studs was increased, the strength increased and the initial portion of the load-slip curve (elastic stiffness) increased. However, there was no direct relationship between the number of studs and the ultimate load. For example, Issa noted that doubling the number of connectors did not double the capacity of the specimen. The ultimate strength was increased for a greater number of shear pockets. The finite element analysis results indicated the maximum shear stress in the interface occured in regions surrounding the shear studs. Issa reported the finite element results showed a good correlation with the experimental results. The finite element results did not capture the post-peak portion of the load-slip curve.

Issa compared his test results with equations developed from previous studies to predict the shear strength of welded shear studs, as well as current code provisions. The AASHTO-LRFD[22] shear friction equation was reported to have predicted conservative estimates for the shear strength for shear studs. A cohesion value, c, of 25 psi and friction coefficient, μ, of 0.7 are recommended.

2.1.2.7 Markowski

Markowski[23] investigated the composite action between steel girders and precast panels with different pocket spacing, which was an extension of the study discussed in Section 2.1.1.7. A model was constructed on ½ scale with a 41 ft - 6 in. simply supported girder and precast deck panels. One half of the girder had 1 ft pocket spacing (simulating 2 ft pocket spacing) with one longitudinal row of three shear studs. The other half of the girder had 2 ft pocket spacing (simulating 4 ft pocket spacing) with two longitudinal rows of shear studs, three shear studs per row. There was no prestressing in the transverse direction, but longitudinal post-tensioning was applied at a level of 256 psi. This was close to the desired level of post-tensioning of 250 psi. According to Markowski, the desired level of 250 psi is the level of post-tensioning that is to be supplied for the Door Creek Bridge. The Door Creek Bridge is a bridge will be constructed in the field for a later phase of the research program.

The setup was instrumented with LVDTs and strain gages. The vertical deflection at midspan, the relative slip between the girder and panels at the ends of the span, and strain distribution through the depth at selected intervals along the span were measured. Both a cyclic test and ultimate strength test were conducted. The specimen was subjected to 2 million cycles of load at 2 Hz. The load applied at midspan was based upon creating the same maximum moment in the specimen that would be found by applying an AASHTO vehicle load with a fatigue factor and axle spacing for fatigue applied. Static tests were performed every 400,000 cycles to see if there was any degredation in stiffness. The specimen was also subjected to an ultimate load test.

For the test on the specimen which investigated composite action, there was no significant degradation in stiffness under the cyclic loading regardless of the pocket spacing. However, cracking was observed on the top surface of the shear pockets that were spaced at 2 ft (simulating 4 ft pocket spacing on a full scale model). There were some noticeable differences in the strains on the bottom flange of the girder during the cyclic test. During the ultimate load test, the capacity of the 100 kip actuator used by Markowski was reached. There was no evidence of any cracking or crushing of the concrete. However, a portion of the steel beam did yield during the test. It was also noticed that the end of the beam with the smaller pocket spacing reached its first slip before the end with the larger pocket spacing. At higher loads, the smaller pocket spacing did provide better composite action between the panels and girder. However, the magnitudes of slip for both ends of the girder were very small. A 4 ft pocket spacing was recommended by Markowski.

When a portion of the deck was removed in the vicinity of the shear connectors, it was noticed that cracking occurred along the top of the shear studs. Markowski reported that having shear studs with the same length creates a plane of weakness in the deck where cracks can form.

Markowski presented a method to calculate the flexural capacity of a section assuming partial composite action, which was based upon the work of Seracino[24]. The strain distribution through the depth of the section can be calculated with this method. The strain distribution from Markowski's tests at different levels of loading was compared to the partial interaction strain distribution. Markowski notes that the strain in

the bottom flange of the beam did increase dramatically when the first slip occurred, signifying partial composite action. However, the strain in the top flange matches the full interaction strain distribution. Markowski stated that it was difficult to determine if there was partial composite action or full composite action based upon the analytical models.

2.1.3 Panel Joints

2.1.3.1 Sullivan

Sullivan[35] carried out finite element analyses in SAP[12] and ANSYS[34] to examine the behavior of different transverse joint configurations. The different joints examined were the male-female epoxied joint, a dapped connection, and flat joint between two panels with a CIP (cast-in-place) concrete topping.

The Scioto River Bridge in Columbus, Ohio was modeled in SAP. The bridge consisted of three steel plate girder spans and eight prestressed girder spans. The girders were modeled with frame elements and the deck and parapets were modeled with shell elements. Full composite action was assumed between the girders and panels in all the models. The piers were not modeled. Instead the piers were treated as pin and roller supports because the large stiffness of the piers was not believed to affect the longitudinal membrane behavior of the deck. The loading cases in the SAP model consisted of an 80 psi wheel load placed adjacent to transverse joints at critical locations on the bridge, a wearing surface load of 30 psf, member self weight, and two temperature loads. The first temperature load consisted of a uniform decrease in temperature of 35 °F and a temperature gradient of 15 °F through the depth of the deck that induced compression in the top of the deck. The second temperature load consisted of a uniform temperature decrease of 50 °F and a temperature gradient of 15 °F through the depth of the deck that induced tension in the top of the deck.

Several locations of the bridge were analyzed in SAP under the wheel load case and other load cases to determine the locations that produce large tensile stresses in the transverse joint. A refined model consisting of a two-panel system was modeled in ANSYS. Rotations and lateral, longitudinal, and vertical displacements from the SAP model were applied to the nodes on the boundaries of the two-panel system,

corresponding to a given load case or combination of the cases. These boundary conditions accounted for the rest of the bridge's influence on the 2-panel system.

The applied load cases in the ANSYS models were the same as the load cases in the SAP model. The panels were modeled with brick elements that incorporated cracking and crushing of concrete. The girders were modeled with beam elements. Interface elements were used to model the interfaces between the two panels at the transverse joints. The material properties of the interface incorporated frictional behavior based on the user specified friction coefficient.

Crack patterns, crack widths, longitudinal strain distributions, shear stress distributions and relative vertical displacements between the panels were studied for each of the transverse joint configurations under the various loading conditions. All the joints exhibited at least some cracking. Crack widths were calculated from empirical formulas found in previous research. Sullivan discovered from other research that crack widths as small as 0.002 in. can cause water leakage through the joint. ACI sets a limit on crack widths of 0.013 in. In this study, crack widths as high as 0.018 were discovered.

The longitudinal behavior of the transverse joints was found to be independent of the transverse joint configuration. The analysis revealed that the large longitudinal stresses caused from the temperature loading produced the most adverse effects in the system. The cracks produced from this load were eliminated when post-tensioning was applied at a level of 800 psi in the deck. The cracks were also eliminated if expansion joints were provided at every other pier in the SAP model. From a practical standpoint, including expansion joints at every other pier can create maintenance issues.

Sullivan showed that the vertical behavior of transverse joints was dependent upon the transverse joint configuration. When the post-tensioning was not included in the models, the male-female joint produced the smallest relative vertical displacements and the flat joint with the cast-in-place topping produced the largest relative vertical displacements. Although, the largest relative vertical displacement were still quite small. The flat joint with the cast-in-place topping had a maximum relative vertical displacement of only 0.399×10^{-3} in. The male-female joint had a maximum relative vertical displacement of only 0.99×10^{-4} in. The difference in the performance of the joint configuration was reduced when post-tensioning was incorporated.

2.1.3.2 Gulyas et al.

Gulyas et al.[36] performed lab tests on grouted female-female joints to investigate the performance of different non-shrink grouts. The height of the specimen ranged from 7 in. to 14.25 in. The specimens were 6.5 in. wide and 3.25 in. deep. Two grouts were used in the tests. The first grout was magnesium ammonium phosphate [Mg-NH_4-PO_4]. This is also known as Set 45® Hot Weather grout and was used in studies by Scholz[1], Menkulasi[27], and Wallenfelsz[29]. The 7 day compressive strength was 7260 psi and the 7 day tensile strength was 557 psi. The second grout was another non-shrink grout. The 7 day compressive strength was 5870 psi and the 7 day tensile strength was 390 psi. The details of the mix design for the non-shrink grout is given by Gulyas. A total of 24 specimens were tested, eight using the non-shrink grout and 16 using the Set 45® Hot Weather grout. Each received a sandblasted surface treatment to improve the bond on the surfaces of the keyways. Sixteen of the specimens had keyway surfaces covered with a damp towel prior to grouting. Eight of the Set 45® Hot Weather specimens were intentionally left exposed to the air for several days prior to the grouting of the joints. The specimens with Set 45® Hot Weather grout were given a 7 day air curing treatment after grouting. The specimens with the non-shrink grout were covered in damp towels and plastic for a 7 day curing period after grouting.

Three different types of tests were performed. The first test was a direct tension test. This test simulated shortening of the precast concrete members due to creep and shrinkage and any drying shrinkage of the grout in the keyway. The second test was a vertical shear test. This test simulated a wheel load on one member and no wheel load on the other member. The third test was a transverse shear test. This test simulated differential creep, shrinkage, or temperature movement at the interface between the grout and precast member.

The specimens with Set 45® Hot Weather grout exhibited much higher failure loads than the non-shrink grout. Even the Set 45® Hot Weather specimens that were exposed to air before grouting had failure loads at least 1.45 times the failure load of the non-shrink grout specimens. Allowing the Set 45® Hot Weather specimen to be exposed to the air for several days prior to pouring the grout caused a substantial decrease in

strength, anywhere from 44% to 68%, depending on the type of test run. The longitudinal shear test showed the most substantial difference.

In addition to the transverse joint push-off tests, shrinkage tests were conducted for 3 in. x 3 in. x 10 in. prisms. Three mixes were compared. The first mix was the Set 45® Hot Weather grout. The second mix was the Set 45® Hot Weather grout with an aggregate extension. The third mix was concrete with Portland cement with a water to cement ratio of 0.32. The Set 45® Hot Weather grout mixes, both with and without the aggregate extension, had shrinkage strains five times less than the concrete mix at about 120 days.

Chloride absorption in 4 in. cubes was also monitored over 21 days. The changes in weights of the specimens were monitored over this time period. The Set 45® Hot Weather specimen showed an increase in weight of about 1% and the portland cement concrete specimen showed an increase in weight of about 3%.

2.1.3.3 Kaneko et al.

Kaneko et. al.[37,38] performed finite element and experimental studies to investigate and verify the failure modes of male-female shear keys proposed in formulations using principles of fracture mechanics. The failure mode investigated was the shear-off, or shearing failure. This occurs through the base of the key. Another failure mode of the male-female shear key is the sliding and separation of the female end with respect to the male end. These two failure modes may occur simultaneously. Refer to Sullivan[35] for more on the shearing failure and sliding failure.

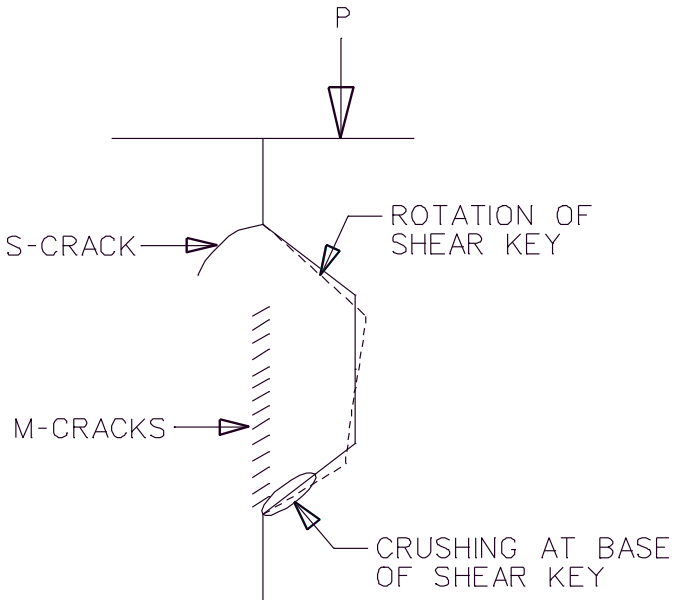

Figure 2.1.2 Proposed Failure Mode for the Male-Female Shear Key

The proposed failure mode of the shear key consists of M-cracks (diagonal multiple cracks) and S-cracks (single curvilinear crack). The failure is initiated by the formation of the S-crack at the corner of the shear key due to high shear stresses, which is shown in Figure 2.1.2. The S-crack continues to propagate under additional load. The propagation of the crack induces the rotation of the shear key. This creates a high stress field at the lower part of the base of the key. The high stress field leads to M-crack development. The cracks are oriented at a certain angle of inclination. If there is no post-tensioning applied across the joint, then the state of stress at the base of the key is close to a pure shear stress state (neglecting longitudinal stresses from flexure). For this state of stress, the M-cracks would be oriented at 45°. Additional loading causes additional M-cracks to form along the base of the key. Eventually the shear key is sheared off at the base by the failure of the compressive struts between the M-cracks. During this process, the male and female end of the joint slip and separate relative to one another. Kaneko derived relationships for the shear stress and the relative slip. The wedge crack model was used to predict the response due to the formation of the S-crack

$$\Delta_s(l) = \sin(\theta)\frac{8\pi}{E(\pi^2-4)}(F-\sin(\theta)-\sigma_p l\cos^2\theta)\ln(l) \qquad [2.29]$$

where,

θ = orientation angle of crack (recommended value of 45°)

E = modulus of elasticity of concrete

F = vertical wedging force

σ_p = lateral prestress

l = assumed crack length

There was no mention about how to calculate the shear stress. However, the average shear stress can be calculated by taking the vertical wedging force, F, and dividing it by the area of the base of the key.

The rotating smeared-crack-band model was used to predict the response due to the formation of the M-cracks

$$\Delta = \varepsilon_y D + \gamma_{xy} L \qquad [2.30]$$

where,

D = depth of the key joint

L = length of the key joint

ε_y = normal strain in the vertical direction

γ_{xy} = shear strain

Determining the shear stress, τ_{xy}, requires using the strain state ε_x, ε_y and γ_{xy} and using stress transformations and constitutive relationships that incorporate inelastic behavior. The constitutive relationships consist of a model for the compressive behavior of concrete and a model for the tensile behavior of concrete. The constitutive relationships used by Kaneko were fairly typical and there is a wealth of literature that proposes such models as well as slight variations[39,40].

Push off tests were performed on male-female shear keys[38]. The vertical slip between the male and female end were monitored along with the applied vertical load. The cracking patterns in the joint were tracked. The cracking observed in the experiment was consistent with the behavior of S-crack and M-crack formation described above. Equations 2.29 and 2.30 also predict the slip of the key fairly well through the entire range of loading for different levels of prestress.

A nonlinear finite element analysis was also carried out to add confidence to the verification study. The model consisted of three node and four node plane stress

elements. Analyses were run with both a multidirectional fixed smeared-crack model and a discrete cracking model (S crack path assumed) to verify the behavior with two different crack models. The finite element model traces the pre-peak stress region of the shear stress vs. relative slip curve considerably well. However, the models were unable to track the post-peak shear stress region on the shear stress vs. relative slip curve.

2.1.4 General Studies on Precast Deck Panel Systems

2.1.4.1 NUDECK System

A great deal work had been done at the University of Nebraska at Lincoln[41,42] in the development of the NUDECK precast deck panel system. The NUDECK system is very similar to typical precast deck panels used. One unique feature is that the NUDECK system utilizes spiral reinforcement around the ends of the prestressing strands. This provides a confining mechanism for the concrete surrounding the strands and reduces the development length of the strands in an overhang.

Another major difference in the NUDECK system lies in the continuity over the girders. Normally full width panels are continuous over the girders with the exception of shear pocket locations. Therefore, there are only discrete locations where there is no precast concrete segment over the girder. The pretensioned strands are continuously embedded in the concrete panels over the entire width. In the NUDECK system, the precast concrete segments only run between the edges of the girders. Continuity over the girders is provided by mild reinforcing steel, properly embedded in adjacent concrete panel spans. When the stress in the prestress force is released, the mild reinforcing bars go into compression, transferring the compressive force between the panels. Over the girder lines, the total compressive force in the continuity bars is equal to the total tensile force in the prestressing strands. The elastic shortening loss in the prestressing strands is equal to the compressive stress gained in the continuity bars. The corresponding strain increment is calculated as:

$$\Delta\varepsilon = \frac{A_p f_{pi}}{A_s E_s + A_p E_p} \qquad [2.31]$$

where,

f_{pi} = tensile stress in the strands just before release

A_s = cross sectional area of the mild reinforcing continuity bars

A_p = cross sectional area of the prestressing strands

E_s = modulus of elasticity of the mild reinforcing continuity bars

E_p = modulus of elasticity of the prestressing strands

Buckling of the continuity bars must also be checked over the length of the gap. The gaps over the girders are filled with grout after the system is post-tensioned together.

Cyclic and ultimate load tests were conducted on two lab specimens. The system was also used on Skyway Drive and West Dodge Bridge in Omaha, Nebraska. Both projects demonstrated the successful implementation and performance of the NUDECK system.

2.1.4.2 Issa et al.

Issa[2] submitted a questionnaire survey to DOT's to see what types of transverse joints were used, the type of bonding material used to fill the joints, the protection system used on the deck, the problems associated with the joints, and the type of connecting system between the panels and girders. Of the states that reported, leaking of the transverse joints was the most common problem. Cracking and deterioration of the system was also reported. This was mostly attributed to poor construction procedures, poor material quality, and inadequate maintenance.

The female-female grouted joint was the most common transverse joint presented by Issa. However, Illinois utilized the male-female joint on the Senneca bridge. Leaking was reported at the joints in this bridge. The vast majority of the bridges described in the report had steel supporting systems with shear studs shot to the girder to obtain composite action.

A field inspection of the bridges reported in the survey was done by Issa[3]. The biggest problems found were leaking and/or cracking at the transverse joints. Issa reported that many of these occurrences can be attributed to poor construction procedures, the configuration of the joint between the adjacent panels, a lack of post-tensioning, or the materials used. Issa recommended that an opening of at least ¼ in. be used between female-female joints to allow for any panel size irregularities. Leaking was reported in this joint configuration when the panels are butted against one another at the

bottom of the joint. Based on the inspections, Issa recommended that longitudinal post-tensioning be used to keep the joint in compression and guard against leaking. Issa reported that very few states use longitudinal post-tensioning. Fewer problems were encountered with bridge decks supported on concrete elements.

2.2 Current Code Provisions

The following sections discuss current code provisions that are applicable to the design and analysis of precast deck panel systems. Models for predicting the variation of the creep coefficient and shrinkage strains with time are discussed first. Methods for calculating prestress loss are discussed next. The equations for prestress loss are not valid for calculating prestress loss in the post-tensioning ducts because the equations do not take in to account the effects of differential creep and shrinkage. Methods for calculating the horizontal shear strength are presented last. The equations for horizontal shear strength are not applicable to the design of the shear pockets for precast deck panel systems the way they are presented. The following chapters investigate whether the equations may be altered for the design of shear pockets in precast deck panel systems.

2.2.1 Creep and Shrinkage of Concrete

The following section discusses various models for predicting creep and shrinkage response of concrete. These models aid in predicting the response of concrete structures and in predicting prestress loss in prestressed concrete structures.

2.2.1.1 ACI-209

The ACI (American Concrete Institute) 209[10] report presents models for predicting creep and shrinkage response of concrete under service conditions. The shrinkage strains can be predicted at any time by

$$(\varepsilon_{sh})_t = \frac{t^{\alpha}}{f + t^{\alpha}} (\varepsilon_{sh})_u \qquad [2.32]$$

where,

t = time from the end of initial curing

α = 0.9 to 1.10 (1.0 recommended value)

f = 20 to 130 days (35 recommended when moist cured for 7 days or 55 days when steam cured for 1-3 days)

$(\varepsilon_{sh})_u$ = ultimate shrinkage strain

= $(780\ \mu\varepsilon)\gamma_{sh}$

γ_{sh} = product of applicable correction factors for nonstandard conditions

The factor γ_{sh} that accounts for nonstandard relative humidity, member sizes, concrete composition, slump, fine aggregate composition, cement content, and air content is

$$\gamma_{sh} = \gamma_\lambda \gamma_{vs} \gamma_s \gamma_\psi \gamma_c \gamma_\alpha \quad [2.33]$$

The creep coefficient can be calculated at any time by

$$v_t = \frac{t^\psi}{d + t^\psi} v_u \quad [2.34]$$

where,

t = time after loading

ψ = 0.4 to 0.8 (0.6 recommended value)

d = 6 to 30 days (10 days recommended)

$v_u = 2.35\gamma_c$

γ_c = product of applicable correction factors for nonstandard conditions

The factor γ_c that accounts for nonstandard curing conditions, relative humidity, member sizes, concrete composition, slump, fine aggregate composition, and air content is

$$\gamma_{sh} = \gamma_{la} \gamma_\lambda \gamma_{vs} \gamma_s \gamma_\psi \gamma_\alpha \quad [2.35]$$

The correction factor accounting for curing is

$$\gamma_{la} = 1.25(t_{la})^{-0.118} \text{ for moist cured concrete other than 7 days,} \quad [2.36]$$

$$\gamma_{la} = 1.13(t_{la})^{-0.094} \text{ for steam cured concrete other than 1-3 days} \quad [2.37]$$

where t_{la} = is the loading age (days). The correction factor for curing only applies to creep.

The correction factor for the ambient relative humidity is:

$$\gamma_\lambda = 1.27 - 0.0067\lambda \quad (\lambda > 40) \quad \text{for creep and} \quad [2.38]$$

$$\gamma_\lambda = 1.4 - 0.01\lambda \quad (40 \le \lambda \le 80) \quad \text{and} \quad [2.39]$$

$$\gamma_\lambda = 3 - 0.03\lambda \quad (80 < \lambda \le 100) \quad \text{for shrinkage} \quad [2.40]$$

where λ = relative humidity (percent). The correction factor for member size can be calculated two separate ways.

The member size correction factor using the average thickness method is:

$$\gamma_h = 1.14 - 0.023h \quad \text{for creep during the first year of loading,} \quad [2.41]$$

$$\gamma_h = 1.10 - 0.017h \quad \text{for creep at ultimate values,} \quad [2.42]$$

$$\gamma_h = 1.23 - 0.038h \quad \text{for shrinkage during the first year and} \quad [2.43]$$

$$\gamma_h = 1.17 - 0.029h \quad \text{for shrinkage at ultimate values,} \quad [2.44]$$

where h = average thickness for the part of the member under consideration (in.).

The second method for calculating the member size correction factor is based on the volume to surface area ratio

$$\gamma_{vs} = \frac{2}{3}\left(1 + 1.13e^{-0.54\frac{V}{S}}\right) \quad \text{for creep and} \quad [2.45]$$

$$\gamma_{vs} = 1.2e^{-0.12\frac{V}{S}} \quad \text{for shrinkage} \quad [2.46]$$

where $\frac{V}{S}$ = volume to surface area ratio (in.). Only the average thickness method or the volume to surface area ratio method should be used.

The correction factor for slump is

$$\gamma_s = 0.82 + 0.067s \quad \text{for creep and} \quad [2.47]$$

$$\gamma_s = 0.89 + 0.041s \quad \text{for shrinkage} \quad [2.48]$$

where s = slump (in.).

The correction factor for fine aggregate composition is

$$\gamma_\psi = 0.88 + 0.0024\psi \quad \text{for creep and} \quad [2.49]$$

$$\gamma_\psi = 0.3 + 0.014\psi \quad (\psi \le 50) \text{ and} \quad [2.50]$$

$$\gamma_\psi = 0.9 + 0.002\psi \quad (\psi > 50) \text{ for shrinkage} \quad [2.51]$$

where ψ = ratio of fine aggregate to total aggregate by weight (%).

The correction factor for cement content is

$$\gamma_c = 0.75 + 0.00036c \quad \text{for shrinkage} \quad [2.52]$$

where c = cement content (lb/yd^3).

The correction factor for air content is

$$\gamma_\alpha = 0.46 + 0.09\alpha \geq 1.0 \qquad \text{for creep and} \qquad [2.53]$$

$$\gamma_\alpha = 0.95 + 0.008\alpha \qquad \text{for shrinkage} \qquad [2.54]$$

where α = air content (%).

When calculating long term deflections or prestress loss in structures where the change of stress over time due to creep and shrinkage is small, an effective modulus can be used. This effective modulus, E_e, accounts for an increase in deflection due to creep

$$E_e = \frac{E_{ci}}{1 + v_t} \qquad [2.55]$$

where,

E_{ci} = modulus of elasticity at the time of loading

v_t = creep coefficient increment from time of loading to time of interest

The modulus of elasticity at the time of loading, E_{ct}, varies with time and is a function of the compressive strength, which also varies with time

$$E_{ct} = 33\sqrt{\omega^3 \frac{t}{\alpha + \beta t}(f_c')_{28}} \qquad [2.56]$$

where,

ω = unit weight of the concrete (lb/ft^3)

α = 4.0 for Type I cement and moist cured

= 2.3 for Type III cement and moist cured

= 1.0 for Type I cement and steam cured

= 0.7 for Type III cement and steam cured

β = 0.85 for Type I cement and moist cured

= 0.92 for Type III cement and moist cured

= 0.95 for Type I cement and steam cured

= 0.98 for Type III cement and steam cured

$(f_c')_{28}$ = compressive strength at 28 days (psi)

The effective modulus method for calculating long term deflections and prestress loss is not accurate when the change in stress over time is significant. An example is when a cast-in-place concrete deck is made composite with a precast concrete girder that

was cast several months earlier. In this situation, additional forces and moments develop in the deck and girder over time from differential creep and shrinkage. A more detailed analysis is warranted for calculating long term losses and prestress losses in the composite system. Refer to Sections 2.1.1-6 for examples of previous studies regarding this effect. The age adjusted effective modulus, E_{ea}, should be used in cases where significant stresses develop over time

$$E_{ea} = \frac{E_{ci}}{1 + \mu \nu_t} \qquad [2.57]$$

where, μ = aging coefficient. The aging coefficient depends on the time of interest with respect to the loading age and the ultimate creep coefficient for the loading considered. See Table 5.1.1 of ACI-209[10] for values for the aging coefficient. Section 2.1.1.2 discusses the aging coefficient further.

The effects of compression steel can be incorporated into an analysis in two ways. The first way is to use the age adjusted effective modulus and include the effect that the compressive forces developed in the concrete are transferred to mild reinforcing steel in the compressive zone. Strain compatibility equations, constitutive equations, and equilibrium equations are used in conjunction with the age adjusted effective modulus. The studies discussed in Section 2.1.1.1 and Section 2.1.1.2 use this method. The second way is to apply an additional multiplier, ζ_r, to the ultimate creep coefficient, v_u. ACI 209 presents several equations to take this in to account

$$\zeta_r = 0.85 - 0.45\frac{A_s'}{A_s} \geq 0.4 \qquad [2.58]$$

for reinforced flexural members considering only creep effects,

$$\zeta_r = 1 - 0.6\frac{A_s'}{A_s} \geq 0.3 \qquad [2.59]$$

for reinforced flexural members considering both creep and shrinkage effects, and

$$\zeta_r = \frac{1}{1 + \frac{A_s'}{A_s}} \qquad [2.60]$$

for prestressed flexural members, where,

A_s' = area of compression steel

A_s = area of tensile steel.

2.2.1.2 CEB-FIB Model Code 1990

The CEB-FIB, *Model Code for Concrete Structures*, 1990[14] also provides time dependent functions to estimate the creep coefficient and shrinkage strains at a given time. The equations presented in this section are in SI units because that is how it is presented in the CEB-FIB Model Code 1990. The shrinkage strains at any time can be predicted by

$$\varepsilon(t,t_s) = \varepsilon_{cso}\beta_s(t-t_s) \quad [2.61]$$

where,

ε_{cso} = notional shrinkage coefficient

β_s = coefficient that describes the development of shrinkage with time

t = age of concrete (days)

t_s = age of concrete at the beginning of shrinkage or swelling

The notional shrinkage coefficient is

$$\varepsilon_{cso} = \varepsilon_s(f_{cm})\beta_{RH} \quad [2.62]$$

where,

$$\varepsilon_s(f_{cm}) = (160+10\beta_{sc}(9-\frac{f_{cm}}{f_{cmo}}))\times 10^{-6} \quad [2.63]$$

f_{cm} = mean compressive strength of concrete at 28 days (MPa)

$$= f_{ck} + 8 \text{ MPa} \quad [2.64]$$

f_{ck} = strength below which 5% of all possible strength measurements for the specified concrete may be expected to fall (analogous to design strength f'$_c$ in ACI-209[10])

f_{cmo} = 10 MPa

β_{sc} = 4 for slowly hardening cements

= 5 for normally or rapid hardening cements

= 8 for rapid hardening, high strength cements

$$\beta_{sRH} = 1-(\frac{RH}{100})^3 \quad [2.65]$$

RH = relative humidity of the ambient atmosphere (%)

$\beta_{RH} = -1.55\beta_{sRH}$ for $40 \le RH < 99$ [2.66]

$\beta_{RH} = 0.25$ for $RH \ge 99$ [2.67]

The development of shrinkage with time is

$$\beta_s(t - t_s) = \sqrt{\frac{\frac{t - t_s}{t_1}}{350\left(\frac{h}{h_o}\right)^2 + \frac{t - t_s}{t_1}}} \quad [2.68]$$

where,

$h_o = 100$ mm

$t_1 = 1$ day

h = notational size of the member

$$= \frac{2A_c}{u} \quad [2.69]$$

u = perimeter of the member in contact with the atomosphere

A_c = cross section of the member

The creep coefficient can be calculated at any time by

$$\phi(t, t_o) = \phi_o \beta_c(t - t_o) \quad [2.70]$$

where,

ϕ_o = notional creep coefficient

β_c = coefficient to describe the development of creep with time after loading

t = age of concrete at the time of interest (days)

t_o = age of concrete at loading (days)

The age of concrete at loading can be adjusted to account for the type of cement used and seasonal variations in temperature, which may produce considerable temperature departures from the mean concrete temperature of 20 °C. The adjusted age may be estimated by

$$t_o = t_{o,T}\left(\frac{9}{2+\left(\frac{t_{o,T}}{t_{1,T}}\right)^{1.2}}+1\right)^{\alpha} \geq 0.5 \qquad [2.71]$$

where,

$t_{1,T}$ = 1 day

α = -1 for slow hardening cements

= 0 normal or rapid hardening cements

= 1 rapid hardening, high strength cements

$$t_{o,T} = \sum_{i=1}^{n} \Delta t_i e^{\left(13.65-\frac{4000}{273+\frac{T(\Delta t_i)}{T_o}}\right)} \qquad [2.72]$$

Δt_i = number of days where a temperature, T, prevails (days)

$T(\Delta t_i)$ = is the corresponding temperature during Δt_i (°C)

T_o = 1 °C

The notional creep coefficient is

$$\phi_o = \phi_{RH}\beta(f_{cm})\beta(t_o) \qquad [2.73]$$

where,

$$\phi_{RH} = 1+\frac{1-\frac{RH}{RH_o}}{0.46\left(\frac{h}{h_o}\right)^{\frac{1}{3}}} \qquad [2.74]$$

$$\beta(f_{cm}) = \frac{5.3}{\sqrt{\frac{f_{cm}}{f_{cmo}}}} \qquad [2.75]$$

$$\beta(t_o) = \frac{1}{0.1+\left(\frac{t_o}{t_1}\right)^{0.2}} \qquad [2.76]$$

The development of creep with time is

$$\beta_c(t-t_o)=\left(\frac{\frac{t-t_o}{t_1}}{\beta_H+\frac{t-t_o}{t_1}}\right)^{0.3} \quad [2.77]$$

where,

$$\beta_H=150(1+(1.2\frac{RH}{RH_o})^{18})\frac{h}{h_o}+250\le 1500 \quad [2.78]$$

When calculating long term deflections and prestress losses, the following formula to estimate the modulus of elasticity at any time may be used with the effective modulus method or age adjusted affective modulus method

$$E_{ci}(t)=\beta_{cc}(t)^{0.5}E_{ci} \quad [2.79]$$

where,

E_{ci} = modulus of elasticity at 28 days

$$=(2.15\times 10^4)\left(\frac{f_{cm}}{f_{cmo}}\right)^{\frac{1}{3}} \quad [2.80]$$

$$\beta_{cc}(t)=e^{s\left(1-\sqrt{\frac{28}{\frac{t}{t_1}}}\right)} \quad [2.81]$$

s = 0.38 for slow hardening cements

= 0.25 for normal and rapid hardening cements

= 0.2 for rapid hardening, high strength cements

2.2.1.3 AASHTO LRFD Specifications

The AASHTO LRFD Specifications provide models for predicting creep and shrinkage response over time. The provisions presented in this section include the 2005 Interims[43] and 2006 Interims[7]. The equations for the creep coefficient and shrinkage strain represent a simplification of the summary of results presented in Section 2.1.1.1. The multipliers applied to Equation 2.82 and Equation 2.83 are the same except for the relative humidity correction factor.

The formula for computing the shrinkage strain is

$$\varepsilon_{sh} = (-480 * 10^{-6}) k_{td} k_{vs} k_{hs} k_f \quad [2.82]$$

The formula for computing the creep coefficient is

$$\psi(t, t_i) = 1.90 k_{td} k_{vs} k_{hc} k_f t^{-0.118} \quad [2.83]$$

where,

t = age of concrete (days) between time load is applied and time being considered.

t_i = age of concrete when the load is initially applied (days)

The relative humidity correction factor is

$$k_{hs} = 2.00 - 0.014H \quad \text{for shrinkage and} \quad [2.84]$$

$$k_{hc} = 1.56 - 0.008H \quad \text{for creep} \quad [2.85]$$

where H = relative humidity (percent).

The V/S ratio correction factor is

$$k_{vs} = 1.45 - 0.13\frac{V}{S} \geq 0.0 \quad \text{for creep and shrinkage} \quad [2.86]$$

The concrete strength correction factor is

$$k_f = \frac{5}{1 + f_{ci}^{'}} \quad \text{for creep and shrinkage} \quad [2.87]$$

where f_{ci}' = for prestressed members: compressive strength at prestress transfer
for non-prestressed members: 80% of strength during service (ksi)

The time-development correction factor is

$$k_{td} = \frac{t}{61 - 4 f_{ci}' + t} \quad \text{for creep and shrinkage} \quad [2.88]$$

where t = age of concrete after loading (days). Factors such as slump, cement content, percent fine aggregate, and air content are not included because of their minor effects.

2.2.1.4 PCI Bridge Design Manual

The PCI Bridge Design Manual's[44] calculations for creep and shrinkage are similar to the ACI 209[10] model. The shrinkage strains can be predicted at any time by

$$S(t, t_o) = \frac{t - t_o}{f + (t - t_o)} (545 \times 10^{-6} k_{cp} k_h k_s k_{st}) \quad [2.89]$$

where,

f = (65- 2.5f_c') for 1-3 days of steam curing

= (45 - 2.5f_c') for 7 days of moist curing

t = age of concrete (days)

t_o = age of concrete at the end of the initial curing period (days)

The creep coefficient can be predicted at any time by

$$C(t,t_o) = \frac{(t-t_o)^{0.6}}{(12-0.5f_c')+(t-t_o)^{0.6}}(1.88k_{la}k_hk_sk_{st}) \quad [2.90]$$

The curing period correction factor is taken from the PCI Bridge Manual and can be found in Table 2.2.1. The relative humidity correction factor is:

$$k_h = 2.00 - 0.0143RH \quad (40 \le RH \le 80) \text{ or} \quad [2.91]$$

$$k_h = 4.286 - 0.0429RH \quad (80 < RH \le 100) \text{ for shrinkage and} \quad [2.92]$$

$$k_h = 1.586 - 0.0084RH \text{ for creep} \quad [2.93]$$

Table 2.2.1 Correction Factor for Curing Period

Moist Curing Period (days)	Shrinkage Factor, k_{cp}
1	1.20
3	1.10
7	1.00
14	0.93
28	0.86
60	0.79
90	0.75

The volume to exposed surface area correction factor is:

$$k_s = 1.2e^{-0.12\frac{V}{S}} \quad \text{for shrinkage} \quad [2.94]$$

$$k_s = \frac{2}{3}\left(1+1.13e^{-0.54\frac{V}{S}}\right) \quad \text{for creep} \quad [2.95]$$

The loading age correction factor for creep is:

$$k_{la} = 1.13t_{la}^{-0.094} \quad [2.96]$$

for t_{la} > 1-3 days of stream curing or:

$$k_{la} = 1.25 t_{la}^{-0.118} \quad [2.97]$$

for $t_{la} > 7$ days of moist curing.

The concrete strength correction factor is:

$$k_{st} = 1.2 - 0.05 f_c' \quad \text{for shrinkage and} \quad [2.98]$$

$$k_{st} = 1.18 - 0.045 f_c' \quad \text{for creep} \quad [2.99]$$

The above equations are valid for concrete strengths up to 12 ksi. If the compressive strength of the concrete is 3 ksi $\leq f_c' \leq$ 5 ksi, then the multiplier for concrete strength, k_{st}, should be eliminated from Equation 2.89 and Equation 2.90.

2.2.2 Estimation of Prestress Loss

There are several effects that contribute to prestress loss. Instantaneous losses are elastic shortening, anchor slip (post-tensioning only), wobble friction (post-tensioning only), curvature friction (post-tensioning only). Losses that occur over time are creep, shrinkage, and steel relaxation.

There are a variety of methods to account for these losses, depending on the level of accuracy required. One method is the lump sum method. In the lump sum method, the effective prestress force is determined by multiplying the initial prestressing force times a coefficient to account for all losses. This coefficient usually ranges from 0.75 to 0.9. Another method to calculate prestress losses is the refined method. Elastic shortening loss, anchorage loss, friction loss, creep loss, shrinkage loss, and relaxation loss are calculated separately and added together. This is the method used by most designers for typical structures.

The most intricate method is the time stepping method. In this method, the instantaneous losses are calculated first from formulas presented in the refined method. Then the remainder of the analysis is divided in to time steps. This method is often time consuming, however, many commercial software packages are available to perform such an analysis. In a given time step, prestress loss is determined by calculating stress redistribution in the system due to creep and shrinkage effects. The methods presented in Sections 2.2.1.1-4 for variation of the creep coefficient and shrinkage strain are used to aid in finding the creep strain and shrinkage strain increments in each time step. A steel

relaxation increment is incorporated into each time step. The more time steps the analysis is divided into, the more accurate the results will be.

The most computationally efficient way to reduce the number of steps is to start with small step sizes and increase them in a logarithmic fashion. However, the results will only be as accurate as the models used to predict creep, shrinkage, and steel relaxation as well as the estimation of the material properties, applied load estimates, construction staging, etc. Therefore, using the time stepping method may not be necessary except in special cases. The time stepping method is used in this research project because there are not typical methods for calculating post-tensioning losses in precast deck panel systems, where typical effects of differential creep and shrinkage losses are unknown.

This section focuses on the refined method for calculating prestress losses. This method is easy to use and often used to check the results obtained from the time stepping method to see if the results are reasonable.

2.2.2.1 AASHTO LRFD Specifications

The AASHTO LRFD Specifications[22] provides models for estimating prestress loss. The provisions presented in this section include the 2005 Interims[43] and 2006 Interims[7]. The approximate method for time dependent losses is presented in this section. The refined method for time dependent losses can be found in AASHTO LRFD Article 5.9.5.4. The background for both of these methods is summarized in Section 2.1.1.1.

The total prestress loss is:

$$\Delta f_{pT} = \Delta f_{pES} + \Delta f_{anchor} + \Delta f_{pF} + \Delta f_{pLT} \quad [2.100]$$

for post-tensioned members and

$$\Delta f_{pT} = \Delta f_{pES} + \Delta f_{pLT} \quad [2.101]$$

for pretensioned members where,

Δf_{pES} = elastic shortening loss

Δf_{anchor} = anchorage loss

Δf_{pF} = friction loss

The elastic shortening loss is given by:

$$\Delta f_{pES} = \frac{E_p}{E_{ci}} f_{cgp} \qquad [2.102]$$

where,

E_p = modulus of elasticity of pretensioning steel

E_{ci} = modulus of elasticity of concrete at transfer

f_{cgp} = concrete stress at the center of gravity of the pretensioning steel due to pretensioning force at transfer and the self weight of the member at the section of maximum positive moment

For post-tensioned members where all the tendons are stressed simultaneously, the elastic shortening loss is zero. For post-tensioned members where all the tendons are not stressed simultaneously, all the tendons except the last tendon will have an elastic shortening loss associated with it.

The anchorage loss for a straight strand with no friction can be expressed as:

$$\Delta f_{anchor} = \frac{\Delta l}{l} E_p \qquad [2.103]$$

where,

Δl = amount of slip experienced by the tendon

l = length of the tendon

The magnitude of the slip depends on the prestressing system used. ¼ in. is a commonly used value. As shown in Equation 2.103, long tendons have small anchorage losses and short tendons have large anchorage losses.

Equation 2.103 assumes the loss is distributed uniformly over the length of the tendon. However, the anchorage loss is usually confined to the area near the jacking anchor (live end), unless the duct is very well greased and the wobble and curvature are small. If the losses are fairly small, they can usually be compensated for by overstressing during jacking.

Losses due to friction between prestressing tendons and the duct wall is:

$$\Delta f_{pF} = f_{pj}(1 - e^{-(Kx+\mu\alpha)}) \qquad [2.104]$$

where,

f_{pj} = stress in prestressing tendon at jacking (ksi)

x = length of a prestressing tendon from the jacking end to the point

of interest (ft)

K = wobble friction coefficient (per ft of tendon)

AASHTO LRFD Table 5.9.5.2.2b-1

μ = coefficient of friction - AASHTO LRFD Table 5.9.5.2.2b-1

α = sum of absolute values of angular change of prestressing steel path from the jacking end, or from the nearest jacking end if tensioning is done equally at both sides (radians)

The term 'Kx' accounts for the wobble curvature (unintentional misalignment of the ducts) and the term '$\mu\alpha$' accounts for the curvature friction (intentional misalignment of the ducts).

The long term loss from creep, shrinkage, and steel relaxation is:

$$\Delta f_{pLT} = 10.0 \frac{f_{pi} A_{ps}}{A_g} \gamma_h \gamma_{st} + 12.0 \gamma_h \gamma_{st} + \Delta f_{pR} \quad [2.105]$$

$$\gamma_h = 1.7 - 0.01H \quad [2.106]$$

$$\gamma_{st} = \frac{5}{1 + f_{ci}'} \quad [2.107]$$

where,

H = relative humidity (percent)

f_{pi} = stress in the strands at transfer after all instantaneous losses (ksi)

A_{ps} = area of prestressing strand (in^2)

A_g = gross cross sectional area (in^2)

f'_{ci} = compressive strength at transfer (ksi).

Δf_{pR} = relaxation loss (ksi)

The relaxation loss in low relaxation prestressing strands is

$$\Delta f_{pR} = \frac{f_{pi}}{30} \left(\frac{f_{pi}}{f_{py}} - 0.55 \right) \quad [2.108]$$

where,

f_{py} = yield strength of strands (ksi) = $0.9 f_{pu}$

f_{pi} = stress in the strands immediately after transfer > $0.55 f_{py}$ (ksi)

2.2.2.2 Tadros Method in the PCI Bridge Design Manual

The PCI Bridge Manual[44] presents the Tadros method for calculating prestress losses. The individual losses are added together to find the total loss in the tendons. For the elastic shortening loss, Equation 2.102 can be used. The loss due to creep is:

$$CR_c = E_p(KC_u \frac{f_{cgp}}{E_{ci}} - (1 + KC_u')\frac{f_{cdp}}{E_c}) \quad [2.109]$$

where,

f_{cgp} = defined in Section 2.2.2.1 (ksi)

f_{cdp} = change in concrete stress at the center of gravity of the prestressing strand due to dead loads except the dead load present at the time the prestressing force is applied (ksi).

E_c = modulus of elasticity of concrete at 28 days (ksi)

E_{ci} = modulus of elasticity of concrete at the time of release (ksi)

E_p = modulus of elasticity of prestressing tendons (ksi)

C_u = ultimate creep coefficient at the time of release

C_u' = ultimate creep coefficient at the time at the time of the superimposed dead loads

$$K = \frac{1}{1 + \frac{E_p}{E_c^*}\frac{A_{ps}}{A}\left(1 + \frac{e_p^2}{r^2}\right)} \quad [2.110]$$

A_{ps} = area of prestressing tendons (in^2)

A = gross cross sectional area of the concrete (in^2)

e_p = eccentricity of the prestressing strands with respect to the centroid of the section (in.)

r = radius of gyration of the gross cross sectional area (in.)

E_c* = age adjusted effective modulus for a gradually applied load at the time of transfer (ksi)

The loss due to shrinkage is:

$$SH = K\varepsilon_{shu}E_p \quad [2.111]$$

where, ε_{shu} = ultimate free shrinkage strain, adjusted for member size and relative humidity (see Section 2.2.1.4). The relaxation loss is given by:

$$CR_s = (1 - 3\frac{SH + CR_c}{f_{po}})KL_r \quad [2.112]$$

where,

f_{po} = stress in the prestressing tendons when the stress in the surrounding concrete is zero (ksi).

L_r = intrinsic relaxation of the strand (see Equation 2.108) (ksi)

The term $1 - 3\frac{SH + CR_c}{f_{po}}$ accounts for the fact that the actual relaxation will be less than the intrinsic relaxation (relaxation that occurs at a constant length found in a laboratory setting).

2.2.2.3 PCI Design Handbook

The PCI Design Handbook[45] presents a method for calculating prestress losses, similar to the methods presented above. The method for calculating the prestress loss due to elastic shortening is the same as Equation 2.102. The loss due to creep is expressed as:

$$CR = K_{cr}\frac{E_p}{E_c}(f_{cgp} - f_{cdp}) \quad [2.113]$$

where, K_{cr} = 2.0 for normal weight concrete and 1.6 for sand-lightweight concrete. The loss due to shrinkage is:

$$SH = E_p(1 - 0.06\frac{V}{S})(100 - RH)(8.2 \times 10^{-6}) \quad [2.114]$$

The loss due to relaxation of the prestressing tendons is:

$$RE = C(K_{re} - J(SH + CR + ES)) \quad [2.115]$$

where:

$$C = 1 + 9(\frac{f_{pi}}{f_{pu}} - 0.7) \quad \text{for} \quad 0.70 \le \frac{f_{pi}}{f_{pu}} \le 0.75 \quad \text{or} \quad [2.116]$$

$$C = \frac{\frac{f_{pi}}{f_{pu}}}{0.19147}(\frac{\frac{f_{pi}}{f_{pu}}}{0.85} - 0.55) \quad \text{for} \quad 0.51 \le \frac{f_{pi}}{f_{pu}} < 0.7 \quad \text{or} \quad [2.117]$$

$$C = \frac{\frac{f_{pi}}{f_{pu}}}{3.83} \quad \text{for} \quad \frac{f_{pi}}{f_{pu}} < 0.51 \qquad [2.118]$$

for stress relieved tendons and

$$C = \frac{\frac{f_{pi}}{f_{pu}}}{0.2125}\left(\frac{\frac{f_{pi}}{f_{pu}}}{0.9} - 0.55\right) \quad \text{for} \quad \frac{f_{pi}}{f_{pu}} \geq 0.54 \quad \text{or} \qquad [2.119]$$

$$C = \frac{\frac{f_{pi}}{f_{pu}}}{4.25} \quad \text{for} \quad \frac{f_{pi}}{f_{pu}} \leq 0.54 \qquad [2.120]$$

for low relaxation tendons,

f_{pu} = ultimate strength of the prestressing tendons (ksi)

Values for K_{re} and J can be found in Table 4.7.1 of the PCI Design Handbook.

2.2.3 Horizontal Shear Design

The code provisions presented in this section aid in the design of the interface between precast deck panels and the supporting girders. The shear capacity of the interface must be greater than the horizontal shear stresses developed at the interface. The horizontal shear stresses are resisted by the cohesion between the concrete and grout, the dowel action of the shear reinforcement crossing the cracked plane, and the clamping force developed in the shear reinforcement. The cohesion consists of frictional resistance that develops at the interface between the two materials, which includes aggregate interlock when both materials at the interface are concrete.

The dowel action can best be described as the shear resistance of the reinforcing bar. A reinforcing bar experiences shear deformations from the relative slip between the two members forming the interface as well as axial deformation from the separation of the two members at the interface caused by a rough crack. The code provisions assume that the two interfaces separate.

The code provisions presented also assume that the shear reinforcement has yielded when the peak load is reached. However, this may not be the case as shown in push-off tests conducted by Wallenfelsz[29]. Although the reinforcement may not yield

prior to the peak load being reached, the behavior of the materials in the vicinity of the reinforcement is fairly nonlinear. Cracking at the interface, local cracking and crushing of the concrete near the shear reinforcement, and frictional behavior are phenomena that complicate the problem. Many of the provisions presented are based on shear-friction theory and may be used in the design of transverse joints between adjacent precast deck panels as well.

2.2.3.1 AASHTO LRFD Specifications

The AASHTO LRFD Specifications[22] provide equations to calculate the nominal shear resistance at an interface. The provisions presented in this section include the 2005 Interims[43]. The nominal shear resistance at the interface between two concretes, grout, or steel cast at different times can be expressed as

$$V_n = cA_{cv} + \mu(A_{vf} f_y + P_c) \leq \min(0.2 f_c' A_{cv}, 5.5 A_{cv}) \qquad [2.121]$$

where,

c = cohesion factor
- = 100 psi for an intentionally roughened surface between two concrete surfaces cast at different times
- = 75 psi for not intentionally roughened surface between two concrete surfaces cast at different times
- = 25 psi for a surface formed by steel and concrete

A_{cv} = area of concrete engaged in shear transfer (in^2)

μ = friction factor
- = 1.0λ for an intentionally roughened surface between two concrete surfaces cast at different times
- = 0.6λ for not intentionally roughened surface between two concrete surfaces cast at different times
- = 0.7λ for a surface formed by steel and concrete

λ = 1.0 for normal density concrete
- = 0.85 for sand-low-density concrete
- = 0.75 for all other low-density concrete

A_{vf} = area of shear reinforcement crossing the interface (in^2)

f_y = yield strength of the shear reinforcement (ksi)

P_c = permanent net compressive force normal to the interface (kips)

f_c' = 28 day compressive strength of the weakest concrete at the interface(s) (ksi)

A_{cv} usually is the product of the width of the top flange and the spacing between the shear reinforcement. However, the shear connectors in precast deck panels are grouped together at the shear pockets. AASHTO LRFD does not address how to handle this situation. For calculations performed in this research program, the capacity of each shear pocket, using the tributary length between the pockets to calculate A_{cv}, is compared to the shear force developed at the pocket, using the tributary length between the pockets. No previous research has been discovered that shows whether using the entire tributary length between the pockets produces accurate predictions of the capacity of the interface at the shear pocket in question.

The shear stress at the interface between the girder and panels can be calculated as

$$v_h = \frac{VQ}{Ib} \qquad [2.122]$$

where,

V = horizontal shear force (kips)

Q = first moment of the area of the slab about the neutral axis of the composite section (in^3)

I = second moment of area of the composite section about the neutral axis of the composite section (in^4)

b = width of section at the interface (in)

when the system behaves elastically.

When the strength of the system is evaluated, there is often cracking present in prestressed girders and the interface between the slab and girder is cracked, resulting in partial composite section. Therefore, only the compressive force developed in the system and the tensile force developed in the tensile reinforcing steel and prestressing strands is considered. Using equilibrium, the following expression is obtained for the horizontal shear force (k/in)

$$V_h = \frac{V_u}{d_e} \quad [2.123]$$

where, d_e = distance between the centroid of the steel in the tension side of the girder to the resultant center of the compressive force in the deck.

The AASHTO LRFD specifications also provide a method for calculating the shear resistance of an interface with steel girders and shear studs or steel channels. This section will address the capacity for a system with shear studs on straight girders with an infinite radius of curvature. When shear studs are used, the specification requires that ratio of the height to the diameter of the shear stud not be less than 4.0. Often, the design of the shear studs is governed by the fatigue limit state instead of the strength limit state. The fatigue limit state is satisfied by placing limits on the pitch, p (in.), of the shear connectors

$$6d \le p \le \frac{nZ_r I}{V_{sr} Q} \le 24 \text{ in.} \quad [2.124]$$

where,

d = diameter of the shear stud (in^2)

n = number of shear connectors in a cross section

I = moment of inertia of the short-term composite section (in^4)

Q = first moment of the transformed area of the slab about the neutral axis of the short term composite section (in^3)

V_{sr} = shear force range under LL+I determined for the fatigue limit state (kips)

Z_r = shear fatigue resistance of an individual shear connector (kips)

The fatigue resistance of an individual shear connector is:

$$Z_r = \alpha d^2 \ge \frac{5.5d^2}{2} \quad [2.125]$$

where,

$$\alpha = 34.5 - 4.28\log(N) \quad [2.126]$$

N = number of cycles

$$= 365(y)n(ADTT)_{SL} \quad [2.127]$$

y = design life (years)

n = number of stress range cycles per truck passage

(see AASHTO LRFD Table 6.6.1.2.5-2)

$(ADTT)_{SL}$ = single lane ADTT

= p(ADTT)

p = see AASHTO LRFD Table 3.6.1.4.2-1

ADTT = %trucks(ADT) (See AASHTO LRFD C3.6.1.4.2)

%trucks = see AASHTO LRFD Table C3.6.1.4.2-1

ADT = 20,000 vehicles per lane per day

The strength of the shear connectors is found by:

$$Q_r = \varphi_{sc} 0.5 A_{sc} \sqrt{f_c' E_c} \leq \varphi_{sc} A_{sc} F_u \quad [2.128]$$

where,

$\alpha_{sc} = 0.85$

A_{sc} = cross sectional area of a shear stud (in^2)

f_c' = 28 day compressive strength of the concrete in the deck (ksi)

E_c = modulus of elasticity of the concrete at 28 days (ksi)

F_u = minimum tensile strength of the shear stud (ksi)

An equation is also given to calculate the total number of shear studs required between sections of maximum positive moment and each adjacent point of zero moment. This equation is also used to determine the number of shear studs required between points of zero moment and the centerline of an interior support

$$n = \frac{\min(0.85 f_c' b t_s, F_{yw} D t_w + F_{yt} b_t t_t + F_{yc} b_c t_c)}{Q_r} \quad [2.129]$$

where,

b = effective width of the slab (in.)

t_s = slab thickness (in.)

F_{yw} = yield strength of the web for steel girders (ksi)

F_{yt} = yield strength of the tension flange for steel girders (ksi)

F_{yc} = yield strength of the compression flange for steel girders (ksi)

D = web depth for steel girders (in.)

b_t = width of the tension flange for steel girders (in.)

b_c = width of the compression flange for steel girders (in.)

t_w = thickness of the web for steel girders (in.)

t_t = thickness of the tension flange for steel girders (in.)

t_c = thickness of the compressions flange for steel girders (in.)

Note that Equation 2.129 assumes the entire compressive stress block falls in the deck.

2.2.3.2 ACI 318 Specifications

ACI 318[26] presents 4 methods that can be used for calculating the horizontal shear strength at an interface between two materials cast at different times. The first method is based on the shear-friction method resulting in the following equation

$$V_n = A_{vf} f_y (\mu \sin \alpha_f + \cos \alpha_f) \quad [2.130]$$

where,

A_{vf} = area of shear reinforcement (in^2)

f_y = yield strength of the shear reinforcement (ksi)

μ = see Equation 2.121

α_f = angle between the shear reinforcement and crack plane

The second method that can be used to calculate the horizontal shear strength is

$$V_n = A_{vf} f_y (0.8 \sin \alpha_f + \cos \alpha_f) + A_c K_1 \sin^2 \alpha_f \quad [2.131]$$

where,

K_1 = 400 psi for normal weight concrete

= 200 psi for lightweight concrete

= 250 psi for sand lightweight concrete

A_c = area of concrete section engaged in shear transfer (in^2)

When using the modified shear friction method,

$$\frac{A_{vf} f_y}{A_c} \text{ or } \frac{A_{vf} f_y \sin \alpha_f}{A_c} \geq 0.2 \text{ ksi} \quad [2.132]$$

for the design equations to be valid.

The first term in Equation 2.131 represents the contribution of friction, with 0.8 representing the coefficient of friction. The second term represents the sum of the resistance to shearing of the aggregates on the crack face and the dowel action of the

shear reinforcement. The shear strength provided by Equation 2.130 and Equation 2.131 can not exceed the maximum shear strength of

$$V_{n\_max} = \min(0.2 f_c' A_c, 800 A_c) \quad [2.133]$$

The third method for calculating the shear strength consists of the following equations

$V_{nh} = 80 b_v d$ for intentionally roughened surfaces without shear reinforcement (lb) [2.134]

$V_{nh} = 80 b_v d$ for surfaces not intentionally roughened with the minimum amount of shear reinforcement, specified in Equation 2.137 (lb) [2.135]

$V_{nh} = (260+0.6\rho_v f_y)\lambda b_v d < 500 b_v d$ (lb) [2.136]

for intentionally roughened surface to an amplitude of ¼ in. with shear reinforcement, where,

b_v = width of contact surface (in.)

d = distance from extreme compression fiber to centroid of tension reinforcement, or 0.8h, whichever is greater (in.)

h = depth of prestressed concrete member (in.)

ρ_v = ratio of shear reinforcement area to area of concrete contact surface

λ = correction factor related to the unit weight of the concrete (see Equation 2.131)

If Equations 2.134-2.136 exceed $500 b_v d$, then Equation 2.130 shall be used to compute the shear strength.

The mimimum amount of reinforcement for Equation 2.135 and Equation 2.136 is

$$A_{v\_min} = 0.75\sqrt{f_c'}\frac{b_w s}{f_y} \geq \frac{50 b_w s}{f_y} \quad [2.137]$$

where,

b_w = web width (in.)

s = spacing of shear reinforcement (in.)

The fourth method presented by ACI 318 for calculating the shear capacity at an interface is based on the change in compressive or tensile force at an interface. The change in compressive force or tensile force is computed at any segment. Shear reinforcement is selected to be able to transfer the compressive force or tensile force across the interface to the supporting element. The horizontal force computed from this method shall not exceed the shear strength provided in Equations 2.134-2.136, where A_c shall be substituted for $b_v d$.

2.2.3.3 PCI Design Handbook

The provisions for horizontal shear strength provided by the PCI Design Handbook[45] are similar to ACI 318[26]. The PCI Design Handbook recommends that the four methods presented in the previous section be used when applicable. There is one major difference between the PCI Design Handbook and the ACI 318 methods. The horizontal shear length, l_{vh}, is used in place of the distance from the extreme fiber in compression to the centroid of the tension reinforcement, d. The horizontal shear length is the distance between the point of zero moment and the maximum moment.

2.3 Summary of Literature Review

This chapter presented previous studies and current code provisions regarding factors contributing to creep and shrinkage behavior, prestress loss, composite action between the bridge deck and supporting girders, transverse joint configurations and behavior, and constructability of the precast bridge deck panel system.

There has been a significant amount of work on the estimate of prestress loss. Methods were proposed for calculating prestress loss in girders taking in to account differential creep and shrinkage when composite action with the deck is considered. However, these methods were not extrapolated to propose methods for calculating long term post-tensioning in precast deck panel systems. Some studies recommended required levels of post-tensioning to keep the transverse joints in compression. Table 2.3.1 presents a summary of the different levels of post-tensioning used in the previous studies, discussed in Section 2.1.1. The focus of these studies dealt with steel girders instead of prestressed, precast concrete girders. Some of these studies did not take differential creep

and shrinkage effects in to account. This research program looked at the long term post-tensioning losses, considering differential creep and shrinkage, and the affects on the system. None of the studies mentioned the effect partial composite action has on the long term effective stress in the deck. A reduction in composite action causes a reduction in the amount of compression present across the transverse joints.

Table 2.3.1 Summary of Different Levels of Post-Tensioning for Previous Studies

Investigators	Initial Level of post-tensioning (psi)	Performance	Type of Study
Harrison and LeBlanc	435	N.A.	Finite Element
Dimmerling et. al.	400	satisfactory	Experimental
Issa et.al.	200 (simply supported spans) 450 (continuous spans)	N.A. N.A.	Finite Element
Issa et.al.	none 208 380	poor satisfactory satisfactory	Experimental Experimental Experimental
Markowski	154	No good. Recommended 250 psi.	Experimental

A great deal of research has been done using push-off test results to recommend preferred grouts, surface preparations, the use of unbonded shear keys, shear connector types, large diameter shear studs, and pocket spacing. Table 2.3.2 provides a summary of the different types of shear connectors used in previous studies, discussed in Section 2.1.2. There has been very limited work on the evaluation of composite action in deck panel systems on bridge mockups using prestressed concrete girders. There is no research results presently available that investigates the performance of the detail with the embedded steel plate with post-installed shear studs, discussed in Section 1.2.1 and Section 1.3. This research program looked at the performance of this new shear stud detail. The code provisions for horizontal composite action do not specifically address

precast deck panels systems or whether the current equations are applicable for such systems. There is even speculation on whether the current equations are correct since the shear connectors are assumed to yield, which isn't always the case. This research program addressed the level of axial strain in the shear connectors as well as whether the AASHTO LRFD shear friction equation was applicable to precast bridge deck panel systems.

Grouted female-female and epoxied male-female transverse joint connections were discussed. Research has shown that both types of joints perform well when the deck is post-tensioned. Finite element studies were able to predict the failure modes of these joints. Although both joints have been used successfully in the past, there has been little work done on addressing the constructability issues associated with these joints and how this can affect the performance. Constructability issues associated with the different shear connectors has not been directly addressed in previous research either. Constructability issues associated with the epoxied male-female joint, grouted female-female joint, and shear connectors were addressed in this research program.

Table 2.3.2 Summary of Different Shear Connector Types for Previous Studies

Investigators	Type of Shear Connector	Type of Test(s)	Number of Tests	Performance
Tadros et. al.	H.R.B.	Flexural	1	Satisfactory
Scholz	none	Push-off	6	Satisfactory
Wallenfelsz	H.R.B. and S.S	Push-off	29	Satisfactory
Menkulasi	H.R.B.	Push-off	26	Satisfactory
	post-installed Dayton Richmond anchors	Push-off	10	Brittle failure.
Badie et. al.	large diameter S.S.	Push-off	45	Satisfactory
		Flexural	1	Satisfactory
Kahn and Slapkus	H.R.B.	Flexural	6	Satisfactory
Issa et. al.	S.S.	Push-off	28	Satisfactory
		Flexural	3	Results Varied.
Markowski	S.S.	Flexural	1	Satisfactory

H.R.B. = hooked reinforcing bars

S.S. = shear studs

Chapter 3
Research Program

3.1 Introduction

An experimental research program and analytical research program were developed in order to accomplish the objectives outlined in Section 1.3. The experimental research program consisted of static and cyclic tests on a simply supported, full scale bridge built at the Virginia Tech Structures Laboratory. The analytical program consisted of finite element analyses using the commercial software DIANA[40].

3.2 Experimental Program

3.2.1 Design of Lab Mockup

The design was based upon a 40 ft long simply supported bridge with 5 girder lines, spaced at 8 ft center to center. This span length was selected because of the limited available floor space in the Virginia Tech Structures Laboratory. The lab mockup consisted of 2 AASHTO Type II girders, 40 ft long, spaced at 8 ft center to center. The AASHTO Type II girder was the most efficient girder to use for the 40 ft simple span. The deck was 8 in. thick, with a 2 ft overhang. The haunch between the panels and girders was 2 in.

3.2.1.1 Design Summary

The design of the lab mockup was done per AASHTO LRFD[22] specifications. The design calculations are located in Appendix A. The Virginia Tech drawings that were produced from the design are found in Appendix B and the fabrication drawings are found in Appendix C.

For the flexural design, the strand pattern for the girders was selected to satisfy service load levels. The girders had 12-1/2 in. diameter Grade 270 strands in a straight pattern. The eccentricity of the strand group below the girder centroid was 7.83 in. The strand pattern selected for the girders also provided a flexural strength that exceeded the required flexural strength. The AASHTO LRFD required flexural strength was defined as $M_{n\_req} = M_u/\phi_b$, where, M_u is the ultimate design moment and ϕ = strength reduction

factor for flexure from AASHTO LRFD. Mild reinforcing bars were also provided in addition to the prestressing strands in the girder. Four No. 5 bars were provided in both the top flange and bottom flange of the girders. The mild steel bars were provided in the girder for two reasons. The first reason was to aid in the layout of the stirrups for the vertical shear design. The mild reinforcing bars provided locations to tie the stirrups to in order to keep the stirrups in place. The second reason the mild reinforcing bars were added was to increase the flexural capacity of the lab mockup. The flexural strength of the lab mockup was calculated to be 24,800 k-in, which was 60% greater than the AASHTO LRFD required flexural strength of 15,500 k-in. The additional flexural capacity was provided to prevent the system from failing prematurely in flexure before gaining insight into the behavior of the horizontal shear connectors.

The AASHTO LRFD required vertical shear strength was 152 k at the critical section. The critical section was 3 ft - 8 in. from the center of the bearing. In order to satisfy this requirement, No. 4 U bars spaced at 20 in. are required. However, No. 5 U bars spaced at 20 in. were provided to prevent the system from failing prematurely in vertical shear before gaining insight in to the behavior of the horizontal shear connectors. The vertical shear capacity with the No. 5 U bars was 230 k.

In order to satisfy the AASHTO LRFD service and strength requirements for the transverse deck design, each panel was provided with 16-½ in. diameter Grade 270 strands. Eight strands were provided 2 ½ in. from the top of the deck (clear spacing) and 8 strands were provided 2 ½ in. from the bottom of the deck (clear spacing). Each panel had a different strand pattern because of the shear pocket layout, the transverse joint configurations, and the post-tensioning blockouts. The panels were approximately 8 ft x 12 ft x 8 in.; slight variations existed between the panel types.

Twelve - ½ in. diameter strands were provided in the longitudinal post-tensioning ducts to provide a compressive stress across the transverse joints. The layout of the strands is discussed in Section 3.2.1.2. The calculated initial level of post-tensioning after all initial losses was -268 psi. The calculated effective level of post-tensioning after all long term losses was -200 psi. The sign convention is negative (-) for compression and positive (+) for tension.

For the horizontal shear connectors, No. 5 hooked reinforcing bars were used for girder 1, and 7 in. long, ¾ in. diameter shear studs were used for girder 2. Equation 2.121 was used to select the required number of connectors per pocket and calculate the capacity provided at a shear pocket. Equation 2.123 was used with the tributary pocket spacing to calculate the design shear force for the pockets. For the shear stud connectors, Equations 2.124-129 were also satisfied.

Because the shear connectors were clustered together in shear pockets instead being dispersed in a more uniform manner along the length of the bridge, the number of required connectors for each pocket was selected instead of a required connector spacing at a given location. The following design procedure was followed for each pocket:

1. The vertical shear force at the location under consideration was calculated.
2. Equation 2.123 was used to determine the shear force per inch.
3. The tributary pocket spacing was calculated. The tributary pocket spacing was half the pocket spacing on each side of the pocket under consideration.
4. The horizontal design shear force was calculated by multiplying the shear force per inch by the tributary pocket length.
5. Equation 2.121 was used to select the number of required shear connectors. The top flange width and the tributary pocket spacing were used to calculate the area of concrete engaged in resisting the shear force. The cohesion value of 75 psi was used for not intentionally roughened (smooth) surface.

In order to provide a more uniform shear connector design, the same number of shear connectors was provided in several pockets. This caused many of the pockets in regions with small shear forces to be over designed. Table 3.2.1 shows the number of connectors required in each pocket using Equation 2.121 and the number of connectors provided in each pocket for both girder 1 and girder 2. More details about the pocket spacing, pocket sizes, and details on the shear stud connector detail are given in the next section. The pocket numbers are shown in Figure 3.2.1(b).

Table 3.2.1 Comparison of Number of Shear Connectors Required and Number of Shear Connectors Provided

(a) Girder 1

pocket #	# bars required	# bars provided	V_{n_prov}/V_{n_req}
1	8	8	1.03
2	8	8	1.11
3	7	8	1.20
4	6	8	1.31
5	5	8	1.44
6	5	8	1.61
7	4	8	1.81
8	4	8	1.90
9	3	8	2.14
10	2	8	2.76
11	3	8	1.87
12	6	10	1.42
13	10	10	1.06
14	12	16	1.25
15	15	16	1.06

(b) Girder 2

pocket #	# bars required	# bars provided	V_{n_prov}/V_{n_req}
1	7	6	0.93
2	6	6	1.00
3	6	6	1.09
4	5	6	1.19
5	5	6	1.31
6	4	6	1.46
7	4	6	1.65
8	4	6	1.70
9	3	6	1.89
10	3	6	2.44
11	4	6	1.60
12	7	8	1.29
13	9	8	0.96
14	11	12	1.14
15	13	12	0.97

3.2.1.2 Lab Mockup Details

Figure 3.2.1 shows a schematic representation of the lab mockup. The bearing pads rested on a support beam that runs perpendicular to the longitudinal axis of the girders. Three post-tensioning ducts were used to accommodate the 12 strands used to

create the desired level of post-tensioning. The live end in Figure 3.2.1 was where the stands were stressed for the post-tensioning operation.

Figure 3.2.1(b) shows the layout of the shear pockets. The pocket spacing was 4 ft at the dead end, 2 ft at the live end, and 2.5 ft for the "transition panel" (Panel Type '3'). The pocket spacing was varied in accordance with the 2nd and 3rd objectives outlined in Section 1.3. The dead end was tested during the live load testing program to look at the performance of the system with 4 ft pocket spacing and the live end was tested during the live load testing program to look at the performance of the system with 2 ft pocket spacing. This is discussed further in Section 3.2.6. Grouted female-female joints were used at the dead end and epoxied male-female joints are used at the live end in accordance with the 2nd and 5th objectives outlined in Section 1.3. Figure 3.2.1(a) and Figure 3.2.1(b) label what will be referred to as the 'inside joints' and 'outside joints.' This terminology will be used during the description of the instrumentation and test setup.

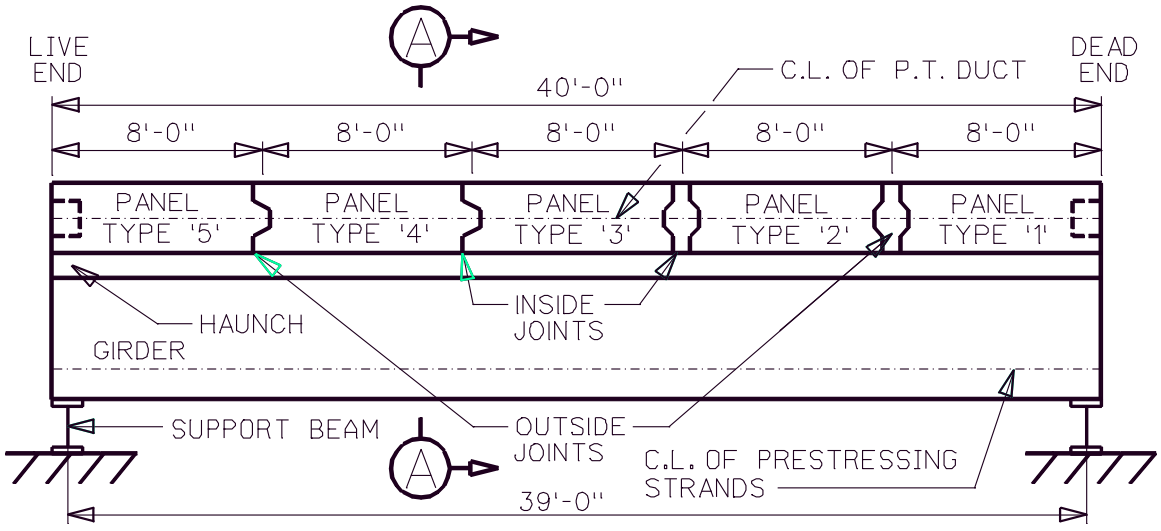

(a)

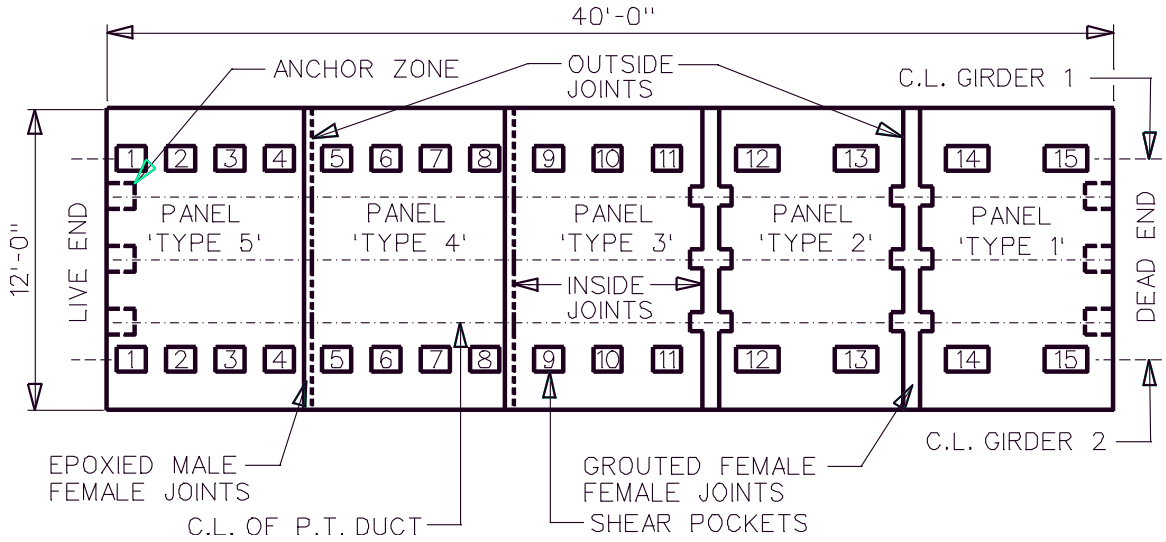

(b)

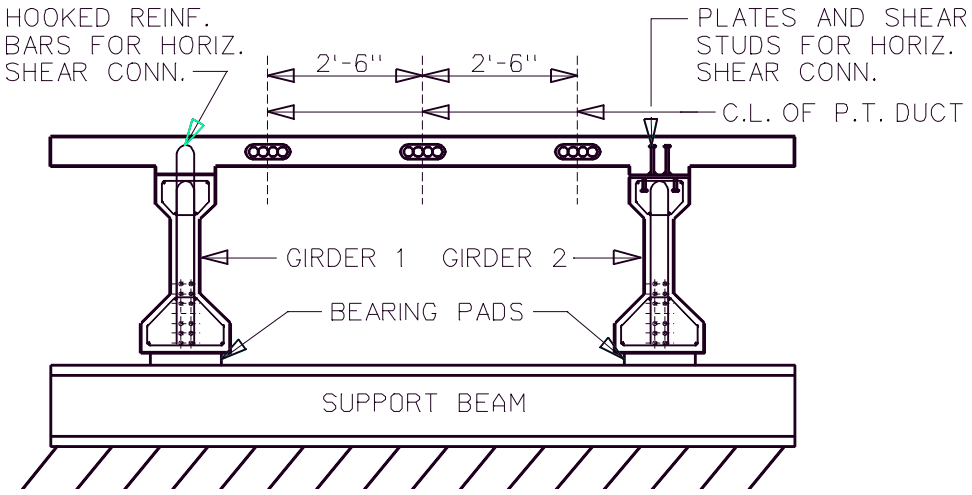

(c)

Figure 3.2.1 Lab Mockup Details (a) Elevation View (b) Plan View (c) Section View

Figure 3.2.1(b) shows the pocket locations. The width of each pocket in the transverse direction of the bridge was 11 in. at the bottom of the pocket. The transverse width of the pocket tapered up to 1 ft at the top of the pocket. The length of the pockets in panel 1 and panel 2 was 1 ft – 5 in. at the bottom of the pocket and tapered to 1 ft – 6 in. at the top of the pocket. The length of the pockets in panel 3, panel 4, and panel 5 was

11 in. at the bottom of the pocket and tapered to 1 ft at the top of the pocket. The length of each pocket was sized to allow for at least a 1 ½ in. gap between the edge of the pocket and the edge of the first shear connector in the pocket. Additionally, the number of different pocket sizes was reduced when possible.

Five, ¼ in. thick plates were placed in the top flange of girder 2 immediately after the concrete was placed in the formwork, as shown in Figure 3.2.2. Five smaller plates were used as opposed to one large plate in order to make placing the plates easier. The shear studs on the bottom of the plate were shot into place prior to casting the girders.

The shear studs on the top of the plate were shot during the construction sequence after the panels were placed on top of the girders. Seven selected shear studs were shot to the top of the girder prior to the panels being placed. This was done so the selected shear studs could be easily instrumented with electrical resistance strain gages. The location of the instrumented shear studs is discussed in Section 3.2.2. More information about the location of the plates, the layout of the shear connectors, and other bridge details is given in Appendix B and Appendix C.

Leveling bolts were used to allow for the panel elevations to be adjusted so the desired haunch height could be obtained. The leveling bolt system consisted of Dayton Richmond F-53 Thin Slab Coil Inserts and B-14 Coil Bolts. Specifications on the leveling bolt system components are given in Appendix D.

Figure 3.2.2 Placement of the Plates in Girder 2.

3.2.2 Instrumentation of Panels and Girders

During the casting operation at Bayshore Concrete Products in Chesapeake, VA, the panels and girders were instrumented with thermocouples and VWGs (vibrating wire gages). The thermocouples and VWGs were placed such that they would be located at the 1/3 points of the span of the bridge. Figure 3.2.3 shows the location of the VWGs and thermocouples through the depth of the cross section. The support beams are not shown for clarity.

Figure 3.2.4 shows a VWG and a thermocouple placed in one of the girders prior to casting the concrete. The thermocouples and VWGs were used to monitor the change in temperature and strain through the casting process as well as during the investigation of the time dependent behavior in the lab, which is discussed in upcoming sections. The VWGs also aided in calculating the curvature of the girder and composite system during the data analysis. The sensitivity of the VWGs was 1 με.

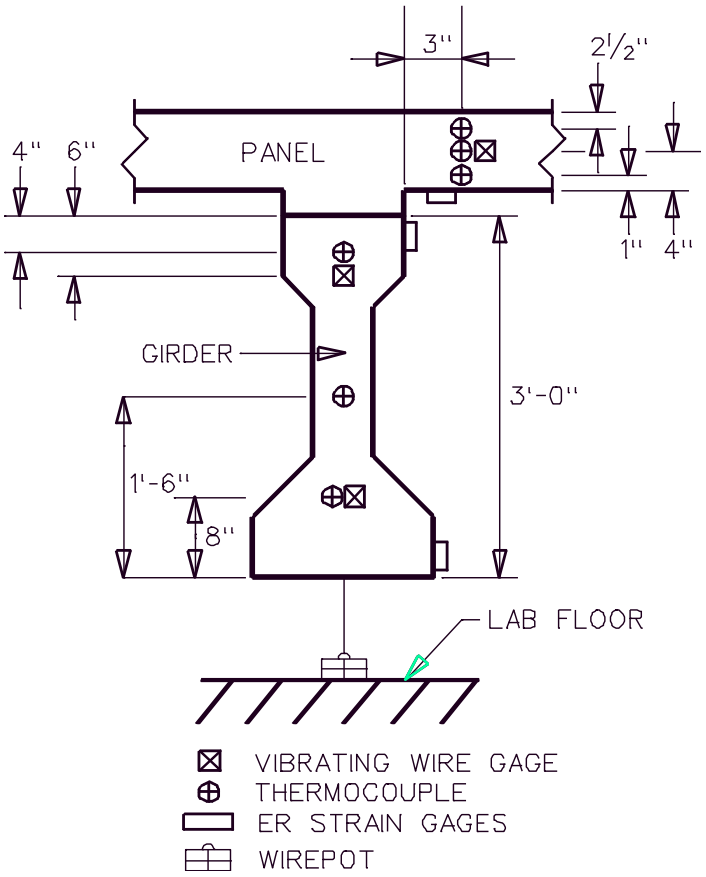

Figure 3.2.3 Location of Instrumentation for Panels and Girders

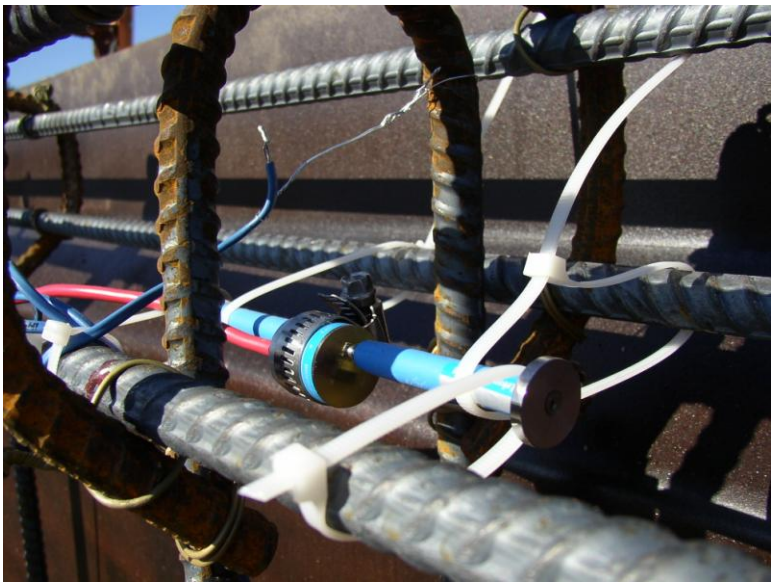

Figure 3.2.4 VWG and Thermocouple in Top Flange of a Girder

The panels and girders were instrumented with ER (electrical resistance) strain gages, wirepots, and LVDT's after arriving at the Virginia Tech Structures Laboratory. Figure 3.2.3 shows the location of the ER strain gages, which were located at the 1/3 points of the span of the bridge. The ER strain gages were used during the cyclic tests and static tests. The sensitivity of the ER strain gages was 5 με. The strain gages aided in establishing strain profiles through the depth, calculating the change in curvature of the composite system, and in establishing whether full or partial composite action was present.

Wirepots were used to measure the vertical displacement of the bridge and any relative displacements that may occur at the transverse joints between the precast deck panels. Figure 3.2.3 shows the location of the wirepots under the girders. The sensitivity of the wirepots was 0.005 in. The wirepots were located directly under the locations of the applied loads. The locations of the applied loads were adjacent to the transverse joints and will be discussed in subsequent sections.

During loading, the displacement measured by the wirepots located under the applied loads included the displacement of the bearing pads. To get the displacement of the bearing pads, wirepots were also placed 1 ft away from the centerline of each bearing pad. These bearing pad displacements were used with the displacements measured by the wirepots located under the applied loads to get the true displacement of the system.

Wirepots were also used to measure any relative vertical displacements that may occur at the transverse joints between adjacent precast deck panels. Figure 3.2.5 shows the setup used with the wirepots to measure the relative vertical displacement between the deck panels.

Figure 3.2.5 Setup to Measure the Relative Vertical Displacement at the Transverse Joints.

LVDTs were used to measure any relative horizontal displacement (slip) that may occur between the panels and girders. The LVDT's were placed 4 ft from each end of the bridge. This location was half way between the first two pockets at the dead end and half way between the second and third pocket at the live end. The setup to measure the relative displacement with the LVDT is shown in Figure 3.2.6. The sensitivity of the LVDTs was 0.005 in.

ER strain gages were placed on selected shear connectors to measure the strain in the horizontal shear connectors during cyclic testing and static testing. Particular attention was paid to how close the shear connectors get to their yield stress at high loads. A nominal yield stress of 60 ksi was used for the hooked reinforcing bars and a nominal yield stress of 50 ksi was used for the shear studs. The corresponding nominal yield strains were 2069 με and 1724 με for the hooked reinforcing bars and shear studs, respectively. The strains in the shear connectors were compared for the different pocket spacings and compared for the hooked reinforcing bar and the shear studs. Figure 3.2.7 shows the locations of the instrumented shear connectors. The terminology will be discussed shortly.

Load cells were placed on one strand in each post-tensioning duct. The load cells were located at the dead end of the bridge. During the stressing operation, the load at the live end was measured with a load cell and compared to the load at the dead end. This was used to determine a typical wobble friction loss in each duct. Elastic shortening losses for the first 11 strands were also extracted from the load cell data. With the initial seating losses, an accurate estimation of the force profile along the length of the strand can be made for the representative strand in each duct. The load cells were also used to measure the loss of force in the strands over time. This was only done until the post-tensioning ducts were grouted.

Table 3.2.2 gives the names of each instrument, the type of instrument, and a description of where it was located in the lab mockup. Even though some names are used more than once, the instruments that are being referred to will be obvious. Table 3.2.2 should be used with Figure 3.2.3 and Figure 3.2.7 to determine the location of the instrument in question. The VWG and thermocouple data was gathered with a Campbell CR23X micrologger and two multiplexers. The ER strain gages, wirepots, LVDTs and load cells were connected to a System 5000 scanner produced by Vishay MicroMeasurements Group, Inc.

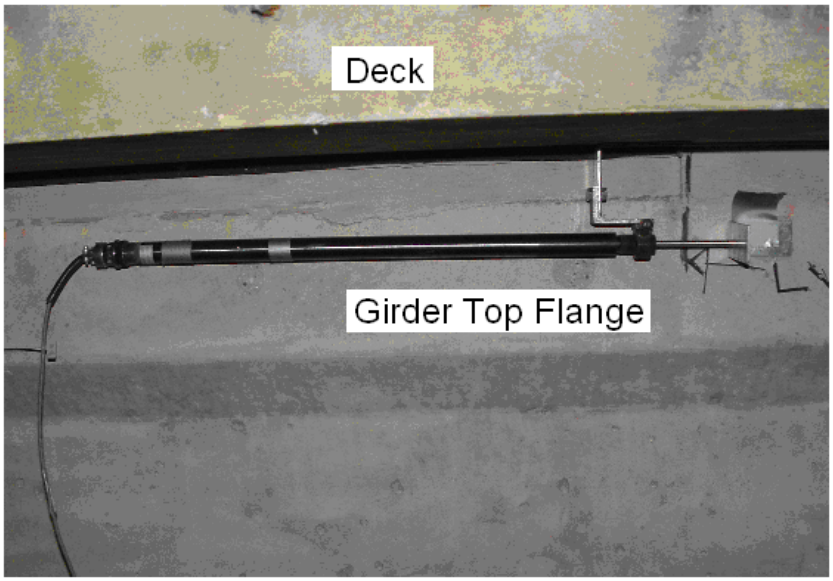

Figure 3.2.6 Setup to Measure the Relative Horizontal Displacement at the Horizontal Interface.

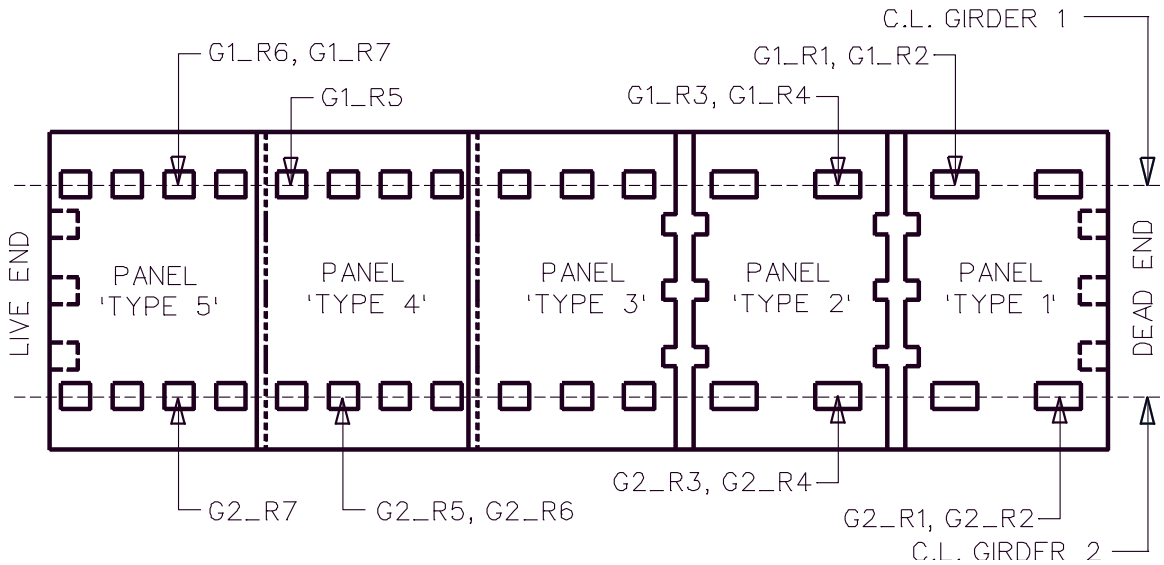

Figure 3.2.7 Locations of Instrumented Shear Connectors

Table 3.2.2 Location of Instrumentation in Lab Mockup

(a) VWGs

Name	Over Girder Line	Description of Location
G1_T_D	Girder 1	In the top flange on the dead end.
G1_B_D	Girder 1	In the bottom flange on the dead end.
G1_T_L	Girder 1	In the top flange on the live end.
G1_B_L	Girder 1	In the bottom flange on the live end.
G2_T_D	Girder 2	In the top flange on the dead end.
G2_B_D	Girder 2	In the bottom flange on the dead end.
G2_T_L	Girder 2	In the top flange on the live end.
G2_B_L	Girder 2	In the bottom flange on the live end.
G1_S2	Girder 1	In panel type 2.
G2_S2	Girder 2	In panel type 2.
G1_S4	Girder 1	In panel type 4.
G2_S4	Girder 2	In panel type 4.

(b) Thermocouples

Name	Over Girder Line	Description of Location
TG1_T_D	Girder 1	In top flange of girder on dead end.
TG1_M_D	Girder 1	In web of girder on dead end.
TG1_B_D	Girder 1	In bottom flange of girder on dead end.
TG1_T_L	Girder 1	In top flange of girder on live end.
TG1_M_L	Girder 1	In web of girder on live end.
TG1_B_L	Girder 1	In bottom flange of girder on dead end.
TG2_T_D	Girder 2	In top flange of girder on dead end.
TG2_M_D	Girder 2	In web of girder on dead end.
TG2_B_D	Girder 2	In bottom flange of girder on dead end.
TG2_T_L	Girder 2	In top flange of girder on live end.
TG2_B_L	Girder 2	In bottom flange of girder on dead end.
TG1_S2_T	Girder 1	In panel type 2 in the top portion of the slab.
TG1_S2_M	Girder 1	In panel type 2 in the middle portion of the slab.
TG1_S2_B	Girder 1	In panel type 2 in the bottom portion of the slab.
TG2_S2_T	Girder 2	In panel type 2 in the top portion of the slab.
TG2_S2_M	Girder 2	In panel type 2 in the middle portion of the slab.
TG2_S2_B	Girder 2	In panel type 2 in the bottom portion of the slab.
TG1_S4_T	Girder 1	In panel type 4 in the top portion of the slab.
TG1_S4_M	Girder 1	In panel type 4 in the middle portion of the slab.
TG1_S4_B	Girder 1	In panel type 4 in the bottom portion of the slab.
TG2_S4_T	Girder 2	In panel type 4 in the top portion of the slab.
TG2_S4_B	Girder 2	In panel type 4 in the bottom portion of the slab.

(c) LVDTs

Name	Over Girder Line	Description of Location
H1	Girder 1	Interface between panels and girders.
H2	Girder 2	Interface between panels and girders.

(d) Load Cells

Name	Over Girder Line	Description of Location
LC A	Duct Closest to Girder 2.	Dead end.
LC B	Middle Duct.	Dead end.
LC C	Duct Closest to Girder 1.	Dead end.

(e) ER Strain Gages

Name	Over Girder Line	Description of Location
G1_R1	Girder 1	See Figure 3.2.7.
G1_R2	Girder 1	See Figure 3.2.7.
G1_R3	Girder 1	See Figure 3.2.7.
G1_R4	Girder 1	See Figure 3.2.7.
G1_R5	Girder 1	See Figure 3.2.7.
G1_R6	Girder 1	See Figure 3.2.7.
G1_R7	Girder 1	See Figure 3.2.7.
G2_R1	Girder 2	See Figure 3.2.7.
G2_R2	Girder 2	See Figure 3.2.7.
G2_R3	Girder 2	See Figure 3.2.7.
G2_R4	Girder 2	See Figure 3.2.7.
G2_R5	Girder 2	See Figure 3.2.7.
G2_R6	Girder 2	See Figure 3.2.7.
G2_R7	Girder 2	See Figure 3.2.7.
PG1_D_L	Girder 1	Lower surface of panel on dead end.
PG1_L_L	Girder 1	Lower surface of panel on live end.
PG2_D_L	Girder 2	Lower surface of panel on dead end.
PG2_L_L	Girder 2	Lower surface of panel on live end.
G1_D_L	Girder 1	Lower surface of girder on dead end.
G1_L_L	Girder 1	Lower surface of girder on live end.
G2_D_L	Girder 2	Lower surface of girder on dead end.
G2_L_L	Girder 2	Lower surface of girder on live end.
G1_D_U	Girder 1	Upper surface of girder on dead end.
G1_L_U	Girder 1	Upper surface of girder on live end.
G2_D_U	Girder 2	Upper surface of girder on dead end.
G2_L_U	Girder 2	Upper surface of girder on live end.

(f) Wirepots

Name	Over Girder Line	Description of Location
A1	Girder 1	1 ft. from end of girder on live end. Used to measure vertical displacment of bearing pads.
B1	Girder 1	Under load applied near inside joint (dead end test setup) or near outside joint (live end test setup) to measure vertical displacement of system.
C1	Girder 1	Under load applied near outside joint (dead end test setup) or near inside joint (live end test setup) to measure vertical displacement of system.
D1	Girder 1	1 ft. from end of girder on dead end. Used to measure vertical displacement of bearing pads.
A2	Girder 2	1 ft. from end of girder on live end. Used to measure vertical displacement of bearing pads.
B2	Girder 2	Under load applied near inside joint (dead end test setup) or near outside joint (live end test setup) to measure vertical displacement of system.
C2	Girder 2	Under load applied near outside joint (dead end test setup) or near inside joint (live end test setup) to measure vertical displacement of system.
D2	Girder 2	1 ft. from end of girder on dead end. Used to measure vertical displacment of bearing pads.
Jt_O	NA	Located at outside transverse joints.
Jt_I	NA	Located at inside transverse joints.

3.2.3 Constructability Study

The fabrication of the panels and girders and the construction of the lab mockup was well documented. During the fabrication of the girders, the practicality and ease of construction of the new shear stud detail for the horizontal shear connector system was examined. Other important observations were also recorded as seen fit. The method for forming the transverse joints, method for creating an efficient strand pattern, and method for creating the shear pockets were examined during the fabrication of the panels.

The different stages of the construction of the lab mockup were examined. The stages included:

1. Placement of the panels on the girders.

2. Pouring the grouted female-female transverse joints.
3. Epoxying the male-female transverse joints.
4. The post-tensioning operation.
5. Placing the formwork for the haunch.
6. Pouring the haunch.
7. Grouting the post-tensioning ducts.
8. Removal of the leveling bolts and lifting eyes.

The duration of each task and notes on the construction process were recorded for each stage. Recommendations were made for the transverse joint and shear connector type that worked best from a constructability point of view.

3.2.4 Time Dependent Testing of Lab Mockup

The strains and temperatures in the VWGs and thermocouples as well as the forces in the load cells at the dead end of the post-tensioning ducts were measured and collected over approximately two months to investigate the time dependent behavior of the lab mockup. If the temperature remained fairly constant, the strains will not be influenced by the temperature. Therefore, the thermocouple data may not be useful if this is the case. This may be true when the girders and panels were placed in the lab.

The VWG data was used to provide insight into the force and moment redistribution produced by creep and shrinkage effects in the composite system. One of the primary interests was whether the initial level of post-tensioning keeps the transverse joints in compression. Although long term stresses could not be measured experimentally in the lab mockup, the experimental data was very useful in verifying the finite element results. The finite element models were capable of estimating the long term longitudinal stresses. The finite element models provided results over a much longer time period than two months so the long term deck stresses could be examined. The time interval in the finite element model was approximately 25 years. This is discussed more in Section 3.3.1. The long term strains in girder 1 were compared to the long term strains in girder 2. This will aid in discovering whether the plates cast with girder 2 for the shear studs acted as compression reinforcement in some regions and reduced the long term strains.

3.2.5 Material Testing

Compression tests and split cylinder tests to measure the compressive and tensile strength of the concrete in the panels and girders were conducted at selected intervals throughout the testing program. The tensile strength of the concrete was calculated by using the equation

$$f_t = \frac{2P}{\pi dL} \qquad [3.1]$$

where,

P = load at which the cylinder failed during the split cylinder test (kips)

d = diameter of the test cylinder (in.)

L = length of the test cylinder (in.)

Compression tests were also performed on the grout in the haunch. The Forney compression machine was used to carry out these tests. Additionally, the modulus of elasticity was obtained at key construction intervals where strains resulting from elastic deformations were available. An estimation of the modulus of elasticity could be back calculated from the experimental strain values. The moduli of elasticity obtained from the experimental data were compared to the modulus of elasticity obtained from Section 8.5.1 of ACI 318[26] for normal weight concrete. The modulus of elasticity was not determined experimentally because of difficulties encountered measuring the deformations for the modulus test.

The cylinders were filled during the casting of the panels and casting of the girders at Bayshore Concrete Products in Chesapeake, VA. The day after the cylinders were filled, the molds were removed. The cylinders then cured at room temperature in the Virginia Tech Structures Laboratory until the time a test was performed with one of the cylinders. The cylinders were 4 in. in diameter and 8 in. in long. The compression and split cylinder tests were performed before the release of the prestress force, at 7 days, 28 days, and during key intervals during the construction process. These key intervals included the time the panels were placed on the girders, the time the post-tensioning was applied, the time the haunch was poured, and immediately before the live load testing began. Multiple breaks were made at each time interval as seen fit. The results were

used to predict limits for the live load tests and help establish material models for the finite element models.

3.2.6 Live Load Test Setup for Lab Mockup

The live load testing program consisted of initial static tests, cyclic testing up to 2 million cycles, intermediate static tests, and final static tests. These tests were performed on both the dead end and live end of the lab mockup in the following order:

1. Initial static test at the dead end,
2. Cyclic testing at the dead end,
3. Intermediate static test at the dead end,
4. Initial static test at the live end,
5. Cyclic testing at the live end,
6. Intermediate static test at the live end,
7. Final static test at the dead end,
8. Final static test at the live end.

Each of these tests is discussed in the following sections. Ponding of water at the transverse joints was also performed before each of the load tests. More details on each of these tests will be presented in subsequent sections. Recall from Figure 3.2.1 in Section 3.2.1 that the live end was where the strands were stressed and the dead end was at the opposite support.

Figure 3.2.8 shows the test setup on the dead end and live end. The shear pockets are left out of the figure for clarity. The loading for each of the two test setups (dead end and live end) consisted of four load patches placed symmetrically about the longitudinal centerline of the bridge. The symmetric loading was done to attempt to create the same loading on each girder. By doing so, the performance of different shear connectors could be compared. The two test setups are symmetric about the transverse centerline (midspan) of the bridge. This allowed the performance of the system with the different pocket spacings to be compared.

Note that the spacing of the four load patches in Figure 3.2.8(a) for each test setup did not match the wheel load spacing and axle spacing for an AASHTO design vehicle. It was decided that loads should be placed adjacent to joints in such a way as to have the

resulting shears and moments in the girders and panels comparable to AASHTO design shears and moments for the lab mockup.

The loads were placed adjacent to the transverse joints to test the performance of the different transverse joint configurations. Although, the longitudinal location of the loading frames was limited by the bolt hole pattern on the longitudinal reaction floor beams in the lab. This did not allow the load patches to be placed at the very edges of the transverse joints. However, it was possible to place the edges of the load patches within 6 in. of the edges of all the transverse joints.

The size of each load patch was 9 in. x 14 in. on the dead end and 9 in. x 18 in. on the live end. The difference in load patch sizes is attributed to the limited number of elastomeric bearing pads available in the lab for the number of projects requesting elastomeric bearing pads. For this study, the size of the load patch size is not an issue since local effects are not a concern.

A spreader beam spans between each pair of wheel loads in the transverse direction. The load was half way between the two load patches, as shown in Figure 3.2.8(b). Each test setup requires two spreader beams, four bearing pads for the load patches, two loading frames, and two hydraulic rams. For the static tests, a 400 kip hydraulic ram was used to apply the load to each spreader beam. For the cyclic tests, a closed-loop, servo-hydraulic testing system was used to apply the loadings.

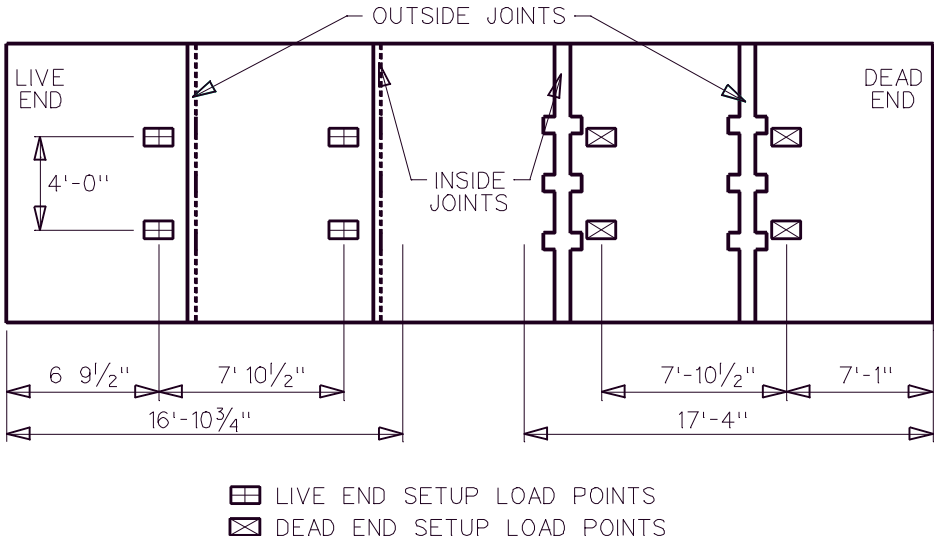

(a)

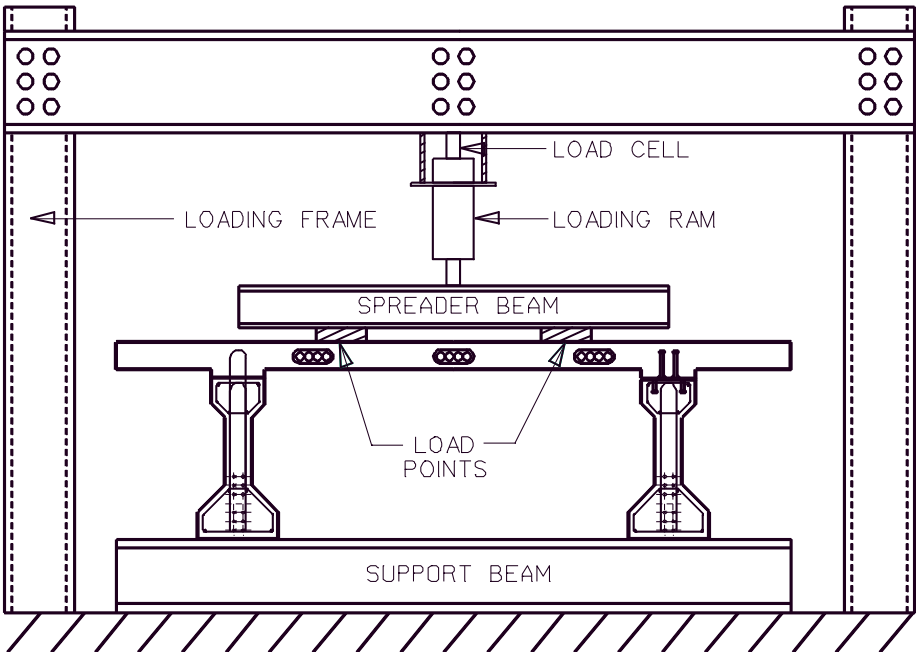

(b)

Figure 3.2.8 Live Load Test Setups (a) Plan View (b) Elevation View

3.2.7 Initial Static Tests for Lab Mockup

For each initial static test (prior to the cyclic testing), a load of 37.33 kips was applied at each wheel load location. This load was determined by using a typical AASHTO design wheel load of 16 kips, multiplying by an impact factor of 1.333 and a

load factor of 1.75. This corresponds to a load of 74.7 k/frame (kip per frame) for each of the two frames used on a given test setup.

The load was gradually increased up to this limit. At load increments of 20 k/frame, the bridge was inspected for flexural cracks, web shear cracking, web flexural cracks (if any flexural cracks were already present), cracking at the horizontal interface, and cracking at the transverse joints.

The data was used to determine if full composite action between the panels and girders over each girder line remained after the load is applied. The performance of the transverse joints and different types of shear connectors was studied.

3.2.8 Cyclic Testing for Lab Mockup

After the initial static test, a total of two million cycles of loading was applied to the bridge. The number of cycles used in this study is the same as that found in previous research on precast deck panel systems by Issa[18] for similar loading conditions. Two million cycles of loading at each end of the bridge was also selected based on the time limits of the testing program. The shape of loading curve over time was a sine wave, with a period of 0.5 sec (frequency of 2 Hz).

For the first 500,000 cycles, the load ranged from 2 k/frame to 29.4 k/frame. This created the AASHTO LRFD design fatigue moment of 2250 k-in for the girder, which was calculated during the design phase of the study. During the cyclic tests, a compressive force of at least 1 kip was always present to prevent rotational movement of the spreader beam and to prevent damage to the bridge. A wheel load for the next 1,500,000 cycles ranged from 2 k/frame to 44.7 k/frame. The range of the loading, 42.7 k/frame, corresponds to two typical AASHTO design wheel loads of 16 kips, multiplied by an impact factor of 1.33. This was greater than the AASHTO LRFD impact factor of 1.15 for fatigue. The load level of 42.7 k/frame produced a maximum moment in the bridge of 3520 k-in, which was 56% greater than the AASHTO LRFD design fatigue moment of 2250 k-in.

Every 100,000 cycles to 300,000 cycles, the cyclic testing was stopped to conduct a static test on the system. The load was gradually increased up to 44.7 k/frame. These intermediate static tests were done to see if there was any loss in stiffness in the lab

mockup due to loss of composite action, cracking, sliding at the joints, etc. throughout the cyclic test program.

3.2.9 Intermediate Static Tests for Lab Mockup

After the cyclic testing was completed for a given test setup, an intermediate static test was performed. The purpose of this test was to attempt to capture some non-linear behavior in the results. These results offer insight into the behavior of the system after cracking, plastic behavior of the reinforcing steel, prestressing strands, and shear connectors, and relative slip at material interfaces occur. The load was gradually increased up to about 130 k/frame, or until sufficient cracking was noticed in the system but the system could still be deemed repairable. A load of 130 k/frame was predicted to cause cracking in the bottom of the girder under the inside load point (see Figure 3.2.8(a)) and cracking at the interface between the haunch and girders.

The load was gradually increased up to this limit. At load increments of 20 k/frame, the bridge was inspected for flexural cracks, web shear cracking, web flexural cracks (if any flexural cracks were already present), cracking at the horizontal interface, cracking at the transverse joints, cracking in the vicinity of the wheel loads on the top of the deck, cracking over the girder lines, cracking on the bottom side of the panels, and cracking in the shear pockets. When the load was above 100 k/frame, the load increments were decreased to every 10 k/frame to 20 k/frame.

The data was used to determine if full composite action between the panels and girders over each girder line remained after the load is applied. The performance of the transverse joints and different types of shear connectors was thoroughly studied.

3.2.10 Final Static Tests for Lab Mockup

After the testing was completed on the dead end and live ends of the bridge, a final static test was performed on the dead end and then the live end. The purpose of this test was to see if required flexural strength of 15,500 k-in and required vertical shear strength of 152 k could be reached before a failure was observed. The failure mode of the system was also noted. The load was gradually increased until failure. An elastic analysis determined an applied load of 187 k/frame would produce a moment equal to the

required flexural strength of 15,500 k-in and an applied load of 212 k/frame would produce a shear equal to the required vertical shear strength of 152 k.

The load was gradually increased in 20 k/frame increments. The bridge was inspected for flexural cracks, web shear cracking, web flexural cracks (if any flexural cracks were already present), cracking at the horizontal interface, cracking at the transverse joints, cracking in the vicinity of the wheel loads on the top of the deck, cracking over the girder lines, cracking on the bottom side of the panels, and cracking in the shear pockets. When the load was above 150 k/frame, the load increments were decreased to every 5 kips to 10 kips. When displacements started increasing in a highly nonlinear manner with respect to the applied load, the analysis was switched to displacement control. The displacement increments used at this point were 0.05 in.

The data were used to determine if full composite action between the panels and girders over each girder line remained after the load is applied. The performance of the transverse joints, different pocket spacings, and different types of shear connectors were thoroughly studied along with the failure modes at each end of the lab mockup.

3.2.11 Durability Study of Transverse Joints

Water was ponded over the transverse joints at selected intervals. The selected intervals were:

1. Before the initial static test,
2. Before the cyclic testing,
3. Before the intermediate static test,
4. After the intermediate static test,
5. After the final static test.

Water was poured from a bucket onto the bridge deck over the transverse joints until the depth of the water was approximately ¼ in. to ½ in. deep. The joints were monitored for a half hour period. During this period, any leaking at the transverse joints was noted.

3.3 Analytical Study

3.3.1 Finite Element Analysis of Time Dependent Behavior

The finite element software DIANA was used to carry out an analysis of the time dependent behavior of the lab mockup to provide insight in to the post-tensioning losses in the system as well as the effective long term stresses across the transverse joints. The results were used to examine whether the initial level of post-tensioning provided in the lab mockup was sufficient to keep the transverse joints in compression. Based on the results presented in Section 5.1, recommendations were made for the initial level of post-tensioning.

A staged, plane stress analysis was run in DIANA. The following was the staging used for the lab mockup:

1. Girder cured for 1.5 days.
2. The strands in the girder were cut. The girder sat and gained strength over the next 22 days.
3. The panels were cast and cured for 2.5 days. The panels then sat in the casting yard and were transported to the lab. The panels continued to sit in the lab. The same environmental conditions were assumed to exist in the casting yard and lab. The girders continued to sit in the casting yard, then the lab. The time period for this step was 71 days.
4. The panels were placed on the girders. The dead weight of the panels was transferred to the girders through the leveling bolts. The non-composite system sat in the lab for a period of 20 days.
5. The first six strands were tensioned during the post-tensioning operation in the deck. The system then remained idle for two days.
6. The last six strands were tensioned during the post-tensioning operation in the deck. The system remained idle for six days.
7. The haunch was cast. The composite system remained idle for 26 days. (This marks the end of the analysis in the lab.)
8. The composite system remained idle for an additional 25 years to look at the long term effects of the bridge.

The model consisted of one girder with a tributary deck width of 6 ft. If the results of the finite element model were in good agreement with the results from the lab mockup, then a three dimensional model would be deemed unnecessary.

Eight node quadrilateral elements were used to model the panels, girder, haunch, and bearing pads. The element size used for this study was approximately 2 in. x 2 in. Using 2 in. x 2 in. elements results in 23 elements through the depth of the composite section. The number of elements used through the depth, along with the higher order polynomial used to model the displacement field, accurately modeled the strain profile through the depth and prevent the model from having an artificially high stiffness. Figure 3.3.1 shows the mesh used for the time dependent behavior models.

The prestressing strands in the girder, the post-tensioning strands in the deck, and all the mild reinforcing steel were modeled with embedded reinforcing bars. Embedded reinforcing bars have no degrees of freedom of their own which makes them computationally cheap. They are embedded in "mother elements", which are the elements that the embedded reinforcement passes through in the geometric layout of the model. The strains in the embedded reinforcement are calculated from the displacement fields of the "mother elements." These embedded reinforcing elements contribute to the stiffness of the system.

A prestress load can be assigned to embedded reinforcement, which was required for the precast bridge deck panel system. Initial losses in the post-tensioning system such as anchor loss, wobble friction loss, curvature friction loss, and elastic shortening were calculated by DIANA. These initial losses were based on the CEB-FIP Model Code 1990.

The concrete in the panels and girders, the grout in the haunch, and the steel for the prestressing steel, post-tensioning steel and mild reinforcing steel were all modeled with linear elastic materials since no cracking or yielding of the steel was anticipated during the time dependent analysis.

Different creep and shrinkage models were used in the preliminary stages to determine which model most accurately modeled the variation of the displacements, strains, and stresses in the lab mockup over time. The creep and shrinkage models available in DIANA[40] were the ACI 209[10] model, the CEB-FIP[14] model code 1990, and

the NEN (Netherlands) 6720[46] model. The NEN 6720 model was immediately removed from the list of possible models for this application because it was only valid for materials with strength and modulus of elasticity that were time independent.

In order to carry out the time steps, regular Newton-Raphson iteration was used with explicit time steps. With regular Newton-Raphson, the stiffness is updated every iteration, which typically results in fewer iterations in a given time (or load) step than modified Newton-Raphson iteration, where the stiffness is only updated at the beginning of a time (or load) step. The time steps were broken up to mimic the logarithmic behavior of the time functions for the creep coefficient and shrinkage strains. The smallest time step used was 10 seconds and the largest time step used was 1000 days.

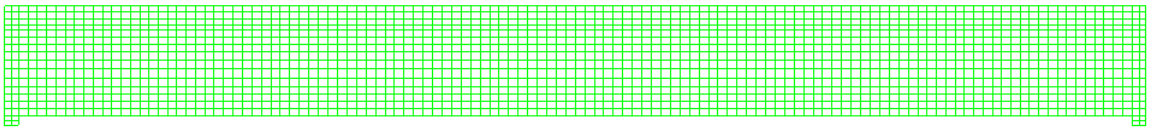

Figure 3.3.1 Mesh for Time Dependent Behavior Models

3.3.2 Finite Element Analysis of Push Off Tests

Finite element models were created in DIANA for push-off specimens to propose a methodology for modeling the shear connectors and the interface between the haunch and girders and interface between the haunch and panels. The modeling methodology for modeling the shear connectors and interfaces for the push-off tests is also used in the finite element models for time dependent effects if necessary (see Section 3.3.1) and the ultimate load tests (see Section 3.3.3). Load vs. relative displacement curves were developed from the finite element results and compared to experimental results produced by Wallenfelsz[29]. Observations were made regarding the relationship between the load vs. displacement curve for the finite element results and Wallenfelsz's results. The finite element slip values were compared to Wallenfelsz's slip values to establish how conservative the finite element models were.

After the finite element models were compared to experimental data and shown to predict the behavior sufficiently, additional models were created in DIANA. Each of the

models had different numbers of shear connectors and different types of shear connectors. The capacities obtained from the finite element models were compared to the capacities obtained from AASHTO LRFD[22] for calculating the horizontal shear capacity. The different types and amounts of shear connectors used for the parametric study were:

1. 2 No. 4 bars,
2. 2 No. 5 bars,
3. 4 No. 4 bars,
4. 4 No. 5 bars,
5. 2-3/4 in. diameter shear studs,
6. 3-3/4 in. diameter shear studs,
7. 4-3/4 in. diameter shear studs.

The results are presented in Section 5.2.

A description of the push-off test specimen is given in Section 2.1.2.3. Figure 3.3.2 shows a representation of the push off test specimen. A plane stress analysis was used first to attempt to match the experimental data. Eight node quadrilateral elements were used to model the panel, girder, shear pocket, and haunch, six node triangular elements were used to model the loading pad, three node beam elements were used to model the shear connectors, and three node interface elements were used to model the interface between the haunch and girder. Beam elements were used instead of truss elements to include the dowel action of the shear connectors. Only the beam elements provide rotational stiffness at the nodes that the beam elements share with the plane stress elements. Interface elements were used to allow slip to occur between the girder and haunch.

It was assumed that a perfect bond existed at the interface of the shear connector(s) and the haunch and the interface between the haunch and panel. The entire length of the interface between the haunch and girder consisted of two dissimilar materials cast at different times. However, the large surface area of grout that passes through the location where the interface between the panel and haunch is located adds strength to the top interface. Therefore, it was assumed that the top interface, between the panel and haunch, was stronger than the bottom interface, between the haunch and girder and cracking would occur at the bottom interface first. It was assumed that the

entire depth of the haunch was filled with grout. If the grout did not fill the entire depth of the haunch, then the strength at the top interface would be less than the strength at the bottom interface. This was verified by studying the cracking patterns in the lab mockup.

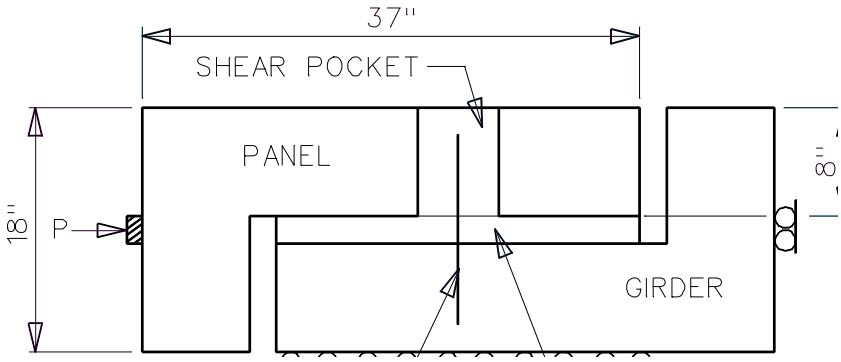

Figure 3.3.2 Push-off Specimen Modeled in DIANA.

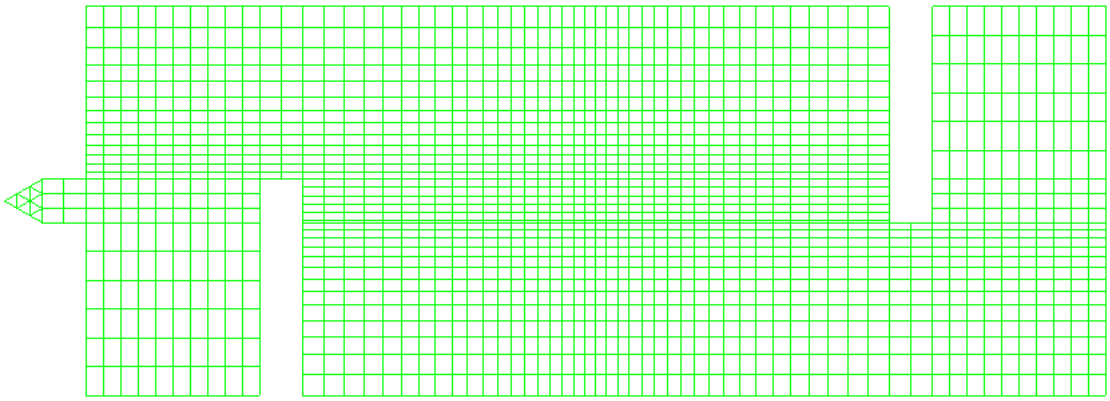

Figure 3.3.3 Mesh for Push-Off Models.

The paving meshing algorithm was used to vary the size of the elements in the model. The paving algorithm produced a quadrilateral mesh on any type of surface. Figure 3.3.3 shows a push-off test model with the paving mesh algorithm applied to generate the mesh. A mesh quality check was run to check the elements for large aspect ratios, large angle deviation at the corners, midnode offsets, warping, and bulging of the midnodes. The mesh was refined in the vicinity of the interface between the haunch and

panel and the shear connectors. Localized cracking and crushing, relative slip, and large stress concentrations in the shear connectors were expected to occur at this location.

Modeling the behavior of the shear connectors in a bridge is a complex problem. When a large shear is transferred from the deck to the girder, the interface cracks causing the two surfaces to separate and slip relative to one another. In turn, a tensile force is developed in the shear connector causing a compressive force and corresponding frictional force to develop at the interface. This frictional force increases the horizontal shear capacity of the system. Accurately modeling this "clamping effect" was difficult to accomplish in DIANA.

DIANA offers several material models that can be used with interface elements. They were examined and considered for the material model for the interface. A crack dilatancy model was first examined. The model of a "rough crack" was only activated after the crack opening in the normal direction of the interface exceeded a user defined limit. In order to exceed this limit, a very small limit can be defined by the user and normal loads in equal and opposite directions at the interface can be applied to create a tensile stress in the interface. Although a rough crack could be simulated, the "clamping effect" was not produced. The rough crack that was activated by the crack dilatancy model did not cause the interface to separate and produce tensile stresses in the shear connectors and frictional stresses in the interface. The Mohr-Coulomb material model was examined next. It was also incapable of capturing the "clamping effect" and results in unstable behavior at higher loads.

A nonlinear, elastic material was selected for the interfaces because of its stable and predictable behavior. The user specifies a normal stress vs. relative opening diagram and a tangential stress vs. slip diagram to define the behavior of the material. The tangential stress vs. slip diagram was defined such that there was still a small amount of shear resistance after the interface "cracks," as shown in Figure 3.3.4. The tangential stress vs. slip diagrams used for the push off tests were derived from data from Scholz[1] and Wallenfelsz[29]. The normal stress vs. relative opening diagram was defined such that the stiffness in the normal direction was very large.

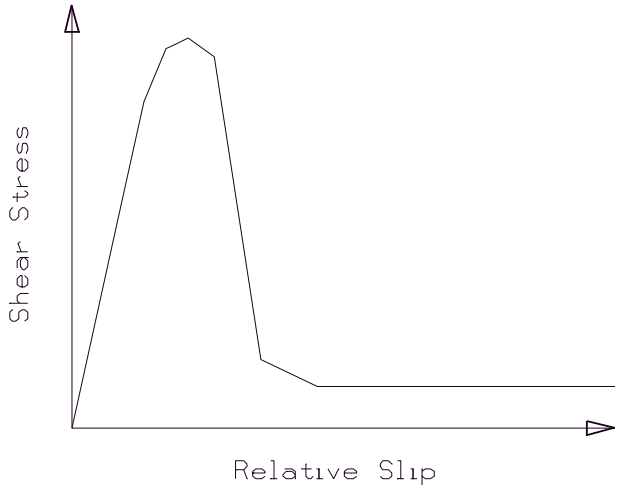

Figure 3.3.4 Tangential Stress vs. Slip Diagram for Interface Material Without Shear Connectors

Neglecting the "clamping effect" was conservative and acceptable for this type of analysis and it resulted in larger slip values and higher strains in the shear connectors. Because the strain levels and slip values were larger than expected, the acceptable number of shear connectors from the parametric study, discussed in Section 3.3.3, was conservative.

As mentioned above, cracking and/or crushing of the concrete occured in the panels, haunch, and girders in the vicinity of the concrete interfaces and shear connectors. Two approaches were examined to attempt to capture this local behavior: A smeared cracking approach and a softened elastic modulus approach.

For the smeared cracking approach, the smeared cracking model was activated in DIANA to model any cracks that form. The cracking model was defined by a tension cut-off model, a tension softening model and a shear retention model. A linear tension cut-off relationship was selected for the tension cut-off model, which is shown in Figure 3.3.5 with a principle stress orientation. This incorporates the influence of a biaxial stress state on the tensile strength of the concrete. As shown in Figure 3.3.5, when a compressive stress exists along one principle stress axis and tension exists along the other principle stress axis, the tensile strength is reduced. A linear tension softening relationship was selected for the tension softening model, which is shown in Figure 3.3.6.

The stress σ_{nn} and strain ε_{nn} are normal to the direction of the crack plane. The total strain is divided into an elastic strain and a crack strain. The same is applied for the total stress. In the formulation of the tension softening model, it is assumed that the crack stress is a function of the crack strain for the one crack that was formed and also assumed that coupling effects with other cracks is ignored. The constant shear retention model was used instead of the full shear retention model. For the full shear retention model, the shear modulus is not reduced after cracking. For this constant shear retention model, the shear modulus is reduced by a user defined amount (β). For the models in this study, it was assumed that 50% of the shear stiffness was lost when the crack was formed (β=0.5). The DIANA User's Manual's manual[40] recommended using β=0.25. However, the value of β was increased to 0.5 to improve the convergence behavior of the model without affecting the results.

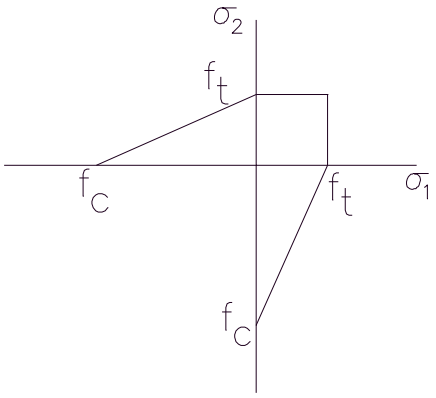

Figure 3.3.5 Tension Cut-Off Model

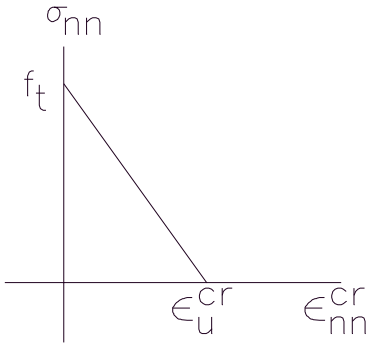

Figure 3.3.6 Tension Softening Model

Crushing was defined by using the Von Mises failure criterion along with a uniaxial, multi-linear stress vs. strain curve to capture the plastic behavior of concrete and grout in compression. For the Von Mises failure criterion, yielding (or crushing) occurs when the distortional strain-energy density at a point becomes greater than or equal to the distortional strain-energy at yield (or crushing) in uniaxial tension or compression. The multi-linear stress vs. strain curve was based upon the modified Hogenstad model presented in MacGregor[39]. The compressive strength of the concrete for the panels and girders was 6 ksi and the compressive strength for the grout in the haunch was 4 ksi.

The second approach to modeling the local cracking and crushing at the interface between the haunch and girder in the vicinity of the shear connectors was the softened elastic modulus approach. In this approach, the region where the localized cracking and crushing occurs was assumed to have very small, constant stiffness through the entire analysis. This "cracked" region is shown in Figure 3.3.7. The stiffness was reduced by decreasing the elastic modulus for the grout in the haunch and concrete in the girder. The factor that the elastic modulus was reduced by and the size of the "cracked" region was determined from the results of the push-off tests run with the smeared cracking approach.

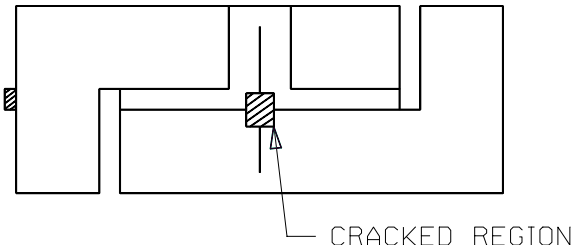

Figure 3.3.7 Cracked Region for Softened Elastic Modulus Approach

The softened elastic modulus approach produced more stable convergence behavior when attempting to capture the unloading portion of the load vs. displacement curve for the push-off tests. This was because the cracking that occurred was localized and the smeared cracking approach was better suited for capturing cracking on a global scale. The results of the two approaches discussed above were compared and one was selected to run the remaining finite element analyses.

The material for the shear connectors was modeled with the Von Mises failure criterion with a uniaxial stress vs. strain curve, similar to the approach for modeling the crushing of the concrete described above. A nominal stress vs. strain curve for Grade 50 steel was used for the shear studs and a nominal stress vs. strain curve for Grade 60 steel was used for the hooked reinforcing bars.

The preliminary models were run with force control and displacement control and were compared to make sure the results and behavior of the system were the same. Displacement controlled analyses were run for the remaining push off test models. Secant iteration was used with adaptive load steps to carry out the load steps. In general, secant iteration results in more stable convergence behavior than other iteration methods when strong nonlinearities, such as cracking, are involved. This is because the stiffness remains positive even when unloading is present for the load vs. displacement curve. Two methods were used to define the load steps. For smaller applied load levels, explicit load steps were used where preliminary analyses indicated the relative slip values were very small, cracking was not extensive, and only the onset of yielding may have occurred in the shear connectors. The size of the load steps was determined from the convergence behavior and decreased in size as the total applied load became larger. For higher applied

load levels, an adaptive load stepping scheme was used where cracking started to become more extensive, relative slip values started to become larger, the stresses in the shear connectors were well in to the plastic range, and the behavior of the system became harder to predict. DIANA determined the size of the next load step based on the user specified desired number of iterations per load step, the actual number of iterations in a given load step, a maximum step size, and a minimum step size.

3.3.3 Finite Element Analysis of Live Load Tests for the Mockup

A series of plane stress finite element analyses were carried out to examine the flexural and shear capacities of the deck panel system compared to predicted values from the design calculations (see Appendix A), any unloading behavior, shear connector behavior, and pocket spacing influence. The failure mode of each model was investigated. Possible failure modes include the failure of one of the horizontal interfaces, flexural failure of the girder, and excessive shear cracks in the girder. If the horizontal interface fails first, the horizontal shear is no longer transferred uniformly from the girder to the deck. Instead, the horizontal shear is transferred from the girder to the deck via the shear connectors at the shear pockets. The widely spaced shear pockets may affect the capacity of the system and the cracking pattern in the girder.

Both the live end setup and dead end setup of the lab mockup were used to examine the behavior of the lab mockup. Details on the setups are given in Section 3.2.6. The entire bridge was modeled in DIANA. One girder was modeled at a time with a 6 ft tributary deck width.

A verification study and a parametric study were carried out to examine the behavior of the deck panel system. For the verification study, the lab mockup was duplicated in DIANA. Because only one girder was modeled at a time and two load conditions were examined (live end setup and dead end setup) the following models were examined for the verification study:

1. Girder 1 with dead end setup for static tests,
2. Girder 2 with dead end setup for static tests,
3. Girder 1 with live end setup for static tests,
4. Girder 2 with live end setup for static tests.

Recall the static tests on the dead end examined the 4 ft pocket spacing and the static tests on the live end examined the 2 ft pocket spacing. Additionally, girder 1 had the hooked reinforcing bars as shear connectors and girder 2 had the shear studs as shear connectors. The results for the finite element models were compared to the experimental results. The load vs. displacement curves, shear connector strains, strain profiles, cracking patterns in the girder, and cracking patterns in the haunch and interface between the haunch and girder were examined and compared.

Once the results of the finite element models were compared to the experimental results, the parametric study was conducted. The parametric study consisted of varying the amount of shear connectors in each pocket and the distribution of the shear connectors among the pockets. This allowed for additional insight in to the influence of the pocket spacing and connector type on the behavior of the deck panel system. The capacities of the models were compared to AASHTO LRFD provisions. As necessary, modifications to current design equations are proposed or new equations are proposed to predict the horizontal shear capacity at an interface. Any unique behavior that the deck panel system exhibits was discussed.

A total of 11 different models were examined for the parametric study. Six of the models were run with No. 5 hooked reinforcing bars as shear connectors and five of the models were run with ¾ in. diameter shear studs as shear connectors. Table 3.3.1 shows the number of shear connectors per pocket for each model examined with a given shear connector type. Model MOCKUP had the exact number of shear connectors used for the lab mockup. Model 2.121_100 had close to the exact number of shear connectors required per pocket using Equation 2.121. Model 2.121_75 had approximately 75% of shear connectors required per pocket using Equation 2.121. Model 2.121_50 had approximately 50% of shear connectors required per pocket using Equation 2.121. Model 2.128_R had close to the number of shear connectors required using Equation 2.128. The shear connectors were distributed in an even manner among the pockets. The connectors were also distributed among the shear pockets so the dead end and live end of the bridge had approximately the same amount of shear connectors. Model 2.128_L had close to the number of shear connectors required using Equation 2.128. Unlike model 2.128_R, the shear connectors were distributed among the pockets such that more shear

connectors were placed in locations with high shear stresses. The results of different models were compared using load vs. displacement curves, Von Mises stresses in the shear connectors, and cracking patterns. The results are presented in Section 5.3.

Figure 3.3.8 shows the mesh for the finite element model. The mesh was refined in the vicinity of the interface between the haunch and girder. Eight node quadrilateral elements were used to model the panels, haunch, girder, and bearing pads. Three node beam elements were used to model the shear connectors. Only the beam elements provide rotational stiffness at the nodes that the beam elements share with the plane stress elements. Three node interface elements were used to model the interface between the haunch and girder. Embedded reinforcing bars were used to model the vertical shear stirrups, the mild longitudinal reinforcing steel, the strands for post-tensioning in the panels, and the strands for prestressing in the girder. Details on the embedded reinforcing bars are given in Section 3.3.1. The material models and nonlinear solution algorithms used for the models of the lab mockup described in Section 3.3.2.

The smeared cracking approach was used instead of the softened elastic modulus approach for two reasons. The first reason was that the cracking in the haunch and the girder in the vicinity of the shear connectors was not as localized as it was for the push-off specimen. The cracking was smeared along the 1 ft-0 in. to 1 ft-6 in. length of the shear pockets. The second reason was that the load vs. displacement curve for the lab mockup did not have an unloading portion, as shown by the experimental data in Chapter 4. Therefore, consideration did not need to be given to replacing the cracking model with a softened elastic modulus approach to stabilize the convergence behavior. Additionally, the models were run under force control since the load vs. displacement curve does not have an unloading portion.

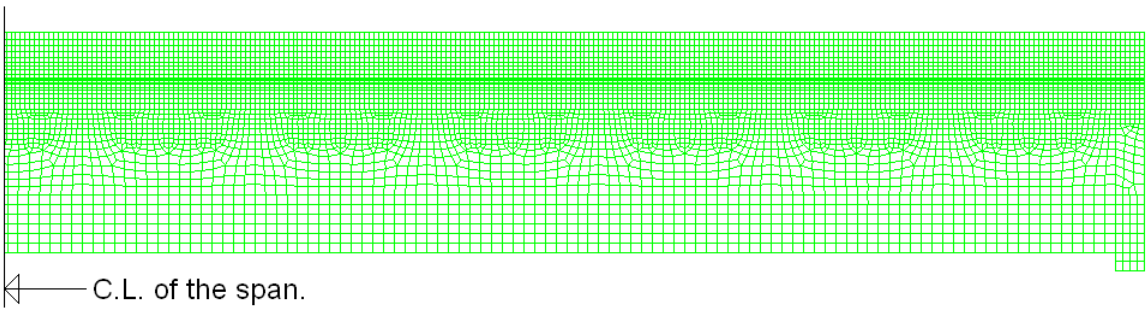

Figure 3.3.8 Mesh for Live Load Tests on Lab Mockup.

Table 3.3.1 Number of Shear Connectors per Pocket for Parametric Study

(a) Hooked Reinforcing Bars

Model Name	MOCKUP	2.121_100	2.121_75	2.121_50	2.128_R	2.128_L
Pocket #						
1	8	8	6	4	4	6
2	8	7	5	4	4	6
3	8	6	5	3	4	6
4	8	6	4	3	4	6
5	8	5	4	2	4	2
6	8	4	3	2	4	2
7	8	4	3	2	4	2
8	8	3	2	2	4	2
9	8	2	2	1	4	2
10	8	1	1	0	4	2
11	8	3	2	1	6	2
12	10	6	4	3	6	6
13	10	9	7	5	6	6
14	16	12	9	6	6	10
15	16	15	11	8	6	10
Total #	140	91	68	46	70	70

(b) Shear Studs

Model Name	MOCKUP	2.121_100	2.121_75	2.128_R	2.128_L
Pocket #					
1	6	7	6	3	6
2	6	6	4	3	6
3	6	6	4	3	6
4	6	5	3	3	3
5	6	5	3	3	3
6	6	4	3	3	3
7	6	4	3	3	0
8	6	4	3	3	0
9	6	3	2	3	0
10	6	3	2	3	0
11	6	4	3	4	0
12	8	7	5	4	0
13	8	9	6	4	5
14	12	11	8	4	9
15	12	13	9	4	9
Total #	106	91	64	50	50

Chapter 4
Experimental Results

This chapter presents the experimental results of the constructability study, time dependent study, material testing, and live load testing on the lab mockup. Design details used in the lab mockup were compared to see how they assisted with rapid construction. Creep and shrinkage strains were examined to study the long term performance of the lab mockup. The live load testing program investigated the different pocket spacings and shear connectors used to investigate their influence on the level of composite action in the lab mockup.

4.1 Fabrication and Constructability Study

4.1.1 Fabrication of the Girders

The formwork, the reinforcement cage, and the stressing of the prestressing strands for the girders was done on 12/12/05 and 12/13/05. The stressing bed was set up so the two girders were in a single line with the prestressing tendons running the length of the entire stressing bed. Refer to Appendix C for more information on the layout of the girders during casting.

Upon arrival at Bayshore on 12/12/05, a conversation took place with the plant manager, Alvin Potter, regarding one of the shear connector plates and a conflict with the lifting eye. The lifting eye consists of a series of strands that are bent to form a hook protruding from the top of the girder. See Appendix C for more on the lifting eye. The ends of the lifting eye are tied into the bottom of the reinforcing cage. The steel plates are installed after the concrete has been cast in girder 2 (see Figure 3.2.2). Therefore, it was not possible to cast plate 5 with the top flange because the lifting eye was in the way. In order to solve the problem, a long slot approximately 8 in. by 2 in. was cut in the steel plate. Caution was exercised not to cut too close to any of the existing studs or near a location where a future stud was to be shot. Figure 4.1.1 shows the slot cut in plate 5 after the concrete was cast.

Figure 4.1.1 Slot in Steel Plate for Lifting Eye

During tying of the steel reinforcing cage, problems were encountered when the height of the longitudinal bars and stirrups in the top flange were checked. Per Alvin Potter, the steel reinforcing cage had to be retied because the bars in the top flange were sitting too low. Potter pointed out that the erection of the steel cage is easier if "courtesy" strands are specified in the top flange in the drawings. "Courtesy" strands are prestressing tendons that are tensioned until the strands are straight. This requires only a small force (4 kips to 5 kips) compared to the force in the other tendons after stressing (31 kips). The stirrups in the top flange can then be hung from the "courtesy" strands and tied into place. The bottom two longitudinal mild reinforcing bars can then be tied to the stirrups.

The girders were instrumented with the VWGs and thermocouples on 12/13/05 from approximately 8 a.m. to 12 p.m. The concrete was placed on 12/13/05 at 3 p.m. and the pour lasted approximately 1 hour. The air temperature was approximately 30 °F. Girder 2 was poured first followed by girder 1. Cylinders, 8 in. long and 4 in. in diameter, were filled during the pour for the material testing phase of the study. The QC (quality control) employees at Bayshore gathered the information on the air content in the concrete, the slump of the concrete, and the temperature of the concrete. The air content in the mix was 7.4%, the slump was 8 ½ in., and the temperature of the concrete mix was 54 °F. The concrete mix design is given in Appendix E. The same mix design was used

for the panels. The expected slump in the mix design was between 0 in. and 7 in. The expected air content in the mix design was between 3% and 7%.

One of the last steps consisted of placing the steel plates in the top flange of girder 2. The construction crew had difficulty in getting each steel plate into place. The problem was not associated with the length of the plates. The construction workers had no problem lifting the plates to the top of the formwork. The problem encountered was trying to fit the steel plates in between the formwork. The width of the steel plate was 12 in. and the top flange width of the girder is 12 in. Slight deviations in the width of the plate or width between the side forms will cause the steel plate not to fit. In order to solve the problem, the construction workers had to remove a selected yolk. The yolk is shown in Figure 1.1.2. The yolks tie the top of the forms together to keep the dimension correct and prevent side forms from bowing outward from the hydraulic pressure of the fresh concrete. After the yolk was removed, a come-a-long was used to temporarily secure the side forms while the steel plate was hammered into place. Then the come-along was tightened and the yolk was hammered back in to place. It is recommended for future projects that a non-full width steel plate be used.

The beams were steam cured from approximately 10:00 p.m. on 12/13/05 until approximately 9:00 a.m. on 12/14/05. Cylinders were broken the morning of 12/13/05 and compressive strength of the girders was greater than the required compressive strength at release. Information on the material testing is found in Section 4.3. The prestressing strands were cut on 12/14/05 at 10:30 a.m. Slight cracking was observed on the top surface of the girder at the ends. This cracking was not believed to be due the tensile strength exceeded at the release of the prestressing force. This was checked during the design phase. These may have been shrinkage cracks.

4.1.2 Fabrication of the Panels

The formwork, the reinforcement cage, and the stressing of the prestressing strands for the panels was done on 12/22/05 and 12/23/05. The layout of the prestressing bed is shown in Figure 4.1.2 and Figure 4.1.3. Each of the five panels had a unique strand layout because of the layout of the horizontal shear connector block-out pockets as shown in Appendix B and Appendix C. When consulting with Bayshore engineers

during the production of the shop drawings, an attempt was made to reduce the number of strand patterns. With some effort, the number of strand patterns was reduced down to three. It is considerably cheaper to have one strand pattern so all the panels can be cast at once. If each panel was cast separately, the entire bed would be used for each operation wasting several hundred feet of strand each time a panel was cast. Instead, all of the strands required for all five panels were run the entire length of the stressing bed. When a strand passed through a given panel that did not call for that particular strand in the strand pattern, it was debonded. The strands were debonded by wrapping a plastic tube around the strand. The plastic tubes are shown in Figure 4.1.3.

Figure 4.1.2 Layout of the Stressing Bed for the Precast Panels

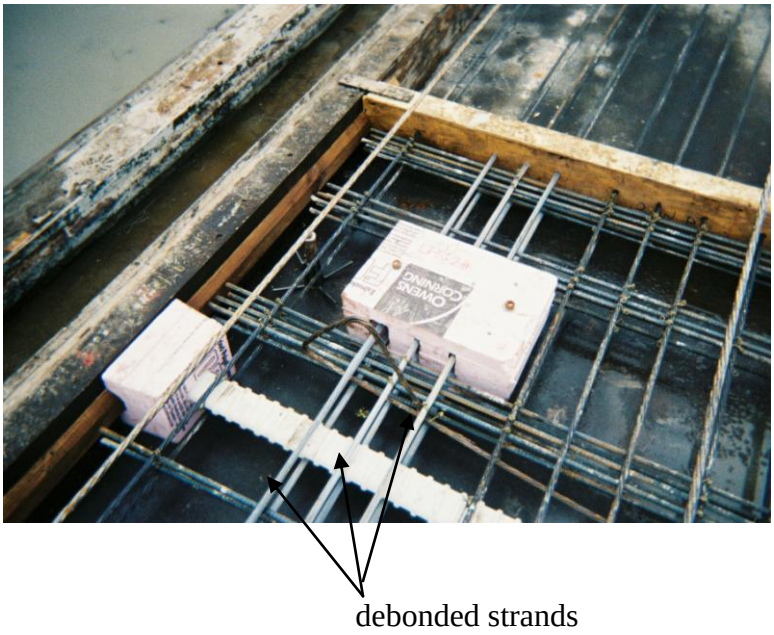

Figure 4.1.3 Formwork for a Transverse Joint

The blockouts for the shear pockets consisted of foam blocks. These blocks are shown in Figure 4.1.2. The transverse joints were formed by attaching wood blocks conforming to the dimensions of the transverse joint to the side form of the stressing bed. This is shown in Figure 4.1.3.

The panels were originally supposed to be cast on 12/23/05. Problems were encountered with pumping standing water out of the casting bed, setting the mild steel within the acceptable tolerances, and the lifting eyes for the panels not having a long enough development length. The pour was delayed until 1/4/06.

On 1/4/06 the panels were instrumented with the VWGs and thermocouples from 8 a.m. until 11 a.m. The pour took place from 3:20 p.m. to 4:10 p.m. The pour started at panel 5 and ended at panel 1. Cylinders, 8 in. long and 4 in. in diameter, were filled during the pour for the material testing phase of the study. Concrete from the first batch was used to fill the cylinders. There were a total of two batches to pour the panels. The QC employees at Bayshore gathered the information on the air content in the concrete, the slump of the concrete, and the temperature of the concrete. The air content in the mix was 5.4%, the slump was 8 in., and the temperature of the concrete mix was 54 °F. The expected slump in the mix design was between 0 in. and 7 in. The expected air content in

the mix design was between 3% and 7%. By the time the concrete was being placed in panel 1, a QC employee noticed that the mix was very fluid. However, no additional cylinders were made.

The stressing bed was steam cured from approximately 10:00 p.m. on 1/4/06 until approximately 9:00 a.m. on 1/5/06 when the strands were originally suppose to be cut. Cylinders were broken the morning of 1/5/06 and compressive strength of the panels was slightly less than the required compressive strength at release. Consideration was given to testing another cylinder later in the day and cutting the strands at that time. However, the uncertainty of the concrete properties in panel 1 and panel 5 was considered. A conversation took place between the QC employees at Bayshore and a Sika chemicals representative. The Sika chemicals representative suggested that the panels be steam cured for an additional day.

On 1/6/06 at 11 a.m. the strands were cut. Considerable time was taken to prepare the stressing bed for releasing the prestressing force. The side forms shown in Figure 4.1.2 were welded to the bottom of the casting bed during the pour. These forms had to be knocked loose to allow the panels to expand laterally due to Poison's effect when the strands are cut. The blockouts for the shear pockets were also originally bolted to the bottom of the casting bed to keep them in place during the pour. The bolts had to be removed prior to the strands being cut. Once the strands were cut, the debonded strands were cut out of the shear pockets.

4.1.3 Placement of the Precast Panels on the Girders

When the panels and girders were delivered to the Virginia Tech Structures Laboratory, they were temporarily stored until construction was ready to begin. The girders were set on the reaction floor of the lab and the panels were stacked on top of each other. Timber blocks were placed in between the panels in the stack to prevent damage to the lifting eyes. This is shown in Figure 4.1.4.

Support beams were bolted to the floor beams. Bearing pads were placed on top of the support beams for the girders to bear on. The bearing pads were placed so the center-of-bearing to center-of-bearing span was 39 ft and the center-to-center spacing of the two girders was 8 ft. Each girder was placed on the bearing pads using two 5-ton

overhead cranes. The diagonal distances between the girders were measured to make sure the girders were square with one another.

The panels were placed on the girders on 3/16/06 from 3:00 p.m. until 4:40 p.m. Three members of the Virginia Tech research team completed the operation. Panel 4 was placed, followed by panel 1, panel 3, panel 2, and panel 5. The order of the placement of the panels was based on the order in which the panels were stacked in the lab. Timber 2 x 4s were placed on top of the girders prior to placing the panels. The leveling bolts were installed at a later date. The wood blocks that the panels originally rested on are shown in Figure 4.1.4.

The hooked reinforcing bars greatly hindered the placement of the panels. The shear pockets were only made 2 in. longer on each side of the outside hooked reinforcing bars. The hooked reinforcing bars were placed within an acceptable tolerance, but not exactly what the shop drawings called for. Therefore, there was less than 2 in. of play to use when placing the panels. This proved to be especially difficult when placing the panels at the live end where the transverse joints were a male-female configuration. Each panel had to be placed on top of the girders and slid together. In many cases, the length of the male protrusion in the male-female joint of 1 in. was very close to the distance from the edge of a shear pocket to the edge of the first hooked reinforcing bar in a shear pocket.

Using the grouted female-female joint allows for the panels to be placed directly on the girders, without having to slide the panels together. The size of the gap between adjacent panels with this joint configuration can be adjusted during construction to account for any small errors that occurred during the fabrication process.

Figure 4.1.4 Girders with Wood Blocks in Place for Panel Erection

The detail with the steel plate and shear studs cast with the top flange of the girder proved to be easy to deal with when placing the panels. Since there were no studs to interfere with the placing of the panels, the panels could slide around freely on girder 2.

The leveling bolts were installed after all the panels were in place. A total of 16 leveling bolts were installed. Typically three leveling bolts are used for each panel. Three leveling bolts are used instead of four leveling bolts to avoid placing a torsional moment on the panels. Four leveling bolts were required in panel 3 because of the shear pocket layout. An air gun was used to install the leveling bolts. Several of the bolts could not be installed immediately because the coil inserts were not flush with the bottom of the panels. This problem was solved by using a jack hammer to widen the hole above the coil insert. This allowed the leveling bolt to be installed at the same angle as the coil insert.

Steel plates approximately 3 in. x 3 in. x ½ in. were placed on top of the girders where the leveling bolts bear on the girders, as shown in Figure 4.1.5. This prevents the leveling bolt from crushing the concrete. Not using the steel plates could cause the leveling bolt to crush the concrete in the area it was bearing, creating a small hole in the top flange of the girder. With the leveling bolt in a hole, a significant frictional force would develop between the leveling bolt and girder during the post-tensioning operation. This would introduce problems with a portion of the post-tensioning force being transferred to the girders during the post-tensioning operation.

Figure 4.1.5 Leveling Bolt Bearing on a Steel Plate

As soon as the leveling bolts were adjusted so the panels were close to the final elevations, the wood blocks were removed. Surveying equipment was used to adjust the panels to their final elevation.

After the panels were set to their final elevations, the post-tensioning strands were fed through the ducts to assure the misalignment of the ducts between adjacent panels was kept to a minimum and all four strands could fit through each duct. Long ropes were then tied around each group of strands. The strands were pulled though the dead end until the strands were only present in panel 1, panel 2, and panel 3. This was done to allow panel 4 to be removed for the epoxying of the male-female joints. Once panel 4 was back in place, the rope could be used to quickly pull the strands back through panel 4 and 5 so the stands could be post-tensioned shortly after the epoxy was placed.

4.1.4 Grouting the Female-Female Transverse Joints

The grouted female-female joints were formed with ¾ in. plyform. Three sheets of plyform were used per grouted joint to form up the bottom surface, each 4 ft x 1 ft-6 in. x ¾ in. One sheet of plyform 1 ft -6 in. x 8 in. x ¾ in. was used to form up each side. Weather stripping was placed around any edges where leaks could possibly occur. The ducts were coupled together with duct tape and small segments of extra plastic duct to bridge the gap. The blockouts for the post-tensioning ducts in the female-female joints are shown in Appendix B and Appendix C. The size of the blockout was 6 in. by 9 in. on

each side of the joint. This allowed enough room to place the duct coupler in the joint and wrap duct tape around the duct segments to prevent grout from leaking in. A duct coupler consisted of a small segment of an extra section of the post-tensioning duct that was shipped with the panels and girders. The coupler could be cut to a desired length to splice the ducts in the two panels together.

An attempt was made to form up the bottom surface of the joint from only the top of the deck surface. This type of forming system would be very advantageous in the field to reduce operations from below. Holes were drilled in the plyform at 30 in. center-to-center. A rope was fed through each hole and a knot was tied at the end so the plyform could be suspended from the ropes. The other end of the rope was fed through a pipe approximately 2 ft long with a hole drilled in the middle. The plyform was turned on it's side, fed through the 1 ½ in. gap between the panels, dropped underneath the panels suspended from the ropes, and then pulled flush against the bottom surface of the panels. In order to try to create a tight seal between the panels and plyform, the pipes were rotated so any slack in the ropes would be taken up by the pipe. Clamps were then used to keep the pipes from turning, allowing the rope to unravel. It was found that this process did not work well. The problem encountered was trying to get the plyform to fit tightly enough against the bottom surface of the panels so the grout would not leak. Instead of using rope, thin, threaded metal rods were used. This required one of the Virginia Tech research team members to hold the plyform in place under the bridge while feeding the threaded metal rod through the hole in the plyform to another person on top of the bridge deck. The person would then slide a washer and nut over the top of the rod and tighten it. The excess length of the threaded metal rod was then cut off. The steel pipe with the threaded metal rod is shown in Figure 4.1.6 in a completed joint.

Figure 4.1.6 Grouted Female-Female Joints with Steel Pipe and Threaded Metal Rod Forming Alternative

The grout was poured on 3/28/06. The grout used for the female-female joints was Five Star® Highway Patch. The product data sheet is found in Appendix F. This grout was selected based on a recommendation provided by Wallenfelsz[29]. The grouting operation took place from 1:00 p.m. to 1:45 p.m. Three members of the Virginia Tech research team completed this operation. The hopper used for mixing the grout is capable of holding and mixing 2 - 50 lb bags of grout. The hopper was placed on top of the bridge deck within 5 – 10 ft of the transverse joints. One person mixed the grout in the hopper, one person poured the grout into the joints, and the other person helped pour bags of grout in to the hopper, vibrate the grout in to place, and level off the top surface of the grout to be even with the top of the deck. Because the grout sets up so quickly, minimal leakage occurred through the bottom formwork.

4.1.5 Epoxying of the Male-Female Transverse Joints

The transverse joints were epoxied on 4/5/06 from 1:20 p.m. to 1:50 p.m. Sikadur 31 Slow Set – SBA was used. This is an epoxy specially formulated for segmental bridges, and was provided at no cost to the research team. Panel 4 was suspended approximately 1 ft above its final elevation. Panel 4 was chosen in order to minimize the number of panels moved during the operation. Expansive foam was placed around the

perimeter of the post-tensioning ducts. This was done to prevent epoxy from leaking into the duct. This operation is shown in Figure 4.1.7.

Epoxy was then placed on each side of panel 4 using chemical resistant gloves. This procedure is shown in Figure 4.1.8. No epoxy was applied to the other surfaces of the male-female joints on panel 3 and panel 5. Once the panels were in place, the rope was used to pull the strands back through the ducts in panel 4 and panel 5. Three members of the Virginia Tech research team performed the epoxying operation. One person operated the crane to lift panel 4 and placed expansive foam around the edges of the ducts while the other two people placed epoxy on the edges of panel 4.

After the procedure was completed, the ends of the transverse joints in the overhangs were not in firm contact. At the time, it was believed these small gaps would close up after the post-tensioning operation was completed.

Figure 4.1.7 Expansive Foam Being Placed Around the Post-tensioning Ducts

Figure 4.1.8 Epoxy Being Placed on a Male-Female Joint

4.1.6 Post-Tensioning Operation

The first six strands were post-tensioned on 4/5/06 from 2:20 p.m. to 4:00 p.m. The last six strands were post-tensioned on 4/7/06 from 9:30 a.m. to 2:30 p.m. Six strands tensioned to approximately 68% of the guaranteed ultimate tensile strength results in a pressure just over 130 psi on the transverse joint. Typically, 50 psi is considered a minimum to adequately seat an epoxied joint. The strands were labeled strand 1 through strand 12. Strand 1 was closest to girder 1 and Strand 12 was closest to girder 2. The strands were stressed in the following order: strand 6, strand 7, strand 2, strand 3, strand 10, strand 11, strand 5, strand 8, strand 9, strand 12, strand 1, strand 4. The strands were tensioned in this order to keep the longitudinal stress distribution in the deck as uniform as possible in the transverse direction. Three people were used when the first six strands were stressed and one person was used when the last six strands were stressed. Before each strand was released, a mark was spray painted on the dead end of the strand a known distance from the edge of the panel. This mark was measured again after the force was released to determine the dead end seating loss.

Typically, strands in flat four strand ducts are stressed individually with a special mono-strand jack. However, since the mono-strand jack was not used for the lab mockup, a stressing chair had to be used to tension each strand. The stressing chair was fabricated at the Virginia Tech Structures Lab and consisted of three steel tubes welded

together. The stressing chair is shown in Figure 4.1.9. Two square steel tubes, 4 in. (O.D.) x 3 in. (I.D.) x 1 ft-6 in. formed the columns that bore on the panels and one square steel tube 4 in. (O.D.) x 3 in. (O.D.) x 2 ft-6 in. formed the beam of the stressing chair.

The strands were fed though a long slot which had been cut out of the beam of the stressing chair. The stressing chair had to be supported on a stack of masonry bricks and wood blocks to get the elevation of the stressing chair to be at the same elevation as the strands. A shim plate was placed against the beam of the stressing chair to conform to the angle the prestressing strand that protrudes from the anchor assembly. A hydraulic ram, a small metal tube used as a spacer, a load cell, and a chuck were then placed over the strand. Each strand was stressed to approximately 28 kips. This was measured with a load cell. Twenty eight kips is approximately 68% of the guaranteed ultimate tensile strength of a ½ in. diameter grade 270 strand. A load cell was also placed at the dead end of one strand in each post-tensioning duct. After the full stressing force was achieved, the wedges were inserted into the anchor plate and tapped in with a hammer. The force was then gradually released by the hydraulic ram.

Using the data from the dead end and live end load cells as well as the measured seating loss at the live end, the variation of the force in each strand along the length of the bridge can be calculated. The force along each strand is shown in Figure 4.1.10. The average force shown in Figure 4.1.10 is the average of all the data points along all the strands. This average force is constant along the length of the bridge. A table summarizing the calculations can be found in Appendix G. The force profile in each strand was calculated as follows

1. The force at the dead end and live end was obtained from load cells. It was assumed that the force measured by the load cell on dead end represented the dead end force for each strand in the post-tensioning duct.
2. The loss in force due to the seating loss at the live end was:

$$\Delta P_a = 2\sqrt{\frac{P_J - P_D}{L} E_{ps} A_{ps} \Delta_a} \qquad [4.1]$$

where,

ΔP_a = loss in force at the live end (kips)

P_J = jacking force at the live end (kips)

P_D = force at the dead end (kips)

L = total length of tensioned strand (in.)

E_{ps} = modulus of elasticity of the prestressing strand (ksi)

A_{ps} = area of one prestressing strand (in^2)

Δ_a = anchor loss measured at the live end (in.)

3. The length from the live end where the maximum force occurs was:

$$l_{\max} = \frac{2A_{ps}E_{ps}\Delta_a}{\Delta P_a} \qquad [4.2]$$

4. The maximum force that occurred at l_{max} was:

$$P_{\max} = P_J - \frac{P_J - P_D}{L} l_{\max} \qquad [4.3]$$

5. The force increased linearly from P_J - ΔP_a at the live end up to the P_{max} at l_{max} from the live end. The force decreased linearly from P_{max} at l_{max} to P_D at the dead end. These assumptions were used to determine a force profile along the length of each strand.
6. The elastic shortening losses at selected increments along the length of a strand were calculated. Because none of the strands were tensioned simultaneously, the first strand that was tensioned experienced elastic shortening losses from the remaining 11 strands that were tensioned. This was calculated by

$$\Delta f_{pES}(x) = \frac{E_p}{E_c} \sum_{i=1}^{\#\_strands} \frac{P(x)}{A_{deck}} \qquad [4.4]$$

where,

E_c = modulus of elasticity of the concrete in the panels at the time the strands were tensioned (ksi)

P(x) = force in the prestressing strand at a distance x from the live end (kips)

A_{deck} = cross sectional area of the deck (in^2)

7. The relaxation losses at selected increments along the length of a strand were calculated

$$\Delta f_{pR1}(x) = \frac{\log(24t)}{45}\left(\frac{\frac{P(x)}{A_{ps}}}{f_{py}} - 0.55\right)\frac{P(x)}{A_{ps}} \qquad [4.5]$$

where,

f_{py} = nominal yield stress of the prestressing strand (ksi)

t = time from the tensioning of strands until the end of the post-tensioning operation (days)

The wobble coefficient is calculated from Equation 2.104. The average wobble coefficient in the 12 strands is 0.001 /ft. Using the force profile for each strand along the length of the bridge, the force and stress across each transverse joint was calculated. These forces and stresses are shown in Table 4.1.1. Refer to Figure 3.2.1 for the locations of the transverse joints.

The deflections of the system were measured with dial gages before and after the deck was post-tensioned. There was no change in the deflection, indicating that none of the post-tensioning force was transmitted to the girder through the leveling bolts. The steel plates the leveling bolts bore on provided a smooth enough surface to allow the panels to slide when the force in the strands was applied.

After all the strands were tensioned, the ends of the transverse joints were still not in complete contact with one another. The panels were in firm contact at the center of the transverse joints. No epoxy seeped out of the joint during the post-tensioning operation. After further observation, it appeared that the ends of panels that make up the transverse joints were bowed. This could have been caused by bowed formwork during the casting operation. It is believed that a good seal at a male-female joint cannot be achieved if there is any bowing in the panels. In order to solve the problem encountered, additional epoxy was injected in to the male-female joints on 5/12/06.

Figure 4.1.9 Stressing Chair used for Lab Mockup

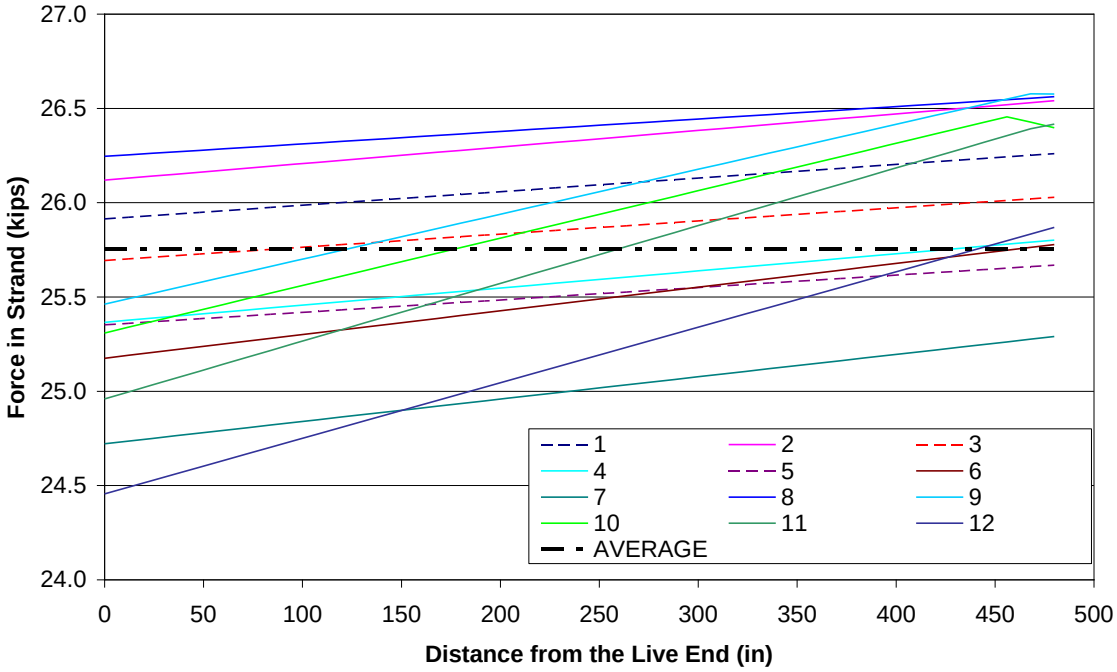

Figure 4.1.10 Variation in Prestress Force for the Strands in the Post-Tensioning Duct Immediately After the Post-Tensioning Operation

Table 4.1.1 Initial Force and Stress Across Each Transverse Joint

Transverse Joint	Force (kips)	Stress (psi)
Outside Epoxied	306	266
Inside Epoxied	308	268
Inside Grouted	310	269
Outside Grouted	312	271

4.1.7 Shooting the Shear Studs

After the post-tensioning operation was performed and before the haunch and shear pockets were poured, the shear studs were shot to the steel plates on girder 2. This operation was performed by one member of the Virginia Tech research team. In order to properly weld the shear studs to the plates, the plates must be connected to one another by small, steel bars. This allows the current to flow from one plate to another. Ceramic ferrules and dirt were removed from the top surface of the girders with an air hose before pouring the haunch.

4.1.8 Grouting the Haunch and Shear Pockets

The formwork for the haunch was placed on 4/11/06 from 10:30 a.m. to 12:00 p.m. and from 5:30 p.m. to 8:10 p.m. Plyform sheets 4 ft x 7 in. x ¾ in. were used to form up the sides of the haunch. Weather stripping was placed between the bottom of the panel and top of the plyform to seal the gap at this interface. The plyform was secured to the girder with concrete stud anchors spaced at approximately 14 in. This is shown in Figure 4.1.11.

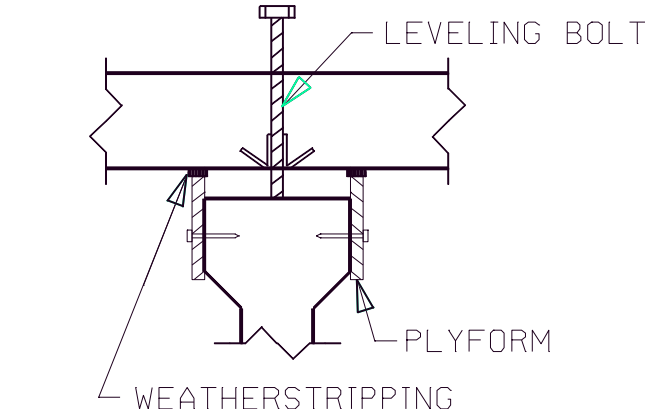

Figure 4.1.11 Formwork Detail for Haunch

The haunch and shear pockets were poured on 4/13/06. The haunch and shear pockets for girder 2 were poured from 2:10 p.m. to 2:55 p.m. The haunch and shear pockets for girder 1 were poured from 3:10 p.m. to 3:40 p.m. The direction of each pour was from the dead end to the live end. Grout cubes were filled from the first few wheelbarrows for the girder 2 pour. The grout placed over girder 1 was considerably more fluid than the grout placed over girder 2.

The grout was mixed in a gasoline powered mortar mixer outside because of the danger of inhaling powder and fumes in confined areas. The grout used was Five Star® Highway Patch, the same grout used for the female-female transverse joints. After mixing, each batch of grout was then placed in a wheelbarrow and transported to the bridge, about 50 ft to 75 ft away, via a forklift. The forklift placed the wheelbarrow on the bridge deck and the grout was poured into a shear pocket directly from the

wheelbarrow. Two wheelbarrows were used during the operation. The grout was vibrated into place. Eight members of the Virginia Tech research team were used to perform this operation. The crew consisted of three people mixing and transporting the grout, two people using wheelbarrows to place the grout into the shear pockets, one person vibrating the grout, and one person shoveling the grout into the shear pockets. One person was also responsible for the grout cubes and pictures.

Many of the early batches of grout were stiff and set rapidly. After mixing several batches of grout, the members of the research team responsible for mixing and transporting the grout were able to produce fairly consistent mixes that were not too stiff.

The formwork was removed on 4/14/06 from 4:30 p.m. to 6:10 p.m. This was done by one member of the Virginia Tech research team. Many of the concrete stud anchors were not easy to remove, so a crow bar, screwdriver, and hammer were used to aid in the removal.

Although the grout was vibrated at each shear pocket to help the grout flow through the haunch to the next shear pocket, a few locations were not completely filled with grout. The two most noticeable locations where this happened were at midspan of girder 1 and girder 2. There were gaps in the haunch in between the shear pockets that were almost the entire depth of the haunch. The length of the gaps was about 4 in. Since these gaps occurred at favorable locations where shear stresses are close to zero, the gaps were not filled with grout.

The leveling bolts were removed on 4/17/06. This process was performed by one member of the Virginia Tech research team. The process took one hour to complete. The bolts had to be removed by using an air powered gun. The process for removing a bolt leaves a void in the haunch and a hole that runs from the top of the deck to the top of the girder. The holes were not filled with grout, however in a field application they would be.

4.1.9 Grouting the Post-Tensioning Ducts

A hand powered Kenrich grout pump was used to grout the post-tensioning ducts. The operating pressure of the pump was 15 psi with an output capacity of 48 cubic feet per hour. Three members for the Virginia Tech research team were used for this

operation. One person operated the hand pump and two people mixed the grout. A 5 gallon bucket was used to mix the grout and transfer it to the reservoir of the hand pump. Five Star® Special Grout 400 with Devoider® Automatic Cavity Preventer was used to fill the post-tensioning ducts. This is a special grout used primarily for this type of application.

The first attempt at grouting the ducts took place on 4/25/06 at 3:00 p.m. The grout was first pumped in at the dead end in the middle duct. The first reservoir from the pump was pumped in without a problem. It was soon determined that the time it took to mix the grout in the 5 gallon bucket would be insufficient to complete the process because the batches were too small. The mortar mixer was then used for the next batch. The time it took to get the mortar mixer into place and mix the next batch of grout was about 10 minutes.

Grout was pumped in and a leak was observed. The grout was leaking through a gap between two of the wedges in the post-tensioning anchor plate. The grouting operation was stopped for the day. Since the first grouting attempt showed that the hand pump does create enough pressure to spring a leak between the wedges or any other gaps at the anchor plate, the blockouts for the post-tensioning anchorage device were completely grouted at the live end. At the dead end, the gaps were sealed with an expansive foam. The blockouts for the post-tensioning anchorage device at the dead end could not be filled with grout because of the load cells that were in place.

The grouting process was completed on 4/27/06 from 8:00 a.m. to 9:00 a.m. The grout was pumped in from the live end. Several small leaks occurred at the epoxied male-female joints as the grout was being pumped through. Note that this occurred prior to the additional epoxy injected into the transverse joints on 5/12/06, as mentioned in Section 4.1.6. No leaks occurred at the grouted male-female joints as the grout was pumped into the post-tensioning ducts.

The grout was able to flow through the ducts and out of the vent on the dead end of the bridge for the outer two ducts. However this did not occur for the middle duct. This was because the middle duct was partially filled with grout at the dead end from the first grouting attempt on 4/25/06. Therefore, there was no guarantee that the duct was completely filled after the grouting process was stopped.

This completed the construction phase of the research program. Other operations performed in the field that were not performed on the lab mockup include but are not limited to:

1. Installing conduit,
2. Milling the surface of the deck,
3. Placing a barrier rail,
4. Placing a wearing surface,
5. Grinding the surface of the strands to be flush with the edges of the precast members.

4.1.10 Recommendations based on Constructability Study

This section provides recommendations for the precast deck panel system regarding the strand pattern, the transverse joint configuration, the shear connectors, and the post-tensioning operation. These recommendations are based on the results of the constructability study.

4.1.10.1 Strand Pattern

When laying out the strand pattern for the precast panels, the panel production and stressing bed layout should be considered. Minimizing the number of strand patterns allows for more panels to be cast in a stressing bed at one time with fewer strands having to be debonded in panels that do not require a specific strand.

4.1.10.2 Transverse Joints

From purely a construction standpoint, the grouted female-female joint is better than the epoxied male-female joint. Neither of the joints takes significantly more time than the other to fabricate. The female-female joints allow the panels to be placed on the girders without having to slide the panels together while avoiding conflicts with the horizontal shear connector layout. The female-female joint configuration is also more forgiving if the edges of the panels are bowed. The variation in the gap between the adjacent panels along the length of the joint caused by bowing can be compensated for by allowing at least a ½ in. gap between the panels at the joint. A gap of at least 1 ½ in. is

recommended if the grout is going to be vibrated in to place. The one advantage that the male-female joint has is that it is more aesthetically pleasing if an overlay is not going to be provided on the bridge deck. In the majority of cases, an overlay is provided.

4.1.10.3 Shear Connectors

The steel plate with post-installed shear studs is a better detail for the system to resist the horizontal shear forces compared to the hooked reinforcing bars, from a construction standpoint. From a fabrication standpoint, it is quicker to place the steel plate with the shear studs in the wet concrete than tying the hooked reinforcing bars in with the reinforcing steel cage.

The steel plate detail allows the leveling bolts to bear directly on the girders since the majority of the top surface of the girder is steel. Girders with hooked reinforcing bars need to have a steel plate placed on top of the girder so none of the post-tensioning force is transferred to the girder via a frictional force that develops between the leveling bolt and girder.

The steel plate detail with the post-installed shear studs also allows the panels to be moved during erection without having to worry about conflicts with the shear connector layout. Erecting panels with shear connectors already in place may damage the shear connectors if the panels collide with them. The steel plate detail is also better from a safety standpoint since the tripping hazard is eliminated. When determining the size of the steel plate to place in the top flange, it is recommended that the width of the steel plate be at least 1½ in. smaller than the width of the top flange of the girder so problems will not occur trying to fit the plate between the formwork for the top flange. Additionally, this provides cover to protect the steel plate from the corrosive environment.

4.1.10.4 Post-Tensioning Operation

During the post-tensioning operation, the force may be partially transferred from the deck to the girders via the leveling bolts. This happens if the interface between the leveling bolt and girder is rough enough to develop a significant frictional force. This frictional force can be reduced by using lubricated steel plates for the leveling bolts to

bear on. Dial gages, or similar instrumentation to measure the deflection of the system, can be used to monitor any change in deflection that may take place during the post-tensioning operation. In place of instrumentation to measure any change in deflection, strain gages are just as effective in detecting any force that may be transferred to the girder during the operation. Surveying equipment may be used to detect any force transfer to the girder when the use of strain gages or dial gages is not feasible.

4.2 Time Dependent Behavior

4.2.1 Time Dependent Behavior During Fabrication

Figure 4.2.1 shows the strains in Girder 1 up until 24 minutes after the strands were cut and Figure 4.2.2 shows the temperature in Girder 1 up until 24 minutes after the strands were cut. All strains reported in subsequent figures have been adjusted for strains produced from the thermal expansion of the steel material in the vibrating wire gage with respect to the surrounding concrete. Recall that Table 3.2.2 in Section 3.2.2 defines the notation for each gage presented in the legend of the following figures. The strains in the girder increased fairly linearly up until about 0.35 days from the moment the concrete was cast. From this point up until the strands were cut, the strains decreased as the temperature increased.

The temperature increased steadily causing temperature induced strains to develop in the girder. The temperature then began to drop around 0.79 days from the moment the concrete was cast. This coincides with the time the formwork was removed. It is difficult to translate strains into stresses prior to cutting the strands. Temperature evolution, strength gain, elastic modulus gain, bond development, and other effects make it difficult to determine the stress in the concrete immediately prior to cutting the strands.

At release of the prestressing strands, Figure 4.2.1 shows that the net increase in compressive strain is greater in the bottom of the girder than in the top of the girder, as expected. Similar behavior is observed for girder 2 during casting, as shown in Appendix H. The average elastic loss in girder 1 using the vibrating wire gage data was -8.56 ksi. The average elastic loss in girder 2 using the vibrating wire gage data was -9.31 ksi. The elastic shortening losses were calculated by first averaging the elastic shortening strains from two vibrating wire gages. The two vibrating wire gages were located at the centroid

of the strand group at the 1/3 points of the girder span, as discussed in Section 3.2.2. The average strain was then multiplied by an elastic modulus of 28,500 ksi. The predicted elastic loss calculated during the design phase was -9.62 ksi. This calculation is shown in Appendix A.

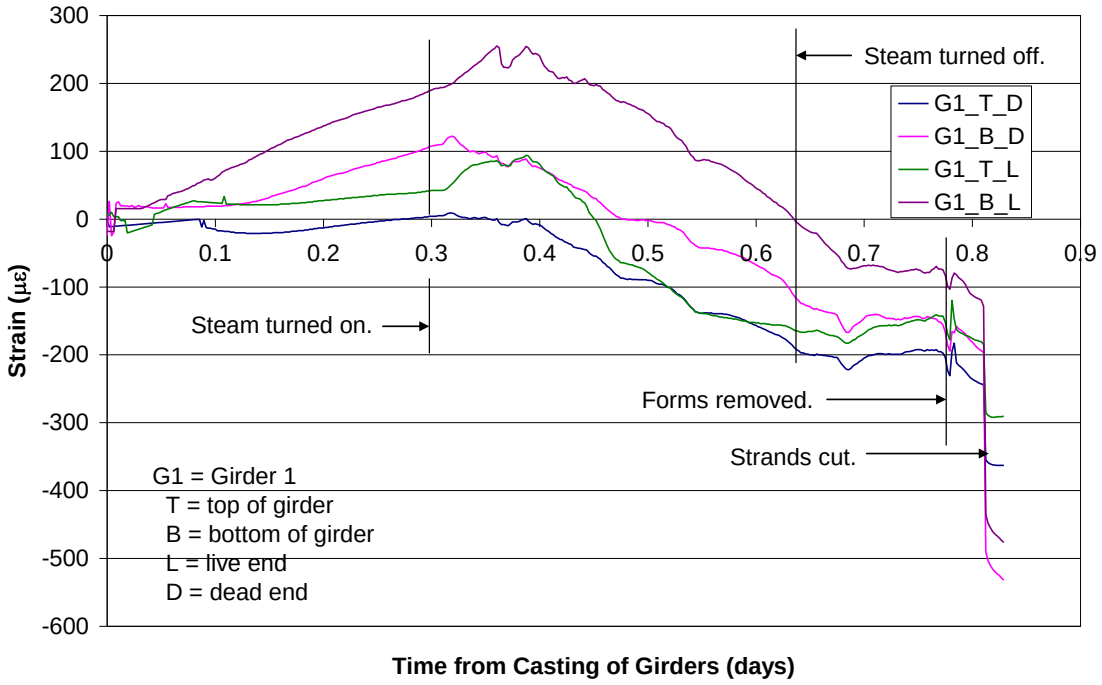

Figure 4.2.1 Variation of Strain with Time During Casting and Strand Release for Girder 1.

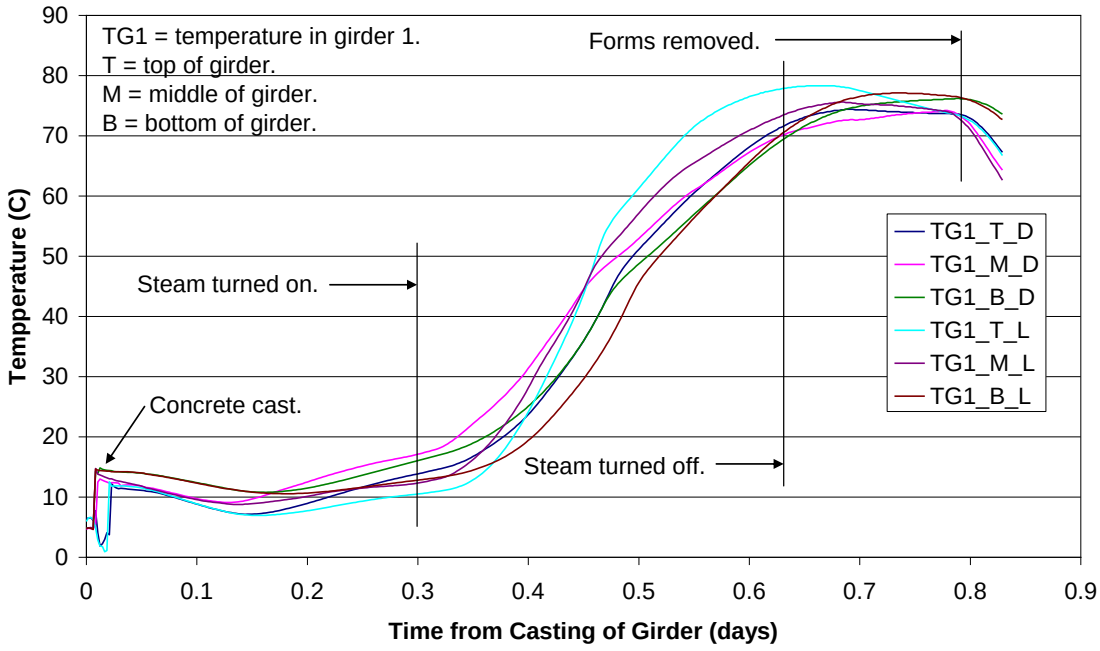

Figure 4.2.2 Variation of Temperature with Time During Casting and Strand Release for Girder 1.

The temperature in the panels up until 15 minutes after the strands are cut is shown in Figure 4.2.3. All the thermocouples were in agreement with one another from the time the steam was turned on in the stressing bed until day 1.5. At this point, the temperature in panel 4 started to decrease at a faster rate than the temperature in panel 2. Panel 4 may have been uncovered before panel 2 after the steam was turned off. This can't be confirmed since none of the Virginia Tech research team members were present at the time. Around day 1.9, the temperatures in the panels increased slightly. This may have been due to a significant rise in the ambient temperature which caused the internal temperature to temporarily rise. Figure 4.2.4 shows the strains during the duration of the casting operation. As discovered with the girders, the increase in temperature caused temperature induced strains to develop in the panels. This was expected for members that are confined during the curing process. The strains started to increase (decrease in compressive strain) as the temperature decreased from day 1.6 to day 1.9. The strains associated with the elastic shortening of the panels from the prestress force are not picked

up by the VWGs since the VWGs were oriented perpendicular to the prestressing strands. The purpose of the VWGs was to study the longitudinal strains in the bridge deck.

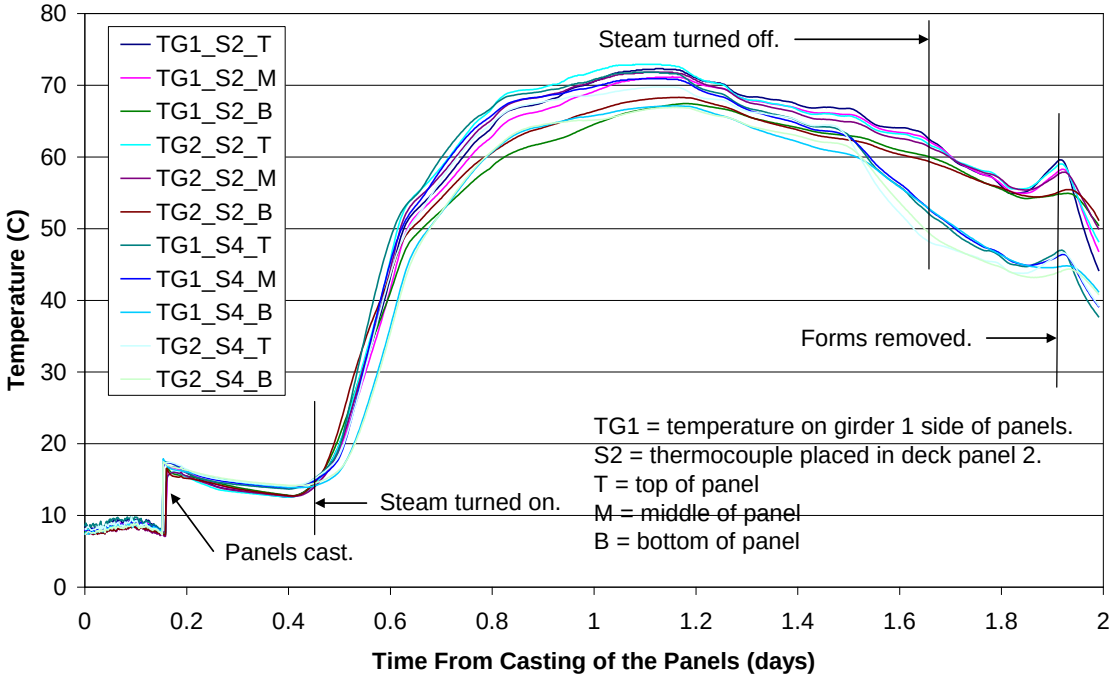

Figure 4.2.3 Variation of Temperature with Time During Casting and Strand Release for the Precast Panels

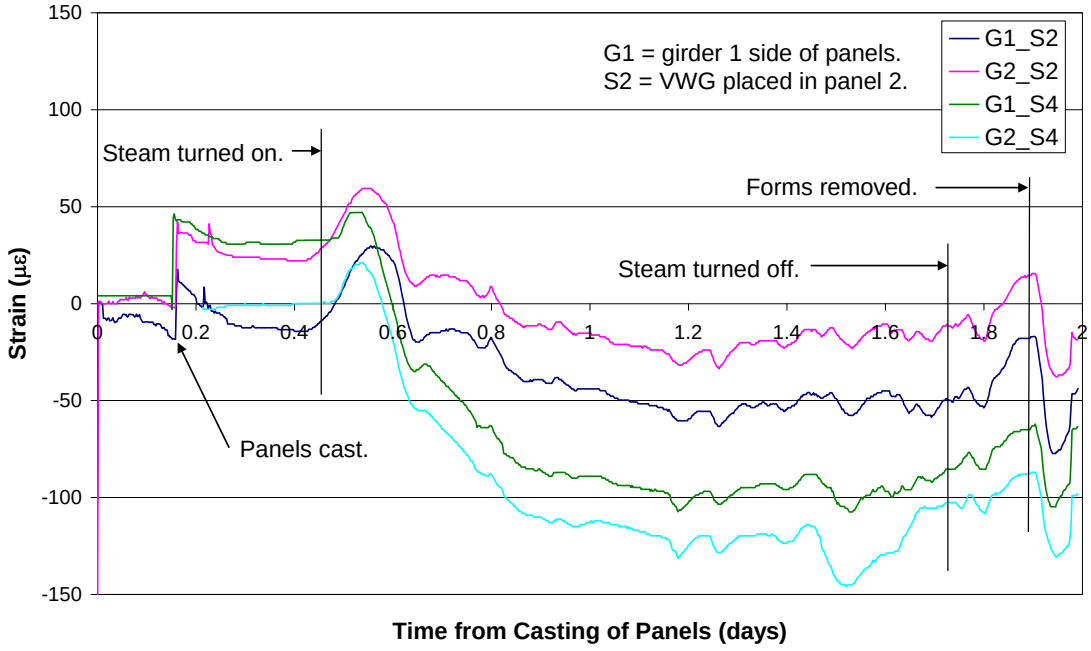

Figure 4.2.4 Variation of Strain with Time During the Casting and Strand Release of the Precast Panels

4.2.2 Time Dependent Behavior During Construction

After the panels and girders were shipped to the Virginia Tech Structures Lab, the Campbell system was reattached to the lab specimen. Data from the VWGs was gathered from the time the panels were placed on the girders until the end of the time dependent study. Figure 4.2.5 displays the strains in girder 1, Figure 4.2.6 displays the strains in girder 2, and Figure 4.2.7 displays the strains in the panels during the time intervals in the lab. Figure 4.2.8 displays the curvature in girder 1 during the time intervals in the lab. Notice that the start of the analysis in the lab is measured from the time the girders were cast. Problems were encountered with gage G2_B_D throughout the study. The gage stopped working at day 118. The general behavior of each member will be discussed here along with the effects that key construction stages have on the system. The sign convention is positive (+) for tensile strains and tensile strain increments and negative (-) for compressive strains and compressive strain increments. The sign convention for curvature is positive (+) when the deck is in compression and the bottom of the girder is

in tension and negative (-) when the deck is in tension and the bottom of the girder is in compression.

During the 92nd day from the time the girders were cast, the panels were placed on the girders. The elastic strains associated with adding the panels are shown by an instantaneous gain or loss in strain in the plots. Table 4.2.1 compares the average VWG strains in the girders to the expected strains in the girders. The average curvature in girder 1 was 4.12 με/in. The expected curvature in girder 1 was 5.17 με/in.

Table 4.2.1 Comparison of Measured and Calculated Strains for Panel Placement on the Girders

	VWG Measurement (με)		Calculated (με)	$\varepsilon_{VWG\_avg}/\varepsilon_{calc}$
VWG Location	Girder 1	Girder 2		
Top	-62	-56	-72	0.82
Bottom	27	32	40	0.74

The expected elastic strains were calculated using the equation

$$\varepsilon_{predict} = \frac{M_{p\_DL} y_{VWG}}{I_g 57\sqrt{f'_c}} \qquad [4.6]$$

where,

M_{p_DL} = dead load moment of the panels at the location of the vibrating wire gages (VWG), 13 ft-4 in. from the supports (k-in)

y_{VWG} = distance from the centroid of the girder to the location of the top or bottom vibrating wire gage (in.)

I_g = second moment of area of the girder (in^4)

f'_c = compressive strength of the concrete in the girder at the time the panels are placed (psi)

Equation 4.6 was derived using the flexure formula and Hooke's Law[50]. Linear, elastic behavior of the concrete is assumed for the flexure formula and Hooke's Law. The expected curvature was calculated using the equation

$$\kappa_{predict} = \frac{M_{p\_DL}}{I_g 57\sqrt{f'_c}} \qquad [4.7]$$

Linear, elastic material behavior is assumed when calculating the curvature in Equation 4.7[50].

One of the first trends observed in the data in Figure 4.2.5 and Figure 4.2.6 is that the steel plate in the top flange in girder 2 apparently does act as compression reinforcement by reducing creep strains. The creep strains the girders experience were calculated from immediately after the panels were added to the end of the analysis. The total time increment is 54 days. The average creep strain associated with the two VWGs in the top flange on girder 1 was -107 με. The average creep strain associated with the two VWGs in the top flange of girder 2 was -88 με. This was a small, but noticeable difference in strain. Although there are five separate, discontinuous steel plates in girder 2, they still function as compressive reinforcement to some degree.

These creep strains are not only associated with the dead load of the panels, but also the dead load of the haunch, as well as from additional forces and moments introduced in the girder over time caused by differential creep and shrinkage in the composite system. Creep associated with the dead load of the composite system will cause the system to deflect downward. Creep associated with the prestressing in the girders will cause the system to deflect upward. Creep associated with the change in the post-tensioning force in the deck after composite action is present will cause the system to deflect downward. Differential shrinkage will cause the system to deflect downward since the panels were cast after the girders. These individual quantities are difficult to extract from the total creep and shrinkage measured by the VWGs.

At day 103, the strains in the girders indicate the girders cambered up for a period of approximately 8 hours. The panels were being repositioned during this time to get them to their final elevations. The removal of a panels caused the girders to camber upward. This operation was done prior to the grouting of the female-female transverse joints.

At day 112, the strains indicate the girders cambered upward for a period of 7 hours, then cambered back to approximately their original position. This elastic deformation was from the temporary removal of panel 4 to prepare the lab mockup for the post-tensioning operation. Table 4.2.2 shows the measured and calculated strains associated with the removal of panel 4. The change in curvature in girder 1 was 1.57

με/in, compared to the expected change in curvature of 1.72 με/in. The deformation does not appear to effect the rate at which the system creeped after day 112 compared to before day 112, so this event does not appear to have an impact on the results.

Table 4.2.2 Comparison of Measured and Calculated Strains for Removal of Panel 4

	Measured (με)		Calculated (με)		$\varepsilon_{VWG}/\varepsilon_{calc}$ (Live End)	$\varepsilon_{VWG}/\varepsilon_{calc}$ (Dead End)
VWG Location	Live End	Dead End	Live End	Dead End		
Top	24.2	11.7	28.3	15.7	0.86	0.75
Bottom	-10.6	-4.7	-15.7	-8.7	0.68	0.54

During day 113 and day 115, the first six strands and last six strands were tensioned in the post-tensioning ducts of the panels. There was some concern prior to the operation that some of the post-tensioning force might be transferred to the girders via frictional forces developed at the interface between the leveling bolts and the top surface of the girders. However, there was no indication that any significant force was transferred to the girder, as shown in Figure 4.2.5 and Figure 4.2.6.

As can be seen in Figure 4.2.7, the average elastic strain in the four VWGs in the deck panels associated with the post-tensioning was -75 με. The expected elastic strain associated with the post-tensioning force was -66 με. The creep strains the panels experience were calculated from immediately after the completion of the post-tensioning operation to the end of the analysis. The total time increment was 34 days. The average creep strain associated with the four VWGs in the panels was -40 με.

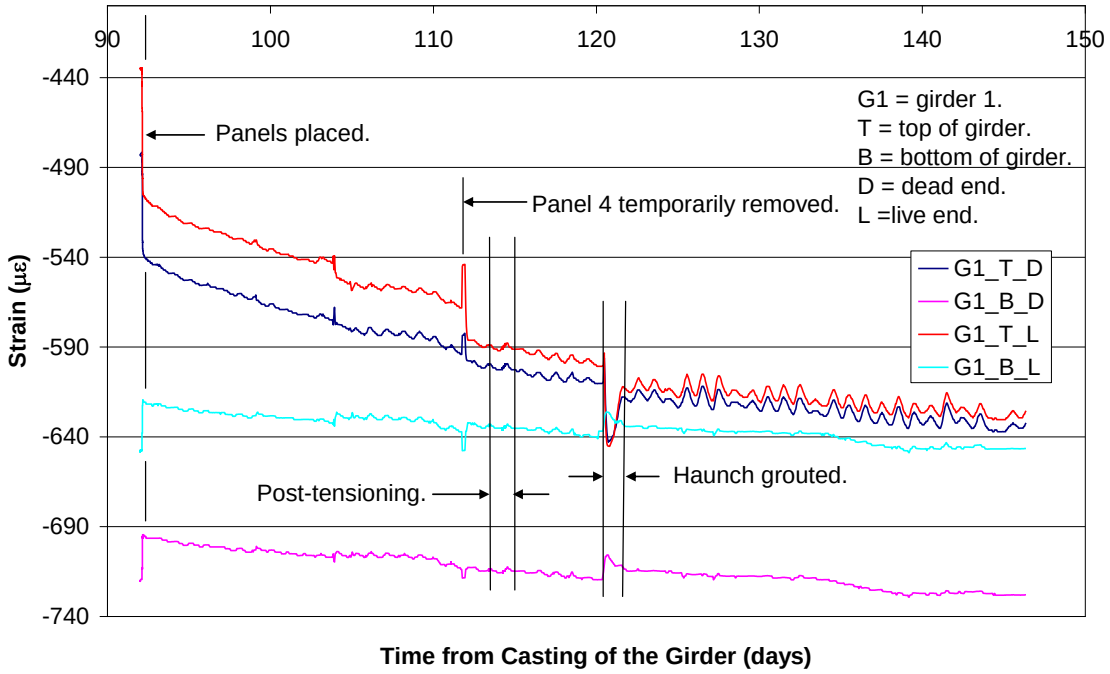

Figure 4.2.5 Variation of Strain with Time for Girder 1 in the Lab

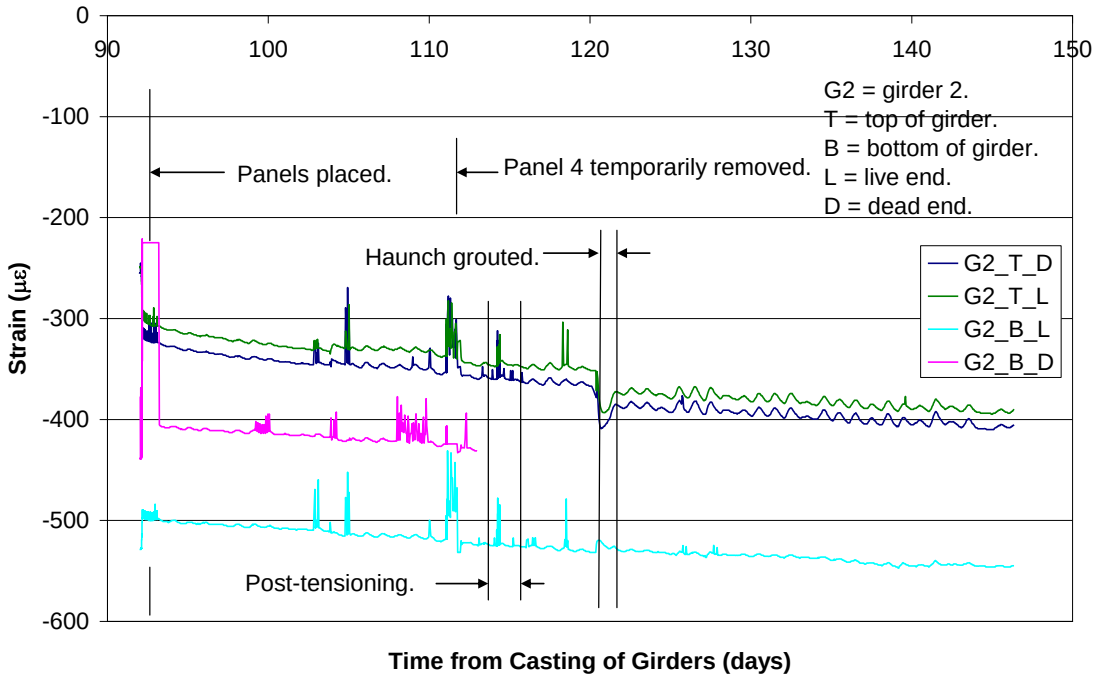

Figure 4.2.6 Variation of Strain with Time for Girder 2 in the Lab

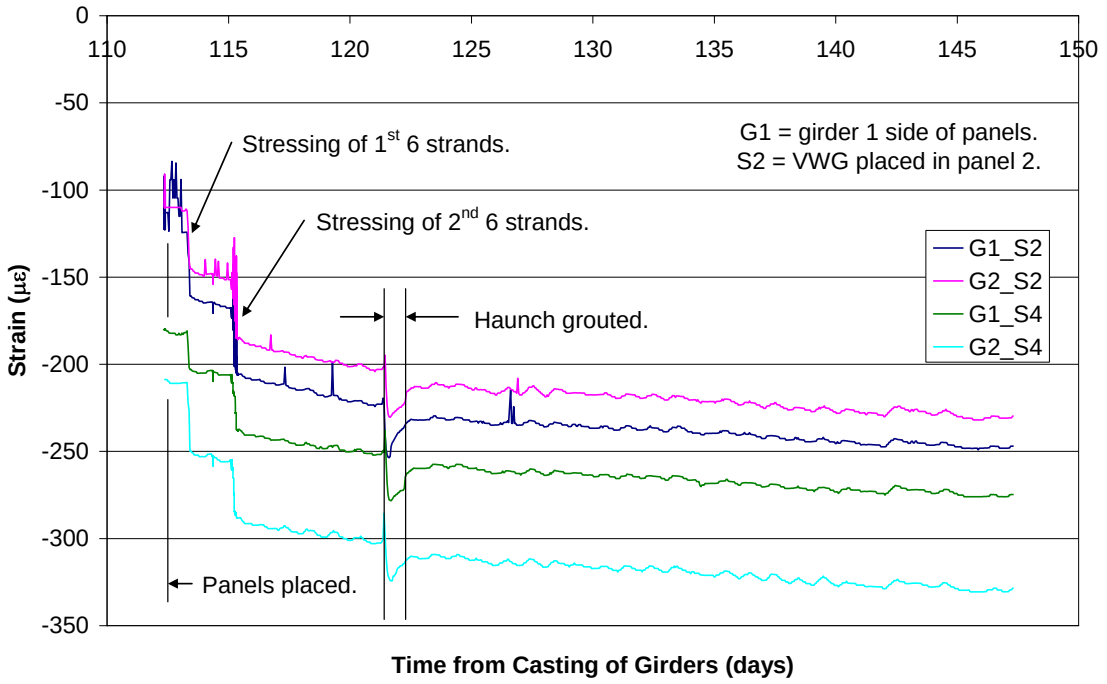

Figure 4.2.7 Variation of Strain with Time for the Precast Panels in the Lab

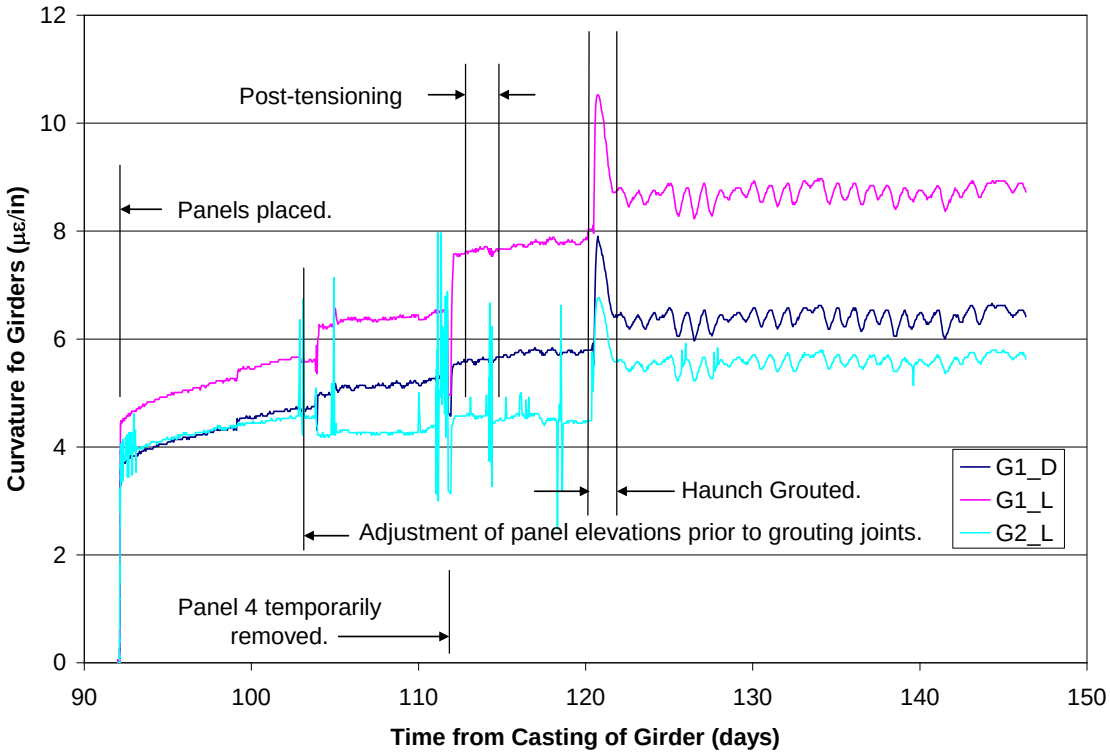

Figure 4.2.8 Variation of Curvature with Time for Girder 1 and Girder 2 in the Lab

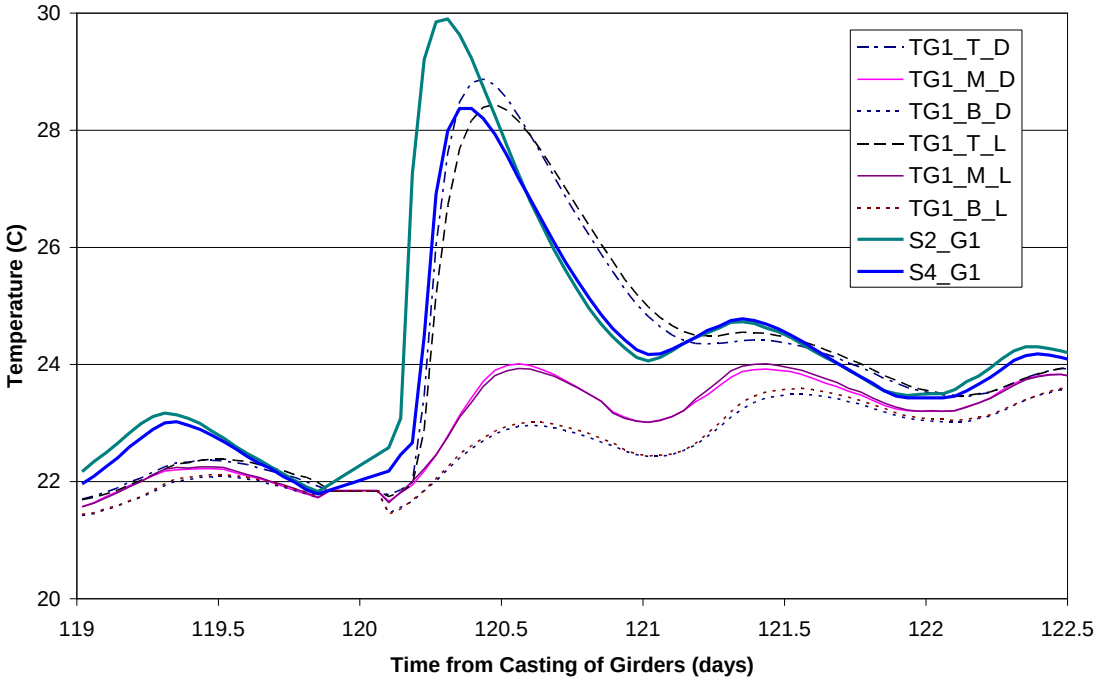

Figure 4.2.9 Variation of Temperature with Time in Girder 1 During Casting of the Haunch

During day 120, the haunch was cast. The system cambered upward during this process due to a temperature gradient introduced in the system from the heat of hydration. Figure 4.2.9 shows the variation in temperature in girder 1 during the casting process. The temperature change was greatest in the deck and smallest in the bottom of the girder. Notice that the maximum temperature change was reached in the panel first, followed by the top of the girder, then the middle of the girder. The bottom of the girder takes the longest to reach its maximum temperature change. A similar trend was observed in girder 2.

Figures 4.2.5 to 4.2.9 can be used to examine the behavior of the system from the effects of the haunch being poured. From day 120.25 to day 120.5, the compressive strains decreased (tensile strain increment) in the girders and panels from the temperature increase caused by the heat of hydration reaction. Figure 4.2.8 shows that there is a negligible change in the curvature in the girders from day 120.25 to day 120.5. During this time increment, the haunch was curing and gaining strength. The haunch reached an

average cube compressive strength of 2.3 ksi 1 hour after the haunch was cast and an average cube compressive strength of 3.4 ksi less than 12 hours after the haunch was cast. The system was changing from a non-composite system to a composite system. Additionally, the haunch was shrinking. This introduced compressive strains in the panels and top of the girders from the effects of shrinkage of the haunch and thermal strains that vary from the varying temperature profile.

From day 120.5 to day 120.75, compressive strain increments developed in the top of the girders and in the panels. Tensile strain increments developed at the bottom of the girders. The system cambered downward during this time increment. As mentioned above, the compressive strains developed in the top of the system are partially due to the shrinkage of the haunch. The temperatures in the girders and panels decreased over this time increment. This temperature decrease also contributed to the compressive strain increments developed during this time increment.

From day 120.75 to day 121.5, tensile strain increments developed in the top of the girders and panels. Compressive strain increments developed at the bottom of the girders. The system cambered upward during this time increment. After day 121, the temperature changes in the panels and girders were only due to the small daily fluctuations in temperature.

When comparing the strains in the girders and panels from day 120.25 to day 121.5, it is clear that residual strains and a residual curvature develop in the system. The changes in strain and curvature may be due to shrinkage of the haunch, the varying axial thermal strains and thermal strain gradients, and the change from a non-composite system to a composite system, as well as the dead load of the haunch. The average residual strain in the VWGs in the panels was -8.82 με. Using the compressive strength data in Section 4.3 along with Section 8.5.1 of ACI 318, the residual stress was approximately -45 psi. The average residual strain in the top VWGs in the girders and bottom VWGs in the girders was -9.41 με and 5.24 με, respectively. This corresponds to average residual stresses in the top VWGs and bottom VWGs of -44 psi and 25 psi, respectively. The average calculated residual curvature in the girders was 0.65 με/in. This corresponds to an average calculated residual moment of 156 k-in. Using Equation 2.3, the calculated

residual deflection at midpsan was 0.018 in., assuming the residual curvature is constant along the length.

The dead load of the haunch creates a stress of -44.4 psi at the level of the top VWGs in the girders and 24.6 psi at the level of the bottom VWGs in the girders. The calculated change in curvature in the girder caused by the dead load of the haunch was 0.66 με/in. When comparing the change in strains from the VWGs and the corresponding approximated stresses to the calculated stresses for the addition of the dead load of the haunch, it appears the net effect the residual thermal strains and residual shrinkage strains have on the system are negligible. However, the average residual strain in the panels of -8.82 με was likely due to thermal effects and shrinkage effects since the dead load of the haunch is carried by the girder. From a design standpoint, the effects from thermal strains and shrinkage strains arising from the casting of the haunch do influence the behavior of the system during the casting operation. However, the net effect they had was negligible and does not need to be considered in design.

4.3 Material Testing

Compression tests and split cylinder tests were performed to measure the compressive strength and tensile strength of the concrete in the panels and girders as well as the cube compressive strength of the grout in the haunch. The tests adhered to ASTM standards ASTM C 39: Standard Test Method for Compressive Strength Cylindrical Concrete Specimens[47], ASTM C 496: Standard Test Method for Splitting Tensile Strength for Cylindrical Conrete Specimens[48], and ASTM C 109: Standard Test Method for Compressive Strength of Hydraulic Cement Mortars Using 2 in. Cube Specimen (modified)[49]. These tests were performed at key intervals outlined in Section 3.2.5. Figure 4.3.1 shows the results from the compression tests and Figure 4.3.2 shows the results from the split cylinder tests. The tensile strengths were obtained using Equation 3.1. Note that the compressive strength reported for grout in the haunch is the *cube* compressive strength. The results are used to aid in generating material models in DIANA as well as predicting the response of the lab mockup.

The measured tensile strength of the concrete at 28 days for the panels and girders was compared to the equation

$$f_t = 7.5\sqrt{f'_{c28\_avg}} \quad [4.8]$$

where, f'_{c28_avg} = the average 28 day compressive strength for the panels or girders from Figure 4.3.1. The average measured tensile strength for the panels was 811 psi. The calculated tensile strength for the panels was 653 psi. This resulted in a difference of 24% between the average measured value and the calculated value from Equation 4.8. The average measured tensile strength for the girders was 673 psi. The calculated tensile strength for the girders was 610 psi. This resulted in a difference of 10% between the average measured value and the calculated value from Equation 4.8.

The moduli of elasticity of the concrete used in the girders and panels were calculated using the VWG data at stages where elastic deformations take place. For the girders, the modulus of elasticity was calculated at the release of strands for the girders and at the time the panels were placed on the girders. For the panels, the modulus of elasticity was calculated at the time the strands were post-tensioned in the deck. The modulus of elasticity was not obtained directly from modulus tests because of the difficulty in obtaining accurate measurements.

At the release of the strands in the girders, the average modulus of elasticity calculated using the VWGs was 4220 ksi for the girders. The average modulus of elasticity was calculated using the equation

$$E_{VWG} = \frac{1}{8}\sum_{i=1}^{8} \frac{1}{\varepsilon_{VWG}}\left(\frac{-P}{A_g} - \frac{Pe_g y_{VWG}}{I_g} + \frac{My_{VWG}}{I_g}\right) \quad [4.9]$$

where,

ε_{VWG} = strain in the top or bottom vibrating wire gage

P = prestressing force in the girder at the time the strands were released (kips)

A_g = cross sectional area of the girder (in^2)

I_g = second moment of area of the girder (in^4)

e_g = eccentricity of the strand group in the girder (in.)

y_{VWG} = distance from the centroid of the girder to the location of the top or bottom VWG (in.)

M_{g_DL} = dead load of the girder at the location of the VWG, 13 ft-4 in.

from the supports (k-in)

The eight VWGs produced eight moduli of elasticity. The eight values were averaged, as shown in Equation 4.9. The value of the modulus of elasticity at the release of the strands in the girders was 3830 ksi when using the equation presented in Section 8.5.1 of ACI 318. The compressive strength used to calculate the modulus of elasticity was 4.52 ksi. There was about a 10% difference between the modulus of elasticity from the ACI 318 equation and Equation 4.9.

When the panels were placed on the girders, the average modulus of elasticity calculated using the VWGs was 6380 ksi for the girders. The average modulus of elasticity was calculated using the equation

$$E_{VWG} = \frac{1}{8}\sum_{i=1}^{8} \frac{M_{p\_DL} y_{VWG}}{I_g \varepsilon_{VWG}} \qquad [4.10]$$

where, M_{p_DL} = dead load moment of the panels at the location of the vibrating wire gages (VWG), 13 ft-4 in. from the supports (k-in). The value of the modulus of elasticity when the panels were placed on the girders was 4790 ksi using the equation presented in Section 8.5.1 of ACI 318. The compressive strength used to calculate the modulus of elasticity was 7.06 ksi. There was about a 33% difference between the modulus of elasticity from the ACI 318 equation and Equation 4.10. The cause for the large value for E_{VWG} is unknown.

At the time the strands were post-tensioned in the deck, the average modulus of elasticity calculated using the VWGs was 3580 ksi for the panels. The average modulus of elasticity was calculated using the equation

$$E_{VWG} = \frac{P_{average}}{A_{deck} \frac{1}{4}\sum_{i=1}^{4} \varepsilon_{VWG}} \qquad [4.11]$$

where,

$P_{average}$ = the average post-tensioning force in the deck along the length of the lab mockup (kips)

A_{deck} = cross sectional area of the deck (in^2)

The four VWG in the panels were averaged to produce the average modulus of elasticity, as shown in Equation 4.11. The value of the modulus of elasticity at the time the strands

were post-tensioned in the deck was 4880 ksi using the equation presented in Section 8.5.1 of ACI 318. The compressive strength used to calculate the modulus of elasticity was 7.32 ksi. There was about a 14% difference between the modulus of elasticity from the ACI 318 equation and Equation 4.11. Table 4.3.1 presents a summary of the comparisons for the elastic moduli calculations above.

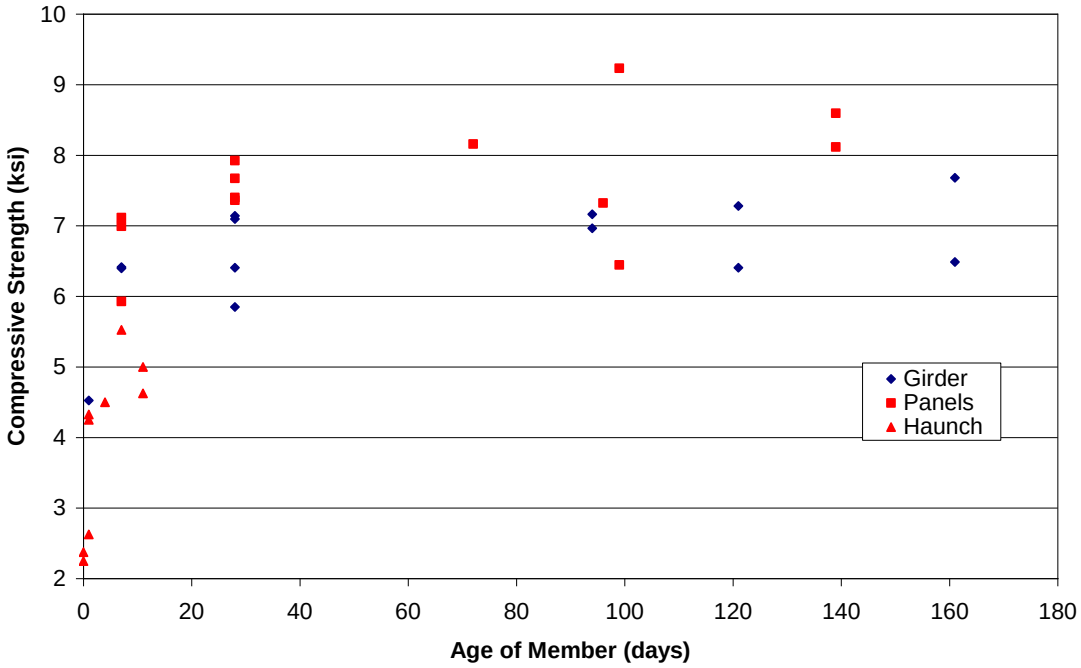

Figure 4.3.1 Compressive Strength of Materials used for Lab Mockup

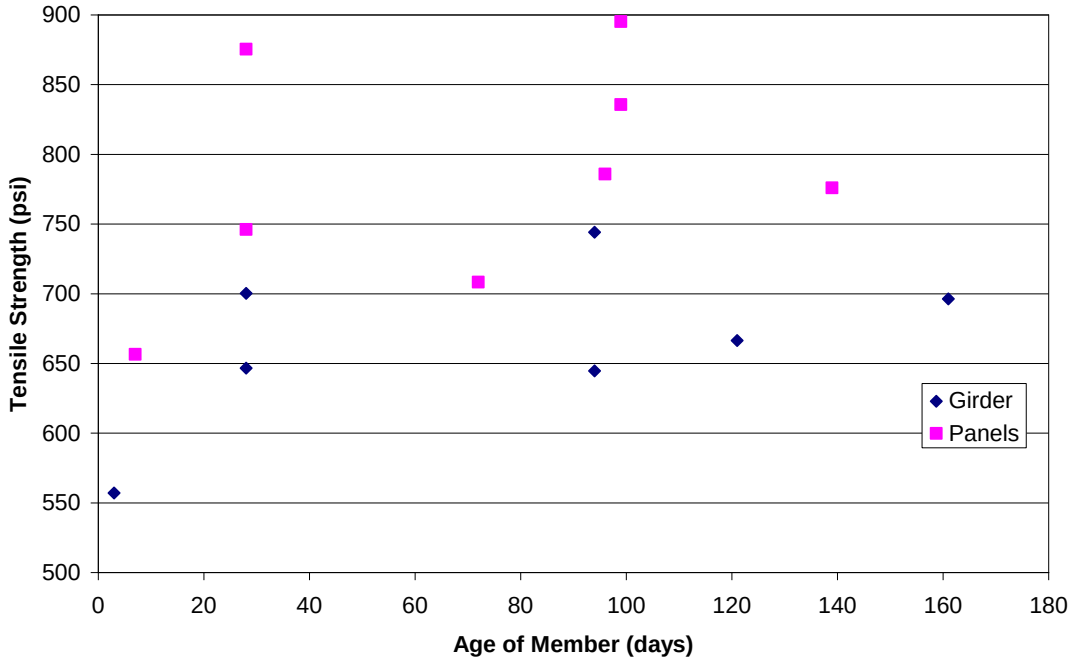

Figure 4.3.2 Tensile Strength of Materials used for Lab Mockup

Table 4.3.1 Comparison of VWG Calculation and ACI 318 Calculations for the Elastic Moduli

	f'c (ksi)	E_{VWG} (ksi)	E_{ACI318} (ksi)	E_{VWG}/E_{ACI318}
Strand Release for Girders	4.52	4220	3830	1.10
Panel Placement	7.06	6380	4790	1.33
Post-Tensioning of Deck	7.32	3580	4880	0.73

4.4 Live Load Testing on the Dead End

4.4.1 Initial Static Test on the Dead End

Figure 4.4.1 shows the deflections of the dead end of the lab mockup during the initial static test at the outside loading point and at the inside loading point. Recall that Figure 3.2.8 indicates the inside and outside loading points. In Figure 4.4.1, G1 denotes

girder 1, G2 denotes girder 2, INSIDE denotes the deflection at the loading point adjacent to the inside joint, and OUTSIDE denotes the deflection at the loading point adjacent to the outside joint.

When the final load of 68.6 k/frame was reached, no cracking was observed in the girders or panels. There was no cracking at the transverse joints and no relative vertical movement between adjacent panels was measured by the wirepots. No cracking was observed at the horizontal interfaces at the haunch. The LVDTs also showed no indication of relative slip. The strains in the shear connectors were well below the nominal yield strain. The lab mockup performed well under loading conditions outlined in Sections 3.2.6 and 3.2.7 for the initial static test.

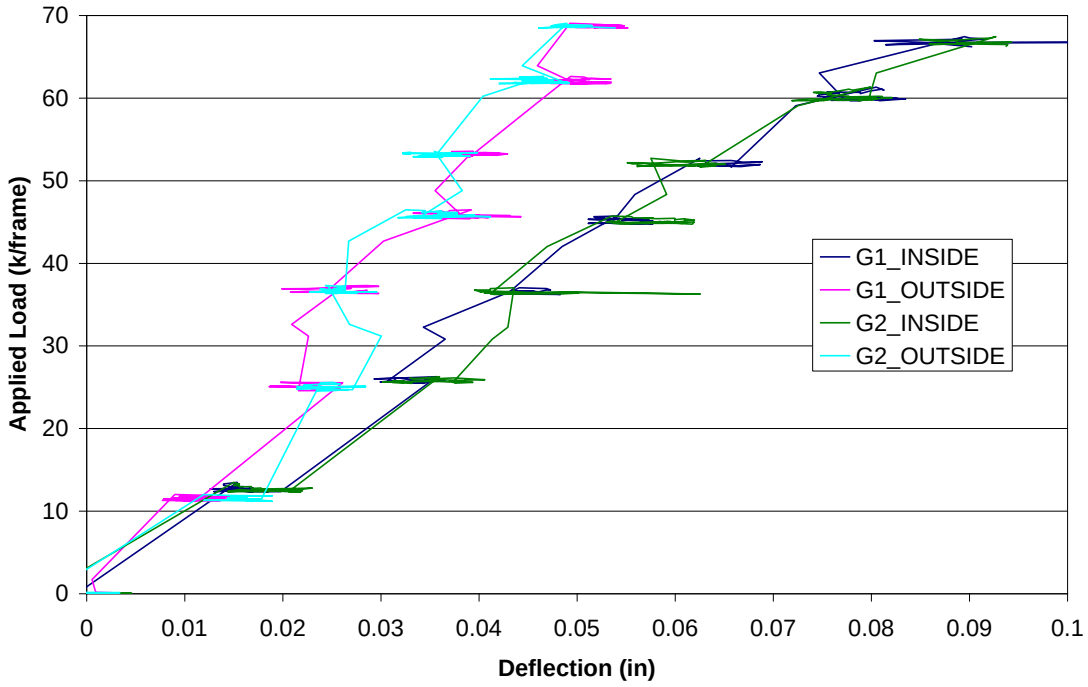

Figure 4.4.1 Deflection During the Initial Static Test at the Dead End

4.4.2 Cyclic Testing on the Dead End

The lab mockup was subjected to two million cycles of load. Static tests were performed approximately every 100,000 cycles. Details on this portion of the test program are presented in Section 3.2.8.

Figure 4.4.2 shows the deflections as measured by the wirepots at the dead end of the lab mockup at a load of 40 k/frame with respect to the number of cycles that had been performed. One trend observed was the increase in the deflection of girder 2 after 1.7 million cycles. However, neither the LVDTs or strain gages in the shear studs indicate girder 2 was experiencing a loss in composite action. The variation in the deflections during the cyclic testing was less than 0.029 in.

Figure 4.4.3 shows the stress in the bottom layer of prestressing strands in the girders at a load of 40 k/frame with respect to the number of cycles that had been performed. The stress was determined by first establishing a linear strain profile through the depth of the composite section with the ER strain gage readings. Refer to Section 3.2.2 for the location of the ER strain gages. Once the strain profile was established, the strain at the level of the bottom layer of strands was interpolated from the strain profile. The strain at this location was multiplied by the elastic modulus of the prestressing strand of 28,500 ksi. If cracks formed from the cyclic testing, the strains in the VWGs would increase. This would have caused the stress in the strands to also increase. The stress in the bottom layer of strands was monitored to see if it exceeded the allowable stress range of 10 ksi. The allowable stress range of 10 ksi is from the fatigue check in the design calculations presented in Appendix A. There was no indication that the stress in the strands increased with the number of cycles from fatigue effects. The stress in the strands for girder 1 at 150,000 cycles was smaller than the other stress readings for the entire range of cycles. This was believed to be from instrumentation error as opposed to a change in the physical behavior of the system.

The strains in the shear connectors were very small. The largest strain observed was 16 με in connector G1_R3 at 150,000 cycles, which was less than 1% of the nominal yield strain. This indicates the shear connectors were not engaged in resisting the horizontal shear stresses developed during the cyclic testing. This also indicates that there was no slip since the connectors were not engaged in resisting the horizontal shear stresses. This was confirmed by the LVDT readings as well as the observation that there was no cracking at the interfaces.

There was no cracking at the transverse joints and no relative vertical movement between adjacent panels was measured by the wirepots. No cracking was observed in the

girder or deck. The cyclic testing had minimal effects, if any, on the degree of composite action in the lab mockup.

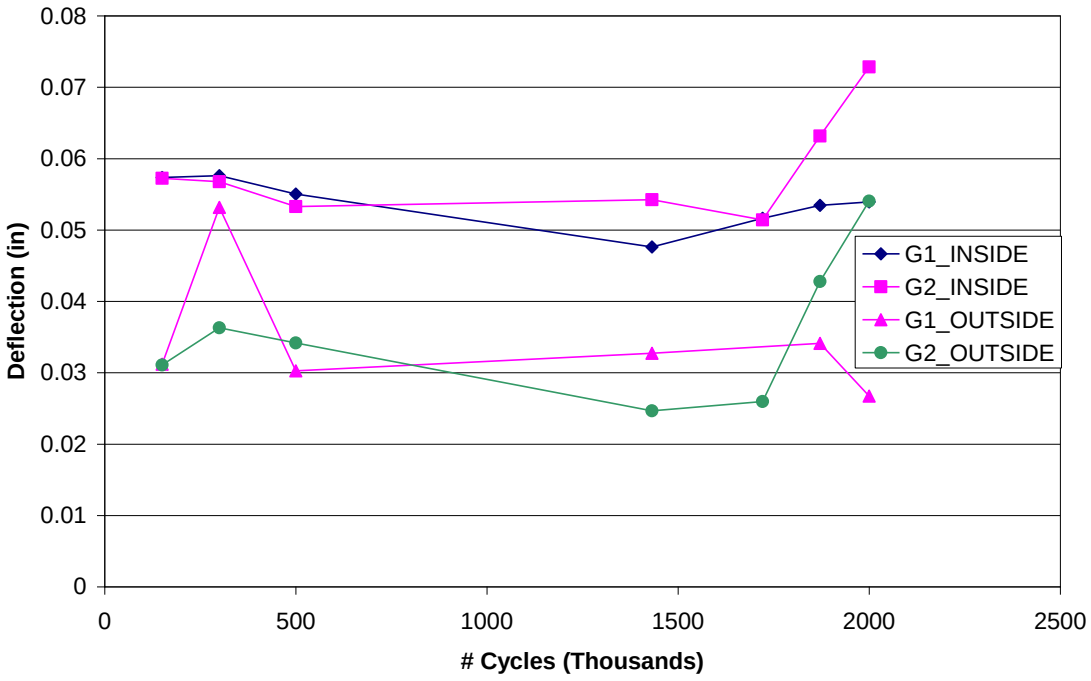

Figure 4.4.2 Variation of Deflections at 40 kips with the Number of Cycles at the Dead End

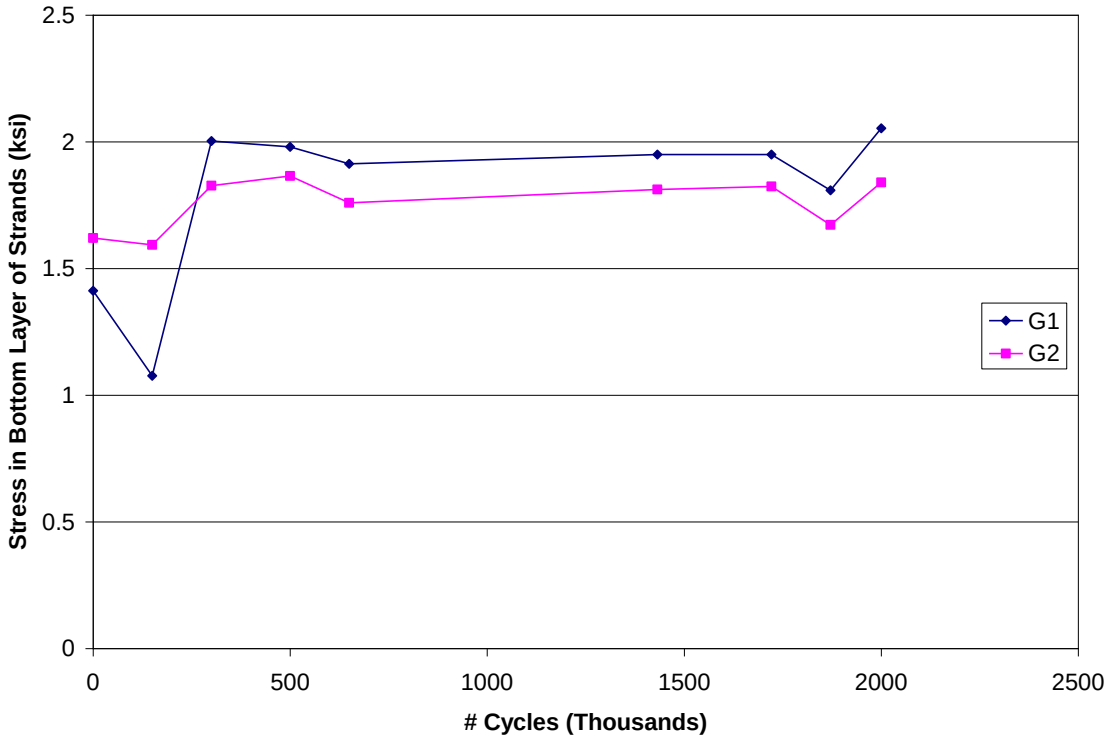

Figure 4.4.3 Variation of Stress in Bottom Layer of Strands at 40 kips with the Number of Cycles at the Dead End

4.4.3 Intermediate Static Test on the Dead End

Figure 4.4.4 shows the deflections of the dead end of the lab mockup during the intermediate static test at the outside loading point and at the inside loading point. Figure 4.4.5 shows the cracking patterns in girder 1 and girder 2 at the dead end. The cracking patterns shown in this figure are on the outside surfaces of the girders. Signs of web shear cracking occurred around 65 to 70 k/frame. The first web shear crack was calculated to occur at 119 k/frame. This was based on an elastic analysis, comparing the principle stresses in the girder to the modulus of rupture. Web shear cracking was more pronounced at 96 k/frame. Flexural cracks occurred at the bottom of the girders, under the inside load point at 118 k/frame. The first flexural crack was calculated to occur at 126 k/frame. This was based on an elastic analysis, comparing the principle stresses in the girder to the modulus of rupture. When the final load of 123 k/frame was reached, significant web cracking was observed. Measured crack widths varied from 0.005 in. to 0.009 in. Crack lengths as long as 29 in. were measured. The angles at which the cracks

formed and propagated were estimated to be between 35° and 45°. The lab mockup was unloaded at 123 k/frame to prevent further damage that might have influenced the results for the live load testing at the live end. According to the data, no relative slip occurred at the transverse joints or at the horizontal interfaces at the haunch.

When comparing Figure 4.4.4 with Figure 4.4.1, there was some indication of a decrease in stiffness based on the vertical deflections. As previously mentioned, the cyclic testing did not affect the performance of the lab mockup. The stiffness decreased when the applied load was above 96 k/frame for the intermediate static test. Figure 4.4.4 shows how the stiffness decreased by 29% at the inside loading point and by 33% at the outside loading point. Even with the decrease in stiffness, the lab mockup's peak deflections were still less than 0.22 in. at 3.85 times the AASHTO design wheel load of 16 kips. The calculated deflection of the girder at the inside wirepot location was 0.20 in. at the peak load. The calculated deflection was done with uncracked, gross section properties.

The strain levels in the shear connectors were less than 2% of the nominal yield strain. No relative slip occurred at the horizontal interfaces and no relative vertical movement occurred between adjacent panels. The intermediate static test had minimal effects on the degree of composite action of the lab mockup.

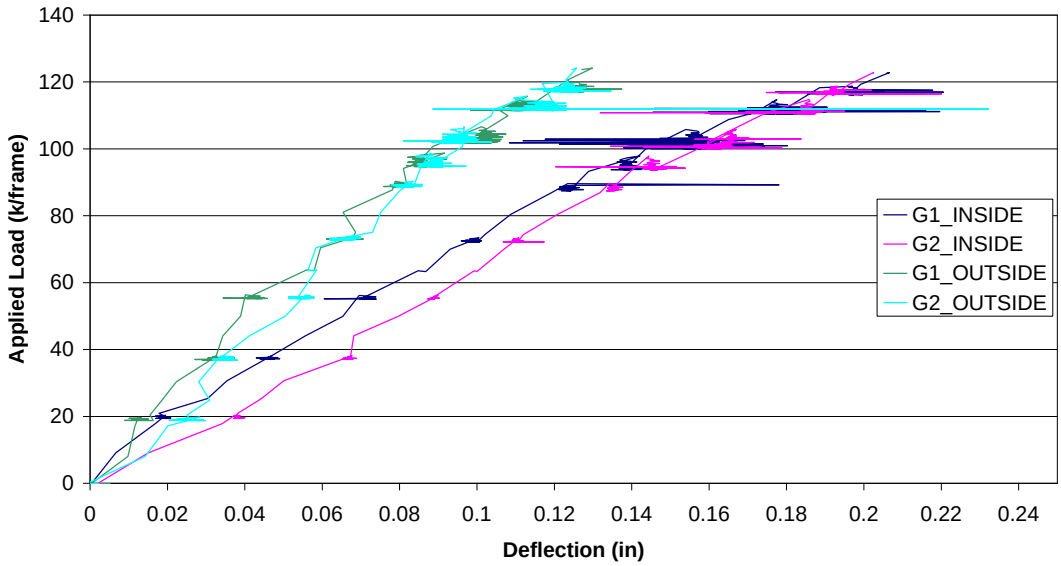

Figure 4.4.4 Deflections During the Intermediate Static Test at the Dead End

(a)

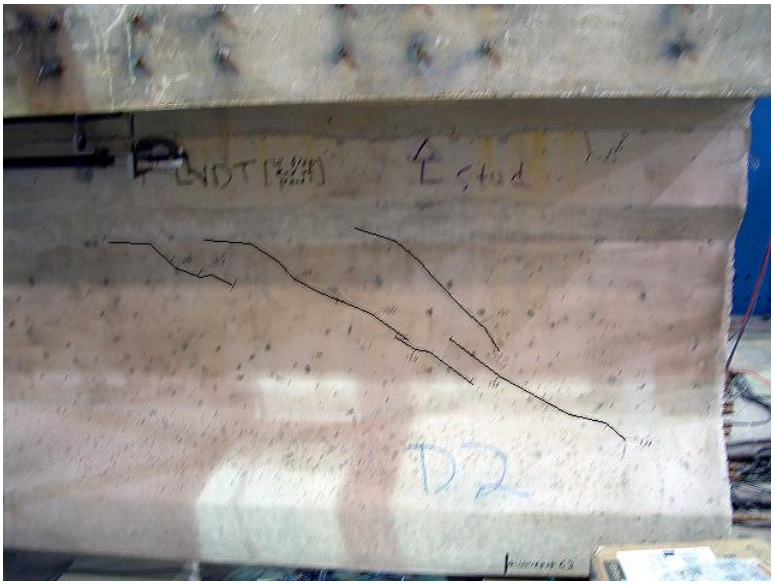

(b)

Figure 4.4.5 Cracking Patterns at the Dead End of (a) Girder 1 (b) Girder 2 During the Intermediate Static Test

4.4.4 Final Static Test on the Dead End

During the final static test, the load was increased up to 249 k/frame. At this load, a punching shear failure occurred under the wheel load located adjacent to the outside female-female joint and adjacent to girder 1. The wheel load causing the punching shear failure was 125 k, compared to the design punching shear capacity (ϕV_{n_punch}) of 113 k and nominal punching shear capacity (V_{n_punch}) of 126 k. The calculations for the punching shear capacity are shown in Appendix A. The punching shear failure is shown in Figure 4.4.6. In order to continue with the testing, the location of the wheel loads shown in Figure 3.2.8(a) were changed from a transverse spacing of 4 ft to 8 ft. With the modified live load setup, the wheel loads were centered over the girder, preventing a punching shear from taking place.

(a) (b)

Figure 4.4.6 Punching Shear Failure at the Dead End (a) Bottom Surface of Deck (b) Top Surface of Deck

Figure 4.4.7 shows the deflections of the dead end of the lab mockup during the final static test at the outside loading point and the inside loading point. The vertical stiffness values were compared for the different static tests. The concept of the equivalent vertical stiffness is shown in Figure 4.4.8. The flexural stiffness, shear stiffness, and axial stiffness all resisted the load in the vertical direction, producing an equivalent vertical stiffness. Rotations were assumed to be small enough such that the vertical component of the axial stiffness was negligible compared to the other stiffness

terms. The vertical stiffness at each load point was also a function of the flexural stiffness at the supports, as well as the flexural stiffness and vertical stiffness at every other point if the bridge was modeled as a continuous system. The calculation of the vertical stiffness at a load point, $K_{vert}=P/\delta$, was simplified by taking the applied load at the load point, P, and dividing by the vertical deflection at the load point, δ.

The initial vertical stiffness of the lab mockup at the loading points for the final static test was less than the initial vertical stiffness at the loading points during the initial static test and intermediate static test. At the inside loading points, the initial vertical stiffness of the lab mockup was 777 k/in. and 710 k/in. for the initial static test and intermediate static test, respectively. For the final static test, the initial vertical stiffness at the inside load point was 461 k/in. As the load was increased, the vertical stiffness at the load points decreased at a faster rate for the final static test, when compared to the initial static test and intermediate static test. This is shown when comparing Figure 4.4.1, Figure 4.4.4, and Figure 4.4.7. This was due to the number of loading and unloading cycles the dead and live end of the bridge underwent along with the accumulated damage that occurred during the intermediate static test at the dead end and during the intermediate static test at the live end. For applied loads greater than 270 k/frame, the vertical stiffness at the inside load point and outside load point were 10.0 k/in. and 18.3 k/in., respectively. This corresponds to 1.3% and 1.4% of the initial vertical stiffness at the inside load point and outside load point, respectively.

At an applied load of 256 k/frame, there was a significant decrease in stiffness. This load does not include the dead load of the system. One reason for the decrease in stiffness may be from the prestressing strands in the girders exceeding the nominal yield strain of the prestressing strands. The load at which the prestressing strands exceed the nominal yield strain was calculated to be 269 k/frame. This was confirmed with the finite element models, which are presented in Chapter 5. The finite element results indicated the top layer of prestressing strands reach a strain of 0.012 in./in. at an applied load of 268 k/frame for the dead end load setup.

When 272 k/frame was reached, the load was intentionally reduced to 237 k/frame. The load was then increased up to 287 k/frame. Figure 4.4.7 shows how the vertical stiffness at the load points was greater upon reloading, compared to the vertical

stiffness along the original load path at 272 k/frame for the final static test. Once the applied load reached 272 k/frame again, the vertical stiffness had decreased back to 10.0 k/in. at the inside load point.

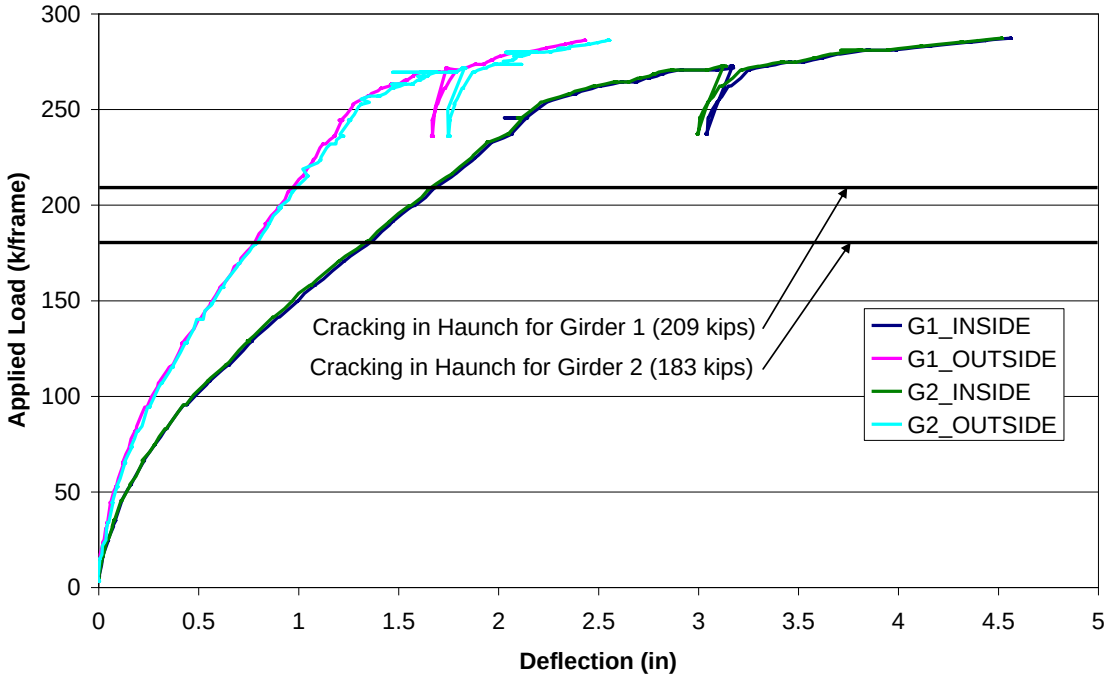

Figure 4.4.7 Deflections During the Final Static Test at the Dead End

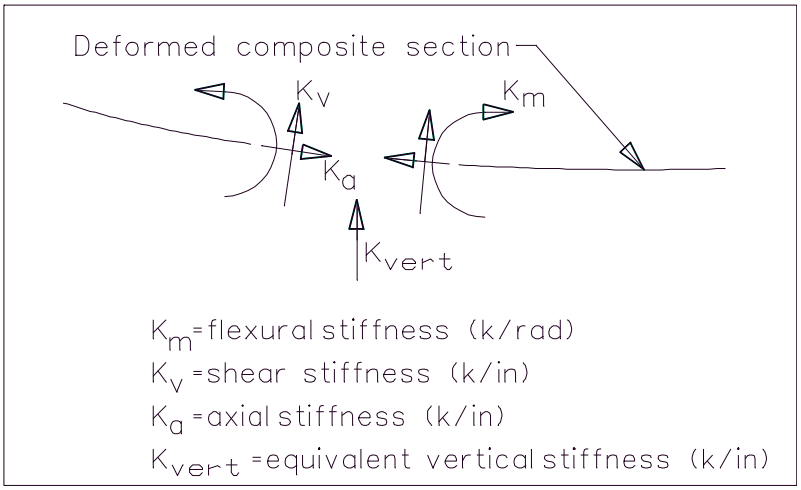

Figure 4.4.8 Equivalent Vertical Stiffness Representation

Another reason for the decrease in stiffness may be from the loss of composite action. Cracking at the interface between the haunch and girder occurred at 209 k/frame for girder 1, and 183 k/frame for girder 2. As the load increased, the cracks continued to propagate. No cracking was observed at the interface between the haunch and deck panels for the entire range of loading. This was believed to be attributed to the large portion of the interface between the panels and haunch that passes through the shear pockets. This part of the interface consists of a monolithic pour of grout through the depth of the shear pocket. The entire interface between the girder and haunch consists of two dissimilar materials cast at different times.

Figure 4.4.9 shows the strains in the shear connectors for the final static test. At an applied load of 256 k/frame, the rate at which the strains increased with respect to the load increased. This indicated that the shear connectors were engaged in resisting the horizontal shear stresses as the cracking at the interface between the haunch and girder continued to increase. The strains in the shear connectors in Figure 4.4.9 were less than 50% of the nominal yield strain for the entire range of applied loads. The strain behavior in the majority of the instrumented shear connectors was the same with the exception of shear connector G2_R4. Problems were encountered with this gage on previous live load tests. This may be a contributing factor to the difference in the strain for this connector when compared to other connectors and may not represent true physical behavior. However, the strain in shear connector G2_R4 was still small and does show the increase in the strain rate at an applied load of 256 k/frame like the rest of the shear connectors. The LVDTs indicated there was no relative slip even though there was cracking at the interface between the haunch and girder and the strain rate in the shear connectors increased.

Figure 4.4.10 shows the cracking pattern at the dead end of girder 1 and girder 2. The cracking pattern for the two girders was very similar. Section 4.4.1 and Section 4.4.3 describe the cracking for load levels below 123 k/frame. As the load increased, the flexural cracks propagated through the depth of the girder and new flexural cracks continued to develop and propagated at locations away from the inside loading points. At 200 k/frame, some of the flexural cracks between the two loading points became flexural shear cracks as the direction of the crack propagation turned toward the inside loading

points. Web shear cracks formed anywhere between 2 ft and 4 ft from the end of the girder at an approximate orientation of 35° to 45° and propagated in both directions. One end of a web shear crack propagated toward the support and the other end of the web shear crack propagated toward the outside load point. At 243 k/frame, flexural cracks formed in the deck panels. Flexural crack widths were as large at 1/8 in. in the girders.

The cracking at the interface between the haunch and girder was more extensive in girder 2, compared to girder 1. Additionally, the cracking at the interface between the haunch and girder occurred at a smaller applied load for girder 2, as shown in Figure 4.4.7. Recall the interface between girder 2 and the haunch consisted of grout from the haunch and the steel plates that were cast with girder 2. The interface between girder 1 and the haunch consisted of grout from the haunch and concrete from girder 1, which has a higher cohesion value. The wirepots at the female-female transverse joints indicated there was no relative vertical movement at the joints.

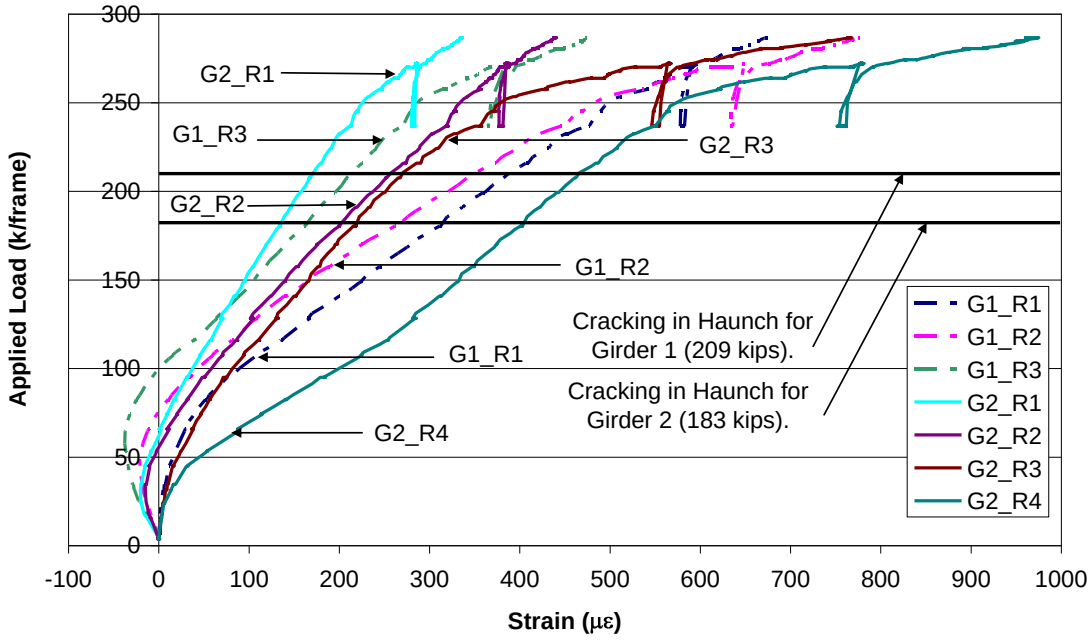

Figure 4.4.9 Connector Strains During the Final Static Test at the Dead End

After the final static test, the bottom surface of the deck between the two girder lines was examined and cracking at the inside and outside grouted female-female joints was observed. The cracking occurred at the interface between the grout for the joint and the concrete for the panels, as shown in Figure 4.4.11. Because cracking patterns were not monitored at this location during the test for safety reasons, the load at which the cracks occurred at was unknown. However, after the conclusion of the first final static test where the punching shear occurred, no cracking was observed at the grouted female-female joints. Therefore, the load at which the grouted female-female joints cracked was greater than 249 k/frame. The load of 249 k/frame was when the punching shear failure occurred.

At 287 k/frame, crushing occurred on the top surface of the bridge deck, adjacent to the inside load points. The applied axial load of 287 k/frame results in an actual flexural capacity of 23,700 k-in., which was 53% greater than the AASHTO LRFD required flexural capacity of 15,500 k-in. As discussed in Section 3.2.1, the flexural capacity was increased in order to gain insight in to the behavior of the shear connectors and influence of the pocket spacing. This was primarily accomplished by adding mild reinforcing steel in the bottom flanges of the girders. When considering the mild reinforcing steel and prestressing steel, the calculated flexural capacity of the lab mockup was 24,800 k-in. This calculation is shown in Appendix A. There was a 4.4% difference when the actual flexural capacity at the dead end of 23,700 k-in was compared to the calculated flexural capacity of 24,800 k-in.

The exceptional performance of the shear connectors at loads above the design loads may be due to over design. One source leading to the over design of the horizontal shear connectors was the shear connector layout. Many shear pockets contain the same number of shear connectors in order to simplify the layout, which is common practice. This leads to pockets in locations with small shears to be over designed. Another source leading to the over design of the horizontal shear connectors has to do with the design loads. As mentioned previously, AASHTO LRFD was used to design the lab mockup. The horizontal interface was designed to resist all dead loads and live loads. Tadros[25] addresses the issue of whether the design loads for horizontal shear design for precast deck panel systems should include non-composite dead loads. However, when extensive

cracking is present, a plastic truss is formed and the loads are redistributed in the system. Based on the truss analogy, the shear connectors should be designed for both non-composite dead loads and composite dead loads in addition to the live loads.

Both the shear studs and the hooked reinforcing bars performed exceptionally well as shear connectors for 4 ft pocket spacing. The strains in the shear connectors were less than 50% of the nominal yield strain. Additionally, the deflections at the inside load points and outside load points were the same for girder 1 and girder 2. The loads at which cracking was observed at the interface between the haunch and girder results in a moment that is 2.5% less than and 11% greater than the required flexural strength, for girder 2 and girder 1, respectively.

(a)

(b)

Figure 4.4.10 Cracking Pattern at the Dead End for (a) Girder 1
(b) Girder 2 During the Final Static Test

Figure 4.4.11 Cracking at the Grouted Female-Female Joint

4.5 Live Load Testing on the Live End

4.5.1 Initial Static Test on the Live End

Figure 4.5.1 shows the deflections of the live end of the lab mockup during the initial static test at the outside loading point and at the inside loading point. When the final load of 70.2 k/frame was reached, no cracking was observed in the girders or panels.

There was no cracking at the transverse joints and no relative vertical movement between adjacent panels was measured by the wirepots. No cracking was observed at the horizontal interfaces at the haunch. The LVDTs also showed no indication of relative slip. The strains in the shear connectors were well below the nominal yield strains. The lab mockup performed well under loading conditions outlined in Sections 3.2.6 and 3.2.7 for the initial static test.

The deflections in Figure 4.4.1 are less that the deflections in Figure 4.5.1. There are two possibilities for the slight difference in stiffness. The cracks that formed at the dead end during the intermediate static test may have more of an influence on the behavior of the live end than originally anticipated. Another possible cause has to do with the load cells. The load cells were re-calibrated before the testing began on the live end of the bridge. There were very minor changes in the calibration values that can produce small changes in the calculated stiffness of the structure. The other possible cause has to do with the transverse joints. The grouted female-female joints may provide a stiffer section at the locations of the joints compared to the epoxied male-female joints.

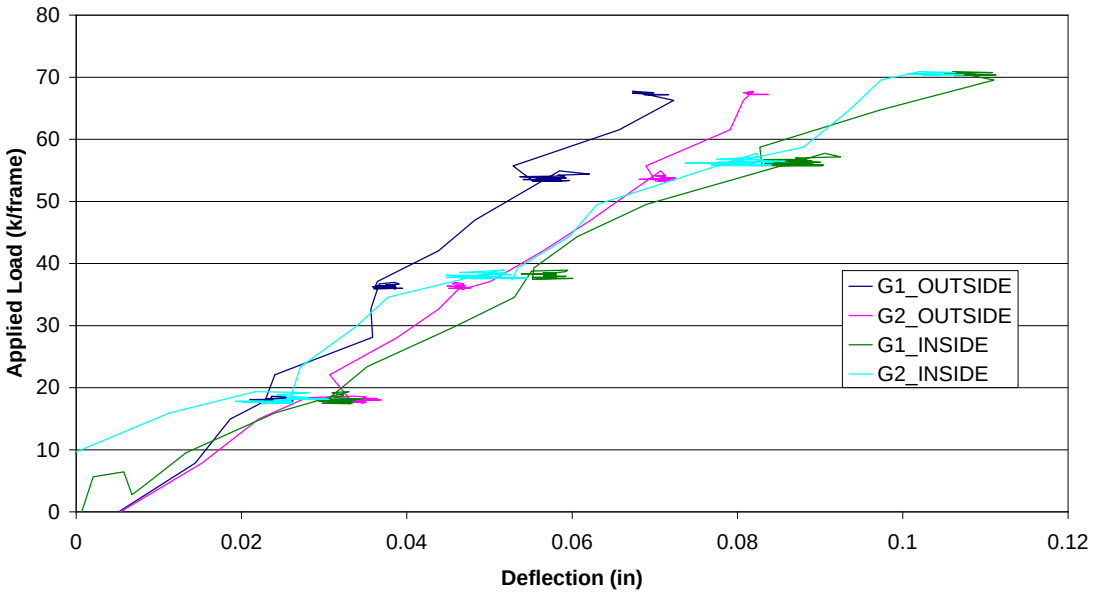

Figure 4.5.1 Deflection During the Initial Static Test at the Live End

4.5.2 Cyclic Testing on the Live End

The lab mockup was subjected to two million cycles of load. Static tests were performed approximately every 100,000 cycles. Details on this portion of the test program are presented in Section 3.2.8.

Figure 4.5.2 shows the deflections of the live end of the lab mockup at 40 k/frame with respect to the number of cycles that had been performed. One trend observed was the increase in the deflection of girder 1 at the inside load point after 1.7 million cycles. The deflection increased from 0.055 in. to 0.090 in. However, neither the LVDTs or strain gages in the shear studs indicate girder 1 was experiencing a loss in composite action. The largest strains in the shear connectors were less than 1% of the nominal yield strain. Additionally, the strains in ER strain gages G1_L_L and G2_L_L did not increase at a higher number of cycles. The high deflection may be caused by a problem in wirepot C1.

Figure 4.5.3 shows the stress in the bottom layer of prestressing strands in the girders at 40 k/frame with respect to the number of cycles that had been performed. The stress was determined by first establishing a linear strain profile through the depth of the composite section with the ER strain gage readings. Refer to Section 3.2.2 for the location of the ER strain gages. Once the strain profile was established, the strain at the level of the bottom layer of strands was interpolated from the strain profile. The strain at this location was multiplied by the elastic modulus of the prestressing strand of 28,500 ksi. If cracks formed from the cyclic testing, the strains in the VWGs would increase. This would have caused the stress in the strands to also increase. The stress in the bottom layer of strands was monitored to see if it exceeded the allowable stress range of 10 ksi. The allowable stress range of 10 ksi is from the fatigue check in the design calculations presented in Appendix A. There was no indication that the stress in the strands increases with the number of cycles from fatigue effects.

As previously mentioned, the strains in the shear connectors were less than 1% of the nominal yield strain. Similar to the cyclic test results for the 4 ft pocket spacing in Section 4.4.2, the shear connectors were not engaged in resisting the horizontal shear stresses developed during the cyclic testing for 2 ft pocket spacing. The cyclic testing had minimal effects on the degree of composite action in the lab mockup.

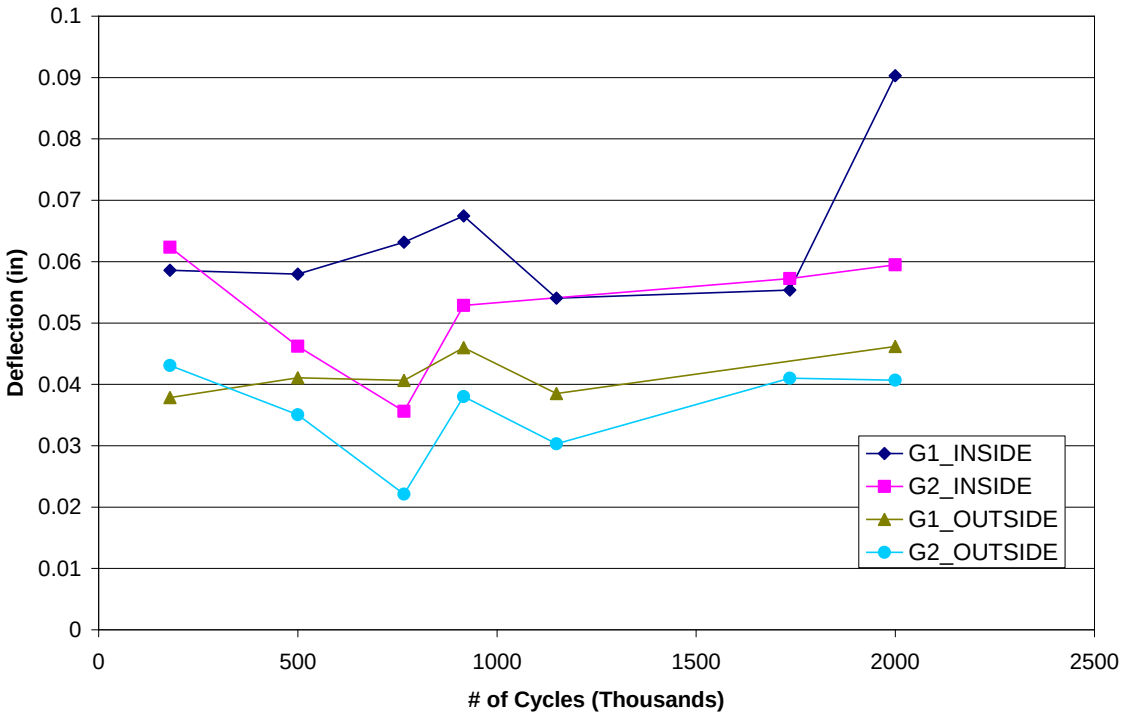

Figure 4.5.2 Variation of Deflections at 40 kips with the Number of Cycles at the Live End

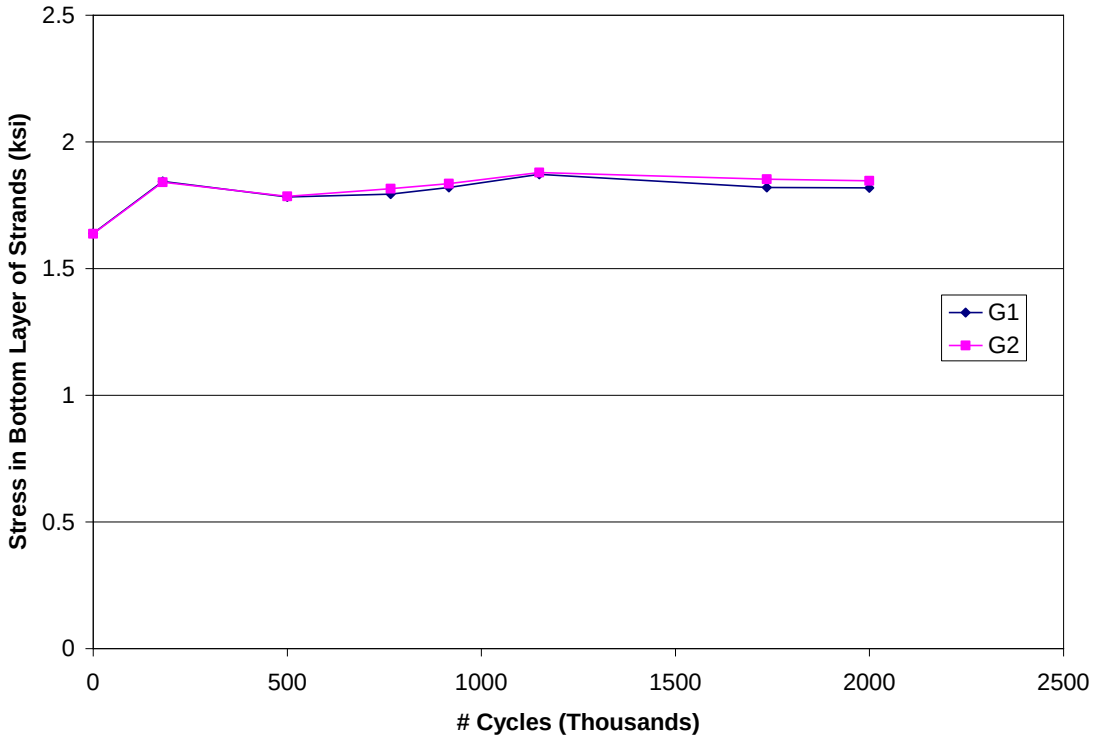

Figure 4.5.3 Variation of Stress in Bottom Layer of Strands at 40 kips with the Number of Cycles at the Live End

4.5.3 Intermediate Static Test on the Live End

Figure 4.5.4 shows the deflections of the live end of the lab mockup during the intermediate static test at the outside loading point and the inside loading point. The load was increased up to 159 k/frame for each load frame. This corresponds to 4.94 times the AASHTO wheel load of 16 k. There was evidence of nonlinear behavior in Figure 4.5.4 for applied loads greater than 130 – 140 k/frame. Web shear cracking occurred at 113 k/frame. The web shear cracking was more significant at 148 k/frame. The first web shear crack was calculated to occur at 119 k/frame. This was based on an elastic analysis, comparing the principle stresses in the girder to the modulus of rupture. The crack widths in the web ranged from 0.007 in. to 0.016 in. when the peak load of 159 k/frame was reached. The angles at which the cracks propagated ranged from 26° to 45°. Flexural cracks formed underneath the applied load points and between the applied load points. The flexural cracks initiated at an applied load of 122 k/frame and continued to

propagate through the depth until the applied load reached 159 k/frame. The first flexural crack was calculated to occur at 126 k/frame. This was based on an elastic analysis, comparing the principle stresses in the girder to the modulus of rupture. At this point, the test was stopped. Many of the cracks propagated 27 in. vertically from the bottom fiber of the girder. The flexural crack widths varied from 0.008 in. to 0.016 in. when the peak load of 159 k/frame was reached.

At 139 k/frame, there were cracks in the haunch. This cracking in the haunch occurred over a length of 20 in. However, no relative slip occurred at this location. Although cracking in the girder had decreased the stiffness of the system, it was believed that the decrease in stiffness was not from a loss in composite action and that full composite action still was present. This was verified by examining the strain levels in the shear connectors. The maximum strain was 133 με, which was 8% of the nominal yield strain. This indicated there was not any relative slip to engage the shear studs and cause them to yield. The epoxied male-female joints also showed superior performance. No visible cracking was noticed and there was no relative vertical movement at the epoxied male-female joints.

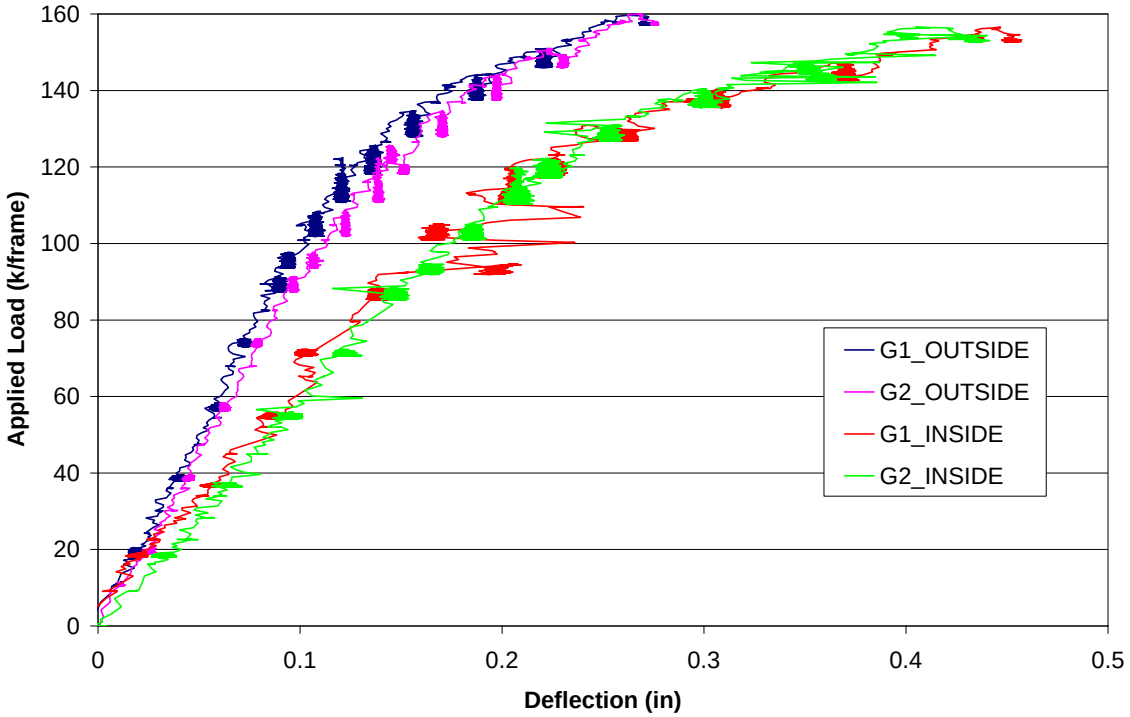

Figure 4.5.4 Deflection During the Intermediate Static Test at the Live End

4.5.4 Final Static Test on the Live End

Figure 4.5.5 shows the deflections of the live end of the lab mockup during the final static test at the outside loading point and the inside loading point. The initial vertical stiffness of the lab mockup at the loading points was less than the initial vertical stiffness at the loading points during the initial static test and intermediate static test on the live end. At the inside loading points, the initial vertical stiffness of the lab mockup was 679 k/in. and 638 k/in. for the initial static test and intermediate static test, respectively. For the final static test, the initial vertical stiffness at the inside load point was 246 k/in. As the load was increased, the vertical stiffness at the load points decreased at a faster rate for the final static test, when compared to the initial static test and intermediate static test. This is shown when comparing Figure 4.5.1, Figure 4.5.4, and Figure 4.5.5. This was due to the many loading and unloading cycles the dead and live end underwent along with the cracking that occurred during the intermediate static test and final static test at the dead end and during the intermediate static test at the live

end. For applied loads greater than 279 k/frame, the vertical stiffness at the inside load point and outside load point was 9.5 k/in. and 25.7 k/in., respectively. This corresponds to 1.4% and 2.6% of the initial vertical stiffness at the inside load point and outside load point, respectively.

At an applied load of 296 k/frame, the lab mockup was completely unloaded. The stiffness of the lab mockup as it was unloaded was similar to the initial stiffness before the final static test. After the lab mockup was completely unloaded, the residual deflection was 0.96 in. at the outside load point and 2.07 in. at the inside load point. The residual deflections can be attributed to:

1. Cracks that remained open upon unloading.
2. Residual strains in the prestressing strands and mild reinforcing steel.
3. Residual slip at the interface between the haunch and girder from rough cracks.

Cracking occurred at the interface between the haunch and girder at applied loads of 260 k/frame and 196 k/frame for girder 1 and girder 2, respectively. The rate the strains in the shear connectors increased with respect to the applied load was greater than the strain rate increase prior to cracking in the haunch. Figure 4.5.6 shows the strains in the shear connectors for the final static test at the live end. The increase in the strain rate with respect to the load indicates the shear connectors were engaged in resisting the horizontal shear stresses after cracking at the interface between the haunch and girder. However, the increase in the strain rate after cracking at the interface was not as apparent for the final static tests at the live end as it was for the final static test at the dead end. After the lab mockup was unloaded, there were residual strains in many of the instrumented shear

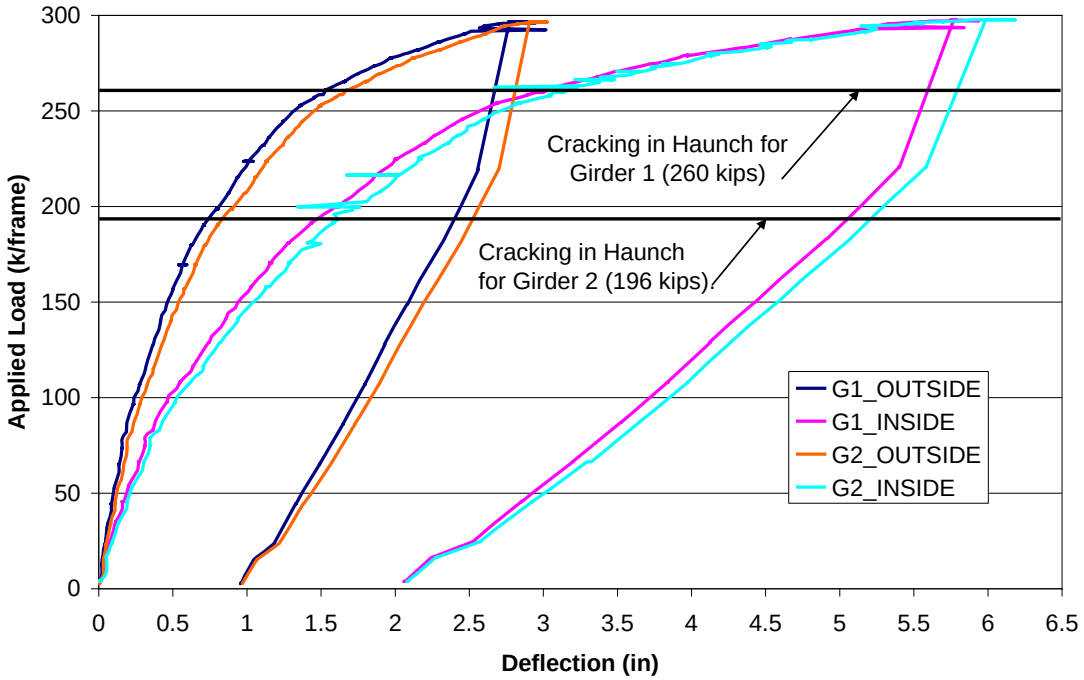

Figure 4.5.5 Deflections During the Final Static Test at the Live End

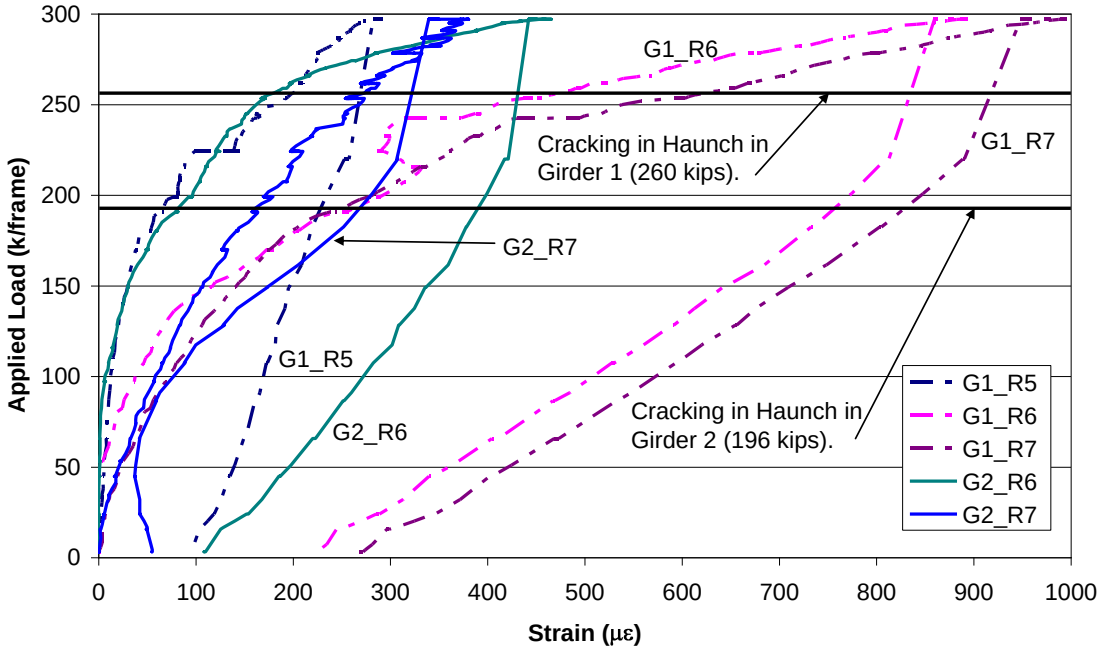

Figure 4.5.6 Connector Strains During the Final Static Test at the Live End

connectors. This was likely due to residual slip at the interface, which does not allow the shear connectors to return to their undeformed configuration. The residual strains in the shear connectors did not result from nonlinear material behavior. The strains in the shear connectors are less than 50% of the nominal yield strain for the entire range of applied loads.

After cracking occurred at the interface between the haunch and girder for both girder 1 and girder 2, the strains in shear connectors G1_R6 and G1_R7 are two to two and a half times as great as the strains in the other shear connectors at an applied load of 296 k/frame. The strains in shear connectors G1_R6 and G1_R7 are also noticeably greater than the strains in the other shear connectors for applied loads as small as 174 k/frame. At 174 k/frame there was no cracking at the interface for each girder. The shear connectors G1_R5 and G2_R6 are located in panel 2 and are subjected to smaller shear loads than shear connectors G1_R6, G1_R7, and G2_R7. Since G1_R6 and G1_R7 are located in girder 1, the larger strains may partially be from the effects of having two concrete interfaces as opposed to having an interface between concrete and steel.

Figure 4.5.7 shows the cracking pattern at the live end of girder 1 and girder 2. The cracking pattern for the two girders was very similar. However, the shear cracks in girder 1 were more dispersed when compared to the shear cracks in girder 2. Additionally, not as many shear cracks were noticed in girder 1. Section 4.5.1 and Section 4.5.3 describe the cracking for low load levels below 159 k/frame. The cracking patterns and progression of the cracks for the final static test at the live end were the same as the description for the cracking patterns and progression of the cracks final static test at the dead end in Section 4.4.4. The wirepots at the epoxied male-female joints indicate there was no relative vertical movement at the joints. Cracking was observed at the inside male-female joint an applied load of 260 k/frame, as shown in Figure 4.5.8. This was the same load at which cracking was observed on the bottom surface of the deck near the joint.

At an applied load of 296 k/frame, crushing was observed on the top surface of the bridge deck. This is shown in Figure 4.5.9. The crushing that occurred during the final static test on the live end was more pronounced than the crushing that occurred

during the final static test on the dead end. The applied load of 296 k/frame results in a flexural capacity of 24,500 k-in., which was 58% greater than the AASHTO LRFD required flexural capacity of 15,500 k-in. As discussed in Section 4.4.4, there was additional capacity in the lab mockup, which is partially from the restraint provided by the bearing pads at the supports. For the final static test at the live end, the failure load was 1.2% less than the calculated flexural capacity of 24,800 k-in.

The shear studs and hooked reinforcing bars performed well as shear connectors with 2 ft pocket spacing. The strains in the shear connectors were less than 50% of the nominal yield strains. The deflections at the inside load points and outside load points are the approximately the same for girder 1 and girder 2. Although, when the deflections are looked at in Figure 4.5.5 at a specific load level, girder 2 had slightly larger deflections than girder 1. The loads at which cracking was observed at the interface between the haunch and girder was 39% greater and 4% greater than the required flexural strength for girder 1 and girder 2, respectively.

(a)

(b)

Figure 4.5.7 Cracking Pattern at the Live End for (a) Girder 1

(b) Girder 2 During the Final Static Test

Figure 4.5.8 Cracking at the Epoxied Male-Female Joint

Figure 4.5.9 Crushing in the Top of the Bridge Deck

4.6 Comparison of Pocket Spacing and Connector Types

4.6.1 Stiffness

Table 4.6.1 shows the vertical stiffness values at the inside load points for the static live load tests performed. The initial vertical stiffness values during the initial static tests at the live end and dead end of the lab mockup have a 13% difference. The flexural cracks on the dead end from the intermediate static test influenced the initial stiffness at the live end. This was one reason for the difference in the calculated initial stiffness at each end. Other possible reasons are discussed in Section 4.5.1. The connector strains were low at this point during the live load testing program and there was no cracking at the interfaces. Therefore, the 2 ft pocket spacing and 4 ft pocket spacing are assumed to provide the same initial degree of composite action. As discussed in Section 4.4.4 and Section 4.5.4 and shown in Table 4.6.1, the stiffness at the dead end and live end of the bridge degraded with each live load test that was performed. The difference in the initial stiffness values for the final static tests at the dead end and live end was larger than the difference in the initial stiffness values for the intermediate static tests at the dead end and live end because the extent of cracking during the final static test on the dead end was greater than the extent of cracking during the intermediate static test on the dead end.

The difference in stiffness at each end of the lab mockup was not believed to be from a larger loss in composite action at one end of the lab mockup compared to the other

for a particular live load test. The strain levels in the shear connectors are comparable for both ends of the lab mockup during the live load tests. During the final static tests, the peak strains in the shear connectors are less than 50% of the nominal yield strain and cracking was not observed at the interface between the haunch and girder until the final static tests at 183 k/frame. The difference in the initial stiffness at each end of the lab mockup was due to the influence of the existing cracks at the opposite end of the bridge. Both the dead end of the lab mockup and the live end of the lab mockup experienced the same loss in the degree of composite action during the live load testing program. This was because both the dead end and live end of the lab mockup:

1. Were subjected to the same number of tests,
2. Were subjected to the same load levels during each test,
3. Started out with the same initial stiffness during the initial static tests,
4. Ended with the same stiffness at the end of the live load testing program.

These results lead to the observation that the pocket spacing does not influence the stiffness of the lab mockup.

Figures 4.4.1, 4.4.4, 4.4.7, 4.5.1, 4.5.4, and 4.5.5 can be used to compare the stiffness values for girder 1 and girder 2 at the inside loading points and outside loading points. None of these figures indicate that the deflections for girder 1 and girder 2 were significantly different for a given loading point and a given static test. This showed the stiffness for the two girders was approximately the same at a given load level. Because the stiffness of the two girders was the same and the cracking patterns and extent of the cracking was similar, the degree of composite action between the girder and haunch must be approximately the same. This means the shear studs and hooked reinforcing bars provide the same stiffness contribution. Additionally, the low strain levels in both types of shear connectors show that any slip at the interface was very small and does not fully engage the shear connectors, indicating a high level of composite action still exists with both pocket spacings and both connector types at the conclusion of the live load testing program.

Table 4.6.1 Comparison of Vertical Tangential Stiffness Values at the Inside Load Points

	Initial Stiffness (k/in.)			Final Stiffness (k/in.)
Static Test	Initial	Intermediate	Final	Final
4 ft (Dead End)	777	710	461	10.0
2 ft (Live End)	679	638	246	9.50
K_{dead}/K_{live}	0.87	0.90	0.53	0.95

4.6.2 Fatigue

Figures 4.4.2 and 4.5.2 show the deflections of the lab mockup at an applied load of 40 k/frame. The deflections for each end of the bridge are small and do not show a substantial increase in the deflections with respect to the number of cycles performed on a given end of the lab mockup. The average deflection at the outside load point for both ends of the mockup was approximately 0.04 in. and the average deflection at the inside load point for both ends of the bridge was approximately 0.055 in. for both ends of the lab mockup. Additionally the average deflection at each load point for each girder was the same. During the cyclic testing on the dead end of the lab mockup, the deflections appear to increase for a larger number of cycles for girder 2 . However, Section 4.4.2 indicates the strain levels in the shear studs are still less than 1% of the nominal yield strain for the entire range of cycles and no cracking was observed at the interface between the haunch and girder. The larger deflection of 0.09 in. at 2 million cycles at the inside loading point for girder 1 at the live end was believed to be from a problem with the wirepot. Figures 4.4.3 and 4.5.3 show the stress in the bottom layer of strands at 40 k/frame. The average stress in the bottom layer of strands is approximately 1.8 ksi for both ends of the bridge and is the same for girder 1 and girder 2. Neither the pocket spacing nor the connector type have an influence on the stiffness of the lab mockup or the fatigue performance of the bottom row of strands for the cyclic testing.

4.6.3 Strength

Both the live end and dead end of the lab mockup failed in flexure by crushing of the concrete on the top surface of the bridge deck. The maximum moment reached

during the final static tests on the dead and live ends of the lab mockup were 23,700 k-in. and 24,500 k-in., respectively. The difference in the maximum moments for the two tests is 3%. The AASHTO LRFD required flexural capacity of the lab mockup was 15,500 k-in. The pocket spacing had very little influence upon the flexural capacity of the lab mockup. The maximum shear reached during the final static tests on the dead and live ends of the lab mockup are 206 k and 213 k, respectively. The required vertical shear capacity of the lab mockup is 152 k. This calculation is shown in Appendix A. The lab mockup with either the 2 ft pocket spacing or 4 ft pocket spacing was capable of exceeding the required vertical shear strength. Section 3.2.1 discusses the design of the lab mockup and how the flexural design and vertical shear design were modified such that the lab mockup would not fail before the horizontal shear forces exceeded the horizontal shear design capacities in the regions with high shear forces.

Table 4.6.2 shows the ratio of the resulting horizontal shear force at each shear pocket from the final static tests to the nominal horizontal shear capacity at each shear pocket. Pocket 1 was closest to the live end of the bridge with the 2 ft pocket spacing and pocket 15 was closest to the dead end of the bridge with the 4 ft pocket spacing. The regions from the support to the outside loading point had the highest shear, based on the shear diagram for the loading conditions. The region with the highest shear incorporates all the pockets within the exterior panel. The horizontal shear force developed at each pocket during the final static tests is 19% higher and 24% higher than the nominal horizontal shear capacity at the dead end and live end, respectively. This indicates the number of shear connectors can be reduced and the lab mockup can still reach the required flexural strength, the required vertical shear strength, and the required horizontal shear strength. The finite element study presented in Chapter 5 investigates the issue of reducing the number of shear connectors in the shear pockets while still providing the required strength for the system.

Table 4.6.2 Ratio of Applied Horizontal Shear to Horizontal Shear Capacity for the Final Static Tests

pocket #	$V_{applied}/V_{prov}$ Dead End	$V_{applied}/V_{prov}$ Live End
1	0.47	1.24
2	0.47	1.24
3	0.47	1.24
4	0.47	1.24
5	0.47	0.37
6	0.47	0.37
7	0.47	0.37
8	0.52	0.41
9	0.56	0.58
10	0.56	0.58
11	0.64	0.67
12	0.49	0.67
13	0.52	0.70
14	1.19	0.49
15	1.19	0.49

The shear connector layout used for the lab mockup provided sufficient strength which exceeds the nominal horizontal shear strength for the pockets in the outside panels (panel 1 and panel 5). Both the 2 ft pocket spacing and 4 ft pocket spacing are capable of providing the required strength. Additionally, the strain levels of less than 50% of the nominal yield strain at maximum loads in all of the connectors indicate both the hooked reinforcing bars and the shear studs perform well as shear connectors.

During the final static test at the dead end, cracking occurred at the interface between the haunch and girder 1 at an applied load of 209 k/frame and cracking occurred at the interface between the haunch and girder 2 and an applied load of 183 k/frame. These applied loads correspond to 111% of the required flexural strength and 99% of the required vertical shear strength for girder 1 and 97% of the required flexural strength and 86% of the required vertical shear strength for girder 2. During the final static test at the live end, cracking occurred at the interface between the haunch and girder 1 at an applied load of 260 k/frame and cracking occurred at the interface between the haunch and girder 2 and an applied load of 196 k/frame. These applied loads correspond to 138% of the required flexural strength and 123% of the required vertical shear strength for girder 1

and 104% of the required flexural strength and 92% of the required vertical shear strength for girder 2.

The exceptional performance of the lab mockup under flexural loads, vertical shear loads, and horizontal shear loads along with the low strain levels in the shear connectors show that both 2 ft pocket spacing and 4 ft pocket spacing are acceptable as well as either hooked reinforcing bars or shear studs as shear connectors. The only possible exception to this is the combination of shear studs with 4 ft pocket spacing. For this combination, cracking occurs at the interface between the haunch and girder at 86% of the required vertical shear strength. However, cracking was expected to occur at the interface in order to engage the shear connectors in resisting the horizontal shear forces.

4.7 Durability of Transverse Joints

The grouted female-female joints performed exceptionally well in all stages of the durability test outlined in Section 3.2.12. No leaking occurred at the transverse joints during the ponding tests. However, a small leak was discovered at the inside male-female joint during the intermediate static test on the live end of the bridge. The leak was noticed around an applied load of 122 k/frame. After the intermediate live load test on the live end of the bridge was completed and the load was completely removed, the leaking stopped. Water was ponded to complete stage 4 of the durability test described in Section 3.2.12. No leaking was discovered.

Water must have leaked into the transverse joint during stage 3 of the durability test. The water did not leak all the way through the joint to the bottom of the deck panels during this stage. During the intermediate static test on the live end, the epoxy must have cracked enough to allow water that was trapped during the 3rd stage of ponding to leak all the way through the joint. When the load was removed, the crack closed back up and did not allow water to leak all the way through the joint during stage 4. No leaking was observed when ponding was performed for stage 5 of the durability study of the transverse joints.

4.8 Summary of Experimental Results

The experimental results provided insight in to constructability issues associated with the deck panels system, as well as time dependent behavior and the performance of the different shear pocket spacings and shear connector types. The transverse joints proved to be more of a constructability issue than a strength or fatigue issue when subjected to moments that cause compression in the deck. The grouted female-female joint configuration prevented leaking at the joints and allowed for rapid placement of the panels on the girders during construction. The time dependent study showed that the creep and shrinkage strains in the deck at the end of the 2 month evaluation period were only 40 με, indicating the creep and shrinkage losses for the post-tensioning force were small. The live load testing program showed that both 2 ft and 4 ft pocket spacing performed well. Both types of shear connectors examined, the shear studs and the hooked reinforcing bars, also performed well.

Chapter 5
Finite Element Results

This chapter presents the finite element results of the time dependent study, the push-off test models, and the lab mockup models. The time dependent results provide insight in to the behavior of the lab mockup at different construction stages as well as the response due to differential creep and shrinkage. The effect of the initial level of post-tensioning provided in the lab mockup on the long term stresses in the deck is discussed. The peak loads reached by the push-off test models are compared to experimental data and the AASTHO LRFD shear friction equation. These comparisons are used to establish how conservative the modeling methodology is for modeling the shear connectors and material interfaces. The results of the lab mockup models are compared to the experimental data presented in Chapter 4. The results of the parametric study are presented to provide insight in to the influence of the connector type and pocket spacing on the deck panel system.

5.1 Time Dependent Analysis Results

5.1.1 Verification of Finite Element Models for Time Dependent Behavior of Lab Mockup

A phased, time dependent analysis was run in DIANA. The eight phases outlined in Section 3.3.1 were followed for this model. Preliminary analyses indicated the ACI 209 model grossly over predicted the creep and shrinkage strains. The CEB-FIP model code 1990 creep and shrinkage model modeled the behavior of the mockup more accurately than the ACI 209 model. The CEB-FIP model code 1990 was used for all the finite element models. The creep and shrinkage functions used for the concrete in the girders and panels were also used for the grout in the haunch. The geometric properties and material properties from Section 3.2.1 and Section 4.3 were used for the panels, girders, and haunch.

Figure 5.1.1 shows the finite element strains in girder 1 compared to the experimental strains in girder 1. Figure 5.1.2 shows the finite element strains compared to the experimental strains in the panels. Because the experimental results revealed the

creep and shrinkage behavior of girder 1 and girder 2 were very similar, only girder 1 was modeled in DIANA for the time dependent study. The experimental results presented in Figure 5.1.1 and Figure 5.1.2 were adjusted such that the residual strains developed in the girders and panels during the casting operation were neglected. The effects from the heat of hydration were not included in the finite element models.

In order to get a better correlation between the experimental results and finite element solution, a higher modulus of elasticity was used than predicted from Section 8.5.1 of ACI 318 [26]. The modulus of elasticity predicted from Section 8.5.1 of ACI 318 was increased by 10% for the girder and by 8% for the panels. Increasing the modulus of elasticity was justified by the comparisons in Section 4.3 between the experimentally determined values of the modulus of elasticity and the predicted values from Section 8.5.1 of ACI 318.

There were still some differences between the experimental results and the finite element results. The finite element strains were 19% higher than the average experimental strains in the top of the girder. The finite elements strains were 26% higher than the average experimental strains in the bottom of the girder. The finite element strains were 15% higher than the average experimental strains in the panels. The error partially resides in the accuracy of the creep and shrinkage models.

The rate at which the compressive strains increased for the finite element results was very close to the rate at which the compressive strains increased for the experimental results. The magnitude of the strains from the elastic shortening during the post-tensioning operations matches the experimental data exceptionally well. This indicates that the parameters used to define the development of the elastic modulus with time were accurate.

From the experimental data, the average force during the jacking operation at the live end of the bridge was 27.9 k. After the strands were tensioned, the average force in the strands was 25.8 k, after the elastic shortening loss, anchor loss, friction loss, and initial relaxation loss were accounted for. Details on calculating these losses are presented in Section 4.1.6. The average force in the strands 34 days after the start of the post-tensioning operation was 25.6 k. This resulted in an instantaneous loss of 2.1 k and a loss of 0.17 k over the first 30 days. For the finite element solution, the force during the

jacking operation was 30.9 k. The average initial force in the strands was 28.7 k, after the elastic shortening loss, anchor loss, and friction loss were accounted for. The average force in the strands 34 days after the start of the post-tensioning operation was 28.5 k. This resulted in an instantaneous loss of 2.25 k and a loss of 0.13 k over the first 34 days. The loss due to creep and shrinkage in the finite element model was 0.04 k smaller than the loss from the experimental data. This difference in force corresponds to a 31% difference.

Recall from Chapter 3 that not all 12 strands were instrumented. One of the strands that was not instrumented could have had a force that was significantly higher or lower than the force in a strand that was instrumented. The force in the strand that was not instrumented would have affected the post-tensioning loss in a strand that was instrumented, and visa versa. For the finite element results, the average jacking force at the live end for the three instrumented strands was used. This also could have affected the results. However, both the experimental results and finite element results indicated the post-tensioning losses were small. This was expected since the age of the panels at the time the strands were first tensioned was 91 days.

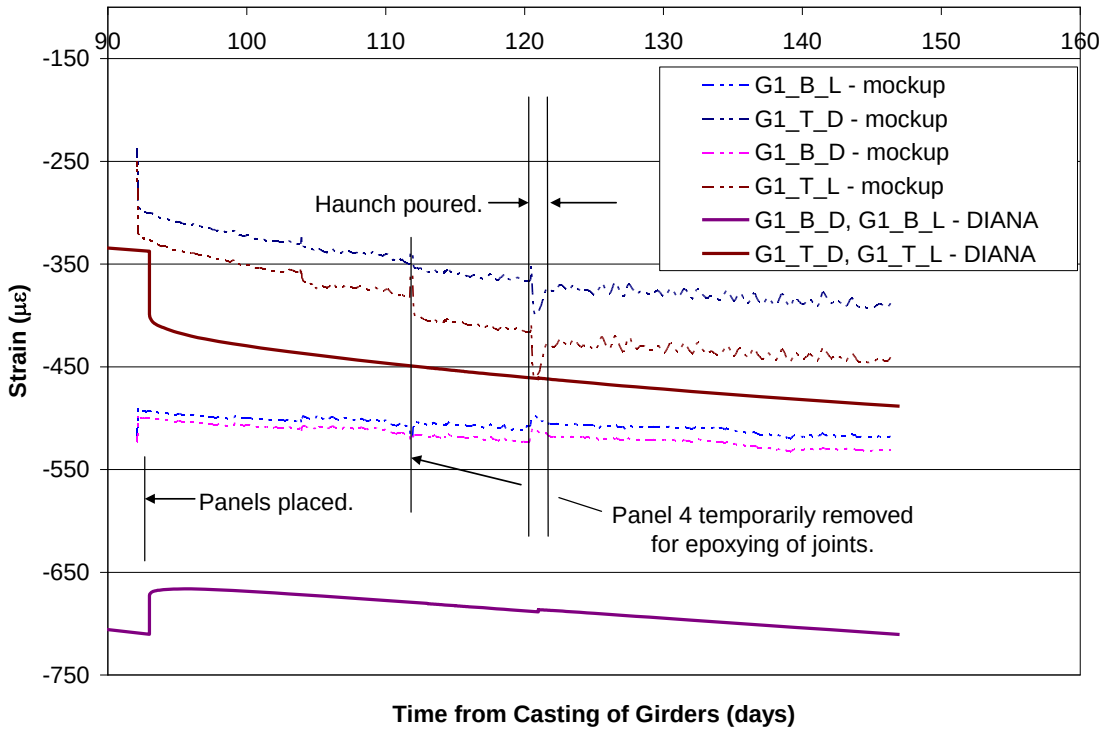

Figure 5.1.1 Comparison of Strains in Girder 1 from Finite Element Results to Strains in the Lab Mockup

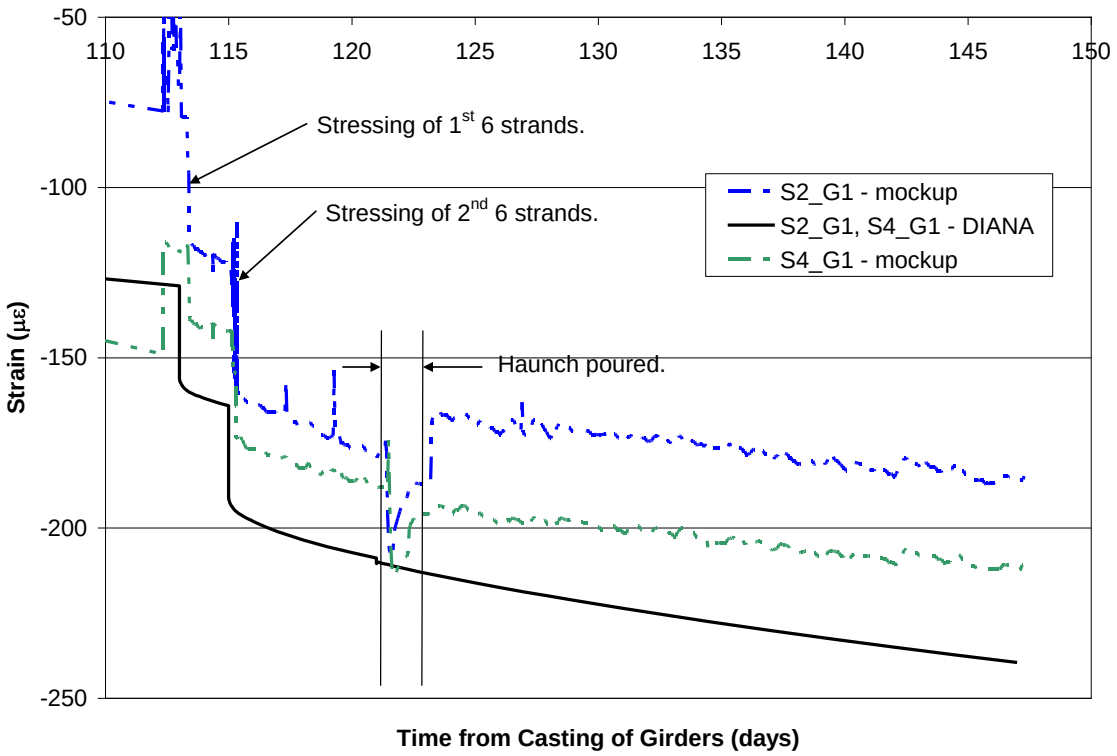

Figure 5.1.2 Comparison of Strains in Panels from Finite Element Results to Strains in the Lab Mockup

5.1.2 Further Look at the Time Dependent Behavior of Lab Mockup

Figure 5.1.3 shows the finite element results for the strain profile through the depth of the lab mockup at selected time intervals after the system was made composite. The location of the strain profile is 13 ft-4 in. from the support. The time intervals indicated were measured from the time the girders were cast. The haunch was poured on day 121 making the system composite. During the early time intervals of the composite system, there was little change in strain in the girder, haunch, and deck. Additionally, the curvature remained fairly constant over the duration of the analysis. The curvature in the girder was 9.94 με/in at day 121 and 9.78 με/in at day 147. At day 10,647, the curvature in the girder was 12.1 με/in, creating a net change in curvature of 2.20 με/in over the duration of the analysis. The differential creep and shrinkage in the composite system cause the system to undergo fairly uniform axial changes in strain compared to the change in curvature.

Figure 5.1.4 shows the stress profile through the depth of the lab mockup at selected time intervals after the system was made composite. Similar to the strain profile behavior, the stress profile does not have any significant changes for the early time intervals. The change in the compressive stress in the girder undergoes a fairly uniform decrease over time. The largest change observed during the early time intervals was a 74 psi increase in stress in the haunch. At day 10,647, the average stress in the haunch was 468 psi, which was greater that the expected cracking stress of $6\sqrt{f'_c} = 6\sqrt{4010} = 380$ psi. By the time the haunch was poured, the girders and panels have experienced most of their shrinkage. The grout in the haunch was restrained during the shrinkage process, creating tensile stresses. The tensile stresses could have been reduced if

1. The panels and girders were not as old at the time of the grouting operation.
2. The post-tensioning operation was performed closer to the time of the grouting operation.
3. A very low shrinkage grout was used.

Additionally, the increase in tensile stress in the haunch occurs more gradually over time than expected. The average stress in the haunch at day 4887 was 371 psi and the average stress in the haunch at day 10,647 was 468 psi, resulting in a change in stress of 97 psi over this time interval. The cause of a significant change in stress at an old age for the haunch may be attributed to the notational size of the member, as defined in Equation 2.69. The small perimeter that was exposed to the atmosphere for the haunch caused the notational size of the member to increase. This increased the value of β_H defined in Equation 2.78, and reduced the development of the creep coefficient with time, as defined in Equation 2.77. For this situation, the reduction in the development of the creep coefficient with time lead to the development of higher stresses in the haunch. In order for the haunch to reach a creep strain associated with the reduced creep coefficient, more time passes compared to a member that has a lower notational size. This means the age of the panels and girders was even greater and the incremental axial creep strains associated with the post-tensioning are smaller, leading to a larger axial restraint force and tensile stresses in the haunch.

The mathematical model may not account for the exchange of moisture between the haunch and the girder and panels. This decrease in the "effective" notational size would ultimately increase the development of the creep coefficient and shrinkage strain with time and increase the tensile stresses developed.

Like the compressive stresses in the girder, the compressive stresses in the deck also decrease over time. However, the decrease in the compressive stress at the top of the deck was noticeably larger than the decrease in compressive stress at the bottom of the deck. The stress at the top of the deck at day 121 was -268 psi and the stress at the bottom of the deck at day 121 was -261 psi. The stress at the top of the deck at day 10,647 was -180 psi and the stress at the bottom of the deck at day 10,647 was -221 psi. The average force in one strand after the initial losses was 28.7 k, which corresponds to an initial stress in the deck of -298 psi. The average force in one of the strands at day 10,647 was 26.8 k. This results in a post-tensioning loss of 1.88 k, or 12.3 ksi, which is a 6.6% loss. This was expected since the strands were post-tensioned at a panel age of 91 days. Although the post-tensioning loss was small, this does not correspond to a small loss of compressive force in the deck. The compressive stress in the top of the deck decreased by -118 psi, which was a reduction in compressive stress of 39.6%.

The increase in compressive strains in the structure can be misleading. Although the deck, haunch, and girder were contracting with time, the viscoelastic behavior of concrete causes the stresses to decrease with time in this case. This relaxation effect is illustrated in Figure 5.1.3 and Figure 5.1.4, showing the compressive strains in the deck, haunch, and girder increased with time and the compressive stresses in the deck and girder decreased over time and the tensile stresses in the haunch increased over time.

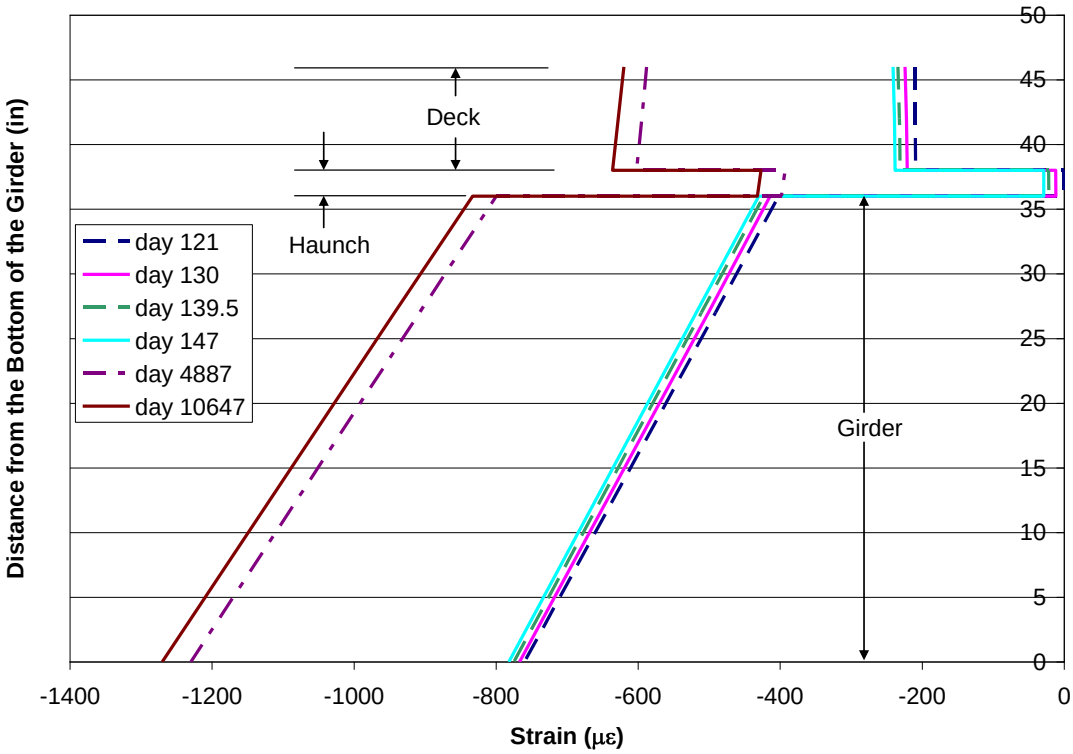

Figure 5.1.3 Strain Profiles in Composite Section for Different Times During the Service Life

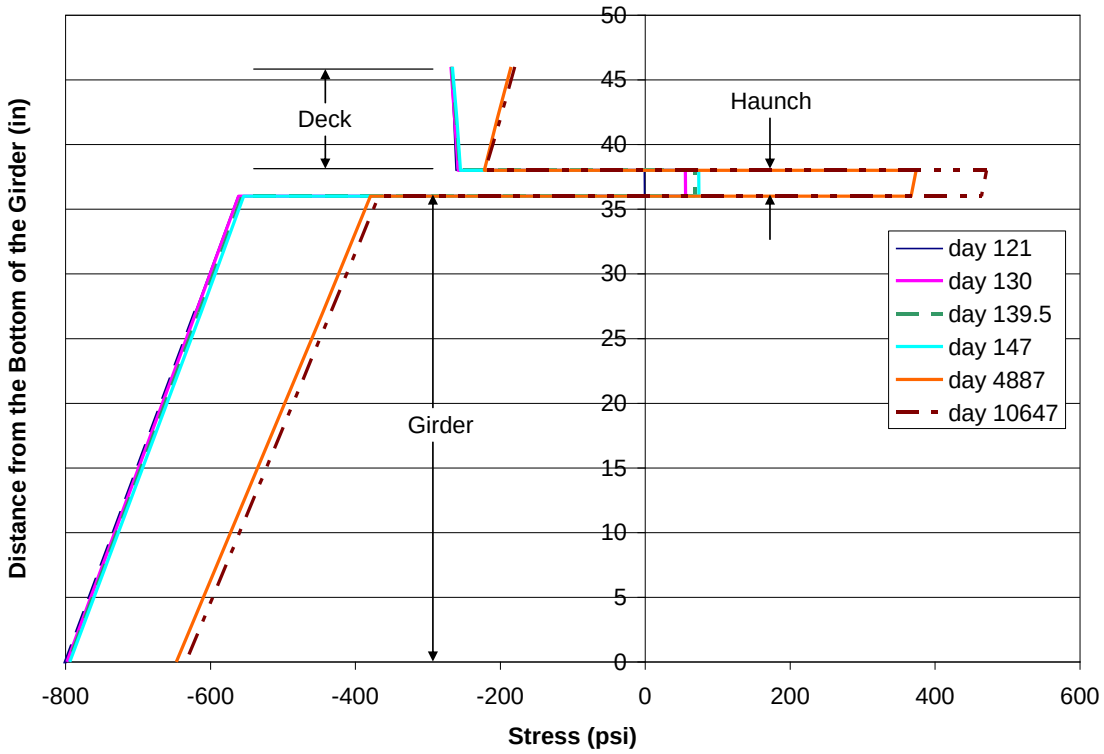

Figure 5.1.4 Stress Profiles in Composite Section for Different Times During the Service Life

5.1.3 Estimation of Post-Tensioning Losses and Recommended Initial Levels of Post-Tensioning

As summarized in Section 2.1.1.6, Issa recommends an initial post-tensioning level of -200 psi for simply supported bridges to keep the joints in compression under live loads. It was assumed this recommendation was based on the application of service loads, not factored loads. Recall that the sign convention is positive (+) for tensile strains and tensile strain increments and negative (-) for compressive strains and compressive strain increments. A post-tensioning level of -100 psi was needed to secure the tightness of the joint under live loads and an additional -100 psi was included to account for creep and shrinkage effects. The results of the finite element study on the lab mockup showed the reduction in the compressive stress in the top of the deck was 118 psi and the reduction in the compressive stress in the bottom of the deck was 77 psi. This resulted in an average reduction in the compressive stress in the deck of 97.5 psi, which was surprisingly close to Issa's lump sum estimate of 100 psi for the losses due to creep and

shrinkage, considering Issa's research is based on deck panel systems with steel girders. Based on Issa's recommendation, the compressive stress at the bottom of the deck of -221 psi was adequate to counteract the tensile stresses developed at the bottom of the deck from service loads. The initial level of post-tensioning of -298 psi proved to be adequate. Although a lower initial level of post-tensioning may have been satisfactory as well.

In addition to Issa's recommendations for initial levels of post-tensioning, which is discussed in more detail in Section 2.1.1.6, a detailed creep and shrinkage analysis is an alternative. The analysis can be simplified by using the age adjusted effective modulus approach with strain compatibility equations, constitutive relationships, and equilibrium equations. The general method is discussed in Section 2.1.1.2.

5.2 Push-Off Test Results

5.2.1 Verification of Finite Element Models for Push-Off Tests

The finite element results based on the smeared cracking approach (see Section 3.3.2) were compared to Wallenfelsz's results for push-off specimen tests. The load vs. relative slip behavior was compared to evaluate the modeling methodologies proposed for the shear connectors and material interfaces described in Section 3.3.2. The comparisons will also be used to predict whether the results for the finite element models for the live loads on the lab mockup will be conservative and reliable.

Figure 5.2.1 shows the finite element results for the push-off test compared to Wallenfelsz's results at small relative slip values. Hooked reinforcing bars were used by Wallenfelsz for this particular series of tests. The number and size of reinforcing bars were varied in each of the tests. Either 2 No. 4 bars or 2 No. 5 bars were used. The finite element model used 2 No. 5 bars.

The finite element results match Wallenfelsz's results very well up until a relative slip of 0.02 in. At this point, the finite element solution diverged. Cracking developed in the vicinity of the shear connectors, as shown in Figure 5.2.2. The peak load reached for the finite element results was 48.5 k. The finite element results indicated the peak strain in the shear connector occurs near the interface of the haunch and girder. There was a rapid decrease in strain in the shear connectors as the distance from the haunch was

increased. This may partially explain why the Wallenfelsz's results indicated the strain levels were low. It was difficult to place the ER strain gage on the shear connector close to the interface between the haunch and girder. Additionally, the ER strain gage was wrapped in an aluminum sheet to protect it. The aluminum sheet facilitates slip between the grout and the aluminum sheet itself, affecting the measured local strain and strain gradient along the length of the shear connector. The issue of localized strains is explored more in Section 5.3.

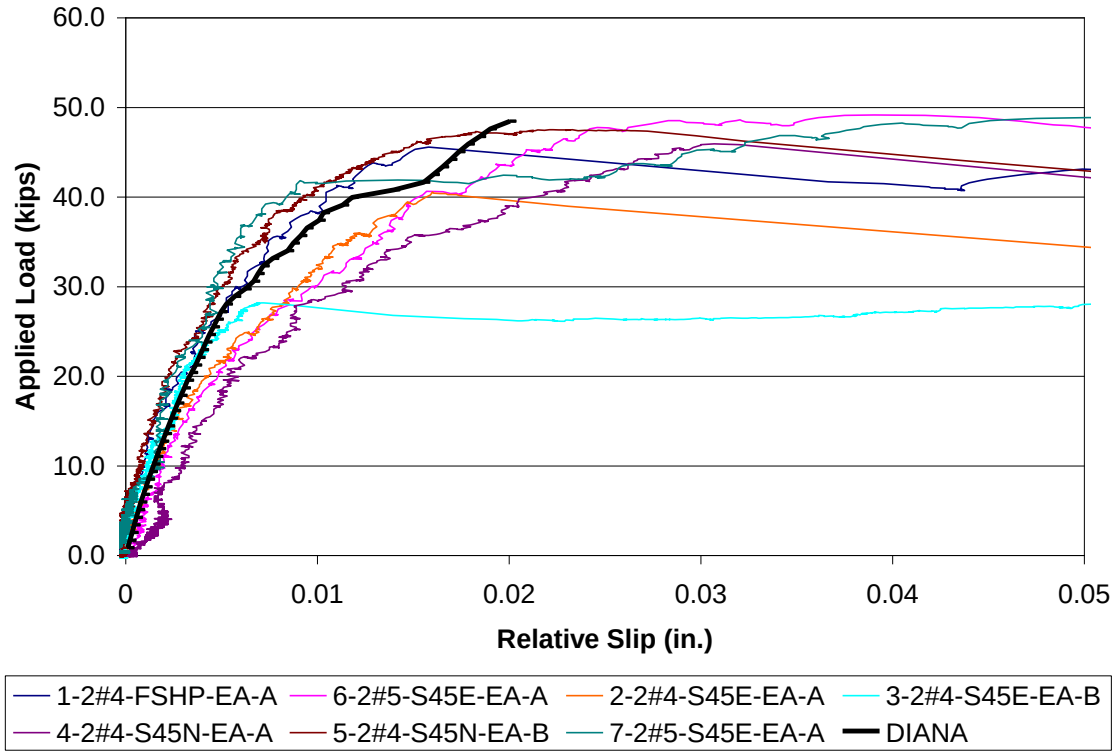

Figure 5.2.1 Comparison of Relative Slip of Push Off Specimen at Small Relative Slip Values Using a Smeared Cracking Approach

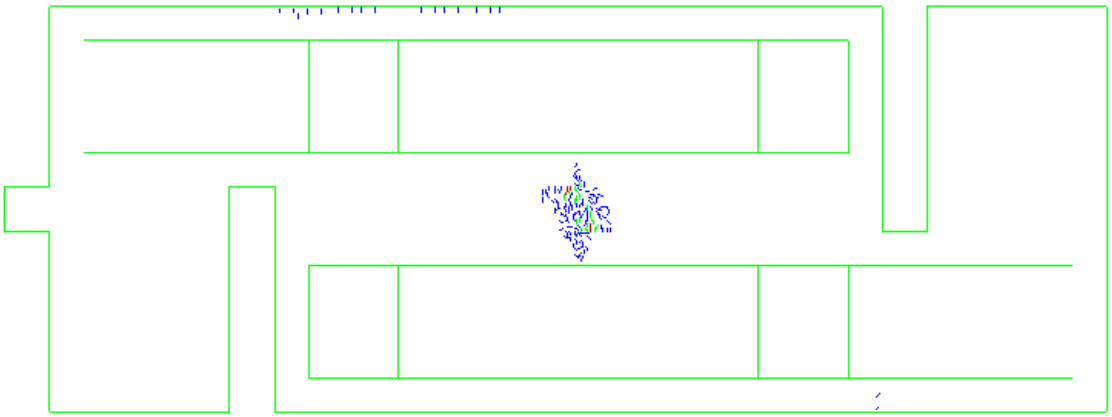

Figure 5.2.2 Cracking Pattern in Push-Off Test Specimen at 48.5 k.

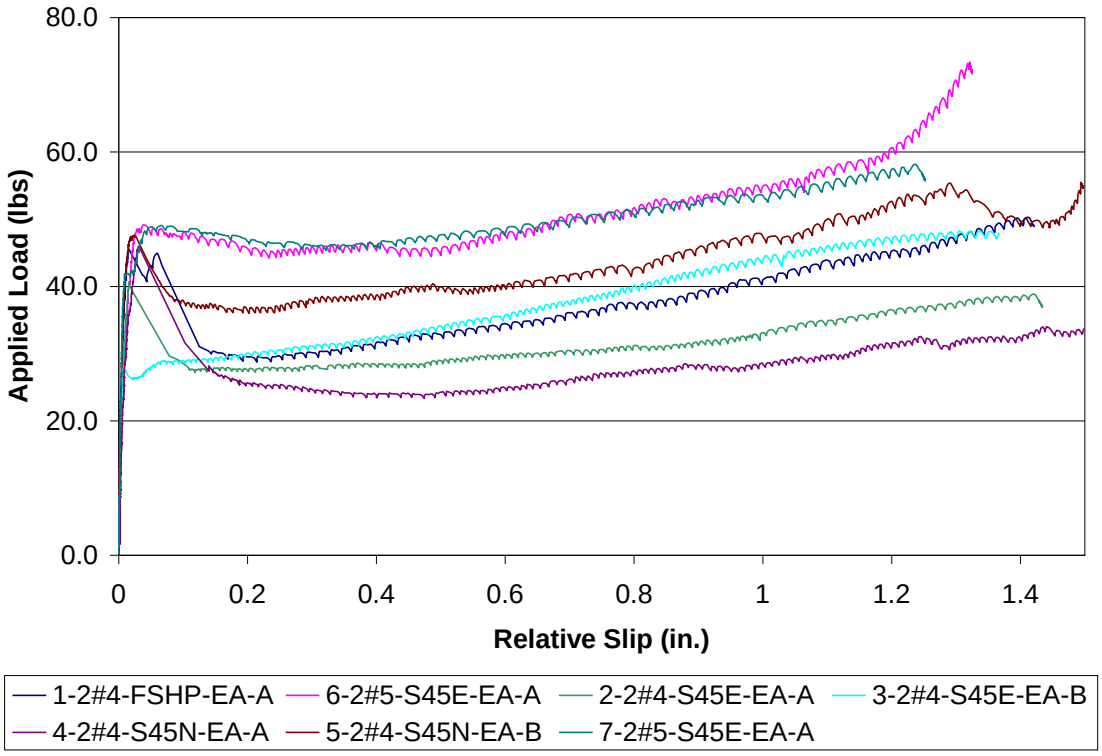

Figure 5.2.3 Relative Slip of Push Off Specimen by Wallenfelsz

Figure 5.2.3 shows relation of the full range of relative slips at the horizontal interface performed by Wallenfelsz. In most of the test results, there was a sudden drop in load and a large increase in the relative horizontal slip after the peak load was reached.

The only way to pick this up in the finite element solution was to run a displacement controlled analysis. The finite element model had not captured the unloading portion of the load vs. relative slip curve because it was run under force control. Additionally, there were convergence problems associated with the localized cracking that occurs in the vicinity of the shear connector and interface when the smeared cracking model was used instead of the discrete cracking model. This is discussed in Section 3.3.2.

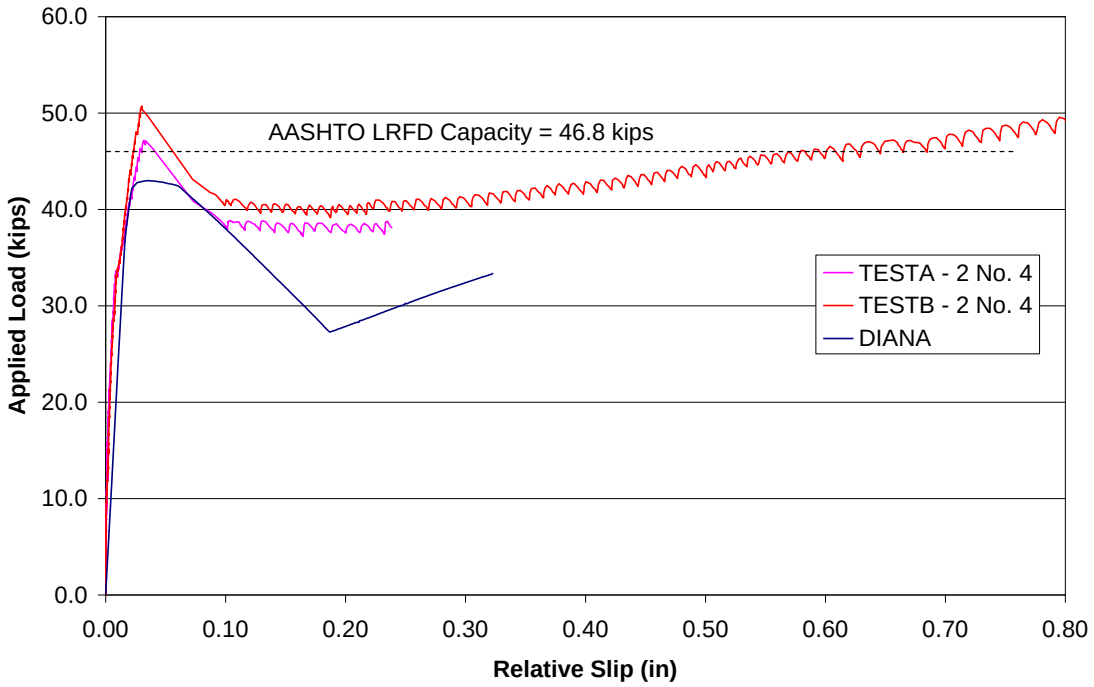

Figure 5.2.4 Comparison of Relative Slip of Push Off Specimen for 2 No. 4 bars with the Softened Elastic Modulus Approach

In order to help stabilize the convergence behavior when attempting to capture the post-peak behavior of the load vs. displacement curve, the softened elastic modulus approach was adopted, as discussed in Section 3.3.2. The elastic modulus used to simulate the cracked region is 0.25% of the elastic modulus for concrete in the panel and girder. The size of the softened elastic zone was approximately 2 in. by 2 in., as determined from the results of the analyses with a smeared cracking model activated.

Figure 5.2.4 shows the finite element results compared to Wallenfelsz's results with 2 No. 4 bars as the shear connectors. Figure 5.2.5 shows the finite element results

compared to Wallenfelsz's results with 2 No. 5 bars as the shear connectors. The softened elastic modulus approach resulted in a more stable convergence behavior of the model. Both of the finite element models for hooked reinforcing bars used as shear connectors underestimated the peak load reached by Wallenfelsz as well as the capacity predicted by Equation 2.121, the AASTHO LRFD shear friction equation. The

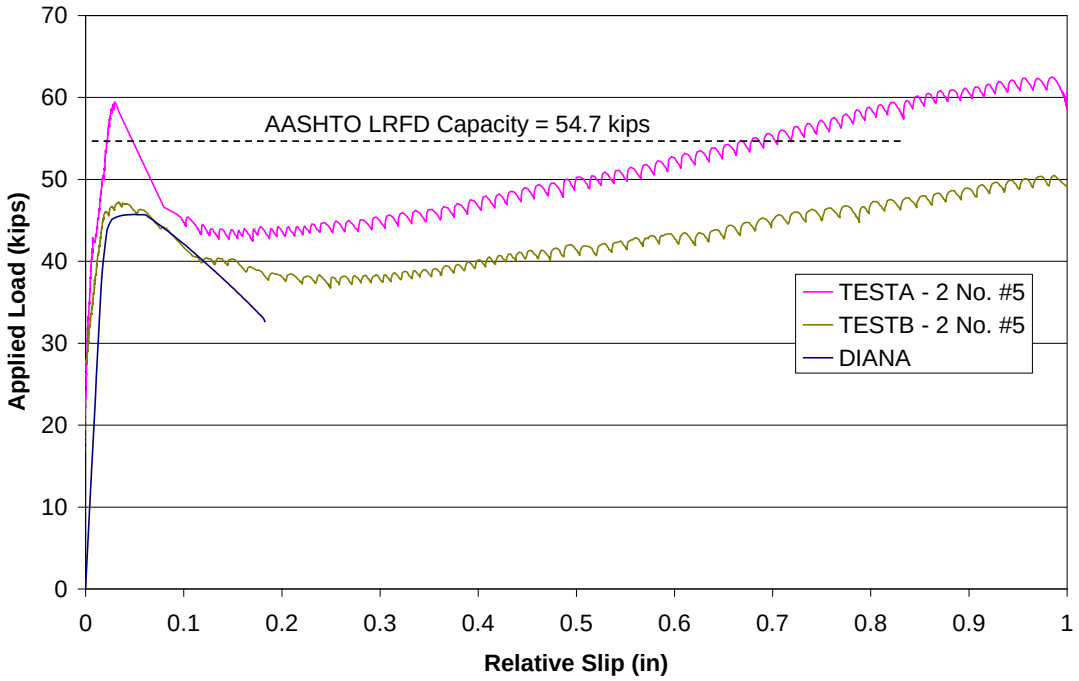

Figure 5.2.5 Comparison of Relative Slip of Push Off Specimen for 2 No. 5 bars with the Softened Elastic Modulus Approach

peak load for the finite element model with 2 No. 4 bars was 42.0 k and the peak load for the finite element model with 2 No. 5 bars was 45.7 k.

The stiffness of the finite element models was less than the stiffness from Wallenfelsz's results prior to the peak load being reached. This was expected when using the softened elastic modulus approach because a region was specified as being "cracked" by reducing the elastic stiffness when, in fact, the region had not cracked yet. For applied loads greater than 40 k, localized cracking in the vicinity of the shear connector and interface was significant enough that the softened elastic modulus approach accurately

captured the slip values and corresponding loads. For applied loads less than 40 k, the localized cracking in the vicinity of the shear connectors and interface was not as significant. Therefore, the smeared cracking approach was more applicable for capturing the gradual progression in the number of cracks and the propagation of the cracks.

When the results for the smeared cracking approach and softened elastic modulus approach are compared for a model with 2 No. 5 bars, the smeared cracking approach results in a peak load that was approximately 6% higher than the model using the softened elastic modulus approach. However, both approaches accurately capture the load vs. displacement behavior of the push-off specimen. The smeared cracking approach was more accurate at capturing the peak load and the softened elastic modulus approach was able to capture the post-peak behavior of the specimen for slip values up to approximately 0.2 in.

For slip values between 0.1 in. and 0.2 in., the finite element model was not able to capture the behavior of the push-off specimen as accurately as it did for slip values between 0 in. and 0.1 in. As stated earlier, the purpose of the finite element models for the push-off specimen is to propose a modeling methodology for modeling the shear connectors in the finite element models for the lab mockup. The experimental results presented in Chapter 4 revealed that the slip values at the interfaces were much less than 0.2 in.

The softened elastic modulus approach was also applied to the push-off models with shear studs as shear connectors. Figure 5.2.6 shows finite element results for the push-off test compared to Wallenfelsz's results with three shear studs as the shear connectors. The shear studs are ¾ in. in diameter. The slip value of 0.12 in. was where the peak load for the finite element results and Wallenfelsz's results occur. The slip values for the finite element model are higher than the slip values for the Wallenfelsz results at a given load. Using the softened elastic modulus approach and the modeling methodology for the shear connectors and interface resulted in an underestimation of the peak load. This is shown for the results with the hooked reinforcing bars as shear connectors. With the clamping effect neglected in the finite element model, the frictional resistance from the clamping force was not developed, reducing the capacity of the model. Although the magnitudes of the slip and applied load do not match the

Wallenfelsz data exactly, the behavior of the two sets of results was the same according to Figure 5.2.6.

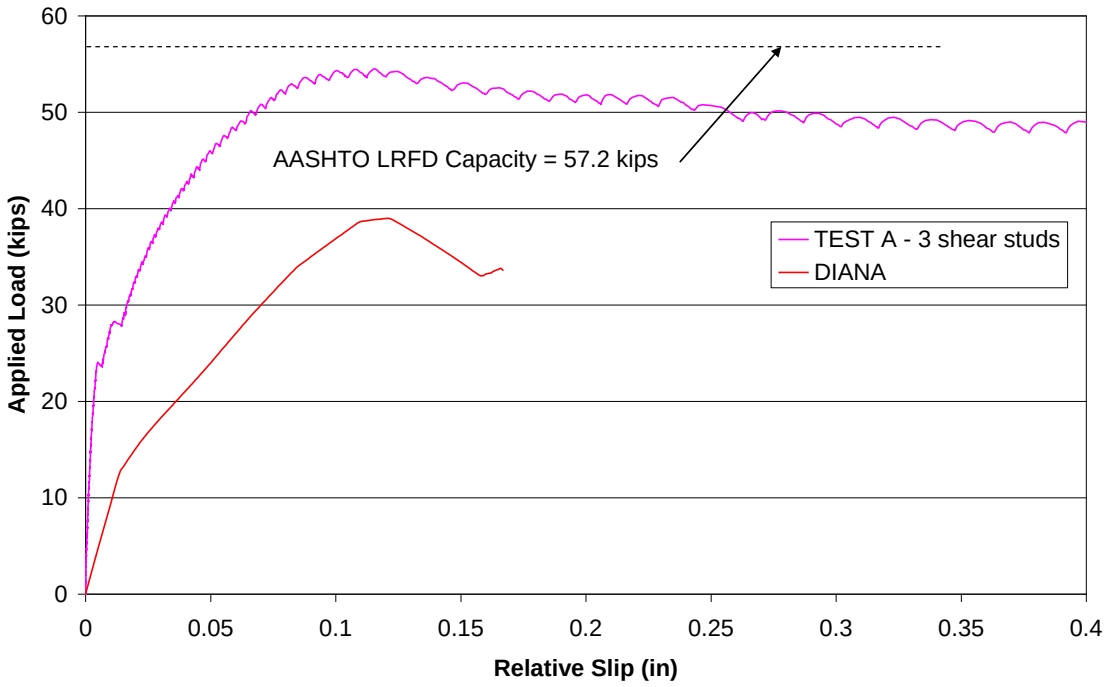

Figure 5.2.6 Comparison of Relative Slip of Push Off Specimen for 3 Shear Studs with the Softened Elastic Modulus Approach

5.2.2 Further Assessment of the Modeling Methodology for Shear Pockets

Figure 5.2.7 compares the peak loads reached by the finite element models to the calculated shear capacity from Equation 2.121, the AASHTO LRFD shear friction equation, for different amounts of shear connectors. For both the models with the hooked reinforcing bars and models with the shear studs, the peak load reached was always less than the shear capacity from the AASHTO LRFD shear friction equation. Additionally, as the number of shear connectors provided was increased, the rate at which the peak load increased in the finite element model was less than the rate at which the shear capacity increased for the AASHTO LRFD shear friction equation.

Shear friction theory assumes the shear connectors yield when the peak load is reached. However, Wallenfelsz's results revealed this was often not the case for the push-off specimen. This explains the difference in the rate of increase in the capacity for

the AASHTO LRFD shear friction equation and the peak loads from the finite element results.

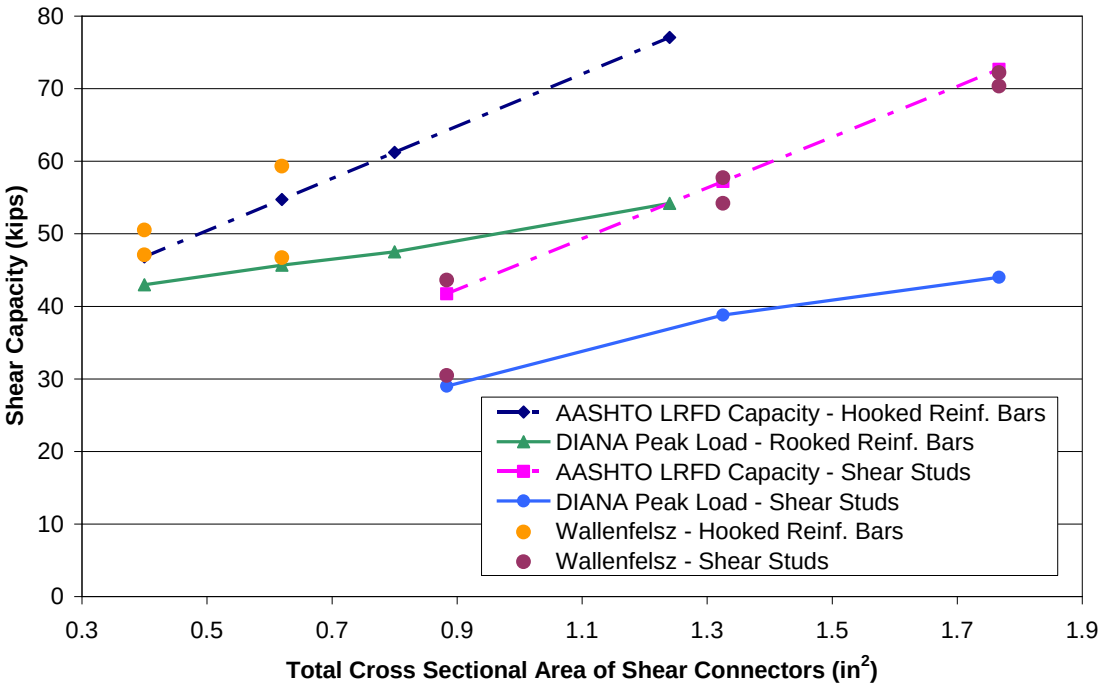

Figure 5.2.7 Comparison AASHTO LRFD, DIANA, and Experimental Capacities from Push-Off Tests

Table 5.2.1 Comparison of Percent Yield at Peak Load with Wallenfelsz's Results

Number of Connectors	DIANA		Wallenfelsz
	σ_e (ksi)	% yield	% yield
2 No. 4	17	28	41
2 No. 5	24	40	57
4 No. 4	23	39	N.A.
4 No. 5	30	49	N.A.
2 studs	17	34	33
3 studs	32	63	73
4 studs	31	63	73

This was also the case for the finite element results. The Von Mises stresses are calculated for the stress state for each shear connector combination. The Von Mises stresses can be directly compared to the uniaxial yield stress for the connectors. The

percent of the yield stress in the connector at the time the peak load was reached in the finite element model is compared to Wallenfelsz's results in Table 5.2.1. Wallenfelsz did not perform push-off tests on specimen with 4 No. 4 bars or 4 No. 5 bars. There was a good correlation between the finite element results and Wallenfelsz's results. Although, the connectors from Wallenfelsz's results were closer to yielding by the time the peak load was reached compared to the finite element results. Both sets of results show that as the number of connectors is increased,the connectors are closer to yielding at the peak load. The issue of the level of strain in the shear connectors when the design load is reached for deck panel systems is discussed in Section 4.4 and Section 4.5 and is explored further in Section 5.3.

The finite element results for the push-off specimen reveal the modeling methodology proposed for the shear connectors and the material interface provides an accurate representation of the behavior of push-off specimens as well as a conservative estimate of the shear capacity of a push-off specimen. The approach can be applied to modeling the shear connectors in shear pockets for the lab mockup. The results of the lab mockup will provide conservative results for the horizontal shear transfer behavior by underestimating the degree of composite action under a given load and shear connector layout.

The smeared cracking approach was used in liu of the softened elastic modulus approach for the lab mockup because the cracking in the shear pockets will be smeared along the entire length of the pocket. The finite element models for the push-off tests showed the softened elastic modulus approach and the smeared cracking approach produced similar results.

5.3 Live Load Analysis Results

5.3.1 Verification of the Finite Element Models for the Live Load Tests

5.3.1.1 Load vs. Deflection Response for the Lab Mockup

Due to the sequence of the load tests during the experimental live load testing program (see Section 3.2.6), the load vs. displacement behavior of the system was different during the final static test compared to the load vs. displacement behavior during the intermediate static test at a given location. This point is illustrated in Figure

5.3.1 for the experimental results for the intermediate and final static tests on the live end of girder 1. After the intermediate static test was performed on the live end, the cracking was significant enough that the initial vertical stiffness of the lab mockup during the final static test on the live end was less than it was during the intermediate static test.

The finite element models do not behave in the manner described above. Once the load was removed, the cracks close and the initial vertical stiffness of the lab mockup was always the same. Figure 5.3.1 shows the unloading and reloading behavior of the finite element model. The model was loaded up to 198 k, then the load was reduced to 0

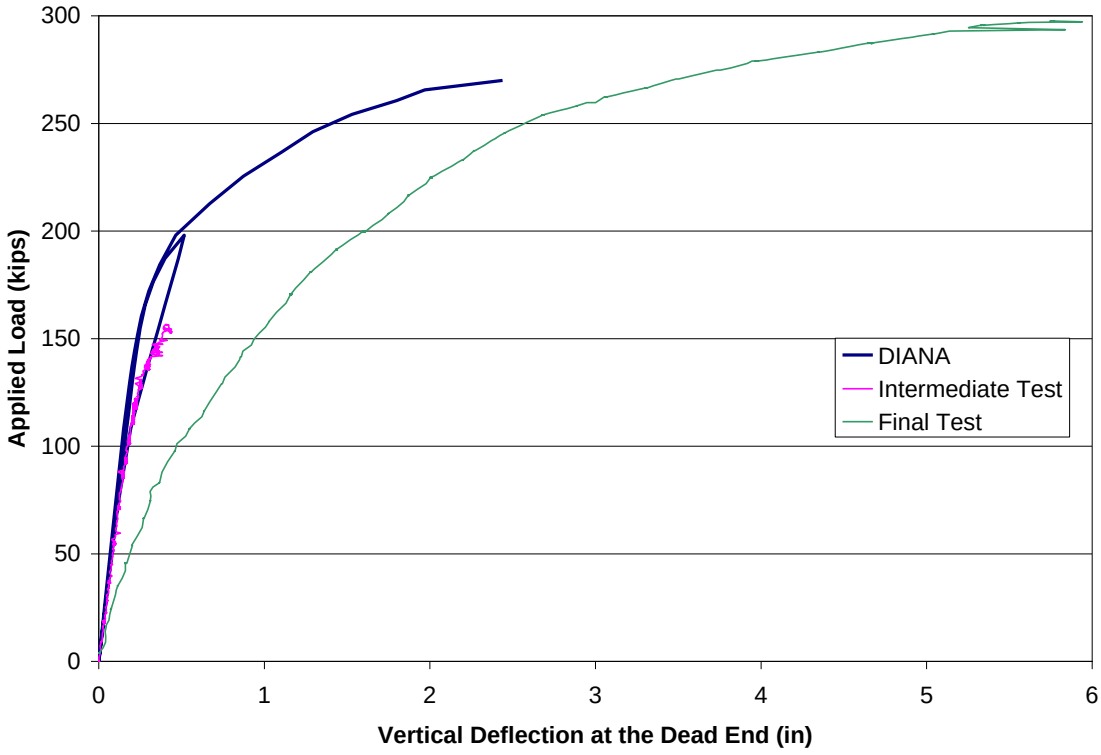

Figure 5.3.1 Unloading and Reloading Behavior of Finite Element Models at the Inside Loading Point

k, and finally it is loaded until failure. After the load is reapplied, the original vertical stiffness of the system at the load point was recovered. Because of this hysteresis effect, the finite element results are compared to both the intermediate static tests and final static tests. The load vs. displacement response is discussed for one finite element model and very similar behavior is observed for the displacements for the other models. The results for the rest of the models are found in Appendix I.

Figure 5.3.2 shows the displacement behavior for girder 1 at the live end of the lab mockup at the inside load point. The initial stiffness of the finite element model matched the initial stiffness of the experimental results up until to an applied load of 127 k/frame. At this point, nonlinear behavior was observed in the system due to the development of multiple flexural cracks under the load points as well as the beginning of shear cracks in the web of the girder. Because the peak load for the intermediate live load test was only 159 k/frame, the results from the final static test were compared to the finite element results for applied loads greater than 159 k/frame. The stiffness of the finite element model was greater than the stiffness of the final static test results

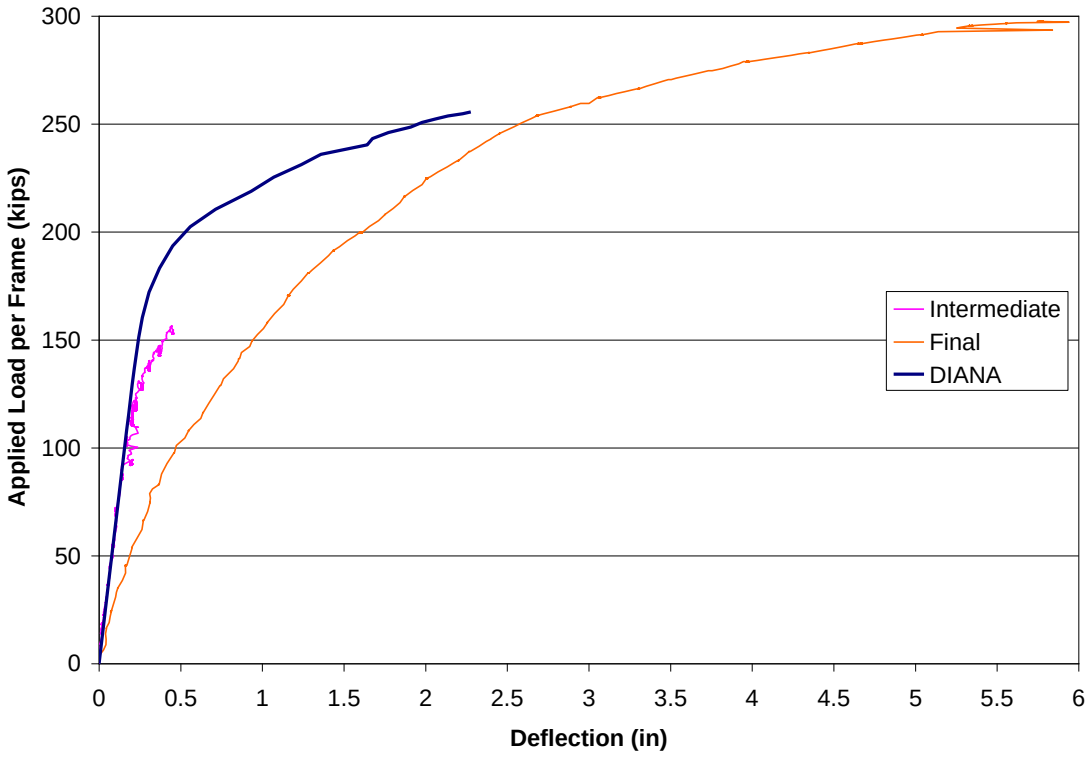

Figure 5.3.2 Deflections in the Finite Element Model for Girder 1 at the Live End Compared to Experimental Results

for applied loads less than approximately 190 k/frame because of the unloading and reloading effect. The stiffness of the finite element model decreased at a faster rate than the experimental results from the final static test for applied loads greater than 190 k/frame. For applied loads approaching the capacity of the lab mockup and the capacity

of the finite element model, the stiffness of the finite element model was very close to the stiffness of the lab mockup. The finite element results diverged at an applied load of 256 k/frame. Divergence does not necessarily indicate the structure modeled had "failed." With the multiple nonlinearities associated with this model (see Section 3.3.2), numerical difficulties were encountered at higher applied loads. This was especially true with the presence of extensive cracking, leading to a numerical collapse when there was no stiffness left at an integration point because of cracking. The finite element models for the parametric study were capable of reaching an applied load ranging from 84% to 143% of the required flexural strength of the lab mockup, depending on the amount and type of shear connectors used. This is discussed more in Section 5.3.2.

5.3.1.2 Strains in the Shear Connectors in the Lab Mockup

Table 5.3.1 shows a comparison of the axial strain in the shear connectors at each end of the bridge with the different shear connectors used. Recall that 2 ft pocket spacing was used at the live end of the bridge and 4 ft pocket spacing was used at the dead end of the bridge. The experimental strains listed in Table 5.3.1 are taken from the ER strain gages mounted on the shear connectors. The ER strain gages on the shear connectors were located approximately 1 in. from the top face of the top flange of the girder. The finite element strains listed in Table 5.3.1 are the strains in the shear connectors 0.25 in. from the top face of the top flange of the girder. This was done to capture the high strains that develop in the region for larger slip values. In general, the finite element strains were smaller than the experimental strains for a large portion of the applied load. This underestimation of the axial strain may be due to the clamping effect being ignored. Other possible discrepancies associated with local behavior of the connectors and slip at the interface are:

1. Accuracy of localized cracking and crushing based on mesh refinement.
2. Connectors that had nodes at the same x, y coordinate but had different z coordinates were lumped together in the same plane for the sake of the plane stress analysis. This created a stiff spot in the model that may have lead to premature localized cracking and crushing.

3. A perfect bond between the reinforcement and shear connectors was assumed to exist.
4. Accuracy of the shear stress vs. relative slip relationship at the interface.
5. Ability of the combination of the mesh layout for the connectors and the shape functions for the beam elements to represent the true deformed configuration of the shear connector.

At higher levels of applied load, the finite elements strains were higher than the experimental strains. As mentioned previously, at higher loads a steep strain gradient developed through the depth of the connector with the maximum strain occurring at the interface between the girder and haunch. In Table 5.3.1(a), the average connector strain in pocket 13 from the finite element results was 742 με at an applied load of 252 k/frame. The corresponding experimental strain was 291 με. Note that the experimental reading did not capture the high strain value in the connector because of the location of the ER strain gage. Additionally, the finite element model cannot model the local effects completely accurately. Therefore, the peak strain in the connectors for the finite element results may slightly overestimate the strain. This will lead to a shear connector, or series of shear connectors, yielding prematurely and leading to higher slip values and a lower corresponding degree of composite action. For the sake of the parametric study in evaluating the current shear connector design provisions in AASHTO LRFD, this is satisfactory. When the average connector strain in pocket 13 at the top of the haunch was examined at the dead end with hooked reinforcing bars as shear connectors, the finite element strain was 282 με, which compares very favorably with the experimental strain of 291 με. This also illustrated how steep of a strain gradient can be encountered in the shear connectors through the depth of the haunch.

Although the strains in the shear connectors from the finite element results were much larger than the corresponding experimental strains at higher applied loads, both sets of results do show that in many of the cases the shear connectors did not yield. There were two cases in Table 5.3.1 were the shear connectors did yield, according to the finite element results. In Table 5.3.1(b) in pocket 3 at an applied load of 252 k/fame, the finite element strain was 2150 με, which was just above the nominal yield strain of 2070 με for

the hooked reinforcing bars. In Table 5.3.1(c) in pocket 13 at an applied load of 196 k/frame, the finite element strain was 2040 με, which was 18% above the yield strain of 1720 με for the shear studs. However, when looking at the strains in the connectors at the top of the haunch for these cases, the finite elements strains were 503 με and 882 με for hooked reinforcing bars and shear suds, respectively. These strains were well below the nominal yield strain.

The finite element strains also reflected the trends observed with the experimental strains, when higher levels of applied load were considered. For example, when applied loads of 218 k/frame and higher are considered, the finite element and experimental results both showed that the shear connectors in pocket 14 had higher strains than the connectors in pocket 13 in Table 5.3.1(a). Similar trends are observed in Table 5.3.1(b)-(d). Additionally, both sets of results show the low participation of pocket 6 in Table 5.3.1(d). When considering all the pockets in Table 5.3.1, pocket 6 is the farthest from the support.

Table 5.3.1 Comparison of Axial Strain in the Shear Connectors

(a) Dead End with Hooked Reinforcing Bars

Pocket #	Applied Load per Frame (kips)	Experimental Strain (με)	DIANA Strain (με)
13	108	15	16
	151	105	28
	201	199	86
	218	231	148
	235	262	375
	252	291	742
14	108	60	13
	151	165	40
	201	325	108
	218	380	370
	235	433	765
	252	490	1300

(b) Live End with Hooked Reinforcing Bars

Pocket #	Applied Load per Frame (kips)	Experimental Strain (με)	DIANA Strain (με)
3	108	81	23
	151	144	64
	202	287	169
	219	346	774
	236	403	1330
	252	558	2150
5	108	14	9
	151	31	21
	202	82	64
	219	89	110
	236	152	506
	252	191	1590

(c) Dead End with Shear Studs

Pocket #	Applied Load per Frame (kips)	Experimental Strain (με)	DIANA Strain (με)
13	108	95	16
	151	167	69
	182	220	933
	196	239	2040
15	108	70	13
	151	141	328
	182	204	633
	196	227	676

(d) Live End with Shear Studs

Pocket #	Applied Load per Frame (kips)	Experimental Strain (με)	DIANA Strain (με)
3	108	81	15
	151	108	34
	183	144	85
	196	168	349
6	108	10	21
	151	31	30
	183	61	52
	196	86	67

5.3.1.3 Strain Profiles for the Lab Mockup

The strain profile through the depth of the lab mockup at a distance of 13 ft-4 in. from the dead end of the bridge is shown in Figure 5.3.3. The section was taken through girder 1 which contains hooked reinforcing bars for shear connectors. Two different applied load levels were examined, 108 k/frame and 122 k/frame. The experimental data that the finite element results were compared to for the strain profiles was taken from the intermediate static tests. After the intermediate static tests were completed, all 4 of the ER strain gages along the bottom of the girders, G1_D_L, G1_L_L, G2_D_L, and G2_L_L from Table 3.1 no longer worked because of the extent of cracking that occurred during the tests. The strain profile from the finite element model showed satisfactory correlation with the experimental data. The largest differences between the finite element results and experimental results existed at the bottom of the girders. There were three possible causes for the differences in the strains toward the bottom of the girders. Part of the difference could be attributed to the restraint provided by the bearing pads, which had a tendency to decrease the strains. As described in Section 3.3.4.1, the boundary

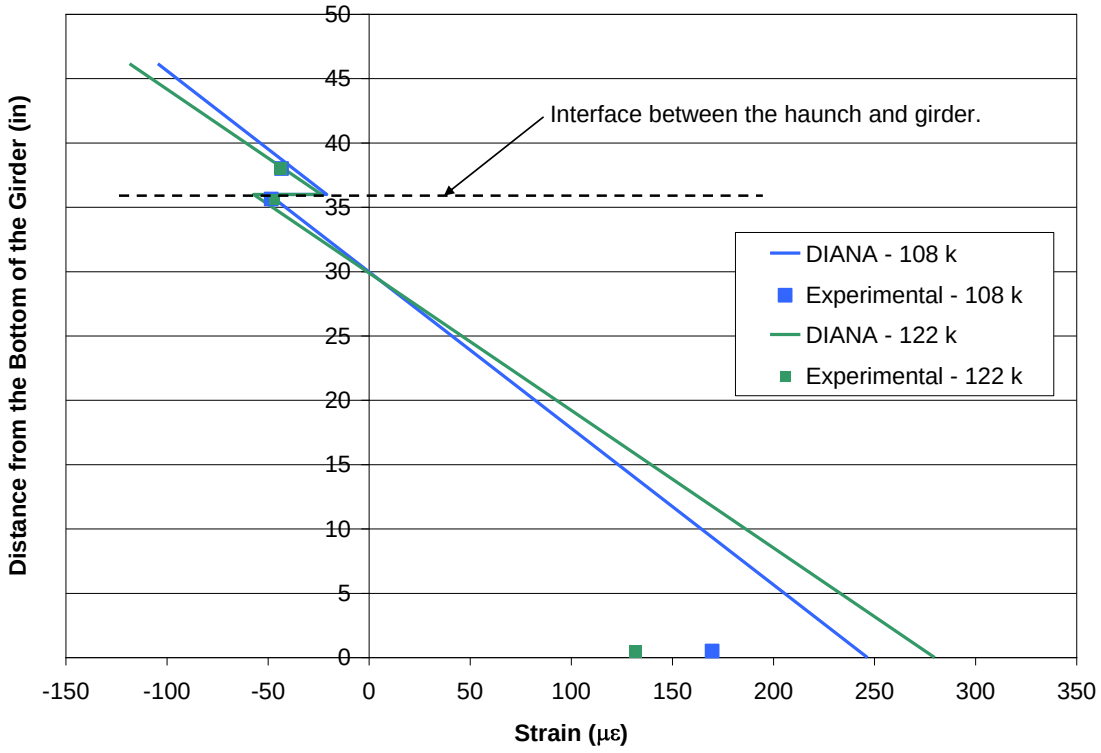

Figure 5.3.3 Strain Profile at the Dead End for Hooked Reinforcing Bar Connectors

conditions for the finite element model consisted of a pin and roller system. Therefore, the bottom flange was not restrained from expanding, resulting in larger finite element strains. The second cause had to do with the effect of the level of composite action on the strain distribution. The results in Section 5.2.1 and Section 5.2.2 showed the method used for modeling the shear pockets resulted in reduced levels of composite action compared to Wallenfelsz's results. This caused the curvature to increase and resulted in larger finite element strains at the bottom of the girder. The third cause had to do with the tension stiffening effect. When cracking occurred in the lab mockup, there was still uncracked concrete between the existing cracks with tensile strength. The level of tension in the concrete ranged from zero at the location of the cracks to a maximum tensile strain in the concrete between the location of the cracks. Therefore, the level of strain in the strain gages was affected when cracks were located in the vicinity of the shear connectors. For the finite element models, tension stiffening was not taken in to account. This effect had caused the experimental strains to be larger, relative to the finite element strains. Additionally flexural cracking occurred at 118 k/frame and 122 k/frame at the dead end and live end of the lab mockup. Depending on the location of the cracks relative to the strain gage, the experimental strain at 122 k/frame may be less than the experimental strain at 108 k/frame. This is shown in Figure 5.3.3.

Figure 5.3.3 shows the finite element strains were close to the experimental strains. The finite element strains were taken from the strain profile at the same depth through the cross section that the strain gages were located at. The experimental strains are compared to the finite element strains in Table 5.3.2. This was done for two load levels, 108 k/frame and 122 k/frame. Both sets of results showed a loss of composite action based on the discontinuities at the interface. Additionally, if full composite action was present and the strain in the top of the girder was a compressive strain, the strain in the bottom of the panel should have shown a higher compressive strain when subjected to positive curvature. Similar observations are made for girder 2 with the shear studs at the dead end of the bridge. The strain distribution for this combination can be found in Appendix I.

Table 5.3.2 Comparison of Experimental Strains and Finite Element Strains for the Lab Mockup Verification Study

	108 k/frame		122 k/frame	
ER Strain Gage Name	Experimental (με)	DIANA (με)	Experimental (με)	DIANA (με)
G1_D_U	-48.4	-46.5	-47.0	-53.6
PG1_D_L	-43.3	-37.4	-43.8	-42.2

The strain profile through the depth of the lab mockup at a distance of 13 ft-4 in. from the live end of the bridge is shown in Figure 5.3.4. The section was taken through girder 2 which contains shear studs for shear connectors. Two different applied load levels were examined, 108 k/frame and 122 k/frame. The ER gages near the interface show that the finite element strains provide strain values close to the experimental values.

When comparing Figure 5.3.4 to Figure 5.3.3, the discontinuity in the strain profile at the interface for the 2 ft pocket spacing at the live end was similar to the discontinuity in the strain profile at the interface for the 4 ft pocket spacing at the dead end. The discontinuity in the strain profile at the interface at the live end with shear stud connectors at a load level of 122 k/frame was 36.5 με. The discontinuity in the strain profile at the interface at the dead end with hooked reinforcing bar connectors at a load level of 122 k/frame was 33.6 με. The small difference in the strain discontinuities can partially be attributed to the pocket spacing and the connector type. Similar observations were made for the shear stud connectors at the dead end and hooked reinforcing bar connectors at the live end, which are shown in Appendix I. The performance of the different pocket spacings, connector types, and quantity of connectors at ultimate load levels will be evaluated in Section 5.3.2.

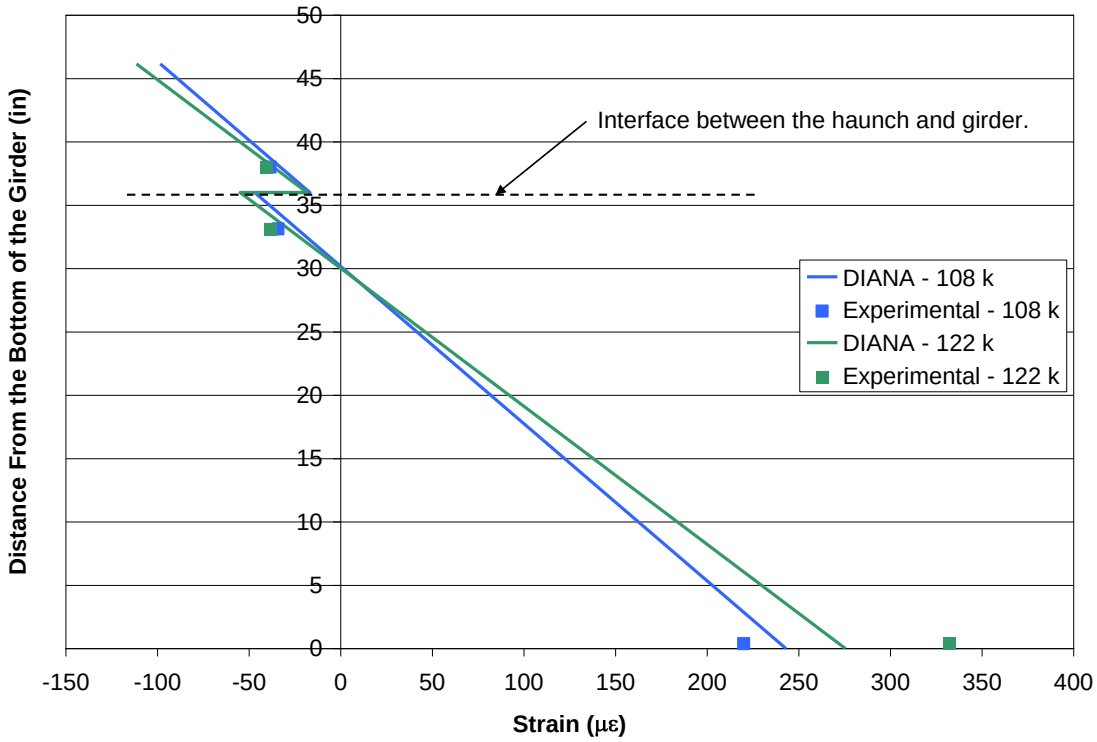

Figure 5.3.4 Strain Profile at the Live End for Shear Stud Connectors

5.3.1.4 Cracking Patterns for the Lab Mockup

The cracking patterns and the loads at which they occur at for finite element results matched the experimental results. The first flexural crack occurred in the lab mockup at 118 k/frame in girder 1. For the finite element results, the first flexural crack occurred at 126 k/frame. The cracking loads in the finite element models were the same for girder 1 and girder 2. Noticeable shear cracking occurred in the lab mockup between 95 and 105 k/frame. For the finite element models, the first shear crack occurred at 119 k/frame. This was the same for girder 1 and girder 2.

Figure 5.3.5 shows the cracking pattern in the lab mockup at the dead end of girder 1 with the hooked reinforcing bar connectors and 4 ft pocket spacing. A very similar cracking pattern occurred in girder 2. The cracking pattern at the dead end was

(a)

(b)

Figure 5.3.5 Typical Cracking Pattern in the Lab Mockup
(a) General Cracking Pattern (b) Flexural Shear Cracks Near Outside Loading Frame

similar to the cracking pattern at the live end. This is discussed in the previous chapter as well as in Section 5.3.2. For applied loads greater than 157 k/frame clear trends in the cracking patterns emerged. As the load increased, the flexural cracks propagated through the depth of the girder and new flexural cracks continued to develop and propagate. The flexural cracks between the two loading frames became flexural shear cracks as the direction of the crack propagation turned toward the inside loading points. The flexural

shear cracks are shown in Figure 5.3.5(b). The web shear cracks form anywhere between 2 ft and 4 ft from the end of the girder at an approximate orientation of 35° to 45° and propagated in both directions. One end of a web shear crack propagated toward the support and the other end of the web shear crack propagated toward the outside loading points.

At an applied load of 157 k/frame, the experimental results showed the flexural cracks under the inside loading points had propagated through the depth of the bottom flange and the depth of the web. Flexural cracks occurred from 12 ft. from the end of the girder to 19 ft from the end of the girder. Some of the web shear cracks ran from the support to the top of the web. At an applied load of 196 k/frame, the flexural cracks under the inside loading points had propagated through the depth of the girder. The flexural cracks occurred from 7 ft from the end of the girder to 27 ft from the end of the girder.

The finite element models matched the crack patterns and the slightly underestimated the degree of crack propagation discussed above for the lab mockup. Figure 5.3.6 shows the cracking patterns in the finite element models at applied load levels of 157 k/frame and 196 k/frame. The distance the flexural cracks propagated through the depth of the girder in Figure 5.3.6(a) is less than what was described for the lab mockup. The flexural cracks only extended through half the depth of the web instead of all the way through the web. The distance the flexural cracks propagated through the depth of the girder in Figure 5.3.6(b) matches what was described for the lab mockup.

For the lab mockup an applied load level of 157 k/frame, the flexural cracks occurred along an approximate length of 7 ft. For the finite element model, the flexural cracks occurred along an approximate length of 8.5 ft. For the lab mockup an applied load level of 196 k/frame, the flexural cracks occurred along an approximate length of 20 ft. For the finite element model, the flexural cracks occurred along an approximate length of 16 ft. The difference in the length of the cracked segments may be the ability to note when the cracks form in the lab mockup. The finite element model will apply the user defined σ-ε relationship for cracked concrete when the principle tensile stress violates the maximum stress condition at any location. However, the smallest of these cracks may not be visible in the lab mockup. Additionally, the cracking model defined in

finite element models will not be identical to the actual physical behavior of the lab mockup.

Cracking occurred in the shear pocket locations, as shown in Figure 5.3.6. The cracks occurred at approximately a 45° angle. These cracks occurred in the finite element model at applied load levels as small as 72 k/frame. These cracks were also common in the lab mockup and are in Figure 5.3.7. These cracks occur in the lab mockup at applied load levels as small as 113 k/frame. For the lab mockup, these cracks occur before any cracks form at the interface between the haunch and girder. For the finite element model, no cracks form at the interface between the haunch and girder. This was because the material model selected for the interface does not generate cracking strain output. The reason these diagonal cracks occur in the haunch at a lower applied load level in the finite element model when compared to the lab mockup has to do with the method for modeling the shear connectors. This was discussed with other differences for modeling small, localized behavior of the connectors and interface in the beginning of Section 5.3.1.2.

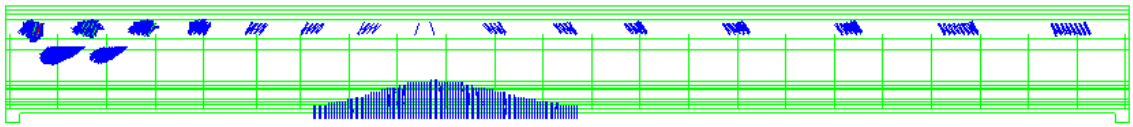

(a)

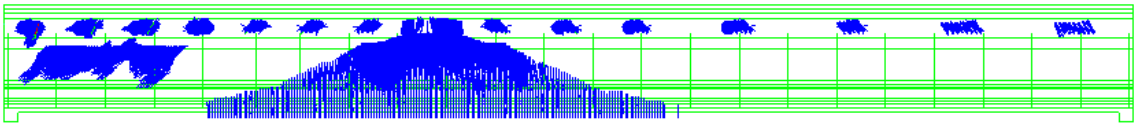

(b)

Figure 5.3.6 Cracking Patterns in the Finite Element Models for the Lab Mockup at an Applied Load Level of (a) 157 k/frame (b) 196 k/frame

Figure 5.3.7 Diagonal Cracking in the Haunch at the Shear Pockets

5.3.2 Parametric Study for the Live Load Tests

5.3.2.1 Load vs. Deflection Response for Different Shear Connector Models

Figures 5.3.8-11 show the load vs. deflection response curves for the different shear connector types and quantities discussed in Section 3.3.3. The location of these vertical deflections was at the inside loading points. The results for the load vs. deflection response at the outside loading points were very similar and can be found in Appendix I. Table 5.3.3 presents the deflection at the inside loading points for each model at a load level producing a maximum moment equal to the required flexural strength.

Recall that model MOCKUP had the exact number of shear connectors used for the lab mockup. Model 2.121_100 had close to the exact number of shear connectors required per pocket using Equation 2.121. Model 2.121_75 had approximately 75% of shear connectors required per pocket using Equation 2.121. Model 2.121_50 had approximately 50% of shear connectors required per pocket using Equation 2.121. Model 2.128_R had close to the number of shear connectors required using Equation 2.128. The shear connectors were distributed in an even manner among the pockets. The connectors were also distributed among the shear pockets so the dead end and live end of the bridge had approximately the same amount of shear connectors. Model 2.128_L had close to the number of shear connectors required using Equation 2.128. Unlike model

2.128_R, the shear connectors were distributed among the pockets such that more shear connectors were placed in locations with high shear stresses.

An applied load of 118 k/frame for the live end test setup or dead end test setup (see Section 3.2.6) produces the design moment for service load levels. An applied load of 187 k/frame for the live end test setup or dead end test setup produces the required flexural strength. Models with larger vertical deflections indicate a larger loss in composite action than models with smaller vertical deflections. At service load levels, the difference in the performance of the different connector quantities was negligible compared to the difference in the performance of the different connector quantities at ultimate load levels. Because the design of the connectors was based on ultimate load levels, the discussion of the different shear connector types and quantities will be limited

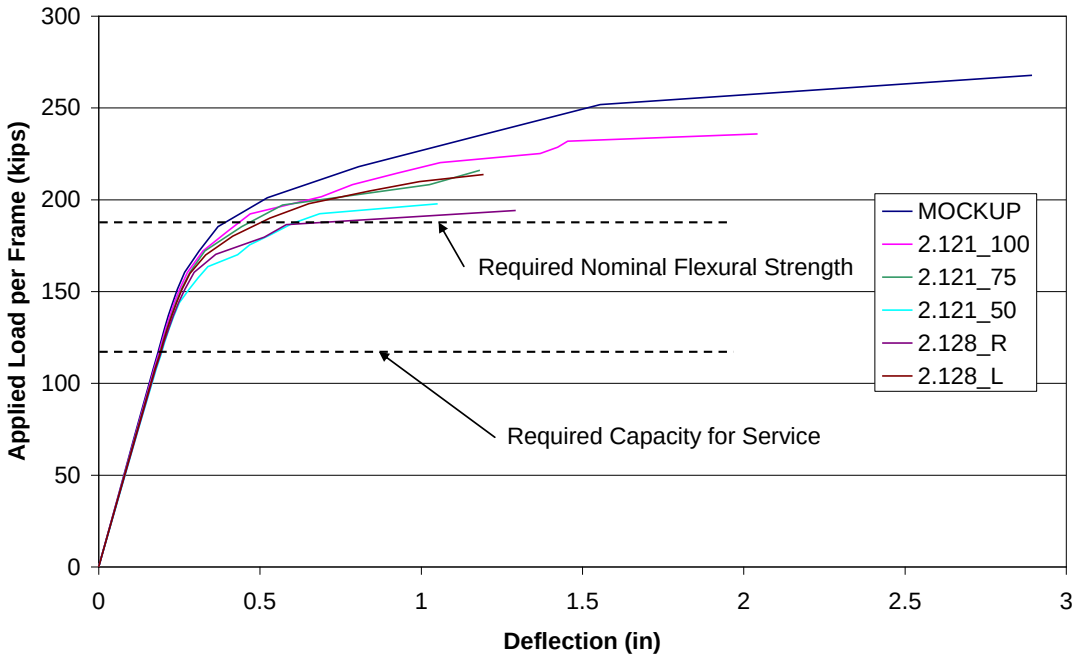

Figure 5.3.8 Comparison of Load vs. Deflection Response for Different Hooked Reinforcing Bar Quantities with 4 ft Pocket Spacing at the Inside Load Point

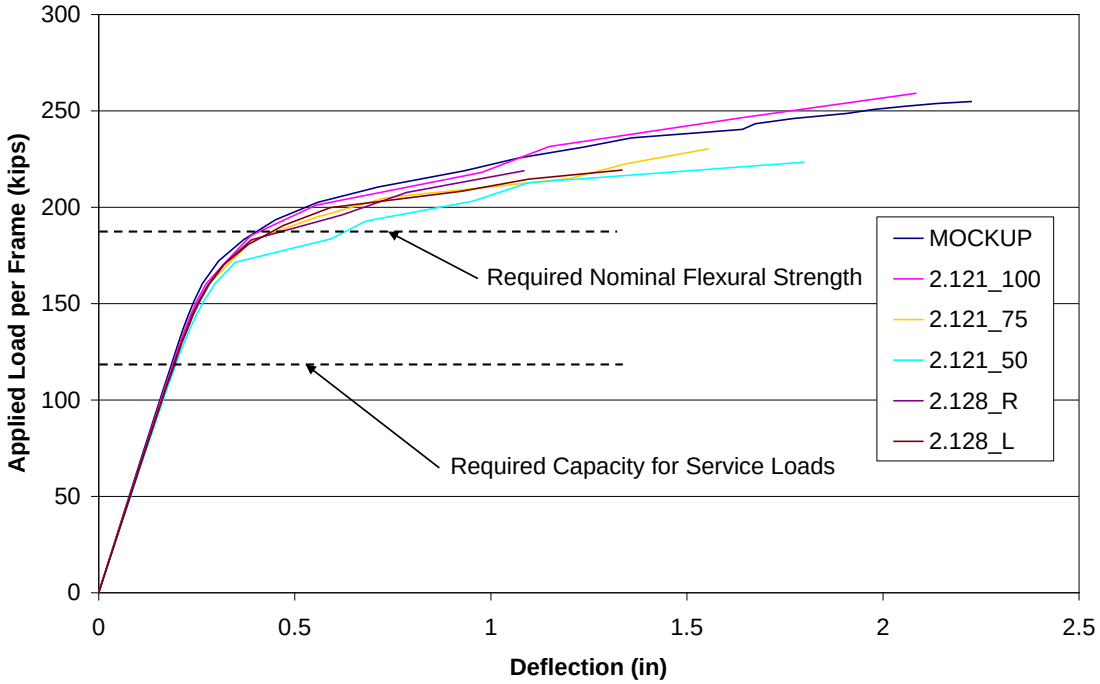

Figure 5.3.9 Comparison of Load vs. Deflection Response for Different Hooked Reinforcing Bar Quantities with 2 ft Pocket Spacing at the Inside Load Point

to ultimate load levels. The peak load for each model in Figures 5.3.8-11 does not indicate the actual capacity of the system for a given shear connector type and quantity. This was the last load step where the solution converged without numerical difficulties.

Small differences in the values of the vertical deflection may be attributed to the convergence behavior of the model. Section 3.3.1.4 describes the load stepping procedure used for the live load models, as well as the iterative procedure. The final incremental deflection for a given load step depends upon the current incremental stiffness, and the size of the out of balance force. The convergence criterion allows a small range of incremental deflections to be satisfactory. Therefore, a different incremental deflection, which results in a different total deflection, may also satisfy the convergence criteria.

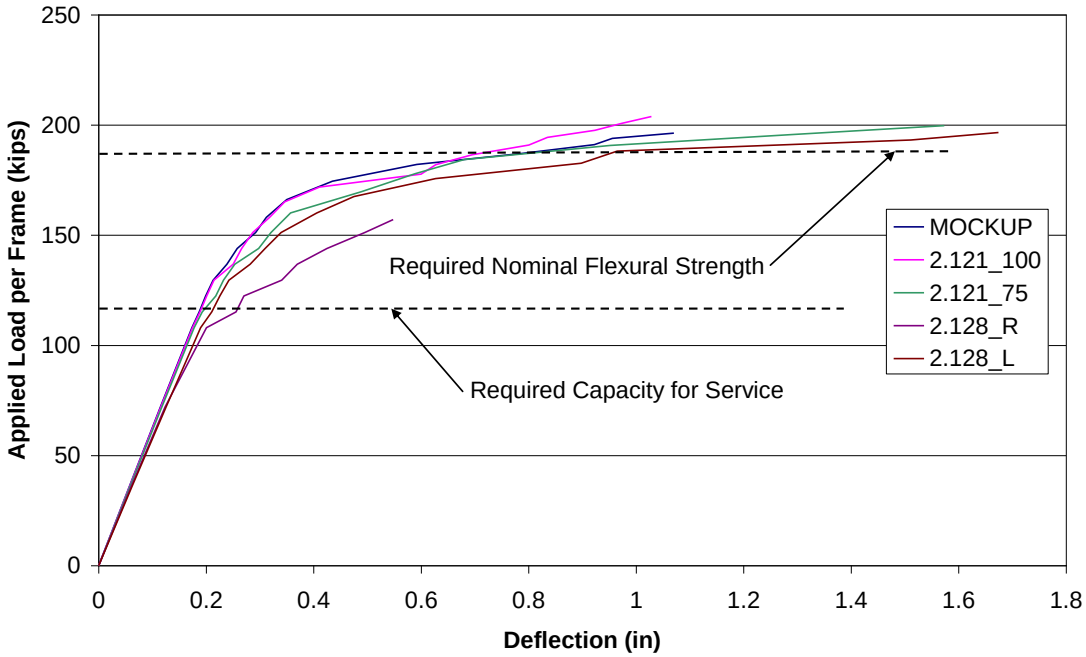

Figure 5.3.10 Comparison of Load vs. Deflection Response for Different Shear Stud Quantities with 4 ft Pocket Spacing at the Inside Load Point

Figure 5.3.8 shows the differences in the response of the system for different hooked reinforcing bar quantities as shear connectors with 4 ft pocket spacing. The MOCKUP model had the lowest vertical deflection of 0.38 in. and the 2.128_R model had the highest vertical deflection of 0.67 in. The 2.121_100 model had a vertical deflection of 0.43 in., which was slightly greater than the vertical deflection of 0.38 in. for the model MOCKUP.

Model 2.121_75 and models 2.128_L had vertical deflections of 0.47 in. and 0.50 in., respectively, at the inside loading point. Additionally, the model 2.121_75 reached a peak load of 216 k/frame and the model 2.128_L reaches a peak load of 214 k/frame. This was more than 14% greater than the load to reach the required flexural strength. The models 2.128_R and 2.121_50 both perform poorly compared to the other models in terms of the vertical deflection at an applied load of 187 k/frame and both models reach a peak load of less than 200 k/frame before convergence problems were encountered.

Figure 5.3.9 shows the differences in the response of the system for different hooked reinforcing bar quantities as shear connectors with 2 ft pocket spacing. Figure 5.3.9 and Table 5.3.3 point out the large loss of composite action for model 2.121_50 with respect to the results of the other models with the same shear connector type and pocket spacing. Unlike model 2.128_R with 4 ft pocket spacing, model 2.128_R with 2 ft pocket spacing performed more like models MOCKUP, 2.121_100, and 2.121_75 with regards to the level of composite action.

Figure 5.3.10 shows the differences in the response of the system for different shear stud quantities as shear connectors with 4 ft pocket spacing. Model 2.128_R provided the largest loss in composite action. The peak load for this model was 157 k/frame, which was 16% less than the load that produces the required nominal flexural strength. The peak loads reached by the rest of the models with shear studs as shear

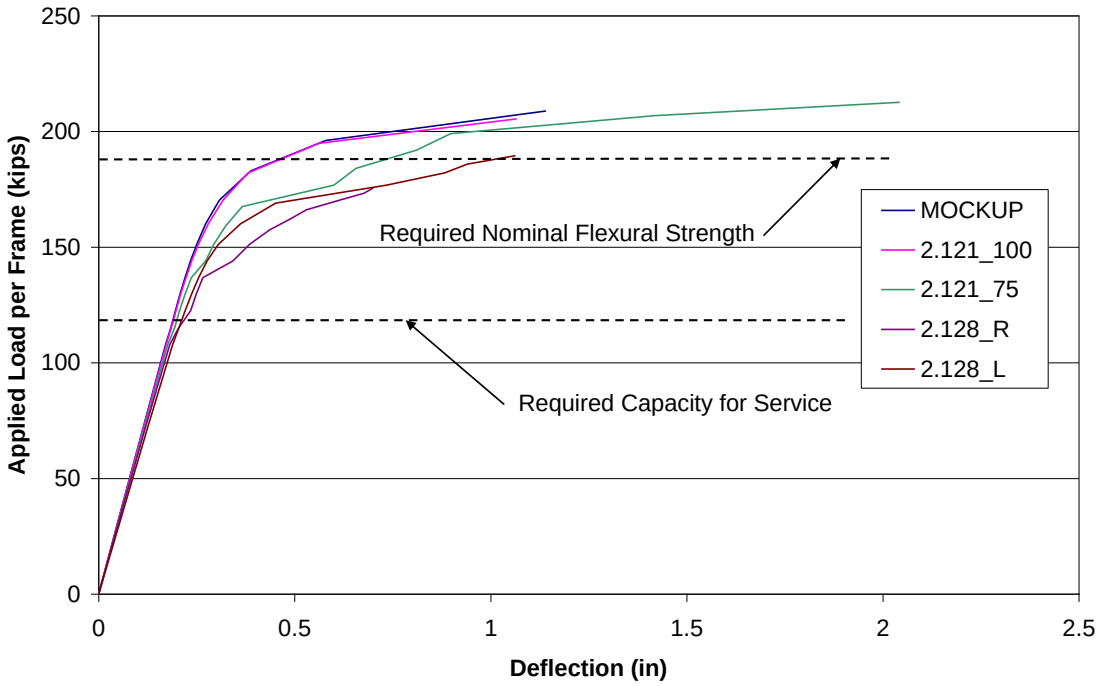

Figure 5.3.11 Comparison of Load vs. Deflection Response for Different Shear Stud Quantities with 2 ft Pocket Spacing at the Inside Load Point

Table 5.3.3 Comparison of Deflections at the Inside Loading Point for Each Model at the Required Flexural Strength

Model Name	Pocket Spacing (ft)	Connector Type	Δ_{inside} (in.)
MOCKUP	4	Reinf. Bars	0.38
2.121_100	4	Reinf. Bars	0.43
2.121_75	4	Reinf. Bars	0.47
2.121_50	4	Reinf. Bars	0.61
2.128_R	4	Reinf. Bars	0.67
2.128_L	4	Reinf. Bars	0.50
MOCKUP	2	Reinf. Bars	0.41
2.121_100	2	Reinf. Bars	0.42
2.121_75	2	Reinf. Bars	0.46
2.121_50	2	Reinf. Bars	0.63
2.128_R	2	Reinf. Bars	0.47
2.128_L	2	Reinf. Bars	0.44
MOCKUP	4	Studs	0.79
2.121_100	4	Studs	0.72
2.121_75	4	Studs	0.80
2.128_R	4	Studs	N.A.
2.128_L	4	Studs	0.96
MOCKUP	2	Studs	0.46
2.121_100	2	Studs	0.46
2.121_75	2	Studs	0.73
2.128_R	2	Studs	N.A.
2.128_L	2	Studs	1.00

connectors with 4 ft pocket spacing were similar, ranging from 196 k/frame to 204 k/frame. Model 2.128_L had a vertical deflection more than 17% larger than the models that reach the load that produces the required nominal flexural strength.

Figure 5.3.11 shows the differences in the response of the system for different shear stud quantities as shear connectors with 2 ft pocket spacing. The models MOCKUP and 2.121_100 had a higher degree of composite action than the remaining models for applied loads greater than 170 k/frame. Model 2.128_R only reached a peak load of 176 k/frame.

5.3.2.2 Von Mises Stresses in the Shear Connectors

For design purposes, the number of connectors was selected based on the stress in the connectors reaching the nominal yield stress of the connector. Therefore, the models

examined during the parametric study that had stresses exceeding the yield stress would result in an undesirable connector layout from a design standpoint. The experimental results from Chapter 4 and finite element results from Section 5.3.1.2 showed the connectors do not typically yield in the axial direction of the connector. However, when slip occurs at the interface between the haunch and girder, the shear stresses in the connectors can become large compared to the axial stresses. Because of the multi-axial stress state in the connectors, it was desirable to examine the Von Mises stresses. The Von Mises stresses can be directly compared to the yield stress for a connector in a uniaxial test. Von Mises stresses are discussed in more detail in Section 3.3.2. Table 5.3.4 presents the maximum Von Mises stresses in the shear connectors at a load level that developed the required flexural strength (187 k/frame). The model 2.121_50 was only considered with hooked reinforcing bars as shear connectors. The model 2.128_R with shear studs as shear connectors was not able to reach the load that creates the required flexural strength. The maximum stress always occurred in one of the pockets near the supports. The models MOCKUP, 2.121_100, and 2.121_75 produced acceptable stress levels when hooked reinforcing bars were used as shear connectors. The models 2.121_50, 2.128_R, and 2.128_L exceed the nominal yield stress. However, the model 2.121_L exceeded the nominal yield stress of 60 ksi for the hooked reinforcing bars with 4 ft. pocket spacing by only 3.8%. This design was very similar to model 2.121_75.

All of the models with shear studs as the shear connectors exceeded the nominal yield stress of 50 ksi when the required flexural strength was reached. According to the results in Section 5.2.2, the models with shear studs overestimated the loss of composite action more than the models with hooked reinforcing bars. The experimental data from Chapter 4 shows that the shear stud quantities used for the finite element model MOCKUP was satisfactory. Therefore, the Von Mises stresses for the models with shear studs were compared to the Von Mises stresses for the model MOCKUP. If the Von Mises stresses for a model with shear studs was similar to the stress level for the model

Table 5.3.4 Maximum Von Mises Stresses in Shear Connectors at the Required Flexural Strength

Model Name	Hooked Reinforcing Bar Connectors		Shear Stud Connectors	
	4 ft Pocket Spacing	2 ft Pocket Spacing	4 ft Pocket Spacing	2 ft Pocket Spacing
MOCKUP	51.5	52.8	59.7	54.1
2.121_100	56.7	54.2	57.6	51.7
2.121_75	59.3	59.6	61.0	62.2
2.121_50	69.9	75.4	x	x
2.128_R	76.7	68.4	67.9 *	68.5 **
2.128_L	62.3	59.2	68.4	67.7

* Occurred at 87.8% of M_{n_req}.
** Occurred at 98.3% of M_{n_req}.

MOCKUP, then the stress level in the connectors for the model under consideration was deemed acceptable. The maximum stresses in the models 2.121_100 and 2.121_75 were comparable to the maximum stresses in the model MOCKUP. The Von Mises stresses in the models 2.128_R and 2.128_L were close to the nominal ultimate strength of 70 ksi for the shear studs and the stresses were considerably greater than the maximum stresses in the model MOCKUP.

5.3.2.3 Cracking Patterns for Different Shear Connector Models

Figure 5.3.12 shows the cracking patterns in selected models at an applied load that creates the required flexural strength. The cracking patterns for the flexural cracks and web shear cracks for selected models were very similar to one another. The web shear cracks all propagated to the outside loading point and the flexural cracks all developed under the inside loading frame.

There are slight variations for each model for the depth of the flexural cracks and extent of the web shear cracking. This was due to the different levels of composite action in each model. At a given load, one model may have had a smaller strain discontinuity at the interface between the haunch and girder compared to another model. This lead to a difference in the strain profile through the depth of the girder. Therefore, at an arbitrary depth in the girder, one model might crack at an earlier load compared to another model.

For models with a smaller degree of composite action, the extent of cracking in the haunch was also greater compared to a model with a larger degree of composite action.

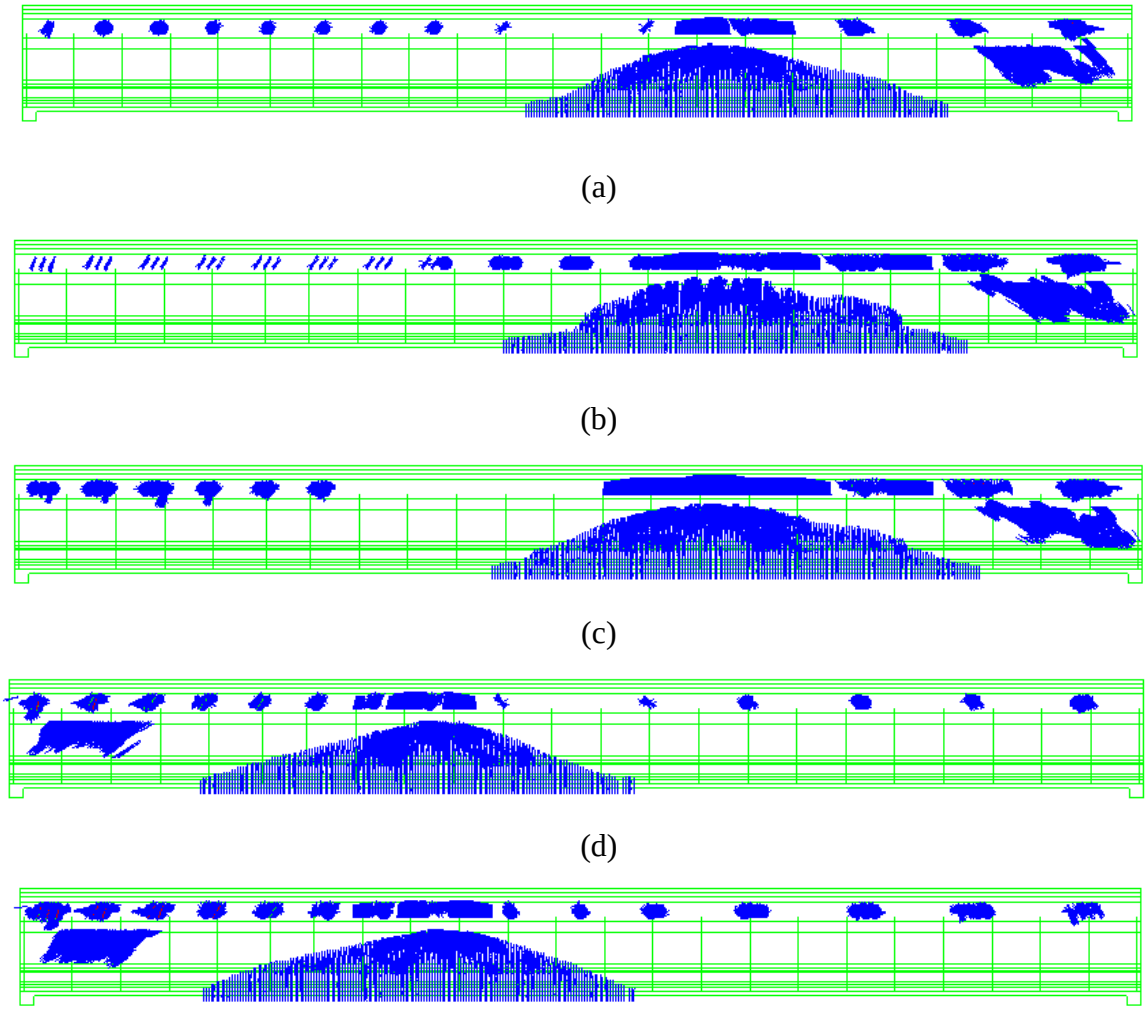

(a)

(b)

(c)

(d)

(e)

Figure 5.3.12 Comparison of Cracking Patterns at the Required Flexural Strength for (a) 2.121_50 with Hooked Reinforcing Bars and 4 ft Pocket Spacing (b) MOCKUP with Shear Studs and 4 ft Pocket Spacing (c) 2.128_L with Shear Studs and 4 ft Pocket Spacing (d) 2.121_50 with Hooked Reinforcing Bars and 2 ft Pocket Spacing (e) 2.121_75 with Shear Studs and 2 ft Pocket Spacing

Figure 5.3.12(c) has more cracks in the haunch at the location of the inside loading point compared to Figure 5.3.12(a).

Although the extent of the cracking was slightly different for each of the models, the cracking patterns are the same. The pocket spacing, the connector type, or the amount of shear connectors does influence the extent of cracking, but not the cracking pattern.

5.3.3 Design Considerations Based on Finite Element Results for Live Load Tests

Based on the results presented in the previous section, several observations were made about the deck panel system with regards to the pocket spacing, the connector type, the distribution of the connectors along the length of the girder, and the quantity of connectors. When comparing Figure 5.3.8 to Figure 5.3.9, 4 ft pocket spacing provided approximately the same degree of composite action as 2 ft pocket spacing when hooked reinforcing bars were used as shear connectors. The only two models that took exception to this statement were models 2.128_R and 2.128_L. For these two models, the 2 ft pocket spacing provided a higher degree of composite action. When comparing Figure 5.3.10 to Figure 5.3.11, the 2 ft pocket spacing clearly provided a higher degree of composite action than the 4 ft pocket spacing when shear studs were used as shear connectors. Figure 5.3.9, Figure 5.3.11, and Table 5.3.3 shows that all of the models examined with 2 ft pocket spacing performed better with hooked reinforcing bars instead of shear studs for shear connectors. However, the difference in the performance of the system with the two different types of shear connectors for models MOCKUP and 2.121_100 was very small. As the number of shear connectors was decreased for models with 2 ft pocket spacing, the models with the shear studs had a larger difference in the degree of composite action when compared to models with hooked reinforcing bars.

The maximum Von Mises stresses discussed in Section 5.3.2.2 indicated that models MOCKUP, 2.121_100, AND 2.121_75 produced acceptable stress levels in the shear connectors. Acceptable stress levels were considered to be less than or slightly above the nominal yield stress. Figures 5.3.8-11 and Tables 5.3.3-4 showed that models 2.121_50 and 2.128_R resulted in a larger loss in composite action and high stress levels

for hooked reinforcing bar connectors. The models 2.128_L and 2.128_R resulted in a larger loss in composite action and high stress levels for shear stud connectors.

It is advisable to use the quantity of connectors provided in models MOCKUP and 2.121_100 for either 2 ft pocket spacing or 4 ft pocket spacing with hooked reinforcing bars and for 2 ft pocket spacing with shear studs. Although, Section 5.2 showed the models with shear studs were more conservative (by producing larger relative slip values compared to experimental data) than models with hooked reinforcing bars. The experimental data showed that the use of shear studs as shear connectors with 4 ft pocket spacing performs as well as any other combination of pocket spacing and connector type. Because the finite element results are conservative, 4 ft pocket spacing is acceptable to use with shear studs as shear connectors. The model 2.121_75 showed that reducing the required number of shear connectors did result in a small loss of composite action, but the stress levels in the connectors were still considered acceptable, based on the discussion in Section 5.3.2.2. This indicates the number of connectors required by AASHTO LRFD for the lab mockup is conservative and can be reduced by as much as 25%, while the stress levels in the shear connectors are still at an acceptable stress level. However, partial composite action must be considered in the design of the composite girder. Partial composite action and its effects on the strain distribution are discussed in Section 2.1.2.1. One method for reducing the amount of shear connectors in a precast deck panel system is to only account for the live loads and composite dead loads during the design of the shear connectors. This is discussed in Section 2.1.2.2, as proposed by Tadros et. al. As discussed in Section 3.2.1, the connectors for the lab mockup are designed for the non-composite dead loads in addition to the composite dead loads and live loads.

The results indicate that there was a large loss in composite action when the connectors in the deck panel system were designed with Equation 2.128 and were redistributed in a uniform manner among the pockets, compared to when the connectors were designed with the same equation and were distributed to locations with high shear forces. However, when 2 ft pocket spacing was used with hooked reinforcing bars as shear connectors, the difference in the load vs. displacement behavior for models 2.128_R and 2.128_L was small compared to any other combination of shear connectors

and pocket spacing. The connector stresses in the shear connectors for 2.128_R were still noticeably larger than the connector stresses for 2.128_L. When it is desirable to have the same number of connectors in each pocket in order to reduce the different shear pocket sizes and strand patterns in the panels, additional shear connectors should be provided at locations with small shear forces instead of distributing the total number of required connectors in a uniform manner among the pockets.

The finite element results show that both the 2 ft pocket spacing and 4 ft pocket spacing performs well for hooked reinforcing bars as shear connectors. The results for the hooked reinforcing bars as shear connectors indicate that the number of connectors required per pocket may be decreased. Two ft pocket spacing performs the best when shear studs are used as the shear connectors. However, when the minimum number of shear studs is provided from the AASHTO LRFD shear friction equation, 4 ft pocket spacing is an acceptable alternative to 2 ft pocket spacing.

Chapter 6
Conclusions and Recommendations

This chapter presents conclusions and recommendations for the construction and design of precast deck panel systems. These are based on the results of the constructability study, the time dependent study, and the live load testing presented in Chapter 4 and Chapter 5. Both the experimental results and finite element results are used to make recommendations for the best deck panel details for rapid construction, the initial level of post-tensioning, pocket spacing, shear connector type, and a horizontal shear design and detailing procedure.

6.1 Conclusions

6.1.1 Constructability Study

6.1.1.1 Transverse Strand Pattern in the Deck Panels

Based on fabrication cost and the ease of fabrication, it was desirable to have one strand pattern. Because of the different pocket spacings used for the lab mockup, it was not possible to use one strand pattern. Using one strand pattern would have reduced the total number of feet of prestressing strands that had to be used during the transverse prestressing operation for the panels. Additionally, the prestressing strand layout and mild reinforcing steel layout within a panel would not have been as congested without the debonded strands.

6.1.1.2 Transverse Joint Configuration

The grouted female-female joint performed well without any problems during construction or when water was ponded for the durability study. The grouted female-female joints were more forgiving when the edges of the panels were bowed. The difference in the gap between the panels was compensated for when the grout was poured for the joints.

The constructability study and durability study revealed that the epoxied male-female joints were susceptible to leaking if the edges of the panel formwork were bowed. If the epoxied male-female joints are required for future projects, tight tolerances must be

used to assure that the two panels forming the epoxied male-female joint are in firm contact with one another along the length of the joint. An alternative is match casting.

Additionally, the grouted female-female joints allowed the panels to be placed on the girders more rapidly when compared to panel placement with epoxied male-female joints. The grouted female-female joints allowed the panels to be placed on the girders without having to slide the panels together while avoiding conflicts with any shear connectors that were already in place.

6.1.1.3 Leveling Bolt System

The Dayton Richmond B-14 coil bolts and F-53 thin slab coil inserts worked well for the leveling bolt system. The weight of the deck panels were supported on three coil bolts without any strength related problems. There was some difficulty adjusting the elevation of some of the panels with the leveling bolt system. In some cases, the thin slab coil inserts were not at a 90° with the bottom of the panel surface. This problem was solved by using a jack hammer to widen the hole above the coil insert. This allowed the coil bolt to be installed at the same angle as the coil insert. In order to avoid this problem in the future, a wider blockout should be provided in case the coil bolt has to be inserted at an angle. This is shown in Figure 6.1.1.

Steel plates provided on top of the girders for the coil bolts to bear on prevented any of the post-tensioning force from getting transferred to the girders during the tensioning operation. The steel plates are shown in Figure 4.1.5 and Figure 6.1.1. Dial gages were used to measure any change in the deflection of the girder to show none of the post-tensioning force was transferred to the girders.

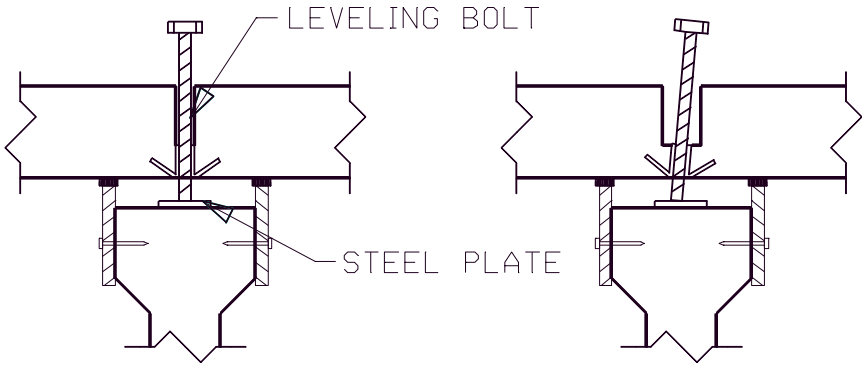

6.1.1 Leveling Bolt Blockouts (a) Old Configuration
(b) New Configuration

6.1.1.4 Formwork for Haunch and Transverse Joints

The methods used to form up the grouted female-female transverse joints and the haunch were presented in Section 4.1.4 and Section 4.1.7, respectively. Both of these methods worked well and minimal leaking was reported during the grouting operations.

6.1.1.5 Grout Specifications

The Five Star® Highway Patch grout was used for the female-female transverse joints and haunch. This grout performed well in terms of providing the required compressive strength in the joints at the time the strands were post-tensioned in the deck. The grout also performed well during the live load testing program. No cracking was observed in the grout for the haunch, transverse joints, and shear pockets.

The finite element time dependent study revealed that it is important to have a grout with very low shrinkage properties. Both the panels and girders restrain the shrinkage of the grout in the haunch, creating large tensile stresses.

6.1.1.6 Shear Connector Type and Pocket Sizes

Using shear studs as shear connectors allows for more rapid placement of the panels on the girders and eliminates a tripping hazard. The width of the steel plate used for the new shear stud detail should be at least 1 ½ in. smaller than the width of the top flange of the girder so problems will not occur when trying to fit the plate between the

formwork for the top flange. This also provides cover to prevent the steel plate from corroding. The width of the steel plate for the new shear stud detail should also be detailed to be at least 1 in. greater than the width of the shear pocket.

When hooked reinforcing bars are used as shear connectors, the size of the shear pockets should be increased to compensate for casting tolerances. For the lab mockup, the sizes of the pockets were detailed such that the distance from the center of the last shear connector in a pocket to the edge of a pocket was 2 in. Based on the difficulties encountered during the placement of the panels, it is recommended that this distance be increased to at least 3 in. when hooked reinforcing bars are used as shear connectors. This distance is not as critical when the shear studs are used as shear connectors since the studs are shot to the steel plates after the panels are placed. The distance of 2 in. can be used in this case.

6.1.2 Time Dependent Behavior

Both the experimental and finite element results showed the level of post-tensioning in the lab mockup was sufficient to keep the transverse joints in compression through the service life of the bridge. The jacking forces at the live end are shown in Table G.1. The average initial level of post-tensioning in the deck for the lab mockup was 269 psi, after considering all instantaneous losses. The experimental results showed the change in strain in the deck from creep and shrinkage effects was only -40 με. The finite element results showed the average reduction in the compressive stress in the deck was 97.5 psi. This resulted in an average compressive stress in the deck of -201 psi at 10,647 days. The successful performance of the initial level of post-tensioning for the lab mockup was expected since the strands were post-tensioned at a panel age of 91 days.

The finite element results showed that significant tensile stresses developed in the haunch. The age of the panels and girders relative to the age of the haunch restrained the shrinkage of the haunch. Recall from Section 5.1.2 that the tensile stresses could have been reduced if

1. The panels and girders were not as old at the time of the grouting operation,

2. The post-tensioning operation was performed closer to the time of the grouting operation, and
3. A very low shrinkage grout was used.

The creep coefficients and ultimate shrinkage strains for the girder, haunch, and deck at the different phases of the construction were calculated in DIANA using the CEB-FIP Model Code 1990. These equations are presented in Section 2.2.1.2.

Because of the effects of differential creep and shrinkage, construction staging, and the relative ages of the panels, girders, and haunch on the long term post-tensioning losses, the equations presented in Section 2.2.2.1 for determining long term prestress losses in precast deck panel systems are not recommended. Issa's[4] recommendation of -200 psi for an initial level of post-tensioning for simply supported bridges can be used to provide an estimate for the required level of post-tensioning in the deck. This initial level of post-tensioning assumes that there will be a reduction in the compressive stress in the deck of 100 psi from creep and shrinkage effects. This loss in compression from creep and shrinkage effects was shown to be a good approximation based on the finite element time dependent results of the lab mockup.

When a more accurate estimate of creep and shrinkage effects on a bridge is desired, there are two approaches. Both methods require that all critical construction stages be considered. One approach is the time stepping method that often requires the use of finite element based commercial software such as DIANA. The other approach is the age adjusted effective modulus method where a single time step is usually used for each construction stage. The development of the forces over these large time steps is compensated for by the aging coefficient. A system of equations is formulated based on equilibrium equations, strain compatibility equations, and constitutive relationships. This was discussed in Section 2.1.1.2.

6.1.3 Live Load Testing Program

6.1.3.1 Transverse Joint Configuration

The performance of a transverse joint configuration was shown to be a constructability issue and not a strength or fatigue issue for a simply supported span configuration. Both the epoxied male-female joints and the grouted female-female joints

performed well when subjected to the vertical loads adjacent to the joints as well as the moments developed from the live loads.

6.1.3.2 Strength and Fatigue Performance

The lab mockup failed in flexure at both the live end and dead end. The moment at which the failure occurred at both ends of the lab mockup was within 4.5% of the calculated flexural capacity. Although the lab mockup did not fail in vertical shear, excessive shear cracking was observed in the girders at both ends of the lab mockup. The peak shear forces in the lab mockup from the live loads were 9% less than the calculated vertical shear capacity.

The experimental results showed the horizontal shear forces developed at the shear pockets exceeded the calculated shear capacities by as much as 24%. The excess capacity of the pockets along with the low strain levels in the shear connectors and high cracking loads in the haunch indicated the number of shear connectors could be reduced in the shear pockets. The finite element results indicated that the number of shear connectors could be reduced by as much as 25%. The method used for modeling the shear connectors neglected the "clamping effect", which produced conservative finite element results by underestimating the level of composite action present.

Creep associated with the dead loads may produce significant shear stresses at the interface. However, shear stresses at the interface associated with creep effects were not included in the analyses presented in Chapter 5. The results showed the AASHTO LRFD shear friction equation was the best equation of the equations examined to use for horizontal shear design.

The finite element results showed that the total number of shear connectors required should not be redistributed evenly among the pockets. The shear connectors should be selected for each pocket.

The lab mockup performed well when subjected to the cyclic testing. The stress range in the strands and the vertical deflection measurements remained constant. The strain levels in the shear connectors were less than 1% of the nominal yield strain.

6.1.3.3 Pocket Spacing

Both the 2 ft pocket spacing and 4 ft pocket spacing performed well. The 2 ft pocket spacing and 4 ft pocket spacing produced levels of composite action that allowed the lab mockup to reach the required flexural strength and the required vertical shear strength. As mentioned in Section 6.3.2, the number of shear connectors used in the lab mockup could be reduced by as much as 25%. This was true for both the 2 ft pocket spacing and 4 ft pocket spacing.

6.1.3.4 Shear Connector Type

Both types of shear connectors worked well based on the live load test results. The hooked reinforcing bars and the new shear stud detail had axial strains less than 50% of the nominal yield strain. The results in Section 5.3.2.2 show the Von Mises stresses were approximately equal to the yield stress of the shear connectors even when the number of shear connectors was reduced by 25%.

6.2 Recommendations

6.2.1 Structural Details

1. The pocket spacing should be kept constant when possible to avoid using more than one transverse strand pattern.
2. The grouted female-female configuration should be used for the transverse joints.
3. The Dayton Richmond B-14 coil bolts and F-53 thin slab coil inserts can be used as the leveling bolt system. The blockout for the coil bolt in the slab should be large enough to account for a coil insert that is not flush with the bottom surface of the panel.
4. Either 2 ft or 4 ft can be used as the interior pocket spacing when AASHTO Type II girders are used.
5. Hooked reinforcing bars or the new shear stud detail can be used as shear connectors.

6.2.2 Grout Specifications

A low shrinkage grout should be used in the haunch, grouted female-female joints, and shear pockets. This is because of the restrained shrinkage provided by precast panels and precast, prestressed girders.

6.2.3 Formwork

The haunch and transverse joints can be formed with plyform and weather stripping. Details are provided in Section 4.1.4 and Section 4.1.7.

6.2.4 Level of Post-Tensioning

A level of post-tensioning of 269 psi is adequate to keep the transverse joints in compression throughout the service life of the bridge. This recommendation is for simply supported spans. A smaller level of post-tensioning may be provided if a more detailed creep and shrinkage analysis is performed.

6.2.5 Design of Shear Connectors

The procedure for selecting the number of shear connectors in each shear pocket is as follows:

1. The factored vertical shear force at the shear pocket under consideration is calculated.
2. Equation 2.123 is used to determine the shear force per inch.
3. The tributary pocket spacing is calculated. The tributary pocket spacing is half the pocket spacing on each side of the pocket under consideration.
4. The horizontal design shear force is calculated by multiplying the shear force per inch by the tributary pocket spacing.
5. Equation 2.121 is used to select the required area of steel per pocket. The top flange width and the tributary pocket spacing are used to calculate the area of concrete engaged in resisting the shear force. Equation 2.121 can be solved for the required area of steel per pocket:

$$A_{s\_pocket} = \frac{\frac{\frac{V_u l_v}{d_v \phi} - b_v l_v c}{\mu} - P_c}{f_y} \quad [6.1]$$

where,

V_u = factored vertical shear force (k)

ϕ = strength reduction factor = 0.9

d_v = distance between the centroid of the steel in the tension side of the girder to the resultant center of the compressive force in the deck (in.)

b_v = width of the surface area engaged in shear transfer (in.)

l_v = tributary pocket spacing (in.)

and μ, c, f_y, and P_c are defined in Section 2.2.3.1. The AASHTO LRFD truck load, AASHTO LRFD lane load, and composite dead loads should be used when determining the shear forces at each pocket in Step 1 of the design procedure above.

For the new shear stud detail shown in Figure 1.2.1, there are two design requirements in addition to the requirements mentioned above. The design of the shear studs on the bottom surface of the steel plate is also done using Equation 2.121. The spacing of the shear studs is determined assuming 2 shear studs will be placed in each row. Equation 2.121 can be solved for the required stud spacing:

$$s = \frac{\mu(2A_{stud} f_y + P_c)}{\frac{V_u}{d_e \phi} - c b_v} \quad [6.2]$$

where, A_{stud} = cross sectional area of one shear connector (in^2), V_u, ϕ, d_e, b_v, and l_v, are defined with Equation 6.1, and μ, λ, c, f_y, and P_c are defined in Section 2.2.3.1. The spacing of the shear studs on the bottom surface of the steel plates should be large enough such that the horizontal shear capacity is limited by

$$V_n \le \min(0.2 f_c' A_{cv}, 5.5 A_{cv}) \quad [6.3]$$

where f_c' and A_{cv} are defined in Section 2.2.3.1. The second additional design requirement for the new shear stud detail is that Equation 2.124 and Equation 2.125 are

satisfied. These equations define the fatigue resistance for an individual shear stud and place limits on the spacing of the shear studs.

6.2.6 Detailing of Shear Connectors and Shear Pockets

From this research program, 2 ft pocket spacing and 4 ft pocket spacing performed well. The results were based on a girder depth of 36 in. In general, the pocket spacing should be determined using the following equation:

$$s_{pocket} \leq d_v \cot(\theta) \qquad [6.4]$$

where θ is the angle at which the shear cracks form at, according to modified compression field theory. The calculation for obtaining θ is outlined in AASHTO LRFD[7]. The angle, θ, can be conservatively taken as 45°. The term d_v is defined with Equation 6.1. The pocket spacing determined from Equation 6.4 should not be greater than 4 ft.

The following are recommended detailing standards when hooked reinforcing bars are used as shear connectors:

1. The reinforcing bars should be properly developed on each side of the haunch.
2. The longitudinal spacing of the hooked reinforcing bars in a pocket is 2 in.
3. The minimum transverse spacing of the hooked reinforcing bars is controlled by the bend diameter and should be no less than 4 times the diameter of the reinforcing bar.
4. The minimum longitudinal distance between the edge of the shear pocket and the center of the first hooked reinforcing bar is 3 in.
5. The width of the shear pocket should be at least 1 in. smaller than the width of the top flange to avoid leaking during the grouting of the haunch.

The following are recommended detailing standards when the new shear stud detail is used as the shear connector system:

1. The shear stud length should be 2 in. less than the sum of the minimum haunch height and the thickness of the deck. If the haunch height varies considerably, more than one shear stud length may have to be used.
2. The minimum thickness of the steel plate should be ¼ in. when used with ¾ in. diameter shear studs.

3. The width of the steel plate should also be 1 in. greater than the width of the shear pocket.
4. The steel plate should be cut to smaller lengths to facilitate easy placement of the plates in the top flange of the girder during fabrication. The length of each plate should be no longer than 10 ft when a ¼ in. thick steel plate is used. This maximum length was selected for handling purposes and ease of installation.
5. The longitudinal spacing of the shear studs in a pocket is controlled by Equation 2.124 and Equation 2.125. These equations place limitations on the spacing based on the fatigue capacity of an individual shear connector.
6. The transverse spacing should not be less than 4 times the diameter of the shear stud.
7. None of the shear studs on the top surface of the plate should fall at the same transverse and longitudinal location as the shear studs on the bottom surface of the steel plate.
8. Any plate that falls in the same location as a lifting eye for the girder will require a slot to be cut through the plate. The shear stud layout should compensate for this.
9. The minimum longitudinal distance between the edge of the shear pocket and the center of the first shear stud is 2 in.
10. A minimum cover of 1 ½ in. should be provided from the edge of the top flange and the steel plate.
11. The width of the bottom of the shear pocket should be at least 4 in. less than the width of the top flange to satisfy requirements 3 and 10.
12. A minimum top flange width of 4d+8” is recommended, where d = stud diameter. This is done to provide at least 2 in. between the edge of the pocket and the shear stud.

Many of the requirements listed above are illustrated in Figure 6.2.1.

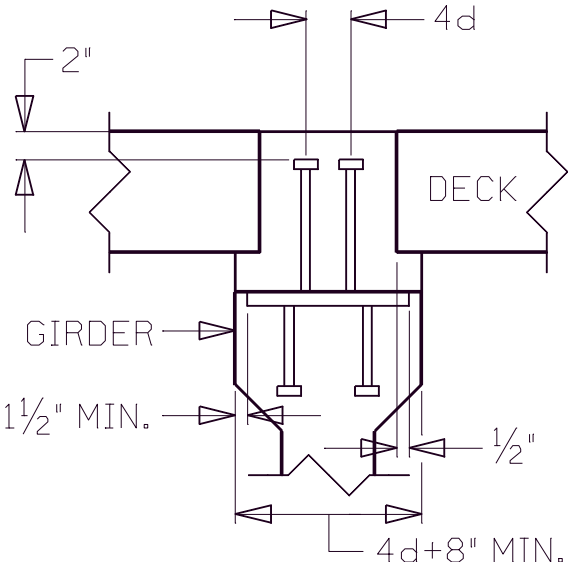

Figure 6.2.1 Requirements for New Shear Stud Detail

6.3 Future Research

The research program did not include an investigation for the transverse deck design for precast deck panel systems. The provisions presented in AASHTO LRFD for transverse deck design were used, as shown in the calculations in Appendix A. No problems were encountered with transverse deck behavior for the lab mockup. Because barrier rail impact tests were not performed for lab mockup, the effects that different confining details have on the transverse strand development length and flexural strength were not investigated.

The lab mockup was only tested in a simply supported configuration. Therefore, the strength of the different transverse joint configurations used for the lab mockup should also be tested in a configuration that produces negative moments at the joints.

Shear stresses associated with the creep of the dead loads were not included in this study. Future studies can determine if these stresses are significant enough to be included in horizontal shear design.

References

1. Scholz, D.P., “Performance Criteria Recommendations for Mortars Used in Full Depth Precast Concrete Bridge Deck Panels,” Virginia Tech, 2004.
2. Issa, M.A., Idriss, A., Kaspar, I.I., Khayyat, S.K., “Full Depth Precast and Precast, Prestressed Concrete Bridge Deck Panels,” *PCI Journal*, January-February 1995, pp. 59-80.
3. Issa, M.A., Yousif, A.A., Issa, M.A., Kaspar, I.I., “Field Performance of Full Depth Precast Concrete Panels in Bridge Deck Reconstruction,” *PCI Journal*, May-June 1995, pp. 82-108.
4. Issa., M.A., Yousif, A.A., Issa, M.A., Kaspar, I.I., “Analysis of Full Depth Precast Concrete Bridge Deck Panels,” *PCI Journal*, January-February 1998, pp. 74-85.
5. Harrison, A., LeBlanc, N.D. (2005). “Design and Construction of a Full-Width, Full-Depth Precast Concrete Deck Slab on Steel Girder Bridge,” *Journal of the Transportation Research Board, No. 1907*, Transportation Research Board, Washington, D.C.
6. Tadros, M.K., Al-Omaishi, N., Seguirant, S.J., Gallt, J.G. “Prestress Losses in Prestensioned High-Strength Concrete Bridge Girders,” National Cooperative Highway Research Program Report 496, National Research Council, Washington, D.C., 2003.
7. American Association of State Highway and Transportation Officials (AASHTO), 2006 Interim *AASHTO Load and Resistance Factor Design Bridge Design Specifications*, Third Edition, Washington, DC, 2004.
8. Wollmann, G.R., Anderson, R.B., Roberts-Wollmann, C.L., “Creep and Shrinkage Effects in Spliced Prestressed Concrete Girder Bridges,” *PCI Journal*, November-December 2003, pp. 92-106.
9. Bazant, Z.P., “Prediction of Concrete Creep Effects Using Age-Adjusted Effective Modulus Method,” *ACI Journal*, April 1972, pp. 212-217.
10. American Concrete Institute Manual of Concrete Practice, “Prediction of Creep, Shrinkage, and Temperature Effects in Concrete Structures,” *ACI 209R-92*, Farmington Hills, Michigan, 2002.

11. Dimmerling, A., Miller, R., Barker, J., Ishmael, K. "Monitoring Precast Deck Panels for Load and Environmental Effects," *National Bridge Conference 2005*, Precast Concrete Institute.
12. *SAP2000*, Computers and Structures, Inc., Berkeley, California
13. *Bridge Designer II*, Interactive Design Systems, San Diego, California.
14. Comite Euro-Internationale du Beton (CEB), "CEB-FIP model code 1990." *Buletin D'Information No. 213/214*, Lausanne, Switzerland, 1990.
15. Peterson, R.J., Ramirez, J.A., "Restraint Moments in Bridges with Full-Span Prestressed Concrete Form Panels," *PCI Journal*, January-February 1998, pp. 54-68.
16. Peterson, R.J., Ramirez, J.A., "Behavior and Strength of Bridges with Full-Span Prestressed Concrete Form Panels," *PCI Journal*, March-April 1998, pp. 80-91.
17. Freyermuth, C., "Design of Continuous Highway Bridges with Precast, Prestressed Concrete Girders," *PCI Journal*, April 1969, pp. 14-39.
18. Issa., M.A., Yousif, A.A., Issa, M.A., "Experimental Behavior of Full Depth Precast Concrete Panels for Bridge Reconstruction," *ACI Structural Journal*, May-June 2000, pp. 397-407.
19. Issa, M.A., Patton, T.A., Abdalla, H.A., Yousif, A.A., "Composite Behavior of Shear Connections in Full Depth Precast Concrete Bridge Deck Panels on Steel Stringers," *PCI Journal*, September-October 2003, pp. 2-15.
20. *ALGOR*, ALGOR, Inc., Pittsburg, Pennsylvania.
21. *PCBRIDGE*, PCLinks, Inc., Gold River, California.
22. American Association of State Highway and Transportation Officials (AASHTO), *AASHTO Load and Resistance Factor Design Bridge Design Specifications*, Third Edition, Washington, DC, 2004.
23. Markowski, S.M., "Experimental and Analytical Study of Full Depth Precast, Prestressed Concrete Deck Panels for Highway Bridges," Thesis (Masters), University of Wisconsin-Madison, 2005.
24. Seracino, R., Oehlers, D.J., Yeo, M.F., "Partial-Interaction Flexural Stresses in Composite Steel and Concrete Bridge Beams," *Engineering Structures*, Volume 23, 2001, pp. 1186-1193.

25. Tadros, M.K., Badie, S.S., Kamel, M.R., "Girder-Deck Connection for Rapid Removal of Bridge Decks," *PCI Journal*, May-June 2002, pp. 58-70.
26. ACI, *Building Code and Requirements for Structural Concrete (ACI 318-02) and Commentary*, American Concrete Institute, Farmington Hills, Michigan, 2002.
27. Menkulasi, F., "Horizontal Shear Connectors for Precast, Prestressed Bridge Deck Panels," Virginia Tech, 2002.
28. American Association of State Highway and Transportation Officials (AASHTO), 200 Interim Revisions to the *Standard Specifications for Highway Bridges*, 16th Edition (1996), Washington, DC, 2000.
29. Wallenfelsz, J.A., "Horizontal Shear Transfer for Full Depth Precast Concrete Bridge Deck Panels," Virginia Tech, 2006.
30. Badie, S.S., Tadros, M.K., Kakish, H.F., Splittgerber, D.L., "Large Shear Studs for Composite Action in Steel Bridge Girders," *Journal of Bridge Engineering*, May-June 2002, pp. 195-203.
31. Kahn, L.F., Slapkus, "Interface Shear in High Strength Composite T-Beams," *PCI Journal*, July-August 2004, pp. 102-110.
32. Kahn, L.F. and Mitchell, A.D., "Shear Firction Tests with High Strength Concrete," ACI Structural Journal, January-February 2002, pp. 98-103.
33. Loove, R.E., Patnaik, A.K., "Horizontal Shear Strength of Composite Beams with a Rough Interface," PCI Journal, January-February 1994, pp. 48-69.
34. *ANSYS*, ANSYS Inc., Canonsburg, Pennsylvania.
35. Sullivan, S.R., "Behavior of Transverse Joints in Precast Deck Panels Systems," Ohio University, 2003.
36. Gulyas, R.J., Wirthlin, G.J., Champa, J.T., "Evaluation of Keyway Grout Test Methods for Precast Concrete Bridges," *PCI Journal*, January-February 1998, pp. 44-57.
37. Kaneko, Y., Connor, J.J., Triantafillou, T.C., Leung, C.K., "Fracture Mechanics Approach for Failure of Concrete Shear Key: Theory", *Journal of Engineering Mechanics*, April 1993, pp. 680-700.

38. Kaneko, Y., Connor, J.J., Triantafillou, T.C., Leung, C.K., "Fracture Mechanics Approach for Failure of Concrete Shear Key: Verification", *Journal of Engineering Mechanics*, April 1993, pp. 701-719.
39. MacGregor, J.G., Reinforced Concrete Mechanics and Design, Third Edition, Prentice-Hall, Upper Saddle River, New Jersey, 1997, pp. 35-74.
40. TNO Building and Construction Research, "DIANA User's Manual," Release 9 2005.
41. Badie, S.S., Baishya, M.C., Tadros, M.K., "NUDECK – A New Prestressed Stay-In-Place Concrete Panel for Bridge Decks," *1998 Transportation Conference Proceedings*, Center for Transportation Research and Education, Iowa State University.
42. Fallaha, S., Sun, C.S., Lafferty, M.D., Tadros, M.T., "High Performance Precast Concrete NUDECK Panel System for Nebraska's Skyline Bridge," PCI Journal, September-October 2004, PP. 40-50.
43. American Association of State Highway and Transportation Officials (AASHTO), 2005 Interim *AASHTO Load and Resistance Factor Design Bridge Design Specifications*, Third Edition, Washington, DC, 2004.
44. Precast Concrete Institute (PCI), *PCI Bridge Design Manual*, Chicago, Illinois, 2001.
45. Precast Concrete Institute (PCI), *PCI Design Handbook*, Fifth Edition, Chicago, IL.
46. NEN. Voorschriften Beton – TGB 1990 (Regulations for concrete. Structural requirements and calculation methods). Tech. Rep. NEN 6720, Nederlands Normalisatie-instituut, 1995.
47. ASTM C 39 (2001). "Standard Test Method for Compressive Strength of Cylindrical Concrete Specimens," *Annual Book of ASTM Standards*, ASTM International, Vol. 04.02, West Conshohocken, PA, 2003.
48. ASTM C 496 (2002). "Standard Test Method for Splitting Tensile Strength of Cylindrical Concrete Specimens," *Annual Book of ASTM Standards*, ASTM International, Vol. 04.02, West Conshohocken, PA, 2003.

49. ASTM C 109 (2002). "Standard Test Method for Compressive Strength of Hydraulic Cement Mortars (Using 2 in. Cube Specimens)," *Annual Book of ASTM Standards*, ASTM International, Vol. 04.01, West Conshohocken, PA, 2003.
50. Boresi, A., Schmidt, R., Advanced Mechanics of Materials, Sixth Edition, John Wiley & Sons, Inc, 2003.

APPENDIX A – DESIGN CALCULATIONS

BRIDGE DECK DESIGN:

AASHTO LRFD Specifications and PCI Bridge Design Manual are used for the design of the precast panels.

LOADINGS FOR BRIDGE DECK *(8.8.2.4.2.3 of PCI Bridge Design Manual)*

The panels are to be designed as simply supported members. The panels are assumed to have a length of 12 ft. and a design width of 8 ft.

Self weight of panel: $\gamma_c := 0.15$ k/ft^3

Construction/Utility Load: $w_{CL} := 0.05$ k/ft^2 = 0.05 k/ft for a 1 ft. strip of deck

Parapet: $w_p := 0.3$ k/ft

Live Load: $P := 16$ k (Based on HS20-44 Vehicle)

Design span length: $S := 8$ ft. This is a conservative design length. This may be reduced if necessary.

Determine the dead load moments, resulting from the construction load and dead load of the panel. The moment resulting from the parapet load will be omitted to conservatively predict the maximum positive moment. The parapet load will be considered when checking the adequacy of the overhang.

Trial depth for panel, $h := 8$ in. (Minimum depth is 8 in. per AASHTO LRFD 13.7.3.1.2)

The trial depth of the panel is used in calculating the section properties. The actual depth of The panel will be an additional 0.5 in. The additional 0.5 in. is used as a wearing surface in the absence of an overlay.

Based upon a 1 ft. strip, the dead load of the panel can be calculated as

$$w_{DL} := \gamma_c \cdot \frac{(h + 0.5) \cdot 12}{144} \qquad w_{DL} = 0.106 \text{ k/ft}$$

$$M_{DL} := \frac{w_{DL} \cdot S^2}{8} \qquad M_{DL} = 0.85 \text{ k-ft/ft}$$

$$M_{CL} := \frac{w_{CL} \cdot 1 \cdot S^2}{8} \qquad M_{CL} = 0.4 \text{ k-ft/ft}$$

The parapet loading will only considered in the design of the overhang.

Determine the effective width of the slab that is used to resist the live load moment.

$W1 := 26 + 6.6 \cdot S$ $W1 = 78.8$ in.

$W2 := 48 + 3 \cdot S$ $W2 = 72$ in.

$W := \min(W1, W2)$ $W = 72$ in.

The clear spacing between the girders is 6 ft. Only one wheel load from the design vehicle will fit on the transverse span. Therefore, the maximum moment in the transverse direction is obtained by placing one wheel load half way between the girders.

$$M_{LT} := \frac{P \cdot S}{4} \qquad M_{LT} = 32 \quad k \cdot ft$$

Use an impact factor, $I := 1.3$

$$M_{LL} := \frac{M_{LT}}{\frac{W}{12}} \cdot I \qquad M_{LL} = 6.933 \quad \text{k-ft/ft}$$

Determine the factored loads used when checking for strength (PCI Bridge Manual 7.3.2):

$\eta := 1.0$ May be changed based upon VDOT's recommendation.

$\gamma_{DL} := 1.25$

$\gamma_{CL} := 1.5$

$\gamma_{LL} := 1.75$

DETERMINE THE TRIAL NUMBER OF STRANDS

$$f_b := \frac{\left| M_{DL} + M_{CL} + M_{LL} \right| \cdot 12}{S_c} \qquad f_b = 0.767 \quad ksi$$

Find the required precompression stress:

$f_P := f_b - f_{ts}$ $f_P = 0.302$ ksi

$P_e := f_P \cdot A_c$ $P_e = 28.971$ k/ft

Assuming a panel width of $b := 8$ ft.

$P_e := P_e \cdot b$ $P_e = 231.77$ k/panel

Assume 30% losses due to jacking and 15% losses due to time dependent effects to determine the trial number of strands. A more accurate estimate of the time dependent losses will be done later.

The prestressing force per strand is

$P_{st} := f_{pu} \cdot 0.70 A_{strand} \cdot 0.8$ $P_{st} = 24.579$ k

$no\_strands := \frac{P_e}{P_{st}}$ $no\_strands = 9.429$

Try using 16 strands.

DETERMINE PRESTRESS LOSSES (PCI Bridge Manual 8.6)

ELASTIC SHORTENING:

$f_{cgp} := \frac{A_{strand} \cdot (0.7 \cdot f_{pu}) \cdot \frac{no\_strands}{b}}{A_c}$ $f_{cgp} = 0.602$ ksi

$\Delta f_{pES} := \frac{E_p}{E_{ci}} \cdot f_{cgp}$ $\Delta f_{pES} = 4.763$ ksi

SHRINKAGE:

Annual average ambient relative humidity, $H := 70$ % for Southwestern Virginia. (PCI Design Handbook – Figure 3.12.2)

$\Delta f_{pSR} := (17 - 0.15H)$ $\Delta f_{pSR} = 6.5$ ksi

CREEP OF CONCRETE:

$f_{cdp} := 0$ Center of prestressing force occurs at the centroid of the cross section of the panel.

$f_{cgp} = 0.602$ ksi

$\Delta f_{pCR} := 12 \cdot f_{cgp} - 7 \cdot f_{cdp}$ $\Delta f_{pCR} = 7.229$ ksi

RELAXATION OF PRESTRESSING STEEL

Relaxation before transfer:

use $t := 1$ day

$K_r := 45$ (Low relaxation strands are assumed to be used. Otherwise, K_r=10.)

$f_i := 0.7 \cdot f_{pu}$ $f_i = 189$ ksi

$\Delta f_{pr1} := \frac{\log(24 \cdot t)}{K_r} \cdot \left(\frac{f_i}{f_{py}} - 0.55 \right) \cdot f_i$ $\Delta f_{pr1} = 1.32$ ksi

Relaxation after transfer:

$\Delta f_{pr2} := 6 - 0.12 \cdot \left| \Delta f_{pES} - 0.06 \right| \Delta f_{pSR} + \Delta f_{pCR} \right|$ $\Delta f_{pr2} = 4.605$ ksi

Total Relaxation loss after transfer:

$\Delta f_{pr} := \Delta f_{pr1} + \Delta f_{pr2}$ $\Delta f_{pr} = 5.925$ ksi

Total losses at transfer:

$\Delta f_{pi} := \Delta f_{pES} + \Delta f_{pr1}$ $\Delta f_{pi} = 6.083$ ksi

Stress in tendon after transfer:

$f_{pt} := 0.7 \cdot f_{pu} - \Delta f_{pi}$ $f_{pt} = 182.917$ ksi

Prestressing force after transfer per panel:

$P_i := no\_strands \cdot A_{strand} \cdot f_{pt}$ $P_i = 447.781$ k

Total losses at service loads:

$\Delta f_{pT} := \Delta f_{pES} + \Delta f_{pSR} + \Delta f_{pCR} + \Delta f_{pr2}$ $\Delta f_{pT} = 23.097$ ksi

Stress in tendon after all losses:

$f_{pe} := 0.7 \cdot f_{pu} - \Delta f_{pT}$ $f_{pe} = 165.903$ ksi

Effective prestressing force per panel:

$P_e := no\_strands \cdot A_{strand} \cdot f_{pe}$ $P_e = 406.131$ k

CHECK STRESSES AT TRANSFER AND SERVICE LOAD FOR MAX. POSITIVE MOMENT

Per PCI Bridge Design Manual, the transfer length is

$l_t := 60 \cdot \frac{d_b}{12}$ $l_t = 2.5$ ft.

The overhang is 2.0 ft. Therefore, the prestress force is not completely transferred to the panel only over the first 6 in. of the design span. In this region, the design moments are low. Therefore, it is not necessary to reduce the prestressing force in this region.

Transfer:

$$f_c := \frac{\frac{-P_i}{b}}{A_c} \qquad f_c = -0.583 \quad ksi$$ Recall that $f_{ci} = -2.4$ ksi **OK.**

Service:

$$f_t := \frac{\frac{-P_e}{b}}{A_c} + \frac{\left(M_{DL} + M_{CL} + M_{LL}\right)\cdot 12}{S_c} \qquad f_t = 0.238 \quad ksi$$ Recall that $f_{ts} = 0.465$ ksi **OK.**

$$f_c := \frac{\frac{-P_e}{b}}{A_c} - \frac{\left(M_{DL} + M_{CL}\right)\cdot 12}{S_c} \qquad f_c = -0.646 \quad ksi$$ Recall that $f_{cs1} = -2.7$ ksi **OK.**

$$f_c := \frac{\frac{-P_e}{b}}{A_c} - \frac{\left(M_{DL} + M_{CL} + M_{LL}\right)\cdot 12}{S_c} \qquad f_c = -1.296 \quad ksi$$ Recall that $f_{cs2} = -3.6$ ksi **OK.**

CHECK FLEXURAL STRENGTH FOR MAX. POSITIVE MOMENT

Ultimate Moment:

$$M_u := \eta\cdot\left(\gamma_{DL}\cdot M_{DL} + \gamma_{CL}\cdot M_{CL} + \gamma_{LL}\cdot M_{LL}\right) \qquad M_u = 13.796 \quad k\text{-}ft/ft$$

Moment Capacity:

$$A_{ps} := no\_strands \cdot A_{strand} \qquad A_{ps} = 2.448 \quad in^2$$

$$\beta_1 := \begin{cases} B \leftarrow 0.85 \text{ if } f_{pc} \le 4 \\ B \leftarrow \max\left[0.85 - 0.05\left(f_{pc} - 4\right), 0.65\right] \text{ if } f_{pc} > 4 \\ B \end{cases} \qquad \beta_1 = 0.75$$

$$b_{eff} := 12 \quad in. \qquad k := 2\cdot\left(1.04 - \frac{f_{py}}{f_{pu}}\right) \qquad k = 0.28$$

$$d_p := h - 2 - 0.25 \qquad d_p = 5.75 \text{ in.}$$

$$c := \frac{\frac{A_{ps}}{2}\cdot f_{pu}}{0.85 8.36\beta_1\cdot\left(b_{eff}\cdot b\right) + k\cdot\frac{A_{ps}}{2}\cdot\frac{f_{pu}}{d_p}} \qquad c = 0.626 \text{ in.}$$

$a := \beta_1 \cdot c$ $a = 0.47$ in.

$f_{ps} := f_{pu} \cdot \left(1 - k \cdot \frac{c}{d_p}\right)$ $f_{ps} = 261.766$ ksi

Check the development length of the strand:

$l_d := \left(f_{ps} - \frac{2}{3} \cdot f_{pe}\right) \cdot \frac{d_b}{12}$ $l_d = 6.299$ ft.

Distance from outer edge of overhang to midspan of first interior span $L := 5.83$ ft.

$L < l_d$ Therefore, the strand is not fully developed at midspan.

$f_{su} := \frac{L \cdot 12}{d_b} + \frac{2}{3} \cdot f_{pe}$ $f_{su} = 250.522$ ksi

$\phi := 1.00$ (AASHTO LRFD 5.5.4.2.1)

$\phi M_n := \phi \cdot \frac{A_{ps}}{2} \cdot f_{su} \cdot \left(d_p - \frac{a}{2}\right) \cdot \frac{1}{12} \cdot \frac{1}{b}$ $\phi M_n = 17.616$ k-ft/ft

Recall that $M_u = 13.796$ k-ft/ft **OK.**

CHECK LIMITS ON REINFORCEMENT (AASHTO LRFD 5.7.3.3)

Maximum amound of reinforcement check:

$c := 0.86$ in.

$d_e := 8 - 2.5 - 0.25$ $d_e = 5.25$ in.

$\frac{c}{d_e} = 0.164$ < 0.42 O.K.

The mild reinforcing steel is placed at the same distance from the top of the deck as the prestressing strands are. Therefore, it is only necessary to perform one check.

Minimum amount of reinforcement check:

$f_r := 0.24\sqrt{f_{pc}}$ $f_r = 0.588$ ksi

$M_{cr} := S_c \cdot \left(\frac{\frac{P_e}{b}}{A_c} + f_r\right) \cdot \frac{1}{12}$ $M_{cr} = 11.911$ k-ft/ft

For overhang:

$1.2 \cdot M_{cr} = 14.294$ k-ft/ft (controls)

$1.33 M_u = 23.43$ k-ft/ft

$\phi M_{np} + \phi M_{nm} = 31.111$ k-ft/ft **O.K.**

For interior span:

$1.2 \cdot M_{cr} = 14.294$ k-ft/ft (controls)

$M_u := 13.79$ k-ft/ft

$1.33 M_u = 18.349$ k-ft/ft

$\phi M_n = 17.616$ k-ft/ft **O.K.**

LONGITUDINAL (DISTRIBUTION) REINFORCEMENT

$\frac{A_{ps}}{2 \cdot b} = 0.153$ in^2/ft (Only consider one layer of steel on a per foot basis.

$S = 8$ ft.

$$p := \left| \begin{array}{l} t \leftarrow \frac{200}{\sqrt{S}} \\ q \leftarrow t \\ q \leftarrow 67 \text{ if } t > 67 \\ q \end{array} \right.$$

$p = 67$ %

$A_{dist} := \frac{p}{100} \cdot \frac{A_{ps}}{2 \cdot b}$ $A_{dist} = 0.103$ in^2/ft

Convert the distribution prestressing steel to an equilalent amount of mild reinforcing steel:

$A_{dist} := \frac{E_p}{E_c} \cdot A_{dist}$ $A_{dist} = 0.662$ in^2/ft

Use # 5 bars: $A_b := 0.31$ in^2/ft

$spa := 12 \cdot \frac{A_b}{A_{dist}}$ $spa = 5.622$ in. Use $s := 6$ in.

Although the spacing provided is slightly more than the required spacing, the prestressing strands provided in the longitudinal direction for the post-tensioning operation will help increase the amount of distribution steel provided.

Therefore, the amount of mild distribution steel provided in the longitudinal direction is

$A_s := \frac{12}{s} \cdot A_b$ $A_s = 0.62$ in^2/ft

Because the deck will be subjected to longitudinal moments, 8.8.2.4.8 of the PCI Bridge Manual must be met to prevent cracking at service loads.

$A_{min\_long} := 0.11 \cdot \frac{A_c}{f_y}$ $A_{min\_long} = 0.176$ in^2/ft OK.

PUNCHING SHEAR CHECK

Per AASHTO LRFD 3.6.1.2.5, the width of the tire contact area is 20 in. and the length of the tire contact area is 10 in. Per PCI Bridge Manual 8.8.2.4.7, the tire pressure is 0.125 ksi.

$V_u := \eta \cdot \gamma_{LL} \cdot 0.125 \cdot 10 \cdot 20$ $V_u = 43.75$ k

Calculate the two-way shear resistance of the deck from AASHTO LRFD 5.13.3.6.3:

$\beta_c := \frac{20}{10}$

Subtract the 2 in. cover and half of the diameter of a prestressing strand from the depth of the slab to find the effective shear depth:

$d_v := 8 - 2 - \frac{0.5}{2}$ $d_v = 5.75$ in.

$f_{pc} := 8.35$ ksi This is the actual compressive strength of the concrete in the deck from the material testing component of this research program.

$b_o := 2 \cdot (20 + 10)$ $b_o = 60$ in. $\phi := 0.9$

$$\phi V_n := \left| \begin{array}{l} V_1 \leftarrow \left(0.063 + \frac{0.126}{\beta_c}\right) \cdot \sqrt{f_{pc}} \cdot b_o \cdot d_v \\ V_2 \leftarrow 0.126 \sqrt{f_{pc}} \cdot b_o \cdot d_v \\ \phi V_n \leftarrow \phi \cdot \min(V_1, V_2) \\ \phi V_n \end{array} \right.$$

$\phi V_n = 113.092$ k O.K.

Determine the number of strands to post-tension the deck:

Estimate the number of 1/2 in. diameter strands that will be used for post tensioning:

Say $f_{pe} := 0.55 f_{pu}$ $f_{pe} = 148.5$ ksi (This is a rough estimate. A more detailed analysis was carried out in DIANA.)

where $f_{pu} = 270$ ksi and $f_{py} := 243$ ksi

The effective stress in the deck should be around 225-250 psi.
Using the following information, the number of strands can be estimated

$A_{strand} := 0.153$ in^2

$t_{deck} := 8$ in.

$b_{deck} := 144$ in^2 (Width of entire deck.)

$A_{deck} := t_{deck} \cdot b_{deck}$

$\sigma := 0.25$ ksi

$$no\_str := \frac{\sigma \cdot A_{deck}}{A_{strand} \cdot f_{pe}} \qquad no\_str = 12.676$$

Check stress with $no\_str := 12$

$$\sigma := \frac{no\_str \cdot A_{strand} \cdot f_{pe}}{A_{deck}} \qquad \sigma = 0.237 \text{ ksi}$$ OK. Try using 12 strands.

GIRDER DESIGN CALCULATIONS

The following table summarizes the design shears and moments for the girder design. The AASHTO LRFD distribution factors were used to obtain the shear and moment for each girder. The shear and moment envelopes based on the following loads:

1. Dead load of the girders, panels, and haunch.
2. AASHTO LRFD design truck and lane loading.

Table A.1 Summary of Shears and Moments for Girder Design

	Service Loads					Factored Loads						Fatigue
Load Case	Load Case 1	Load Case 2	Load Case 3			Load Case 3						
Loading	w_g	w_2	w_{3s}	Lane Load	Vehicle Load	w_{3f}	Lane Load	Vehicle Load	w_{3f}	Lane Load	Vehicle Load	Fatigue Truck
	M (k-ft)	M (k-ft)	M (k-ft)	M (k-ft)	M (k-ft)	V (k)	V (k)	V (k)	M (k-ft)	M (k-ft)	M (k-ft)	M (k-ft)
Distance												
0	0.00	0.00	0.00	0.00	0.00	34.60	18.23	103.95	0.00	0.00	0.00	0.00
0.5	3.79	16.39	13.63	4.70	27.93	33.74	17.78	102.41	17.08	8.22	48.89	10.39
1	7.49	32.37	26.91	9.27	53.97	32.87	17.33	100.88	33.74	16.23	94.45	20.10
1.5	11.09	47.93	39.85	13.73	78.54	32.01	16.89	99.34	49.95	24.03	137.45	29.29
2	14.59	63.08	52.44	18.07	101.96	31.14	16.46	97.81	65.74	31.62	178.43	38.09
2.5	18.00	77.81	64.69	22.29	124.47	30.28	16.03	96.27	81.09	39.01	217.82	46.60
3	21.31	92.13	76.59	26.39	146.22	29.41	15.60	94.74	96.02	46.18	255.89	54.89
3.5	24.53	106.03	88.15	30.37	167.32	28.55	15.18	93.20	110.50	53.15	292.80	63.00
4	27.65	119.52	99.36	34.24	187.79	27.68	14.77	91.67	124.56	59.92	328.64	70.96
4.5	30.67	132.59	110.23	37.98	207.66	26.82	14.36	90.13	138.18	66.47	363.40	78.78
5	33.60	145.25	120.75	41.61	226.88	25.95	13.96	88.59	151.38	72.81	397.04	86.45
5.5	36.43	157.49	130.93	45.11	245.42	25.09	13.56	87.06	164.13	78.95	429.48	93.96
6	39.17	169.32	140.76	48.50	263.20	24.22	13.17	85.52	176.46	84.88	460.61	101.28
6.5	41.81	180.73	150.25	51.77	280.17	23.36	12.79	83.99	188.35	90.60	490.30	108.37
7	44.35	191.73	159.39	54.92	296.25	22.49	12.41	82.45	199.82	96.11	518.43	115.23
7.5	46.80	202.31	168.19	57.95	311.37	21.63	12.04	80.92	210.84	101.42	544.90	121.80
8	49.15	212.48	176.64	60.87	325.50	20.76	11.67	79.38	221.44	106.52	569.62	128.08
8.5	51.41	222.23	184.75	63.66	338.58	19.90	11.31	77.84	231.60	111.41	592.51	134.02
9	53.57	231.57	192.51	66.34	350.59	19.03	10.95	76.31	241.34	116.09	613.54	139.60
9.5	55.63	240.49	199.93	68.89	361.54	18.17	10.60	74.77	250.63	120.56	632.70	144.83
10	57.60	249.00	207.00	71.33	371.44	17.30	10.26	73.24	259.50	124.82	650.02	149.67
10.5	59.47	257.09	213.73	73.65	380.32	16.44	9.92	71.70	267.93	128.88	665.56	154.13
11	61.25	264.77	220.11	75.85	388.24	15.57	9.58	70.17	275.94	132.73	679.42	158.22
11.5	62.93	272.03	226.15	77.93	395.27	14.71	9.26	68.63	283.50	136.37	691.73	161.93
12	64.51	278.88	231.84	79.89	401.51	13.84	8.93	67.10	290.64	139.80	702.64	165.30
12.5	66.00	285.31	237.19	81.73	407.04	12.98	8.62	65.56	297.34	143.03	712.32	168.33
13	67.39	291.33	242.19	83.45	411.97	12.11	8.31	64.02	303.62	146.04	720.96	171.06
13.5	68.69	296.93	246.85	85.06	416.43	11.25	8.00	62.49	309.45	148.85	728.74	173.51
14	69.89	302.12	251.16	86.54	420.49	10.38	7.70	60.95	314.86	151.45	735.86	175.72
14.5	70.99	306.89	255.13	87.91	424.27	9.52	7.41	59.42	319.83	153.85	742.48	177.71
15	72.00	311.25	258.75	89.16	427.84	8.65	7.12	57.88	324.38	156.03	748.72	179.51
15.5	72.91	315.19	262.03	90.29	431.24	7.79	6.84	56.35	328.48	158.01	754.67	181.14
16	73.73	318.72	264.96	91.30	434.49	6.92	6.56	54.81	332.16	159.77	760.35	182.63
16.5	74.45	321.83	267.55	92.19	437.54	6.06	6.29	53.27	335.40	161.34	765.69	183.97
17	75.07	324.53	269.79	92.96	440.30	5.19	6.03	51.74	338.22	162.69	770.53	185.16
17.5	75.60	326.81	271.69	93.62	442.61	4.33	5.77	50.20	340.59	163.83	774.56	186.18
18	76.03	328.68	273.24	94.15	444.21	3.46	5.52	48.67	342.54	164.77	777.36	186.97
18.5	76.37	330.13	274.45	94.57	444.75	2.60	5.27	47.13	344.05	165.50	778.31	187.48
19	76.61	331.17	275.31	94.87	443.77	1.73	5.03	45.60	345.14	166.02	776.59	187.60
19.5	76.75	331.79	275.83	95.04	440.67	0.87	4.79	44.06	345.78	166.33	771.18	187.20
20	76.80	332.00	276.00	95.10	434.72	0.00	4.56	42.53	346.00	166.43	760.77	186.11

GIRDER DESIGN CALCULATIONS

MATERIAL PROPERTIES

$f'_{ci\_deck} := 4$ ksi $\quad E_{ci\_deck} := 57\cdot\sqrt{f'_{ci\_deck}\cdot 100}$ $\quad E_{ci\_deck} = 3.605\times 10^3$ ksi

$f'_{c\_deck} := 6$ ksi $\quad E_{c\_deck} := 57\cdot\sqrt{f'_{c\_deck}\cdot 100}$ $\quad E_{c\_deck} = 4.415\times 10^3$ ksi

$f'_{ci\_girder} := 4$ ksi $\quad E_{ci\_girder} := 57\cdot\sqrt{f'_{ci\_girder}\cdot 100}$ $\quad E_{ci\_girder} = 3.605\times 10^3$ ksi

$f'_{c\_girder} := 6$ ksi $\quad E_{c\_girder} := 57\cdot\sqrt{f'_{c\_girder}\cdot 100}$ $\quad E_{c\_girder} = 4.415\times 10^3$ ksi

$f'_{ci\_h} := 4$ ksi $\quad E_{ci\_h} := 57\cdot\sqrt{f'_{ci\_girder}\cdot 100}$ $\quad E_{ci\_h} = 3.605\times 10^3$ ksi

$f'_{c\_h} := 6$ ksi $\quad E_{c\_h} := 57\cdot\sqrt{f'_{c\_girder}\cdot 100}$ $\quad E_{c\_h} = 4.415\times 10^3$ ksi

$$n_{deck} := \frac{E_{c\_deck}}{E_{c\_girder}} \qquad n_{deck} = 1$$

$$n_h := \frac{E_{c\_h}}{E_{c\_girder}} \qquad n_h = 1$$

Prestressing strands:

$f_{pu} := 270$ ksi $\quad f_{py} := 243$ ksi $\quad E_p := 28500$ ksi

SECTION PROPERTIES

$L := 40$ ft.

$S := 8$ ft.

Girder:

AASHTO Type II

$b_f := 12$ in. $\quad I_g := 50979$ in^4 $\quad A_g := 369$ in^2 $\quad h_g := 36$ in. $\quad b_w := 6$ in.

$c_1 := 20.17$ in. $\quad S_1 := \frac{I_g}{c_1}$ $\quad S_1 = 2.527\times 10^3$ in^3

$c_2 := 15.83$ in. $\quad S_2 := \frac{I_g}{c_2}$ $\quad S_2 = 3.22\times 10^3$ in^3

Deck Slab:

$h_{deck} := 8$

$b_{deck} := \left| \begin{array}{l} A \leftarrow \frac{1}{4} \cdot L \cdot 12 \\ B \leftarrow 12 \cdot h_{deck} + \max\left(b_w, \frac{1}{2} \cdot b_f\right) \\ C \leftarrow S \cdot 12 \\ temp \leftarrow \min(A, B, C, 6 \cdot 12) \\ temp \end{array} \right.$ $b_{deck} = 72$ in.

(AASHTO LRFD Article 4.6.2.6.1)

(Max. effective width of the deck in the lab is 6 ft.)

$A_{deck} := h_{deck} \cdot b_{deck}$ $A_{deck} = 576$ in^2

$A_{deck\_eff} := n_{deck} \cdot A_{deck}$ $A_{deck\_eff} = 576$ in^2

Haunch:

$h_h := 2$ in.

$A_h := h_h \cdot b_f$ $A_h = 24$ in^2

$A_{h\_eff} := n_h \cdot A_h$ $A_{h\_eff} = 24$ in^2

Composite Section:

$y_h := h_g + \frac{h_h}{2}$ $y_h = 37$ in.

$y_{deck} := h_g + h_h + \frac{h_{deck}}{2}$ $y_{deck} = 42$ in.

$h := h_g + h_h + h_{deck}$ $h = 46$ in.

$y_{bar} := \frac{c_2 \cdot A_g + y_h \cdot A_{h\_eff} + y_{deck} \cdot A_{deck\_eff}}{A_g + A_{h\_eff} + A_{deck\_eff}}$ $y_{bar} = 31.91$ in.

$$I_c := \left| \begin{array}{l} I_{g\_c} \leftarrow I_g + A_g \cdot \left| y_{bar} - c_2 \right|^2 \\ I_{h\_c} \leftarrow \frac{1}{12} \cdot n_h \cdot b_f \cdot h_h^{\,3} + A_{h\_eff} \cdot \left| y_{bar} - y_h \right|^2 \\ I_{deck\_c} \leftarrow \frac{1}{12} \cdot n_{deck} \cdot b_{deck} \cdot h_{deck}^{\,3} + A_{deck\_eff} \cdot \left| y_{bar} - y_{deck} \right|^2 \\ I_c \leftarrow I_{g\_c} + I_{h\_c} + I_{deck\_c} \\ I_c \end{array} \right. \qquad I_c = 208733 \quad in^4$$

$$S_{c1} := \frac{I_c}{\left| h_g - y_{bar} \right|} \qquad S_{c1} = 5.104 \times 10^4 \quad in^3$$

$$S_{c2} := \frac{I_c}{y_{bar}} \qquad S_{c2} = 6.541 \times 10^3 \quad in^3$$

$$S_{c3} := \frac{I_c}{\left| h - y_{bar} \right|} \qquad S_{c3} = 1.481 \times 10^4 \quad in^3 \qquad \text{(to top of slab)}$$

$A_c := A_g + A_{h\_eff} + A_{deck\_eff}$ $\qquad A_c = 969 \quad in^2$

Prestressing Strands:

Use 1/2 in. ϕ , grade 270 strands. $\qquad A_{strand} := 0.15$ in^2

ALLOWABLE STRESSES (PCI Bridge Manual 8.2.1.2.2)

Deck:

For design purposes, the deck has an initial compressive stress of 250 psi from the post tensioning operation.

$f_{cs1\_deck} := -0.45 f'_{c\_deck} + 0.25$	$f_{cs1\_deck} = -2.45$ ksi	Allowable compressive stress for dead loads at service.
$f_{cs2\_deck} := -0.6 f'_{c\_deck} + 0.25$	$f_{cs2\_deck} = -3.35$ ksi	Allowable compressive stress for dead and live loads at service.
$f_{cs3\_deck} := -0.4 f'_{c\_deck} + 0.25$	$f_{cs3\_deck} = -2.15$ ksi	Allowable compressive stress for live loads and one half of dead loads at service.
$f_{ts\_deck} := 0.19\sqrt{f'_{c\_deck}}$	$f_{ts\_deck} = 0.465$ ksi	Allowable tensile stress for dead and love loads at service.

Girder:

$f_{ci\_girder} := -0.6 \cdot f'_{ci\_deck}$ $\quad f_{ci\_girder} = -2.4$ ksi — Allowable compressive stress at release.

$f_{ti\_girder} := \left| \begin{array}{l} f \leftarrow 0.0948\sqrt{f'_{ci\_deck}} \\ g \leftarrow f \\ g \leftarrow 0.2 \text{ if } f \geq 0.2 \\ g \end{array} \right.$ $\quad f_{ti\_girder} = 0.19$ ksi — Allowable tensile stress at release.

$f_{cs1\_girder} := -0.45 \cdot f'_{c\_deck}$ $\quad f_{cs1\_girder} = -2.7$ ksi — Allowable compressive stress for dead loads at service.

$f_{cs2\_girder} := -0.6 \cdot f'_{c\_deck}$ $\quad f_{cs2\_girder} = -3.6$ ksi — Allowable compressive stress for dead and live loads at service.

$f_{cs3\_girder} := -0.4 \cdot f'_{c\_deck}$ $\quad f_{cs3\_girder} = -2.4$ ksi — Allowable compressive stress for live loads and one half of dead loads at service.

$f_{ts\_girder} := 0.19\sqrt{f'_{c\_deck}}$ $\quad f_{ts\_girder} = 0.465$ ksi — Allowable tensile stress for dead and live loads at service.

DETERMINE THE TRIAL NUMBER OF STRANDS:

The channel of permissible profiles is shown in Figure A.1. It is based upon the moments determined in the loading section of the calculations, the allowable stresses, and section properties calculated above. The most efficient straight tendon profile consists of 12 strands with an eccentricity of 7.83 in. The equations used in the spreadsheet to determine the limits on the permissible tendon profiles are based off the following equations:

Transfer:

$$\frac{-P_i}{A_g} + \frac{P_i \cdot e_g}{S_1} - \frac{M_g}{S_1} \leq f_{ti\_girder}$$

$$\frac{-P_i}{A_g} - \frac{P_i \cdot e_g}{S_2} + \frac{M_g}{S_2} \geq f_{ci\_girder}$$

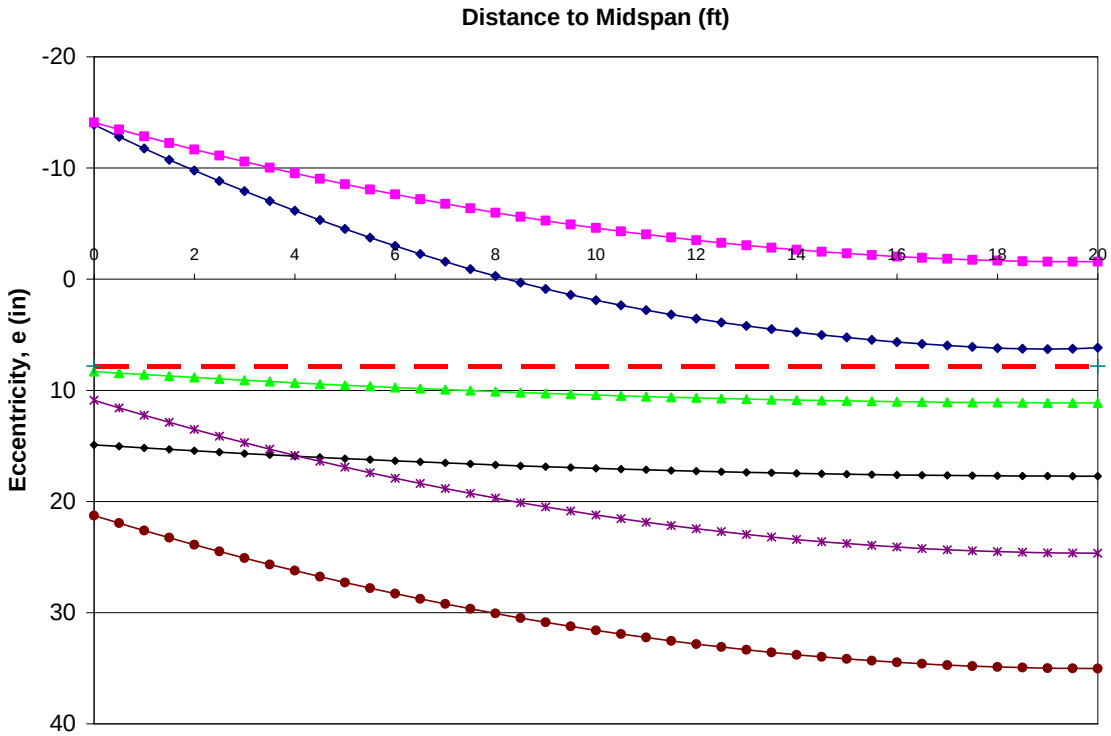

Figure A.1 Channel of Permissible Tendon Profiles for the Girders

Intermediate (Construction Stage):

$$\frac{-P_e}{A_g} + \frac{P_e \cdot e_g}{S_1} - \frac{M_{\omega 2}}{S_1} \le f_{ts\_girder}$$

$$\frac{-P_e}{A_g} - \frac{P_e \cdot e_g}{S_2} + \frac{M_{\omega 2}}{S_2} \ge f_{cs1\_girder}$$

Service:

$$\frac{-P_e}{A_g} + \frac{P_e \cdot e_g}{S_1} - \frac{M_{\omega 3}}{S_1} - \frac{M_{lane} + M_{vehicle}}{S_{1c}} \ge f_{cs3\_girder}$$

(This stress limit was imposed on the total live load. The concrete does not come close to cruching at any location.)

$$\frac{-P_e}{A_g} - \frac{P_e \cdot e_g}{S_2} + \frac{M_{\omega 3}}{S_2} + \frac{0.8 \left(M_{lane} + M_{vehicle} \right)}{S_{2c}} \le f_{ts}$$

(The factor of 0.8 comes from the "Service III" load combination in PCI Bridge Manual 7.3.2.)

where,

M_g The self weight of the girder.

$M_{\omega 2}$ The weight of the girder, haunch, panel and constuction utility load.

$M_{\omega 3}$ The weight of the girder, haunch, panel and barrier.

DETERMINE PRESTRESS LOSSES (PCI Bridge Manual 8.6)

ELASTIC SHORTENING:

Assumed force per strand at transfer: $A_{strand} \cdot 0.7 \cdot f_{pu} = 28.917$

$no\_strands := 12$

$e := 7.83$ in.

$P_i := no\_strands \cdot A_{strand} \cdot 0.7 \cdot f_{pu}$ $P_i = 347.004$ k

$M_g := 921.0$ k-in

$$f_{cgp} := \frac{P_i}{A_g} + \frac{P_i \cdot e^2}{I_g} - \frac{M_g \cdot e}{I_g} \qquad f_{cgp} = 1.216 \text{ ksi}$$

$$\Delta f_{pES} := \frac{E_p}{E_{ci\_girder}} \cdot f_{cgp} \qquad \Delta f_{pES} = 9.615 \text{ ksi}$$

SHRINKAGE:

Annual average ambient relative humidity, $H := 70$ % for Southwestern Virginia. (PCI Design Handbook - Figure 3.12.2)

$\Delta f_{pSR} := (17 - 0.15H)$ $\Delta f_{pSR} = 6.5$ ksi

CREEP OF CONCRETE:

$M_s := 3984 - 921.0$ k-in (Refer to Load Summary)

$$f_{cdp} := \frac{M_s \cdot e}{I_g} \qquad f_{cdp} = 0.47 \text{ ksi}$$

$f_{cgp} = 1.216$ ksi

$\Delta f_{pCR} := 12 \cdot f_{cgp} - 7 \cdot f_{cdp}$ $\Delta f_{pCR} = 11.301$ ksi

RELAXATION OF PRESTRESSING STEEL

Relaxation before transfer:

use $t := 1000$ day

$K_r := 45$ (Low relaxation strands are assumed to be used. Otherwise, K_r=10.)

$f_i := 0.7 \cdot f_{pu}$ $f_i = 189$ ksi

$\Delta f_{pr1} := \frac{\log(24 \cdot t)}{K_r} \cdot \left(\frac{182}{f_{py}} - 0.55 \right) \cdot 18$ $\Delta f_{pr1} = 4.33$ ksi

Relaxation after transfer:

$\Delta f_{pr2} := 6 - 0.12 \cdot \Delta f_{pES} - 0.06 \left| \Delta f_{pSR} + \Delta f_{pCR} \right|$ $\Delta f_{pr2} = 3.778$ ksi

Total Relaxation loss after transfer:

$\Delta f_{pr} := \Delta f_{pr1} + \Delta f_{pr2}$ $\Delta f_{pr} = 8.108$ ksi

Total losses at transfer:

$\Delta f_{pi} := \Delta f_{pES} + \Delta f_{pr1}$ $\Delta f_{pi} = 13.944$ ksi

Stress in tendon after transfer:

$f_{pt} := 0.7 \cdot f_{pu} - \Delta f_{pi}$ $f_{pt} = 175.056$ ksi

Prestressing force after transfer per panel:

$P_i := no\_strands \cdot A_{strand} \cdot f_{pt}$ $P_i = 321.403$ k

Total losses at service loads:

$\Delta f_{pT} := \Delta f_{pES} + \Delta f_{pSR} + \Delta f_{pCR} + \Delta f_{pr2}$ $\Delta f_{pT} = 31.194$ ksi

Stress in tendon after all losses:

$f_{pe} := 0.7 \cdot f_{pu} - \Delta f_{pT}$ $f_{pe} = 157.806$ ksi

Effective prestressing force per panel:

$P_e := no\_strands \cdot A_{strand} \cdot f_{pe}$ $P_e = 289.732$ k

The channel of permissible tendon profiles shows 12 strands with an eccentricity of 7.83 in. works.

CHECK FATIGUE OF STRANDS: (PCI Bridge Manual 8.2.1.9)

Compute the range of stress in the lower strand due to the fatigue truck loading at midspan:

$M_{fatigue} := 186.1$ k-ft $\quad M_{fatigue} \cdot 12 = 2.233 \times 10^3$ k-in

$$\Delta\sigma_{fatigue} := \frac{M_{fatigue} \cdot 12 \cdot \left| y_{bar} - 2 \right|}{I_c} \cdot \frac{E_p}{E_{c\_girder}} \qquad \Delta\sigma_{fatigue} = 2.066 \text{ ksi}$$

$\Delta\sigma_{fatigue}$ is less than the allowable range of 10 ksi OK.

CHECK FLEXURAL STRENGTH FOR MAX. POSITIVE MOMENT

$A_{ps} := no\_strands \cdot A_{strand} \qquad A_{ps} = 1.836 \text{ in}^2$

$$\beta_1 := \begin{cases} B \leftarrow 0.85 \text{ if } f'_{c\_girder} \le 4 \\ B \leftarrow \max\left[0.85 - 0.05 \left| f'_{c\_girder} - 4 \right|, 0.65\right] \text{ if } f'_{c\_girder} > 4 \\ B \end{cases} \qquad \beta_1 = 0.75$$

$$k := 2 \cdot \left(1.04 - \frac{f_{py}}{f_{pu}}\right) \qquad k = 0.28$$

$d_p := h - \left| c_2 - e \right| \qquad d_p = 38$ in.

The longitudinal steel in the deck acts as compression reinforcement in the composite section (see Deck Design calcs):

$A'_s := \frac{b_{deck}}{12} \cdot 0.57$ $\qquad A'_s = 3.432 \text{ in}^2$

$f'_y := 60$ ksi

$$c := \frac{A_{ps} \cdot f_{pu} - A'_s \cdot f'_y}{0.85 f'_{c\_girder} \cdot \beta_1 \cdot n_{deck} \cdot b_{deck} + k \cdot A_{ps} \cdot \frac{f_{pu}}{d_p}} \qquad c = 1.039 \text{ in.}$$

$a := \beta_1 \cdot c$ $\quad a = 0.779$ in.

$f_{ps} := f_{pu} \cdot \left(1 - k \cdot \frac{c}{d_p}\right)$ $\quad f_{ps} = 267.934$ ksi

$\phi := 1.0($ (AASHTO LRFD 5.5.4.2.1)

$\phi M_n := \phi \cdot A_{ps} \cdot f_{ps} \cdot \left(d_p - \frac{a}{2}\right) \cdot \frac{1}{12}$ $\quad \phi M_n = 1.542 \times 10^3$ k-ft

$M_u := 346 + 166.43 + 760.7$ (From Load Summary)

$M_u = 1.273 \times 10^3$ k-ft OK.

For constructability reasons and to increase the flexural capacity of the lab mockup, 4 #5 bars were placed in both the top flange and bottom flange of the girders. The flexural capacity will be calculated with the addition of the mild steel to the girders:

$f'_c := 8.35($ ksi (Actual compressive strength of the girder at the time the deck is post-tensioned.)

$b := 72$ in.

The stress-strain relationship for the mild reinforcing steel:

$$f_s(\varepsilon_s) := \begin{cases} f \leftarrow 29126.21 \cdot |\varepsilon_s| \text{ if } |\varepsilon_s| \le 0.00103 \\ f \leftarrow 13684.21 \cdot |\varepsilon_s| + 15.91 \text{ if } 0.00103 < |\varepsilon_s| \le 0.0029 \\ f \leftarrow 967.57 \cdot |\varepsilon_s| + 53.16 \text{ if } 0.00293 < |\varepsilon_s| \le 0.035 \\ f \leftarrow 288.22 \cdot |\varepsilon_s| + 76.94 \text{ if } 0.035 < |\varepsilon_s| \le 0.08 \\ f \leftarrow 100 \text{ if } |\varepsilon_s| > 0.08 \\ f \end{cases}$$

The stress-strain relationship for the prestressing strands:

$$f_{ps}(\varepsilon_{ps}) := \begin{cases} f \leftarrow 28500 |\varepsilon_{ps}| \text{ if } |\varepsilon_{ps}| \le 0.0086 \\ f \leftarrow 270 - \frac{0.04}{|\varepsilon_{ps}| - 0.007} \text{ if } |\varepsilon_{ps}| > 0.008 \\ f \end{cases}$$

Trial value of the depth of the compression block. It will initially be assumed that the complete compressive stress block is located in the deck:

$c := 2.09($ in.

Using strain compatibility, the constitutive relationships above, and the cross sectional area of steel at a given depth, the force in each layer of steel is calculated. It is assumed the concrete in the top of the deck crushes at a strain of 0.0038.

For the top row of distribution steel in the deck:

$$T_{1a} := f_s\left[0.0038 \cdot \frac{(46 - c - 43.5)}{c}\right] \cdot 1.8 \qquad T_{1a} = 38.173 \quad k$$

For the bottom row of distribution steel in the deck:

$$T_{1b} := f_s\left[0.0038 \cdot \frac{(46 - c - 40.5)}{c}\right] \cdot 1.8 \qquad T_{1b} = 106.42 \quad k$$

For the 4 No. 5 bars in the top flange of a girder:

$$T_2 := f_s\left[0.0038 \cdot \frac{(46 - c - 30)}{c}\right] \cdot 1.24 \qquad T_2 = 96.129 \quad k$$

For the 4 No. 5 bars in the bottom flange of a girder:

$$T_3 := f_s\left[0.0038 \cdot \frac{(46 - c - 8)}{c}\right] \cdot 1.24 \qquad T_3 = 118.646 \quad k$$

For the prestressing strands in the bottom of the girder:

$$T_4 := f_{ps}\left[0.0038 \cdot \frac{(46 - c - 8)}{c} + 0.00618\right] \cdot 1.836 \qquad T_4 = 494.576 \quad k$$

The strain of 0.00619 is the sum of the strain associated with the effective prestress force,

$f_{pe} := 169.5$ ksi $\quad E_p := 2850$ ksi $\quad P := 311.2$ k $\quad A_g := 369$ in^2

$e := 7.83$ in. $\quad f'_{c\_g} := 7.087$ ksi $\quad I_g := 5097$ in^4

$E_g := 57\sqrt{f'_c \cdot 1000} \qquad E_g = 5.21 \times 10^3$ ksi

$$\varepsilon_1 := \frac{f_{pe}}{E_p} \qquad \varepsilon_1 = 5.947 \times 10^{-3}$$

and the strain associated with the decompression of the concrete at the steel centroid,

$$\varepsilon_2 := \left(\frac{P}{A_g} + \frac{P \cdot e^2}{I_g} \right) \cdot \frac{1}{E_g} \qquad \varepsilon_2 = 2.337 \times 10^{-4}$$

$$\varepsilon_1 + \varepsilon_2 = 6.181 \times 10^{-3}$$

The total tensile force is:

$$T := T_{1a} + T_{1b} + T_2 + T_3 + T_4 \qquad T = 853.944 \quad k$$

The compressive force in the deck is obtained by breaking the compressive σ-ε curve up in to an area formed by a parabola, a triangular area, and a rectangular area. The Hogenstad model is used for the compressive σ-ε curve and can be found in MacGregor[39].

$$C_1 := b \cdot \int_0^{0.672c} 5898.2 \cdot \left(0.0038 \cdot \frac{y}{c} \right) - 1156540 \left(0.0038 \cdot \frac{y}{c} \right)^2 dy \qquad C_1 = 509.268 \quad k$$

$$C_2 := \frac{b \cdot 0.15 \cdot \left| 0.9 \cdot f'_c \right| \cdot (c - 0.672 \cdot c)}{2} \qquad C_2 = 27.946 \quad k$$

$$C_3 := b \cdot 0.85 \cdot \left| 0.9 \cdot f'_c \right| \cdot (c - 0.672 \cdot c) \qquad C_3 = 316.717 \quad k$$

The total compressive force in the deck is

$$C := C_1 + C_2 + C_3 \qquad C = 853.93 \quad k$$

The difference between the total tensile force and the compressive force is

$$T - C = 0.014 \quad k$$

The moment arms are the distance from the top of the deck to the centroid of the force of interest. For the calculation of the moment arms for the compressive forces in the deck, the distances from the neutral axis, d_i, area calculated first and then subtracted from the depth of the neutral axis.

$$d_1 := \frac{72 \cdot \int_0^{0.672 \cdot c} y \cdot \left[5898.2 \cdot \left(0.0038 \cdot \frac{y}{c} \right) - 1156540 \left(0.0038 \cdot \frac{y}{c} \right)^2 \right] dy}{72 \cdot \int_0^{0.672 \cdot c} 5898.2 \cdot \left(0.0038 \cdot \frac{y}{c} \right) - 1156540 \left(0.0038 \cdot \frac{y}{c} \right)^2 dy}$$

$d_1 = 0.881$ in.

$d_2 := 0.672 \cdot c + (c - 0.672 \cdot c) \cdot \frac{1}{3}$ $d_2 = 1.639$ in.

$d_3 := 0.672 \cdot c + (c - 0.672 \cdot c) \cdot \frac{1}{2}$ $d_3 = 1.754$ in.

$M_1 := -C_1 \cdot \left| c - d_1 \right| - C_2 \cdot \left| c - d_2 \right| - C_3 \cdot \left| c - d_3 \right|$

$M_2 := T_{1a} \cdot 2.5 + T_{1b} \cdot 5.5 + T_2 \cdot 16 + T_3 \cdot 38 + T_4 \cdot 38$

$M := M_1 + M_2$ $M = 24780$ k-in

MINIMUM AMOUNT OF REINFORCEMENT CHECK: (PCI Bridge Manual - 8.2.2.3.3)

The following two equations must be considered along the span of the girder.

$\phi M_n \geq 1.33 M_u$

$\phi M_n \geq 1.2 \cdot M_{cr}$

The expression that produces the smallest value controls

Determine the expression for the cracking moment:

$$f_r = \frac{-P_e}{A_g} - \frac{P_e \cdot e}{S_2} + \frac{M_{cr}}{S_{c2}}$$

$f_r := 0.24 \sqrt{f'_{c\_girder}}$ $f_r = 0.588$ ksi

$M_{cr} := \left(f_r + \frac{P_e}{A_g} + \frac{P_e \cdot e}{S_2} \right) \cdot S_{c2} \cdot \frac{1}{12}$ $1.2 \cdot M_{cr} = 1.359 \times 10^3$

MAXIMUM AMOUNT OF REINFORCEMENT CHECK:

(PCI Bridge Manual - 8.2.2.3.2)

There will need to be some mild steel to support the stirrups. This will be estimated for this calculation to be 10 - #5 bars. The centroid of the mild reinforcing steel will be conservatively estimated at the centroid of the girder.

$A_{supp} := 3.1 \quad in^2$

$d_{supp} := h - y_{bar} \qquad d_{supp} = 14.09 \quad in.$

$f_{ym} := 60 \quad ksi$

$$d_e := \frac{A_{ps} \cdot f_{ps} \cdot d_p + A_{supp} \cdot f_{ym} \cdot d_{supp} + A_s \cdot f_y \cdot d}{A_{ps} \cdot f_{ps} + A_{supp} \cdot f_{ym} + A_s \cdot f_y} \qquad d_e = 31.798 \quad in.$$

$\frac{c}{d_e} = 0.033$ Less than 0.42. Composite Section meets ductility requirements.

SHEAR DESIGN (AASHTO LRFD 5.8 and PCI Bridge Manual 8.4.3)

Critical Section at Support:

Determine trial value for θ :

Let $\theta := 22$ degrees

or $\theta := \theta \cdot \frac{\pi}{180}$ $\theta = 0.384$ rad

Effective shear depth and effective web width:

$d_v :=$ $d_e \leftarrow h - \left(c_2 - e \right)$ $d_v = 37.611$ in.

$a \leftarrow 0.779$

$d_v \leftarrow d_e - \frac{a}{2}$

$lowlim1 \leftarrow 0.9 \cdot d_e$

$lowlim2 \leftarrow 0.72 \cdot h$

$d \leftarrow \max\left(d_v, lowlim1, lowlim2 \right)$

d

$b_v := 6$ in. for AASHTO Type II girder

Find critical section:

$d_{cr} := \max\left(0.5 \cdot d_v \cdot \cot\left(\theta \right), d_v \right)$ $d_{cr} = 46.545$ in.

The corresponding shears and moments at the section are found using the Load Summary Table from the loading calculations section:

$V_u := 28.55 + 15.18 + 93.$ $V_u = 136.93$ k

$M_u := 110.5 + 53.15 + 292.$ $M_u = 456.45$ k-ft

$M_{DL} := 88.1$ k-ft

$N_u := 0$

Compute the resultant compressive stress in the concrete at the centroid of the prestressing strands, due to the all permanent loads, resisted by the girder alone:

$f_{pc} := \frac{-P_e}{A_g} - \frac{P_e \cdot e^2}{I_g} + \frac{M_{DL} \cdot 12 \cdot e}{I_g}$ $f_{pc} = -0.971$ ksi

Compute the stress in the prestressing strand where the stress in the surrounding concrete is zero:

The delevopment length is

$$l_d := \left(f_{ps} - \frac{2}{3} \cdot f_{pe} \right) \cdot d_b \qquad l_d = 81.365 \quad \text{in.}$$

Recall the section of interest is at $d_{cr} = 46.545$ in.

The effective stress in the strand at the section of interest is

$$f_p := \begin{cases} f \leftarrow \dfrac{d_{cr}}{60 \cdot d_b} \cdot f_{pe} \text{ if } d_{cr} < 60 \cdot d_b \\ f \leftarrow f_{pe} \text{ if } d_{cr} = 60 \cdot d_b \\ f \leftarrow \dfrac{d_{cr}}{d_b} + \dfrac{2}{3} \cdot f_{pe} \text{ if } d_{cr} > 60 \cdot d_b \wedge d_{cr} < l_d \\ f \leftarrow f_{pu} \text{ if } d_{cr} \geq l_d \\ f \end{cases} \qquad f_p = 198.293 \quad \text{ksi}$$

$$f_{po} := f_p + f_{pc} \cdot \frac{E_p}{E_{c\_girder}} \qquad f_{po} = 192.024 \quad \text{ksi}$$

See attached sheet from PCI Bridge Manual for description of calculation.

$$\varepsilon_x := \frac{\dfrac{M_u \cdot 12}{d_v} + 0.5 \cdot N_u + 0.5 \cdot V_u \cdot \cot(\theta) - A_{ps} \cdot f_{po}}{2 \cdot (E_s \cdot A_s + E_p \cdot A_{ps})} \qquad \varepsilon_x = -1.453 \times 10^{-4}$$

where $E_s = 2.9 \times 10^4$ ksi

ε_x will be multiplied by the following factor:

$$F_\varepsilon := \begin{cases} a \leftarrow 1 \text{ if } \varepsilon_x \geq 0 \\ a \leftarrow \dfrac{E_s \cdot A_s + E_p \cdot A_{ps}}{A_{ct} \cdot E_{c\_girder} + E_s \cdot A_s + E_p \cdot A_{ps}} \text{ if } \varepsilon_x < 0 \\ a \end{cases} \qquad F_\varepsilon = 0.106$$

where A_{ct} is definded in PCI Bridge Manual 8.4.3.2, $A_{ct} = 246 \quad in^2$

$\varepsilon_x := \varepsilon_x \cdot F_\varepsilon \qquad \varepsilon_x = -1.542 \times 10^{-5}$

Compute the factored shear stress

$$v := \frac{V_u}{\phi \cdot b_v \cdot d_v} \qquad v = 0.674 \quad ksi \qquad \text{where} \quad \phi = 0.9$$

$$\frac{v}{f'_{c\_girder}} = 0.112$$

Enter Table 5.8.3.4.2.1 of AASHTO LRFD with

$$\frac{v}{f'_{c\_girder}} = 0.112 \quad \text{and} \quad \varepsilon_x = -1.542 \times 10^{-5}$$

to get the new value of θ:

Interpolating between the data in the chart,

$$\theta_1 := 21.4 + \frac{0.112 - 0.1}{0.125 - 0.1} \cdot (22.8 - 21.4) \qquad \theta_1 = 22.072 \quad \text{degrees}$$

$$\theta_2 := 22.5 + \frac{0.112 - 0.1}{0.125 - 0.1} \cdot (23.7 - 22.5) \qquad \theta_2 = 23.076 \quad \text{degrees}$$

$$\theta := \theta_1 + \frac{0.015 - 0.05}{0 - 0.05} \cdot \left| \theta_2 - \theta_1 \right| \qquad \theta = 22.775 \quad \text{degrees}$$

or $\theta := \theta \cdot \frac{\pi}{180} \qquad \theta = 0.397 \quad rad$

Use the new value of θ to run through the <u>second iteration</u>:

Find critical section:

$d_{cr} := \max\left(0.5 \cdot d_v \cdot \cot\left(\theta\right), d_v\right) \qquad d_{cr} = 44.791 \quad in.$

The corresponding shears and moments at the section are found using the Load Summary Table from the loading calculations section:

$V_u := 28.55 + 15.18 + 93.2$ $\quad V_u = 136.93$ k

$M_u := 110.5 + 53.15 + 292.8$ $\quad M_u = 456.45$ k-ft

$M_{DL} := 88.15$ k-ft

$N_u := 0$

Compute the resultant compressive stress in the concrete at the centroid of the prestressing strands, due to the all permanent loads, resisted by the girder alone:

$$f_{pc} := \frac{-P_e}{A_g} - \frac{P_e \cdot e^2}{I_g} + \frac{M_{DL} \cdot 12 \cdot e}{I_g} \qquad f_{pc} = -0.971 \quad \text{ksi}$$

Compute the stress in the prestressing strand where the stress in the surrounding concrete is zero:

Recall the section of interest is at $d_{cr} = 44.791$ in.

The effective stress in the strand at the section of interest is

$$f_p := \begin{cases} f \leftarrow \dfrac{d_{cr}}{60 \cdot d_b} \cdot f_{pe} \text{ if } d_{cr} < 60 \cdot d_b \\ f \leftarrow f_{pe} \text{ if } d_{cr} = 60 \cdot d_b \\ f \leftarrow \dfrac{d_{cr}}{d_b} + \dfrac{2}{3} \cdot f_{pe} \text{ if } d_{cr} > 60 \cdot d_b \wedge d_{cr} < l_d \\ f \leftarrow f_{pu} \text{ if } d_{cr} \geq l_d \\ f \end{cases} \qquad f_p = 194.786 \quad \text{ksi}$$

$$f_{po} := f_p + -f_{pc} \cdot \frac{E_p}{E_{c\_girder}} \qquad f_{po} = 201.055 \quad \text{ksi}$$

$$\varepsilon_x := \frac{\dfrac{M_u \cdot 12}{d_v} + 0.5 \cdot N_u + 0.5 \cdot V_u \cdot \cot(\theta) - A_{ps} \cdot f_{po}}{2 \cdot (E_s \cdot A_s + E_p \cdot A_{ps})} \qquad \varepsilon_x = -2.344 \times 10^{-4}$$

where $E_s = 2.9 \times 10^4$ ksi

ε_x will be multiplied by the following factor:

$$F_\varepsilon := \begin{cases} a \leftarrow 1 \text{ if } \varepsilon_x \geq 0 \\ a \leftarrow \dfrac{E_s \cdot A_s + E_p \cdot A_{ps}}{A_{ct} \cdot E_{c\_girder} + E_s \cdot A_s + E_p \cdot A_{ps}} \text{ if } \varepsilon_x < 0 \\ a \end{cases} \qquad F_\varepsilon = 0.106$$

where A_{ct} is definded in PCI Bridge Manual 8.4.3.2, $A_{ct} = 246 \text{ in}^2$

$\varepsilon_x := \varepsilon_x \cdot F_\varepsilon$ $\varepsilon_x = -2.487 \times 10^{-5}$

Compute the factored shear stress

$v := \dfrac{V_u}{\phi \cdot b_v \cdot d_v}$ $v = 0.674$ ksi where $\phi = 0.9$

The required vertical shear strength is

$V_{n\_req} := \dfrac{V_u}{\phi}$ $V_{n\_req} = 152.144$ k

$$\frac{v}{f'_{c\_girder}} = 0.112$$

Enter Table 5.8.3.4.2.1 of AASHTO LRFD with

$\dfrac{v}{f'_{c\_girder}} = 0.112$ and $\varepsilon_x = -2.487 \times 10^{-5}$

to get the new value of θ:

Interpolating between the data in the chart,

$\theta_1 := 21.4 + \dfrac{0.112 - 0.1}{0.125 - 0.1} \cdot (22.8 - 21.4)$ $\theta_1 = 22.072$ degrees

$\theta_2 := 22.5 + \dfrac{0.112 - 0.1}{0.125 - 0.1} \cdot (23.7 - 22.5)$ $\theta_2 = 23.076$ degrees

$\theta := \theta_1 + \dfrac{0.02485 - 0.05}{0 - 0.05} \cdot \left| \theta_2 - \theta_1 \right|$ $\theta = 22.577$ degrees

or $\theta := \theta \cdot \dfrac{\pi}{180}$ $\theta = 0.394$ rad

The value of θ from this iteration is close enough to the value of θ from the previous iteration. The cooresponding value of β from Table 5.8.3.4.2-1 is

$$\beta_1 := 3.24 + \frac{0.115 - 0.1}{0.125 - 0.1} \cdot (2.94 - 3.24) \qquad \beta_1 = 3.06$$

$$\beta_2 := 3.14 + \frac{0.115 - 0.1}{0.125 - 0.1} \cdot (2.87 - 3.14) \qquad \beta_2 = 2.978$$

$$\beta := \beta_1 + \frac{0.02485 - 0.05}{0 - 0.05} \cdot \left| \beta_2 - \beta_1 \right| \qquad \beta = 3.019$$

The nominal shear capacity of the concrete can be calculated:

$$V_c := 0.0316\beta \cdot \sqrt{f'_{c\_girder}} \cdot b_v \cdot d_v \qquad V_c = 52.729 \quad k$$

Using the actual compressive strength of the concretre in the girder from the material testing component of this research program:

$$V_{c\_test} := 0.0316\beta \cdot \sqrt{7.082} b_v \cdot d_v \qquad V_{c\_test} = 57.287 \quad k$$

Recall that $V_u = 136.93$ k

Therefore, stirrups are needed.

$$V_{s\_req} := \frac{V_u}{\phi} - V_c \qquad V_{s\_req} = 99.415 \quad k$$

Try using #5 double leg stirrups.

$A_v := 2 \cdot 0.31$ in^2

$f_y := 60$ ksi

The required spacing is

$$s := \frac{A_v \cdot f_y \cdot d_v \cdot \cot(\theta)}{V_{s\_req}} \qquad s = 33.847 \text{ in.}$$

Check maximum spacing requirements:

$0.125 f'_{c\_girder} = 0.75$ ksi

Recall that $v = 0.674$ ksi

Because $v < 0.125 f'_{c\_girder}$, the maximum spacing is

$s_{max} := \min(0.8 \cdot d_v, 24) \qquad s_{max} = 24$ in. O.K., use 20 in. spacing.

Check for minimum amount of reinforcement:

$A_{v\_min} := 0.0316\sqrt{f'_{c\_girder}} \cdot \frac{b_v \cdot s}{f_y}$ $A_{v\_min} = 0.262$ in^2/ft

Using $s := 20$ in. $A_{v\_prov} := 0.62$ in^2/ft O.K.

Check the upper limit on the shear capacity:

$V_n := 0.25 f'_{c\_girder} \cdot b_v \cdot d_v$ $V_n = 338.495$ k

the provided capacity is

$V_s := \frac{A_{v\_prov} \cdot f_y \cdot d_v \cdot \cot(\theta)}{s}$ $V_s = 168.248$ k

$V_n := V_c + V_s$ $V_n = 220.977$ k O.K.

$V_{n\_test} := V_{c\_test} + V_s$ $V_{n\_test} = 225.534$ k O.K.

The stirrup spacing will not be changed along the span since the selected spacing of 20 in. is close to the maximum spacing of 24 in. Check if there is a location where stirrups can be eliminated:

$0.5 \cdot \phi \cdot V_c = 23.728$ k

$V_{u\_midspan} := 4.56 + 42.5$ $V_{u\_midspan} = 47.09$ k

The minimum amount of stirrups must be provided along the entire length of the girder.

Use #5 double leg stirrups with 20 in. spacing for 2 in. < L < 39 ft. 10 in.

The design drawings and shop drawings for the deck panels and girders are in Appendix B and Appendix C.

Horizontal Shear Design

Girder 1:

AASHTO LRFD Equation 5.8.4.1-1: $V_n = c*A_{cv} + \mu(A_{vf}*f_y+P_c) \leq MIN(0.2*f'_c*A_{cv},0.8*A_{cv})$

Solving for A_{vf}: **$A_{vf} = (V_{n\_req} - c*A_{cv})/(\mu*f_y)$**

cohesion, c =	**0.075**	ksi	(AASHTO LRFD 5.8.4.2)
yield strength of shear reinforcement, f_y =	**60**	ksi	
ultimate strength of shear reinforcement, f_u =	**100**	ksi	
friction factor, μ =	**0.6**		(AASHTO LRFD 5.8.4.2)
strength reduction factor, ϕ =	**0.9**		(AASHTO LRFD 5.5.4.2.1)
effective deck width, b_{eff} =	**72**	in.	(See girder design calculations)
compressive strength of the concrete, f'_c =	**6**	ksi	
elastic modulus of the concrete, E_c =	**4415**	ksi	
specific weight of the concrete deck, γ =	**0.15**	k/ft^3	
thickness of the deck, t =	**8**	in.	
width of top flange, b_f =	**12**	in.	
A_{cv} = 1 in. *b_f =	12	in^2/in	
depth of compresive stress block for composite section, a =	**0.779**	in	(See girder design calculations)
depth to centroid of prestressing reinforcement, d_p =	**38**	in	(See girder design calculations)
$d_v = d_p - a/2$ =	37.611	in.	
Stud diameter, d =	**0.625**	in.	
stud area, A_{stud} =	0.31	in^2	
Limits on Shear Capacity:			
$V_{n1} = 0.2*f'_c*A_{cv}$ =	14.40	k	
$V_{n2} = 0.8*A_{cv}$ =	9.60	k	

pocket #	x_coord CL	V_{uv} (k)	V_{nh_req} (k/in)	trib width (ft)	trib width (in)	$V_{nh\ req}$ (k)	A_{cv} (in^2)	$A_{s\ req}$ (in^2)	# bars required	# bars provided
1	12	151.30	4.47	2	24	107.27	288	2.38	8	8
2	36	140.33	4.15	2	24	99.50	288	2.16	8	8
3	60	129.36	3.82	2	24	91.72	288	1.95	7	8
4	84	118.39	3.50	2	24	83.94	288	1.73	6	8
5	108	107.42	3.17	2	24	76.16	288	1.52	5	8
6	132	96.45	2.85	2	24	68.38	288	1.30	5	8
7	156	85.48	2.53	2	24	60.61	288	1.08	4	8
8	180	74.51	2.20	2.25	27	59.43	324	0.98	4	8
9	210	60.80	1.80	2.5	30	53.88	360	0.75	3	8
10	240	47.08	1.39	2.5	30	41.73	360	0.41	2	8
11	270	60.80	1.80	3	36	64.66	432	0.90	3	8
12	312	79.99	2.36	3.75	45	106.34	540	1.83	6	10
13	360	101.93	3.01	4	48	144.55	576	2.82	10	10
14	408	123.87	3.66	4	48	175.66	576	3.68	12	16
15	456	145.81	4.31	4	48	206.77	576	4.54	15	16

Girder 2:

AASHTO LRFD Equation 5.8.4.1-1: $V_n = c*A_{cv} + \mu(A_{vf}*f_y+P_c) \leq MIN(0.2*f'_c*A_{cv},0.8*A_{cv})$

Solving for A_{vf}: **$A_{vf} = (V_{n\_req} - c*A_{cv})/(\mu*f_y)$**

cohesion, c =	**0.025**	ksi (AASHTO LRFD 5.8.4.2)
yield strength of shear reinforcement, f_y =	**50**	ksi
ultimate strength of shear reinforcement, f_u =	**65**	ksi
friction factor, μ =	**0.7**	(AASHTO LRFD 5.8.4.2)
strength reduction factor, ϕ =	**0.9**	(AASHTO LRFD 5.5.4.2.1)
effective deck width, b_{eff} =	**72**	in. (See girder design calculations)
compressive strength of the concrete, f'_c =	**6**	ksi
elastic modulus of the concrete, E_c =	**4415**	ksi
specific weight of the concrete deck, γ =	**0.15**	k/ft^3
thickness of the deck, t =	**8**	in.
width of top flange, b_f =	**12**	in.
A_{cv} = 1 in. *b_f =	12	in^2/in
depth of compresive stress block for composite section, a =	**0.779**	in (See girder design calculations)
depth to centroid of prestressing reinforcement, d_p =	**38**	in (See girder design calculations)
$d_v = d_p - a/2$ =	37.611	in.
Stud diameter, d =	**0.75**	in.
stud area, A_{stud} =	0.44	in^2
Limits on Shear Capacity:		
$V_{n1} = 0.2*f'_c*A_{cv}$ =	14.40	k
$V_{n2} = 0.8*A_{cv}$ =	9.60	k

pocket #	x_coord CL	V_{uv} (k)	V_{nh_req} (k/in)	trib width (ft)	trib width (in)	V_{nh_req} (k)	A_{cv} (in^2)	A_{s_req} (in^2)	# studs required	# studs provided
1	12	151.30	4.47	2	24	107.27	288	2.86	7	6
2	36	140.33	4.15	2	24	99.50	288	2.64	6	6
3	60	129.36	3.82	2	24	91.72	288	2.41	6	6
4	84	118.39	3.50	2	24	83.94	288	2.19	5	6
5	108	107.42	3.17	2	24	76.16	288	1.97	5	6
6	132	96.45	2.85	2	24	68.38	288	1.75	4	6
7	156	85.48	2.53	2	24	60.61	288	1.53	4	6
8	180	74.51	2.20	2.25	27	59.43	324	1.47	4	6
9	210	60.80	1.80	2.5	30	53.88	360	1.28	3	6
10	240	47.08	1.39	2.5	30	41.73	360	0.94	3	6
11	270	60.80	1.80	3	36	64.66	432	1.54	4	6
12	312	79.99	2.36	3.75	45	106.34	540	2.65	7	8
13	360	101.93	3.01	4	48	144.55	576	3.72	9	8
14	408	123.87	3.66	4	48	175.66	576	4.61	11	12
15	456	145.81	4.31	4	48	206.77	576	5.50	13	12

APPENDIX B – VIRGINIA TECH DESIGN DRAWINGS

LIST OF DRAWINGS:
SHEET NO. 1 - GENERAL NOTES AND QUANTITIES
SHEET NO. 2 - BILL OF BARS
SHEET NO. 3 - DECK PANELS - PANEL TYPE 1
SHEET NO. 4 - DECK PANELS - PANEL TYPE 2
SHEET NO. 5 - DECK PANELS - PANEL TYPE 3
SHEET NO. 6 - DECK PANELS - PANEL TYPE 4
SHEET NO. 7 - DECK PANELS - PANEL TYPE 5
SHEET NO. 8 - DECK PANELS - ANCHOR ZONE
SHEET NO. 9 - DECK PANELS - LEVELING BOLT
SHEET NO. 10 - DECK PANELS - TRANS. JOINTS
SHEET NO. 11 - GIRDERS - GIRDER TYPE 1
SHEET NO. 12 - GIRDERS - GIRDER TYPE 2

QUANTITIES:

CONCRETE:

	VOLUME (C.Y.)
PANELS	11.10
GIRDERS	7.59
TOTAL	18.69

MILD REINFORCING STEEL:

	WEIGHT (LB.)
PANELS	1186
GIRDERS	1530
TOTAL	2716

PRESTRESSING STEEL:

	WEIGHT (LB.)
PANELS	499
GIRDERS	499
TOTAL	998

MATERIAL PROPERTIES:
ALL MATERIALS SHALL CONFORM TO "AASHTO LRFD BRIDGE CONSTRUCTION SPECIFICATIONS" AND SECTION 5.4 OF "AASHTO LRFD BRIDGE DESIGN SPECIFICATIONS."

CONCRETE:
CLASS P CONCRETE SHALL BE USED.
MIN. 28 DAY COMPRESSIVE STRENGTH OF 6 KSI.
MIN. COMPRESSIVE STRENGTH OF 4 KSI WHEN PRESTRESSING STRANDS ARE CUT.

MILD REINFORCING STEEL:
YIELD STRENGTH OF 60 KSI. ULTIMATE STRENGTH OF 90 KSI. REINFORCING STEEL SHALL CONFORM TO THE REQUIREMENTS OF ASTM A 706.

PRESTRESSING STEEL:
½" DIA. UNCOATED, LOW RELAXATION, SEVEN WIRE, GRADE 270 STRANDS ARE TO BE USED.

CONSTRUCTION TOLERANCES:
ALL CONCRETE DIMENSIONS SHALL BE FABRICATED TO ⅛".

ABBREVIATIONS:
C.L. = CENTERLINE
ELEV. = ELEVATION
NO. = NUMBER
LONG. = LONGITUDINAL
TRANS. = TRANSVERSE
WT. = WEIGHT

VIRGINIA POLYTECHNIC INSTITUTE AND STATE UNIVERSITY
GENERAL NOTES AND QUANTITIES
CREATED BY: SEAN SULLIVAN
CHECKED BY:
DATE: 4/21/05

MARK	NO.	WT.	TYPE	LENGTH	A	B	C	D	E	F	LOCATION
P50L	24	499	1	40'-0"	40'-0"						GIRDER - LONG.
P502	80	499	1	12'-0"	12'-0"						PANELS - TRANS.
M603	20	124	2	4'-1½"	1'-0"	3"	8"				PANELS
M504	72	257	6	3'-5"	1'-2"	4"	5½"	5½"	3"		GIRDERS - STIRRUPS
M505	50	104	6	2'-0"	8"	2½"	2½"	2½"	3"		GIRDERS - STIRRUPS
M506	50	287	5	5'-6"	2'-6"	1¼"					GIRDERS - STIRRUPS
M507	70	219	5	3'-0"	1'-2"	1¼"					GIRDER 1 - STIRRUPS
M508	16	663	1	39'-9"	39'-9"						GIRDERS - LONG.
M409	7	16	4	3'-6"	3"	1'-3"					PANELS
M410	180	902	1	7'-6"	7'-6"						PANELS - LONG.
M411	4	6	1	2'-3"	2'-3"						PANELS
M312	80	120	3	4'-0"	3"	1'-0"	1¾"				PANELS
M313	4	18	1	12'-0"	12'-0"						PANEL 5 - TRANS.

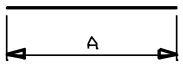

TYPE 1

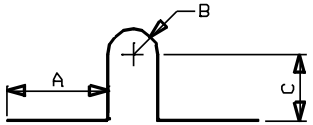

TYPE 2

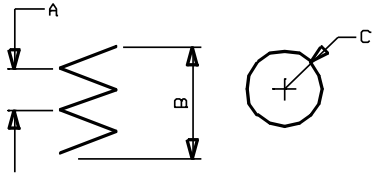

PLAN SECTION

TYPE 3

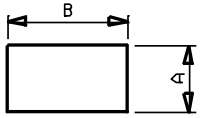

TYPE 4

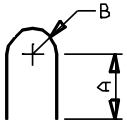

TYPE 5

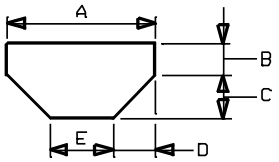

TYPE 6

NOTES:
M = MILD REINF. STEEL
P = PRESTRESSING STEEL

VIRGINIA POLYTECHNIC INSTITUTE AND STATE UNIVERSITY

BILL OF BARS

CREATED BY: SEAN SULLIVAN
CHECKED BY:
DATE: 4/21/05

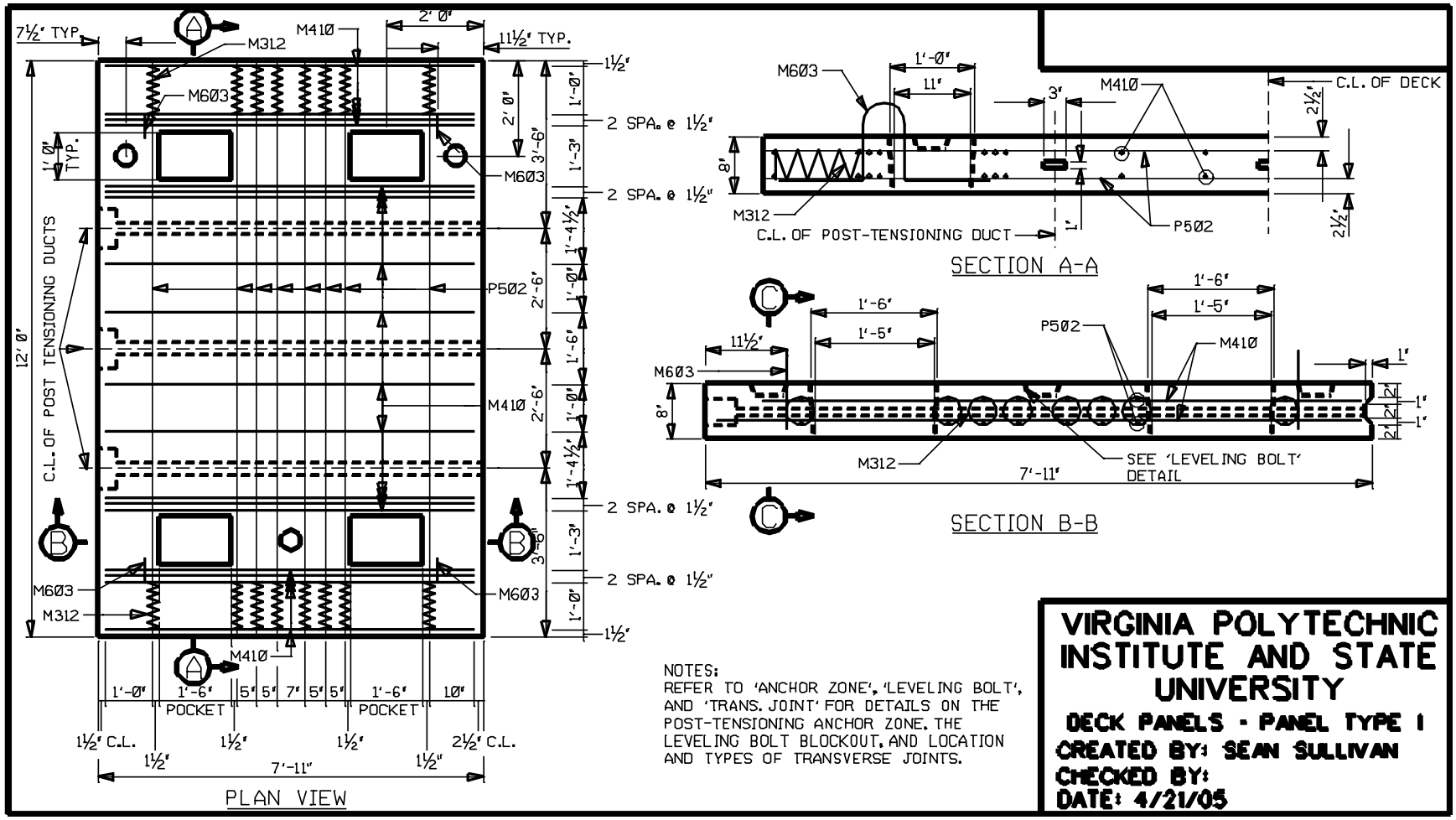
7½" TYP.
M312
M410
2' Ø"
11½" TYP.
M6Ø3
1' Ø" TYP.
C.L. OF POST TENSIONING DUCTS
12' Ø"
P5Ø2
M410
M6Ø3
M312
M6Ø3
M410
1½"
1'-Ø"
3'-6"
1'-3"
2 SPA. @ 1½"
1'-4½"
2'-6"
1'-6"
2 SPA. @ 1½"
1'-3"
1'-Ø"
1½"
1'-Ø"
1'-6"
5" 5" 7" 5" 5"
1'-6"
1Ø"
POCKET
POCKET
1½" C.L.
1½"
1½"
1½"
2½" C.L.
7'-11"
PLAN VIEW
M6Ø3
1'-Ø"
11"
3"
M41Ø
C.L. OF DECK
2½"
8"
M312
C.L. OF POST-TENSIONING DUCT
1"
P5Ø2
2½"
SECTION A-A
1'-6"
1'-5"
1'-6"
1'-5"
P5Ø2
M41Ø
11½"
M6Ø3
1"
8"
2½"
2½"
1"
1"
M312
SEE 'LEVELING BOLT' DETAIL
7'-11"
SECTION B-B
NOTES:
REFER TO 'ANCHOR ZONE', 'LEVELING BOLT', AND 'TRANS. JOINT' FOR DETAILS ON THE POST-TENSIONING ANCHOR ZONE. THE LEVELING BOLT BLOCKOUT, AND LOCATION AND TYPES OF TRANSVERSE JOINTS.
VIRGINIA POLYTECHNIC INSTITUTE AND STATE UNIVERSITY
DECK PANELS - PANEL TYPE 1
CREATED BY: SEAN SULLIVAN
CHECKED BY:
DATE: 4/21/05

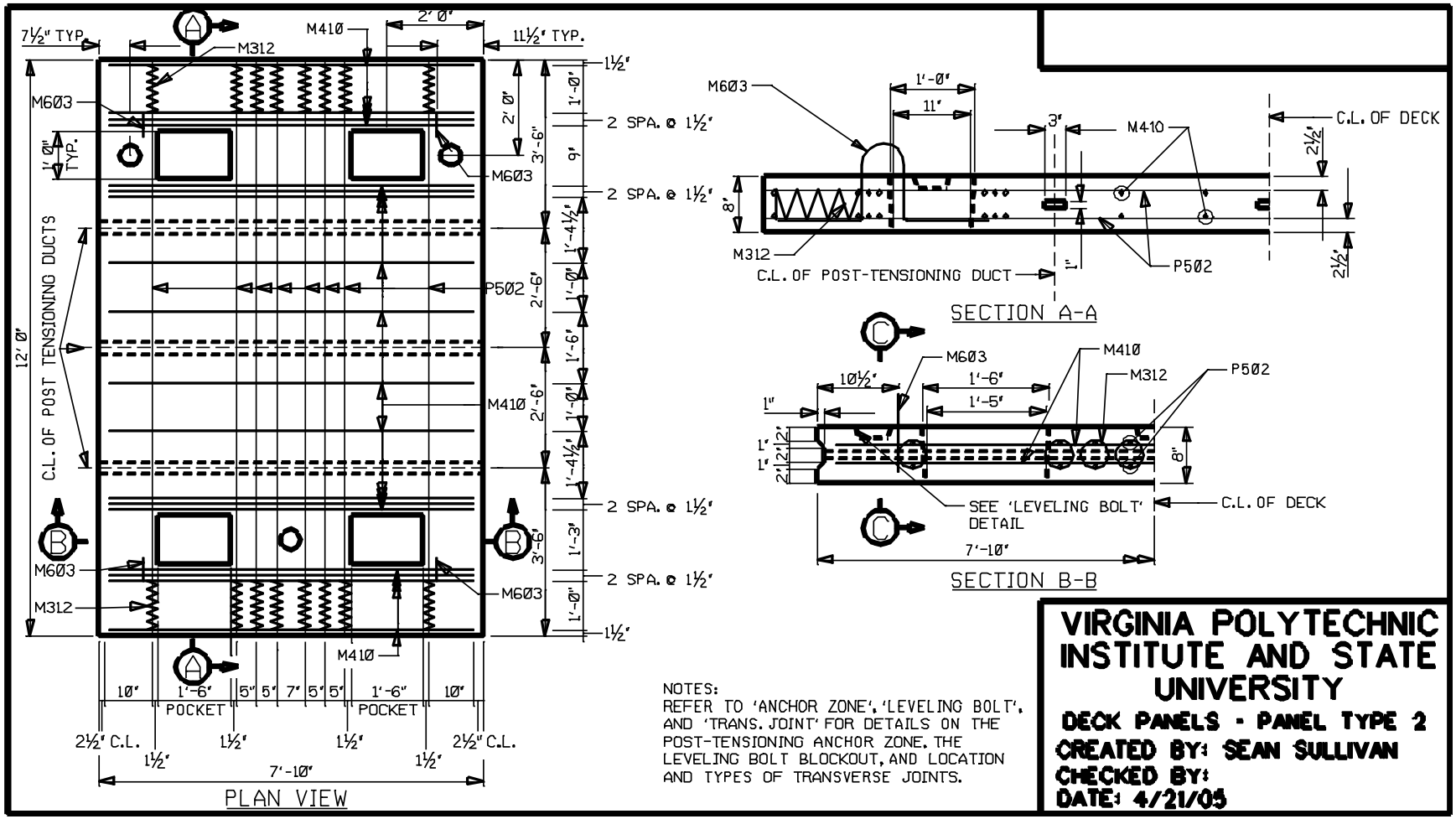

NOTES:
REFER TO 'ANCHOR ZONE', 'LEVELING BOLT', AND 'TRANS. JOINT' FOR DETAILS ON THE POST-TENSIONING ANCHOR ZONE. THE LEVELING BOLT BLOCKOUT, AND LOCATION AND TYPES OF TRANSVERSE JOINTS.

VIRGINIA POLYTECHNIC INSTITUTE AND STATE UNIVERSITY

DECK PANELS - PANEL TYPE 2

CREATED BY: SEAN SULLIVAN

CHECKED BY:

DATE: 4/21/05

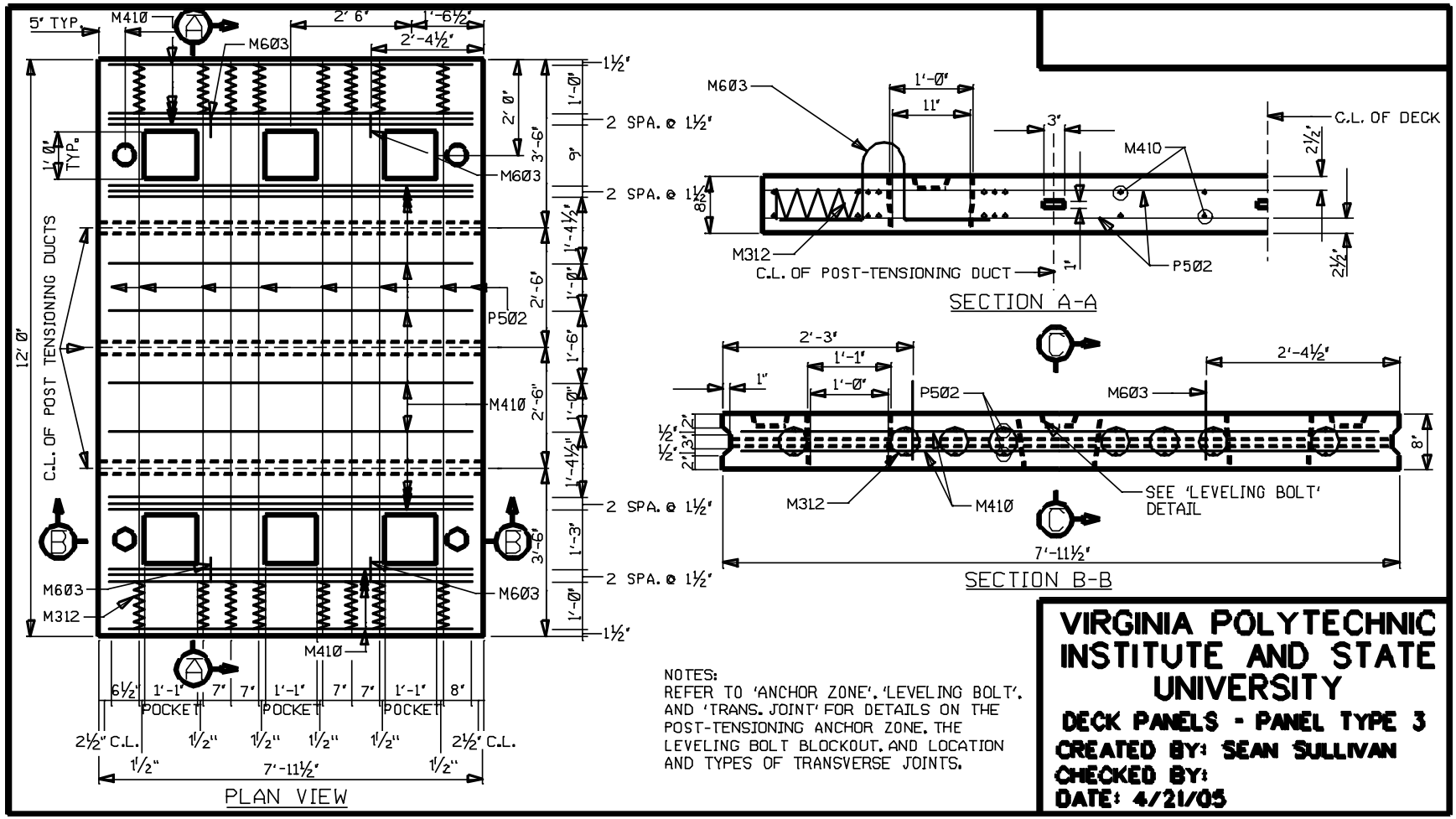

NOTES:
REFER TO 'ANCHOR ZONE', 'LEVELING BOLT', AND 'TRANS. JOINT' FOR DETAILS ON THE POST-TENSIONING ANCHOR ZONE. THE LEVELING BOLT BLOCKOUT. AND LOCATION AND TYPES OF TRANSVERSE JOINTS.

VIRGINIA POLYTECHNIC INSTITUTE AND STATE UNIVERSITY

DECK PANELS - PANEL TYPE 3

CREATED BY: SEAN SULLIVAN

CHECKED BY:

DATE: 4/21/05

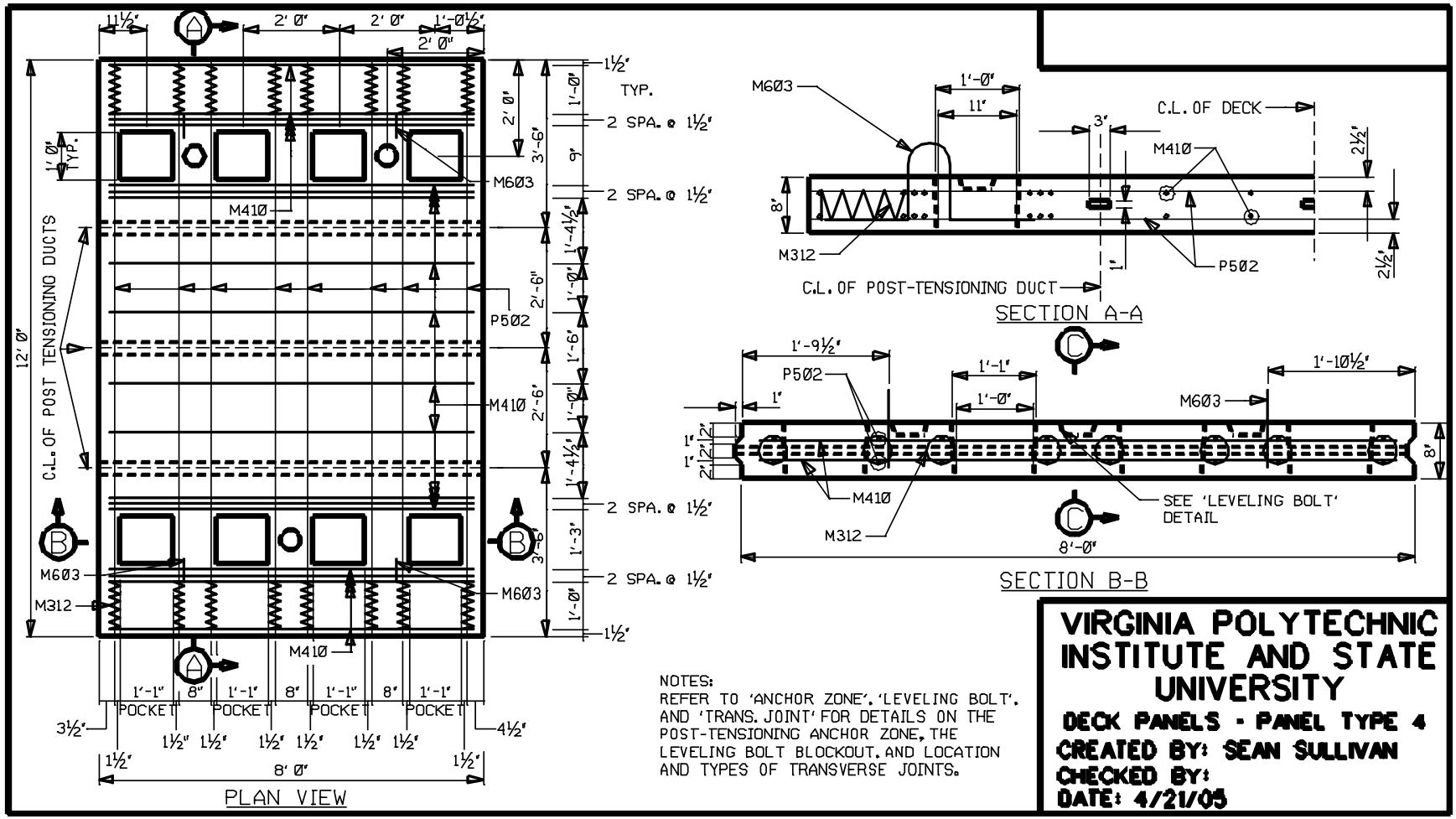
PLAN VIEW
SECTION A-A
SECTION B-B
C.L. OF POST TENSIONING DUCTS
C.L. OF DECK
C.L. OF POST-TENSIONING DUCT
SEE 'LEVELING BOLT' DETAIL
M6Ø3
M41Ø
M312
P5Ø2
NOTES:
REFER TO 'ANCHOR ZONE', 'LEVELING BOLT', AND 'TRANS. JOINT' FOR DETAILS ON THE POST-TENSIONING ANCHOR ZONE, THE LEVELING BOLT BLOCKOUT, AND LOCATION AND TYPES OF TRANSVERSE JOINTS.
VIRGINIA POLYTECHNIC INSTITUTE AND STATE UNIVERSITY
DECK PANELS - PANEL TYPE 4
CREATED BY: SEAN SULLIVAN
CHECKED BY:
DATE: 4/21/05

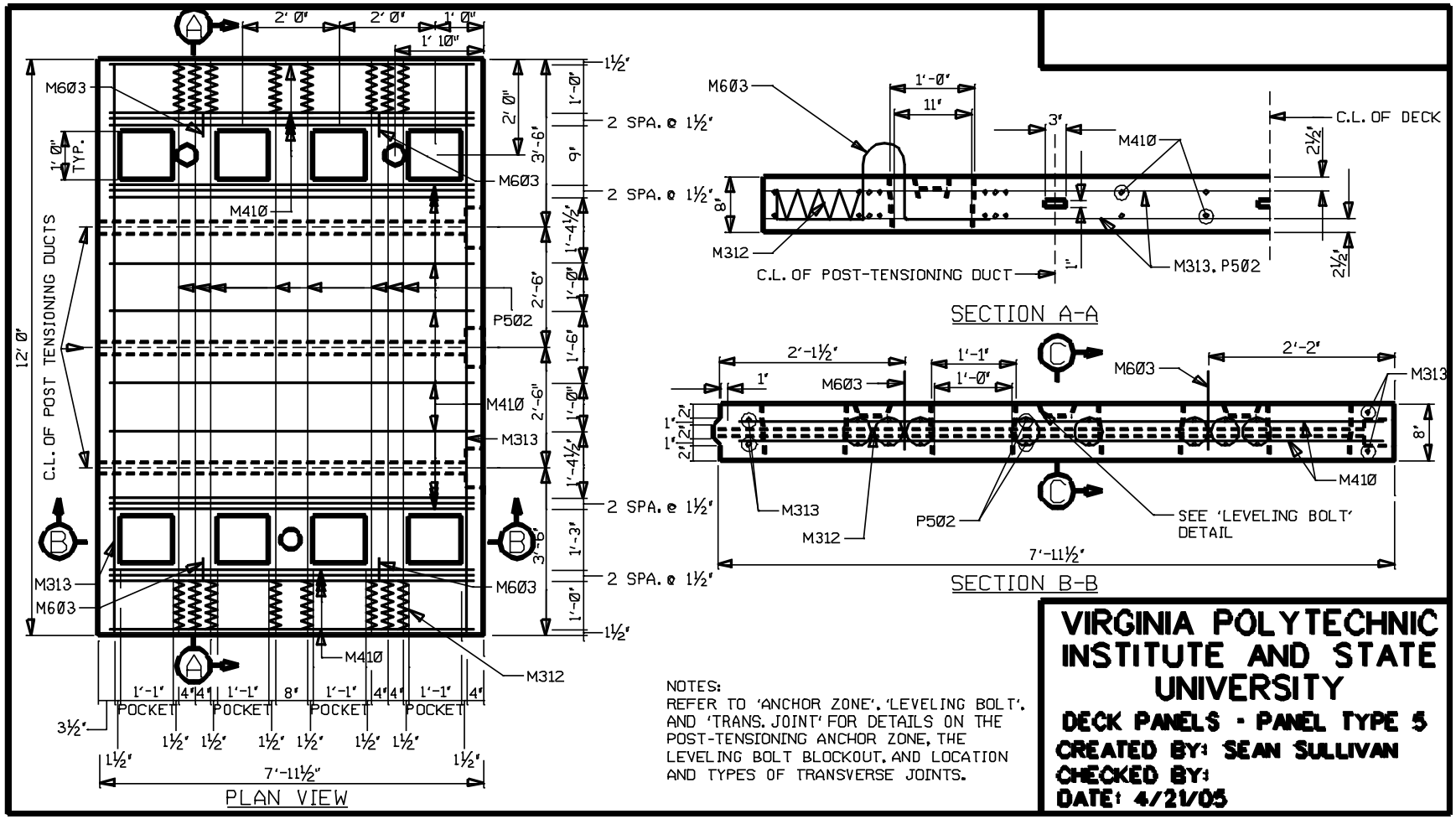
PLAN VIEW
SECTION A-A
SECTION B-B
C.L. OF POST TENSIONING DUCTS
C.L. OF POST-TENSIONING DUCT
C.L. OF DECK
M603
M410
M313
M312
P502
SEE 'LEVELING BOLT' DETAIL
POCKET
NOTES:
REFER TO 'ANCHOR ZONE', 'LEVELING BOLT', AND 'TRANS. JOINT' FOR DETAILS ON THE POST-TENSIONING ANCHOR ZONE, THE LEVELING BOLT BLOCKOUT, AND LOCATION AND TYPES OF TRANSVERSE JOINTS.
VIRGINIA POLYTECHNIC INSTITUTE AND STATE UNIVERSITY
DECK PANELS - PANEL TYPE 5
CREATED BY: SEAN SULLIVAN
CHECKED BY:
DATE: 4/21/05

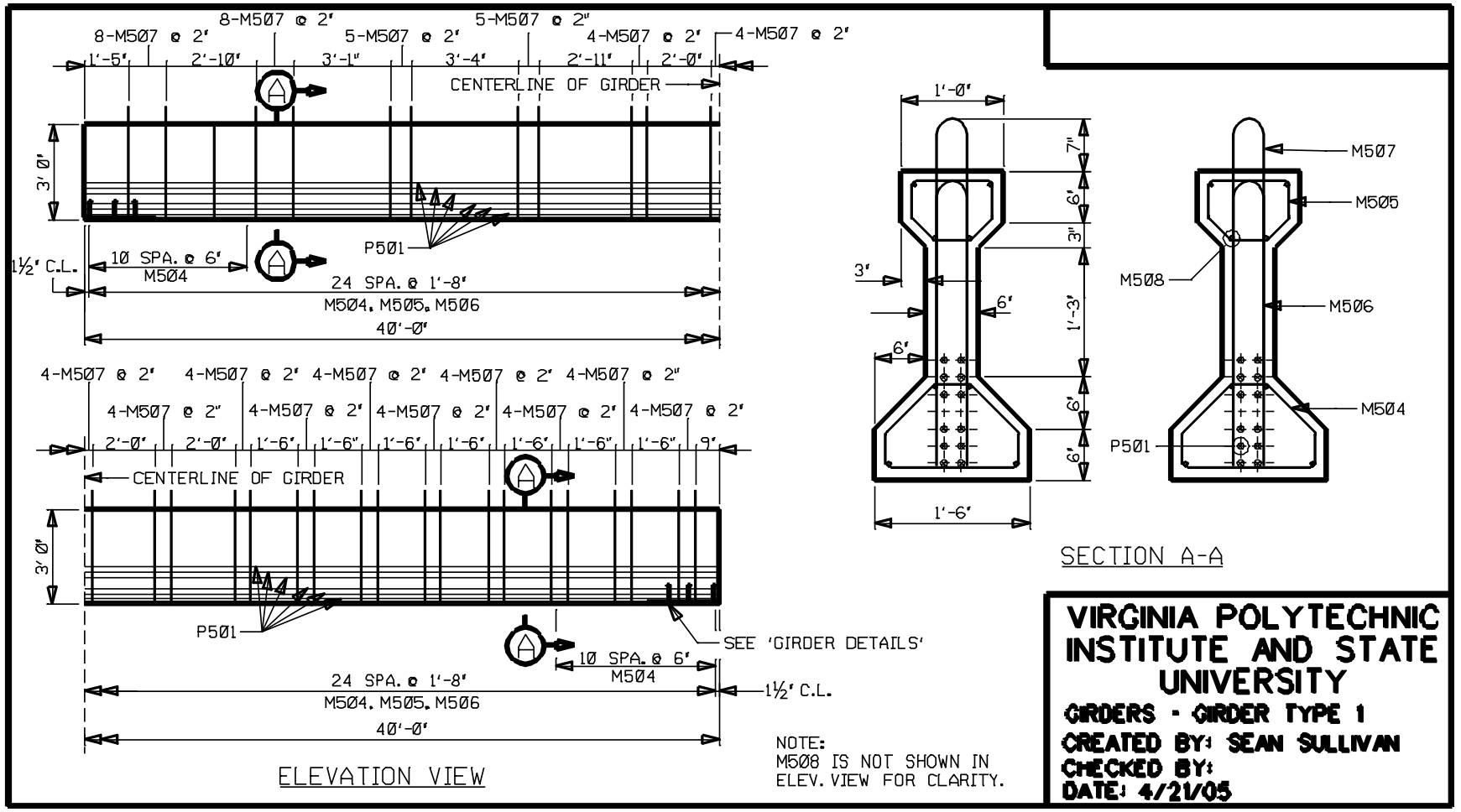
8-M507 @ 2"
8-M507 @ 2"
5-M507 @ 2"
5-M507 @ 2"
4-M507 @ 2"
4-M507 @ 2"
1'-5"
2'-10"
3'-1"
3'-4"
2'-11"
2'-0"
CENTERLINE OF GIRDER
3' 0"
P501
1½" C.L.
10 SPA. @ 6"
M504
24 SPA. @ 1'-8"
M504, M505, M506
40'-0"
4-M507 @ 2"
4-M507 @ 2"
4-M507 @ 2"
4-M507 @ 2"
4-M507 @ 2"
4-M507 @ 2"
4-M507 @ 2"
4-M507 @ 2"
4-M507 @ 2"
2'-0"
2'-0"
1'-6"
1'-6"
1'-6"
1'-6"
1'-6"
1'-6"
1'-6"
9"
CENTERLINE OF GIRDER
3' 0"
P501
SEE 'GIRDER DETAILS'
10 SPA. @ 6"
M504
24 SPA. @ 1'-8"
M504, M505, M506
1½" C.L.
40'-0"
ELEVATION VIEW
1'-0"
7"
6"
3"
1'-3"
6"
6"
3"
6"
6"
6"
1'-6"
M507
M505
M508
M506
M504
P501
SECTION A-A
NOTE:
M508 IS NOT SHOWN IN
ELEV. VIEW FOR CLARITY.
VIRGINIA POLYTECHNIC INSTITUTE AND STATE UNIVERSITY
GIRDERS - GIRDER TYPE 1
CREATED BY: SEAN SULLIVAN
CHECKED BY:
DATE: 4/21/05

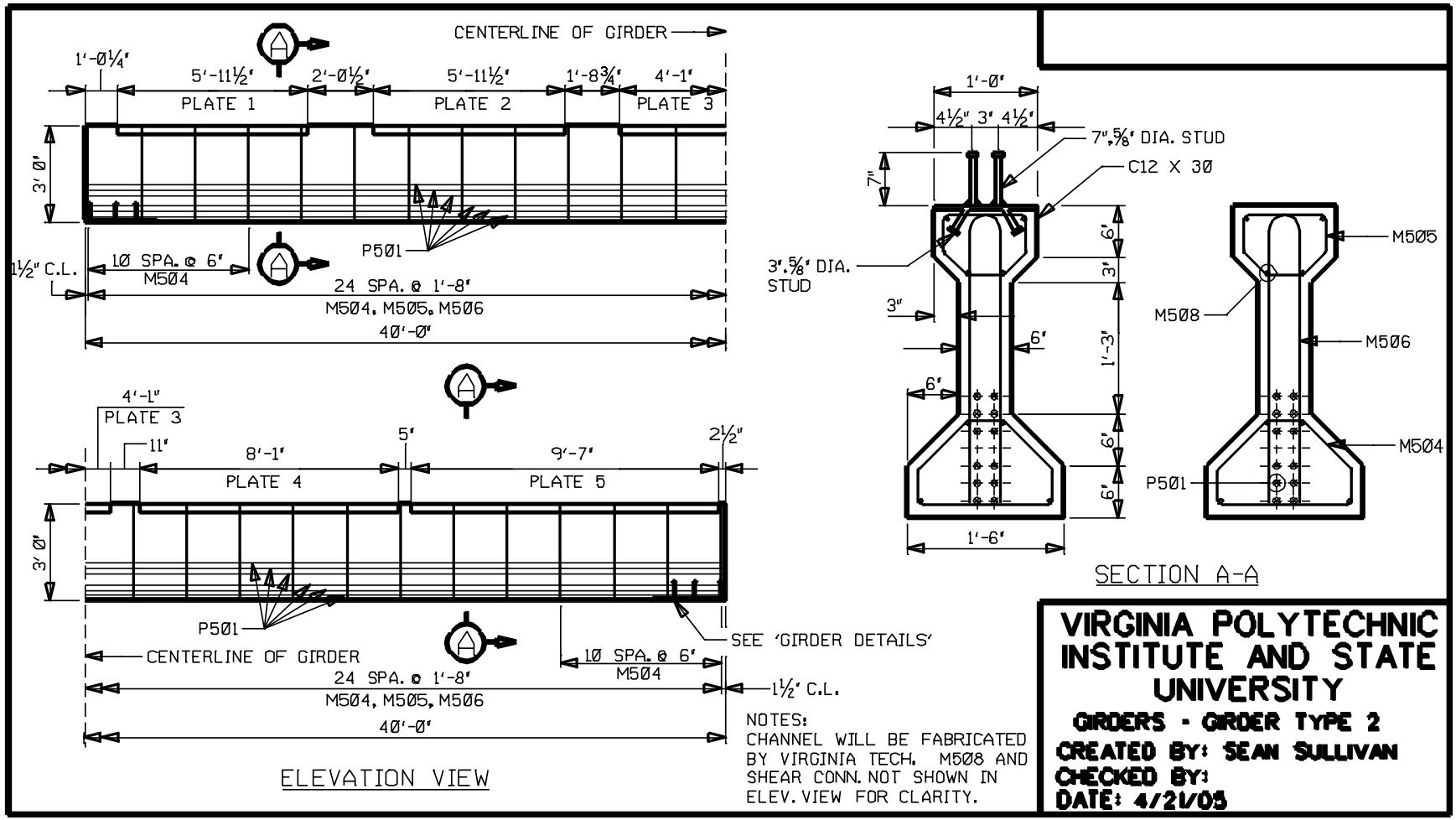
CENTERLINE OF GIRDER
1'-0¼"
5'-11½"
2'-0½"
5'-11½"
1'-8¾"
4'-1"
PLATE 1
PLATE 2
PLATE 3
3' 0"
1½" C.L.
10 SPA. @ 6"
M504
P501
24 SPA. @ 1'-8"
M504, M505, M506
40'-0"
4'-1"
PLATE 3
11"
8'-1"
5"
9'-7"
2½"
PLATE 4
PLATE 5
3' 0"
P501
CENTERLINE OF GIRDER
SEE 'GIRDER DETAILS'
10 SPA. @ 6"
M504
24 SPA. @ 1'-8"
M504, M505, M506
1½" C.L.
40'-0"
ELEVATION VIEW
1'-0"
4½" 3" 4½"
7", ⅝" DIA. STUD
C12 X 30
7"
3", ⅝" DIA. STUD
6"
3"
1'-3"
6"
6"
6"
6"
1'-6"
M505
M508
M506
M504
P501
SECTION A-A
NOTES:
CHANNEL WILL BE FABRICATED BY VIRGINIA TECH. M508 AND SHEAR CONN. NOT SHOWN IN ELEV. VIEW FOR CLARITY.
VIRGINIA POLYTECHNIC INSTITUTE AND STATE UNIVERSITY
GIRDERS - GIRDER TYPE 2
CREATED BY: SEAN SULLIVAN
CHECKED BY:
DATE: 4/21/05

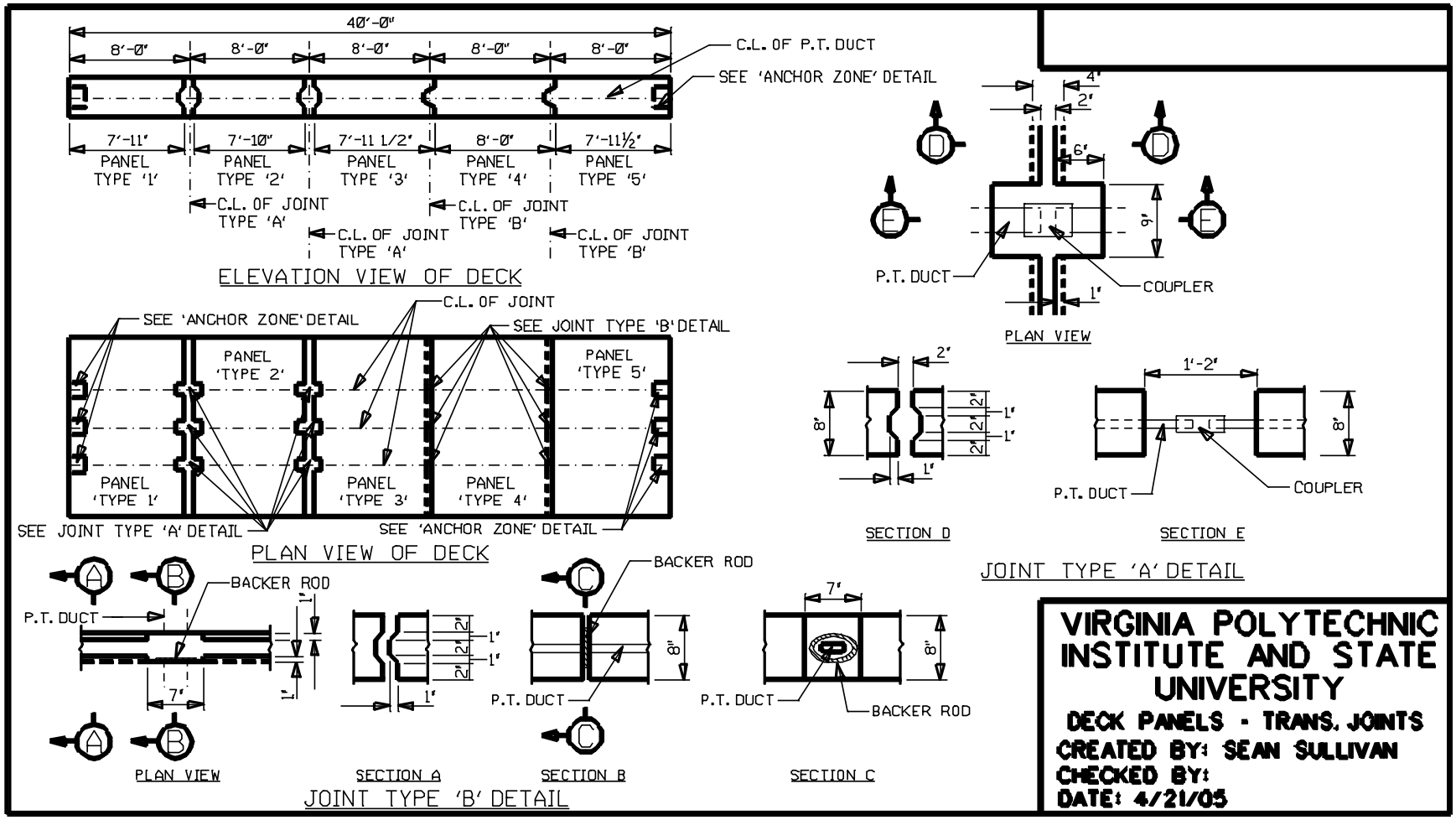
40'-0"
8'-0"
8'-0"
8'-0"
8'-0"
8'-0"
C.L. OF P.T. DUCT
SEE 'ANCHOR ZONE' DETAIL
7'-11"
7'-10"
7'-11 1/2"
8'-0"
7'-11½"
PANEL TYPE '1'
PANEL TYPE '2'
PANEL TYPE '3'
PANEL TYPE '4'
PANEL TYPE '5'
C.L. OF JOINT TYPE 'A'
C.L. OF JOINT TYPE 'B'
C.L. OF JOINT TYPE 'A'
C.L. OF JOINT TYPE 'B'
ELEVATION VIEW OF DECK
SEE 'ANCHOR ZONE' DETAIL
C.L. OF JOINT
SEE JOINT TYPE 'B' DETAIL
PANEL 'TYPE 1'
PANEL 'TYPE 2'
PANEL 'TYPE 3'
PANEL 'TYPE 4'
PANEL 'TYPE 5'
SEE JOINT TYPE 'A' DETAIL
SEE 'ANCHOR ZONE' DETAIL
PLAN VIEW OF DECK
4'
2'
6'
9'
P.T. DUCT
COUPLER
1'
PLAN VIEW
2'
8'
2"
2"
2"
1'
1'
1'
SECTION D
1'-2"
8"
P.T. DUCT
COUPLER
SECTION E
JOINT TYPE 'A' DETAIL
BACKER ROD
P.T. DUCT
1'
7'
1'
2"
2"
2"
1'
1'
PLAN VIEW
SECTION A
BACKER ROD
8"
P.T. DUCT
SECTION B
7'
8"
P.T. DUCT
BACKER ROD
SECTION C
JOINT TYPE 'B' DETAIL
VIRGINIA POLYTECHNIC INSTITUTE AND STATE UNIVERSITY
DECK PANELS - TRANS. JOINTS
CREATED BY: SEAN SULLIVAN
CHECKED BY:
DATE: 4/21/05

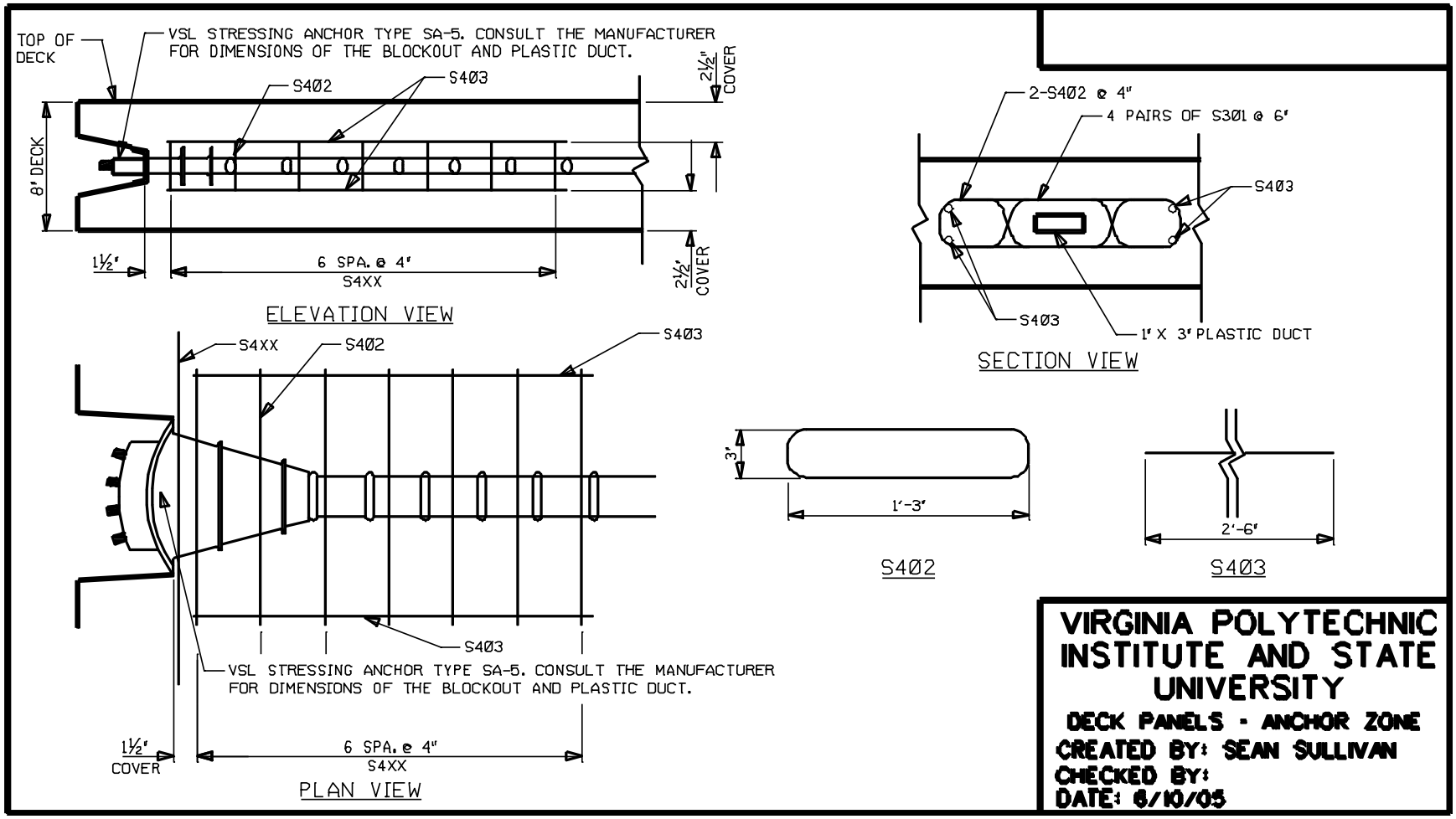
TOP OF DECK
VSL STRESSING ANCHOR TYPE SA-5. CONSULT THE MANUFACTURER FOR DIMENSIONS OF THE BLOCKOUT AND PLASTIC DUCT.
S402
S403
2½" COVER
8" DECK
1½"
6 SPA. @ 4"
S4XX
2½" COVER
ELEVATION VIEW
S4XX
S402
S403
S403
VSL STRESSING ANCHOR TYPE SA-5. CONSULT THE MANUFACTURER FOR DIMENSIONS OF THE BLOCKOUT AND PLASTIC DUCT.
1½" COVER
6 SPA. @ 4"
S4XX
PLAN VIEW
2-S402 @ 4"
4 PAIRS OF S301 @ 6"
S403
S403
1" X 3" PLASTIC DUCT
SECTION VIEW
3"
1'-3"
S402
2'-6"
S403
VIRGINIA POLYTECHNIC INSTITUTE AND STATE UNIVERSITY
DECK PANELS - ANCHOR ZONE
CREATED BY: SEAN SULLIVAN
CHECKED BY:
DATE: 6/10/05

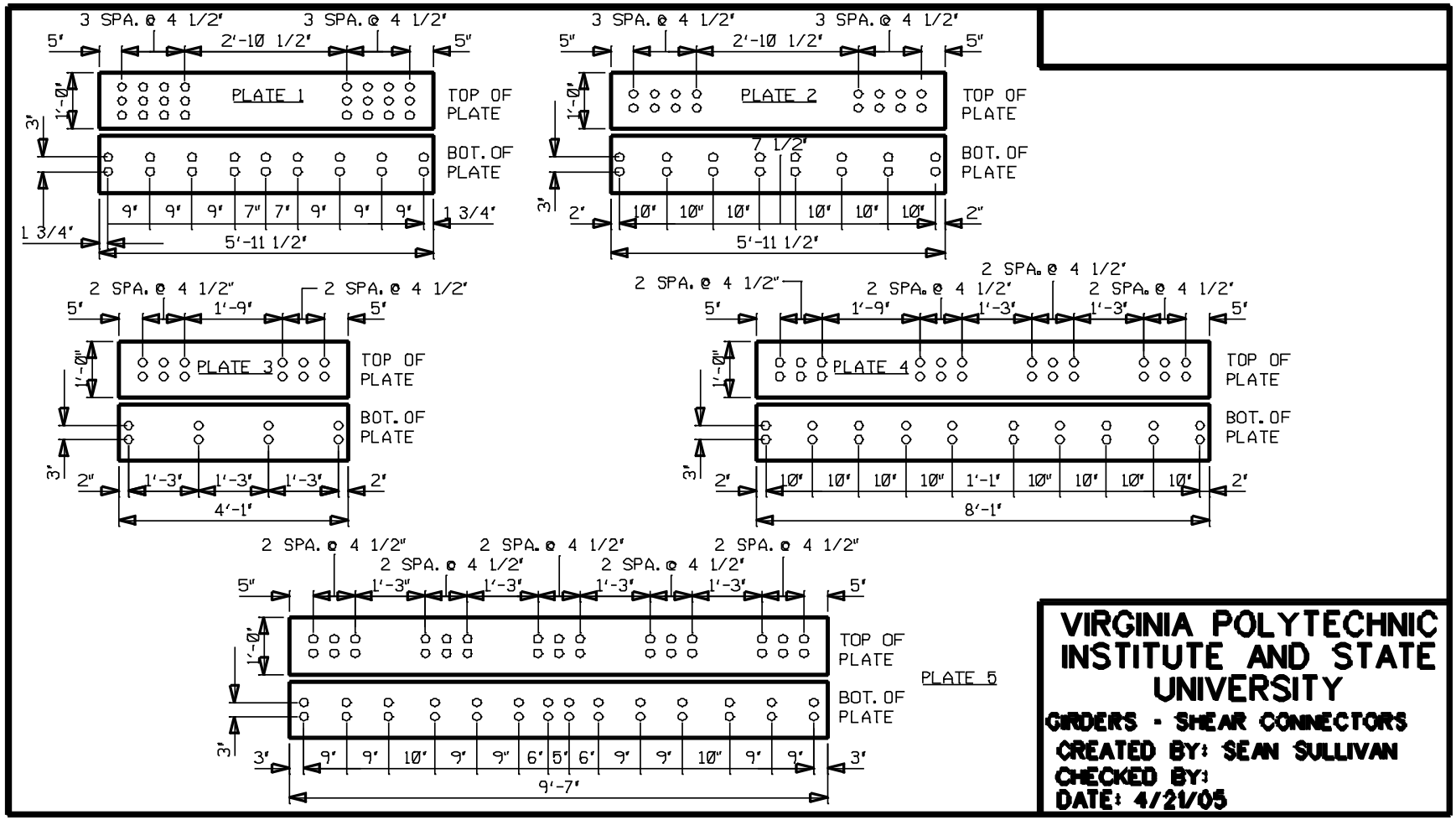
3 SPA. @ 4 1/2"
3 SPA. @ 4 1/2"
5"
2'-10 1/2"
5"
PLATE 1
TOP OF PLATE
BOT. OF PLATE
1'-0"
3"
9" 9" 9" 7" 7" 9" 9" 9"
1 3/4"
1 3/4"
5'-11 1/2"
PLATE 2
7 1/2"
10" 10" 10" 10" 10" 10"
2"
2 SPA. @ 4 1/2"
1'-9"
PLATE 3
4'-1"
1'-3"
PLATE 4
10" 10" 10" 10" 1'-1" 10" 10" 10" 10"
8'-1"
PLATE 5
9" 9" 10" 9" 9" 6" 5" 6" 9" 9" 10" 9" 9"
9'-7"
VIRGINIA POLYTECHNIC INSTITUTE AND STATE UNIVERSITY
GIRDERS - SHEAR CONNECTORS
CREATED BY: SEAN SULLIVAN
CHECKED BY:
DATE: 4/21/05

APPENDIX C – BAYSHORE SHOP DRAWINGS

SLAB TYPE 1	SLAB TYPE 2	SLAB TYPE 3	SLAB TYPE 4	SLAB TYPE 5
BEAM TYPE J				
BEAM TYPE J				

ERECTION PLAN

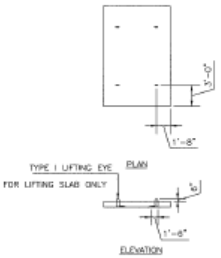

LIFTING EYE DETAIL FOR SLABS

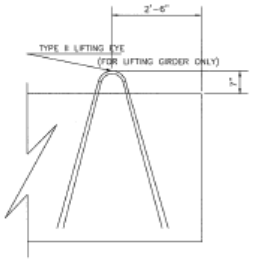

LIFTING EYE DETAIL FOR GIRDERS

NOTES FOR TYPE II GIRDERS:
1.) CONCRETE COMPRESSIVE STRENGTH SHALL BE 6,000 P.S.I. @ 28 DAYS & A MIN. OF 4,000 P.S.I. @ TIME OF RELEASE OF STRANDS.
2.) REINFORCING STEEL SHALL CONFORM TO A.S.T.M. A615 GRADE 60 (BLACK).
3.) PRESTRESSING STRANDS SHALL BE A.S.T.M. GRADE 270 7 WIRE STRAND.
4.) BEAM 3 TO RECEIVE A BROOM FLOAT FINISH, EXCEPT IN THE AREA OF THE #607 BARS (RAKE IN AREA OF #507).
5.) BEAM 3 TO HAVE THE PLATES CAST INTO THE TOP (WOOD FLOAT BETWEEN PLATES).
6.) STRAND SHALL PROJECT 6".
7.) MIX DESIGN NO. 58C-2-05 IS TO BE USED.

NOTES FOR SLABS:
1.) CONCRETE COMPRESSIVE STRENGTH SHALL BE 6,000 P.S.I. @ 28 DAYS, A MIN. OF 4,000 P.S.I. @ TIME OF RELEASE OF STRANDS.
2.) REINFORCING STEEL SHALL CONFORM TO A.S.T.M. A615 GRADE 60 (BLACK).
3.) PRESTRESSING STRANDS SHALL BE A.S.T.M. GRADE 1/2" ø.
4.) SLABS SHALL RECEIVE A BROOM FLOAT FINISH.
5.) STRAND SHALL PROJECT 6".
6.) MIX DESIGN NO. 58C-2-05 IS TO BE USED.

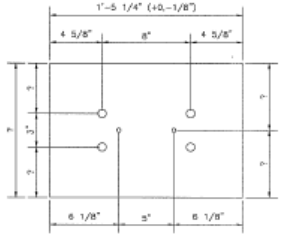

BEARING PLATE PLAN

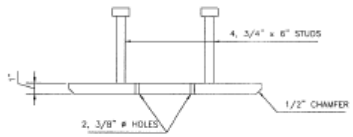

BEARING PLATE ELEVATION

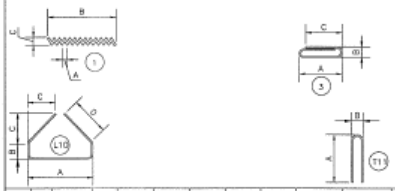

MARK	TYPE	# REQ'D	SPACING	# LENGTH	A	B	C	D	WT (LBS)	COATING
#508	STR.	16	---	39'-8"					41	
#507	T11	70	2'0"	6'-8"	3'-3"	3 3/4"			7	
#505	L10	50	2"	2'-0"	8"	3 1/8"	3 1/2	4 7/8"	2	
#504	L10	94	2"	3'-4 1/2"	1'-5 1/2"	3"	8 3/4"	9 1/2"	4	
#508	T11	50	7'0"	5'-2"	2'-6"	3 3/4"			5	

REINFORCING SCHEDULE PER POUR (GRADE 60) BLACK

TOTAL REINFORCING SCHEDULE (GRADE 60) BLACK

MARK	TYPE	# REQ'D	SPACING	# LENGTH	A	B	C	D	WT (LBS)	COATING
#411	STR.	24	---	2'-3"					2	
#410	STR.	180	---	7'-6"					5	
#409	3	42	2"	3'-6"	1'-3"	3"	10"		2	
#313	STR.	4	---	11'-10"					4	
#312	1	80	3"	3'-11"	3"	1'-0"	3 3/4"		1	

REQ.	B.C.P. SUPPLIED BILL OF MATERIALS	REQ.	SUPPLIED BY OTHERS BILL OF MATERIALS
4	BEARING PLATES	1	PLATE 1
		1	PLATE 2
		1	PLATE 3
		1	PLATE 4
		1	PLATE 5
16	LEVELING BOLTS		
	PT HARDWARE		

REV	DATE	BY	REMARKS
Δ	11-14	AJB	#312 & #504

VIRGINIA POLYTECHNIC INSTITUTE AND STATE UNIVERSITY
TESTING PROGRAM

BAYSHORE CONCRETE PRODUCTS CORPORATION
P.O. BOX 298
CAPE CHARLES, VA. 23310

ERECTION PLAN & MISCELLANEOUS DETAIL

DESIGN			SCALE	DRWG. NO.	REV.
DRAWN	A.J.B	11-10-05	NONE	5756 & 5757 -01	A
CHECKED					

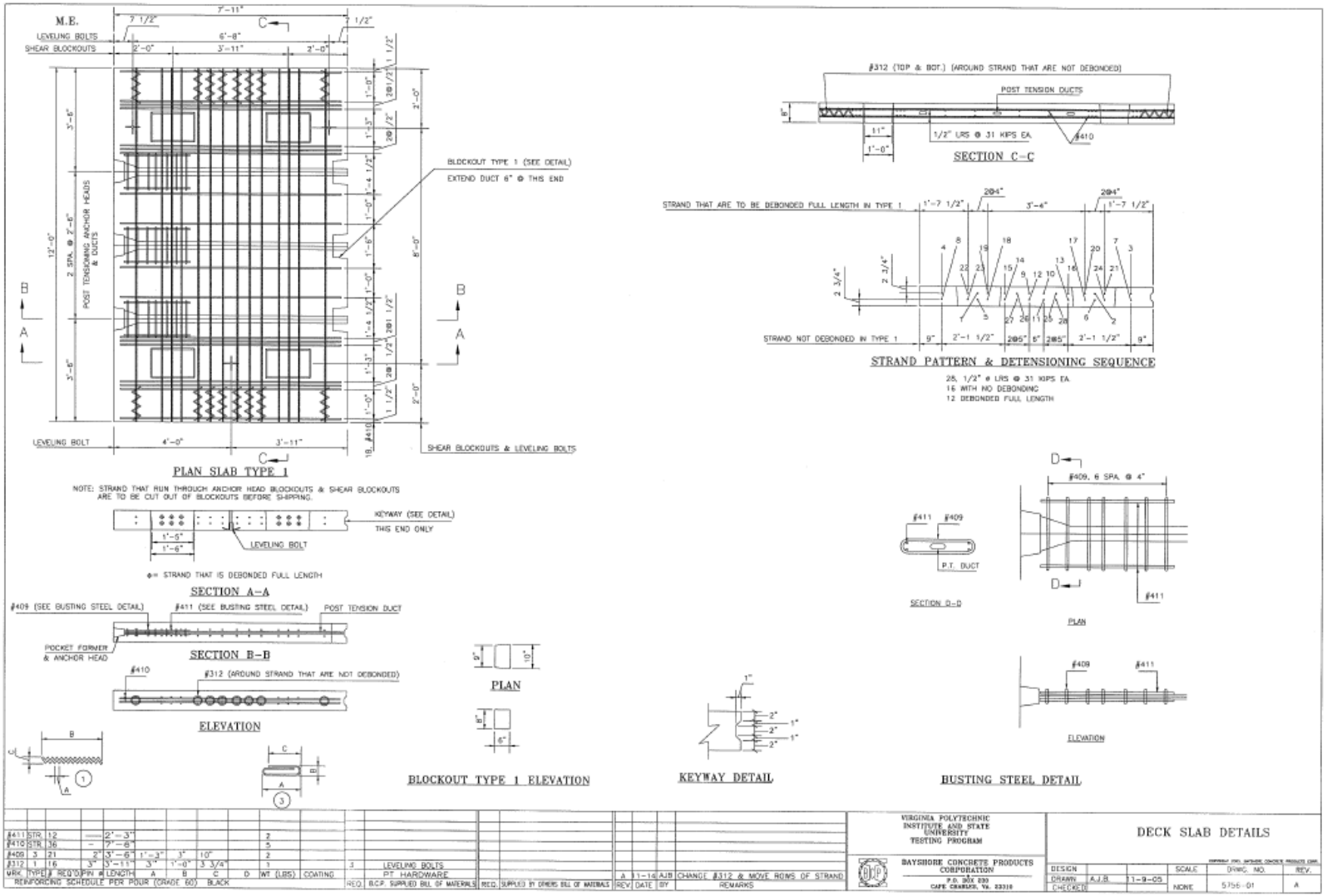

MK	TYPE	# REQ'D	PIN #	LENGTH	A	B	C	D	WT (LBS)	COATING
#411	STR	12		2'-3"					2	
#410	STR	36		7'-8"					5	
#409	3	21		2" 3'-6"	1'-3"	3"	10"		2	
#312	1	16		3" 3'-11"	3"	1'-0"	3 3/4"		3	

REINFORCING SCHEDULE PER POUR (GRADE 60) BLACK

REQ.	LEVELING BOLTS P.T. HARDWARE

REQ.	SUPPLIED BY OTHERS BILL OF MATERIALS

REV	DATE	BY	REMARKS
A	11-16	AJB	CHANGE #312 & MOVE ROWS OF STRAND

VIRGINIA POLYTECHNIC INSTITUTE AND STATE UNIVERSITY
TESTING PROGRAM

BAYSHORE CONCRETE PRODUCTS CORPORATION
P.O. BOX 330
CAPE CHARLES, Va. 23310

DECK SLAB DETAILS

DESIGN		SCALE	DRWG. NO.
DRAWN	A.J.B	11-9-05	NONE
CHECKED			5756-01

REV. A

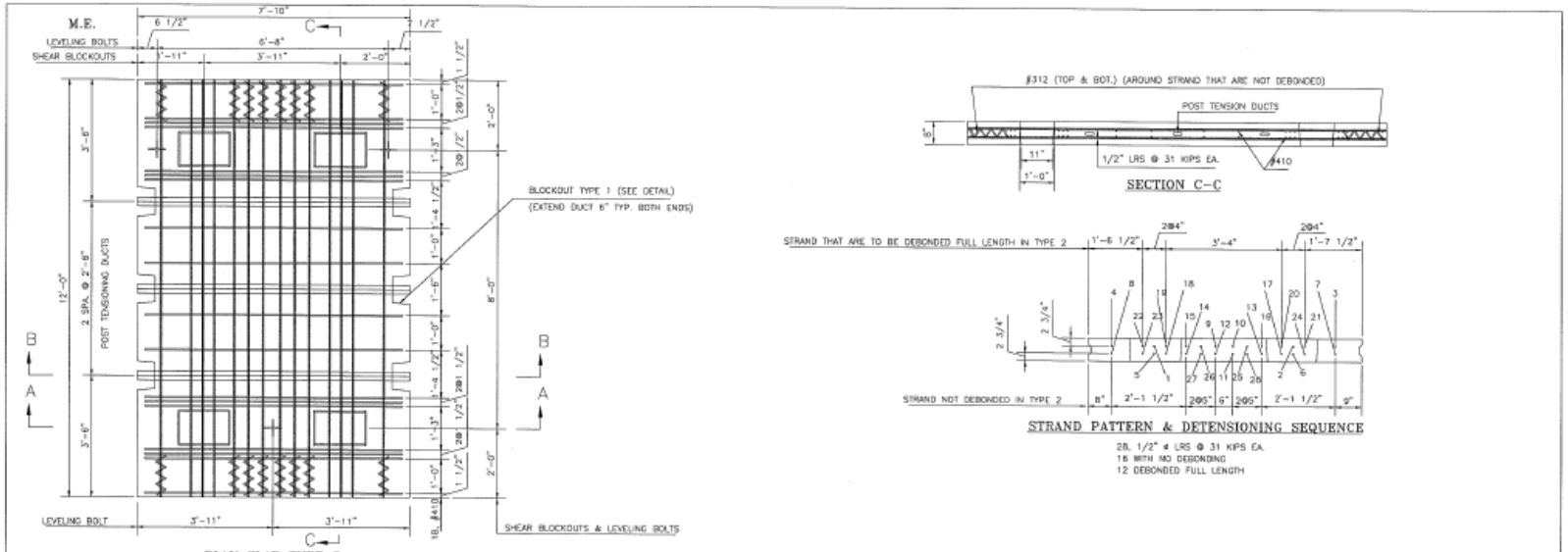

PLAN SLAB TYPE 2

NOTE: STRAND THAT RUN THROUGH SHEAR BLOCKOUTS ARE TO BE CUT OUT OF BLOCKOUTS BEFORE SHIPPING.

⊕= STRAND THAT IS DEBONDED FULL LENGTH

SECTION A–A

SECTION B–B

ELEVATION

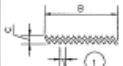

PLAN

BLOCKOUT TYPE 1 ELEVATION

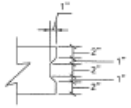

KEYWAY DETAIL

SECTION C–C

STRAND PATTERN & DETENSIONING SEQUENCE

28, 1/2" ⌀ LRS @ 31 KIPS EA.
16 WITH NO DEBONDING
12 DEBONDED FULL LENGTH

MRK	TYPE	# REQ'D	PIN ⌀	LENGTH	A	B	C	D	WT (LBS)	COATING
#411	STR.	0	=	2'-3"					2	
#410	STR.	36	-	7'-6"					5	
#409	3	0		2'-3"-6"	1'-3"	3"	10"		2	
#312	1	16		3'-3"	3'-11"	3"	1'-0"	3 3/4"	1	

REINFORCING SCHEDULE PER FOUR (GRADE 60) BLOCK

REQ'D	PT HARDWARE
3	LEVELING BOLTS

REQ'D BCP SUPPLIED BILL OF MATERIALS

REQ'D SUPPLIED BY OTHERS BILL OF MATERIALS

REV.	DATE	BY	REMARKS
A	11-14	AJB	CHANGE BAR #312 & MOVE ROWS OF STRAND PAT

VIRGINIA POLYTECHNIC INSTITUTE AND STATE UNIVERSITY
TESTING PROGRAM

BAYSHORE CONCRETE PRODUCTS CORPORATION
P.O. BOX 330
CAPE CHARLES, Va. 23310

DECK SLAB DETAILS

DESIGN			SCALE	DRWG. NO.
DRAWN	A.J.B.	11-9-05	NONE	5756-02
CHECKED				

REV. A

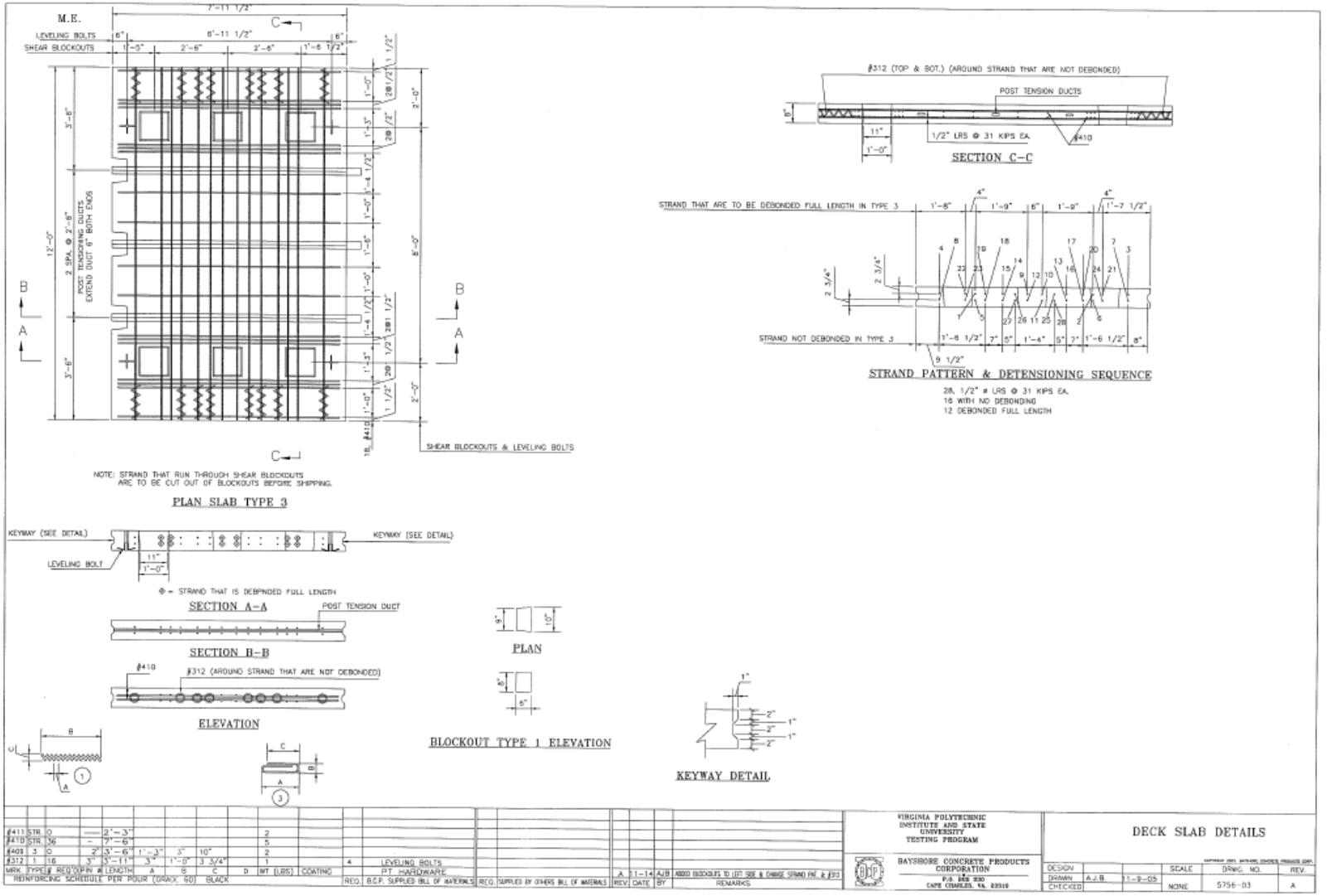

MRK	TYPE	# REQ'D	PIN #	LENGTH	A	B	C	D	WT (LBS)	COATING
#411	STR.	10		2'-3"					2	
#410	STR.	36		9'-6"					5	
#409	3	10		2' 3'-6"	1'-3"	5"	10"		2	
#312	1	16		3' 3'-11"	3"	1'-0"	3 3/4"		1	

REINFORCING SCHEDULE PER POUR (GRADE 60) BLACK

REQ.	P.T. HARDWARE
4	LEVELING BOLTS

REQ. SUPPLIED BY OTHERS BILL OF MATERIALS

REV.	DATE	BY	REMARKS
A	11-14	AJB	ADDED BLOCKOUTS TO LIFT SIDE & CHANGE STRAND PAT. & #312

VIRGINIA POLYTECHNIC INSTITUTE AND STATE UNIVERSITY
TESTING PROGRAM

BAYSHORE CONCRETE PRODUCTS CORPORATION
P.O. BOX 330
CAPE CHARLES, VA. 23310

DECK SLAB DETAILS

			SCALE	DRWG. NO.	REV.
DESIGN					
DRAWN	A.J.B.	11-9-05	NONE	5756-03	A
CHECKED					

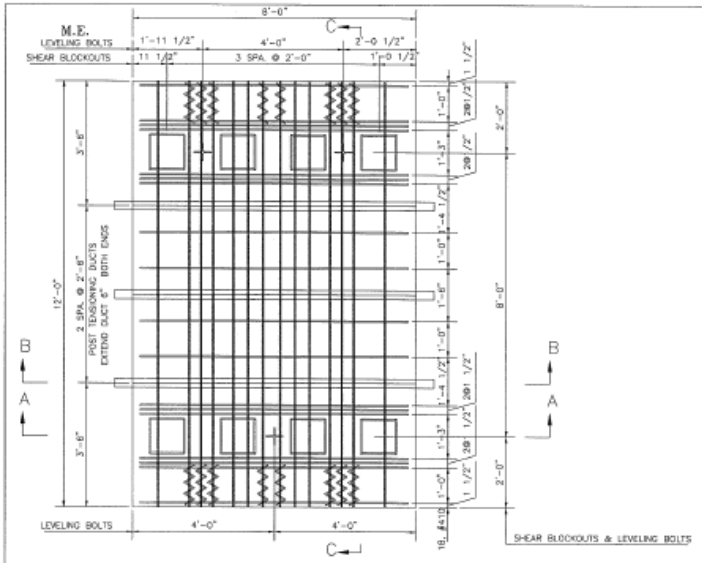

MRK.	TYPE	# REQ'D	PIN ø	LENGTH	A	B	C	D	WT (LBS)	COATING
#411	STR.	0	—	2'-3"					2	
#410	STR.	36	-	7'-6"					5	
#409	3	0	2"	3'-6"	1'-3"	3"	10"		2	
#312	1	16	3"	3'-11"	3"	1'-0"	3 3/4"		1	

REINFORCING SCHEDULE PER POUR (GRADE 60) BLACK

REQ.	B.C.P. SUPPLIED BILL OF MATERIALS
3	LEVELING BOLTS
	PT HARDWARE

REQ. SUPPLIED BY OTHERS BILL OF MATERIALS

REV.	DATE	BY	REMARKS
A	11-14	AJB	CHANGE #312 & MOVE ROWS OF STRAND

VIRGINIA POLYTECHNIC
INSTITUTE AND STATE
UNIVERSITY
TESTING PROGRAM

BAYSHORE CONCRETE PRODUCTS
CORPORATION
P.O. BOX 230
CAPE CHARLES, Va. 23310

DECK SLAB DETAILS

			SCALE	DRWG. NO.	REV.
DESIGN					
DRAWN	A.J.B.	11-9-05	NONE	5756-04	A
CHECKED					

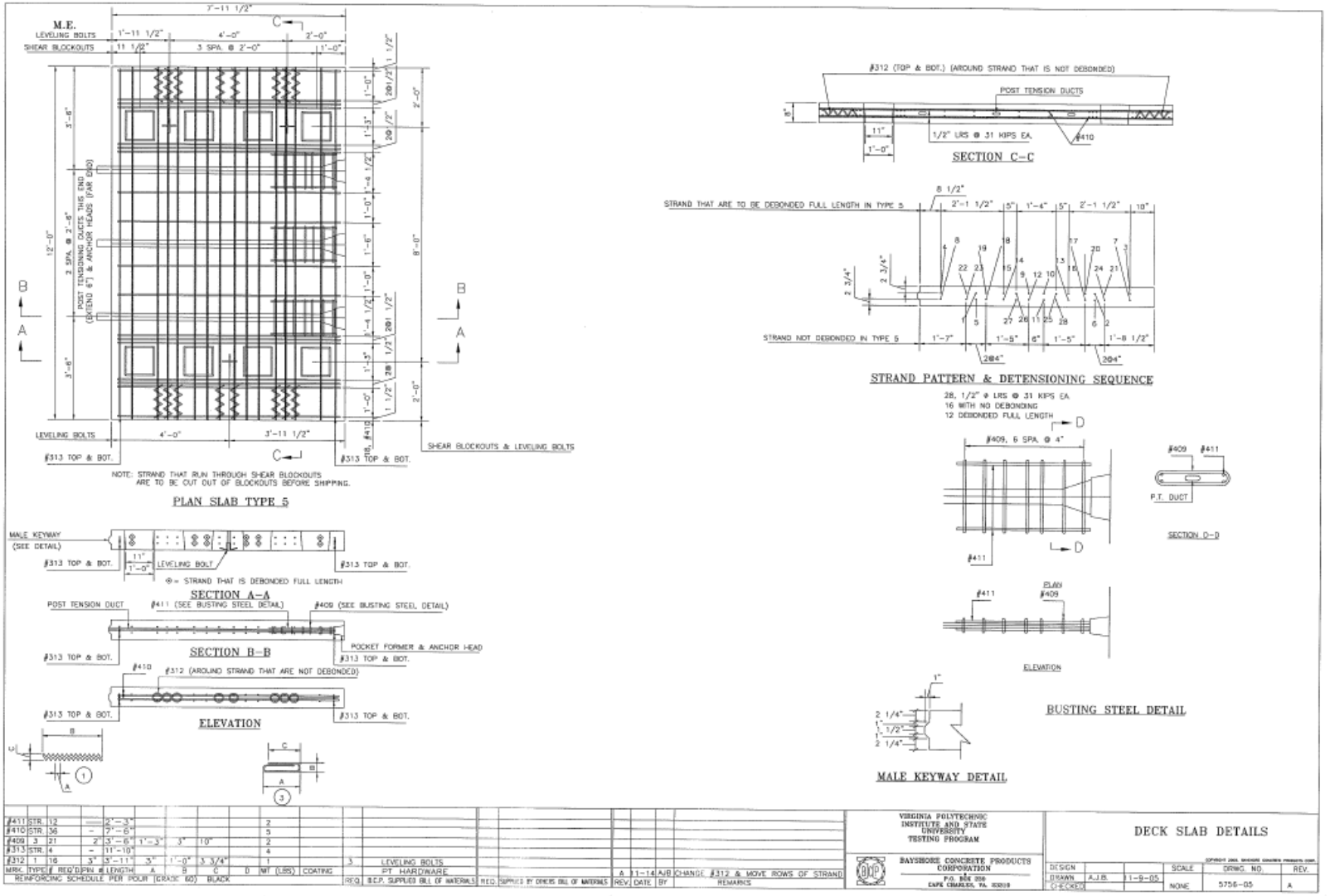

MRK	TYPE	# REQ'D	PIN ø	LENGTH	A	B	C	D	WT (LBS)	COATING
#411	STR.	12		2'-3"					2	
#410	STR.	36		7'-6"					5	
#409	3	21		2'-3"-6"	1'-3"	3"	10"		2	
#313	STR.	4		11'-10"					4	
#312	1	16		3"	3'-11"	3"	1'-0"	3 3/4"	1	

REINFORCING SCHEDULE PER FOUR (GRADE 60) BLACK

REQ.	LEVELING BOLTS PT HARDWARE
3	B.C.P. SUPPLIES BILL OF MATERIALS

REQ. SUPPLIED BY DIRECTS BILL OF MATERIALS

REV.	DATE	BY	REMARKS
A	11-14	AJB	CHANGE #312 & MOVE ROWS OF STRAND

VIRGINIA POLYTECHNIC INSTITUTE AND STATE UNIVERSITY
TESTING PROGRAM

BAYSHORE CONCRETE PRODUCTS CORPORATION
P.O. BOX 250
CAPE CHARLES, VA. 23310

DECK SLAB DETAILS

			SCALE	DRWG. NO.	REV.
DESIGN					
DRAWN	A.J.B.	11-9-05	NONE	5756-05	A
CHECKED					

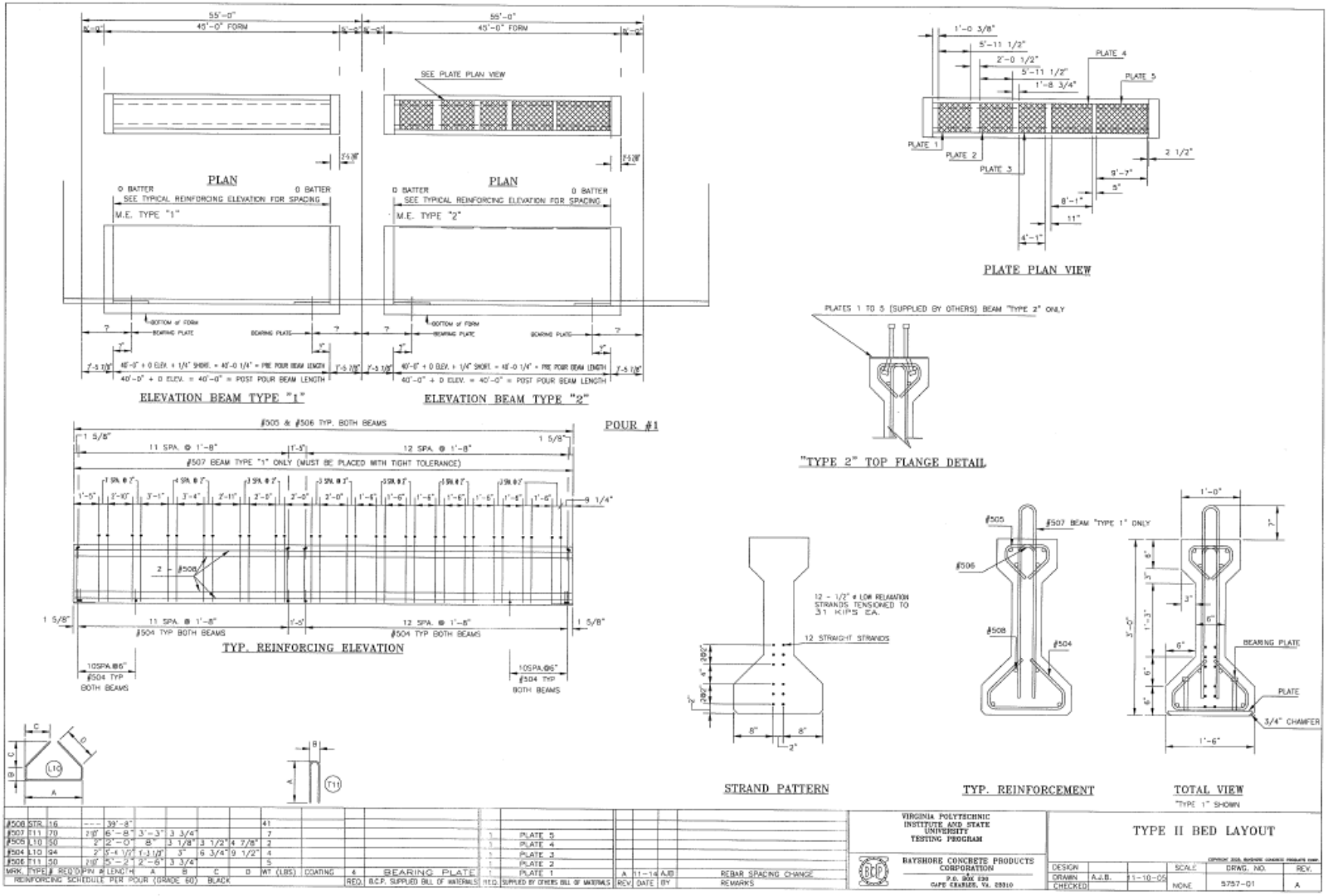

MRK.	TYPE	# REQ'D	PIN #	LENGTH	A	B	C	D	WT (LBS)	COATING
#508	STR.	16	---	39'-8"					41	
#507	T11	70	2'@	6'-8"	3'-3"	3 3/4"			7	
#505	L10	50	2	2'-0"	8"	3 1/8"	3 1/2"	4 7/8"	2	
#504	L10	94	2	5'-6 1/2"	1-1 1/2"	3"	6 3/4"	9 1/2"	4	
#506	T11	50	2'@	5'-2"	2'-6"	3 3/4"			5	

REINFORCING SCHEDULE PER POUR (GRADE 60) BLACK

REQ.	BEARING PLATE
1	PLATE 5
1	PLATE 4
1	PLATE 3
1	PLATE 2
1	PLATE 1

REQ. B.C.P. SUPPLIED BILL OF MATERIALS | REQ. SUPPLIED BY OTHERS BILL OF MATERIALS

REV.	DATE	BY	REMARKS
A	11-14	AJB	REBAR SPACING CHANGE

VIRGINIA POLYTECHNIC INSTITUTE AND STATE UNIVERSITY TESTING PROGRAM

BAYSHORE CONCRETE PRODUCTS CORPORATION
P.O. BOX 830
CAPE CHARLES, VA. 23310

TYPE II BED LAYOUT

			SCALE	DRWG. NO.	REV.
DESIGN					
DRAWN	A.J.B.	11-10-05	NONE	5757-01	A
CHECKED					

APPENDIX D – LEVELING BOLT DATA SHEETS

DAYTON/RICHMOND CONCRETE ACCESSORIES

B-14 Coil Bolts and Minimum Coil Penetration Information

- B-14 coil bolts have fast acting, self-cleaning threads and are available in 3/4", 1", 1-1/4" and 1-1/2" diameter bolts.
- Bolts may be furnished with integrally formed heads or made with B-12 coil rod and B-25 hex nuts securely welded on.
- May be reused—but will wear and must be regularly inspected.
- Must be kept clean and lubricated.
- When determining overall length of lifting bolt, see example on page 26 and 27—you must consider:
  - A. Height of hardware
  - B. Insert Setback
  - C. Minimum coil penetration
- Minimum coil penetration shown in the charts below applies to all coil products.

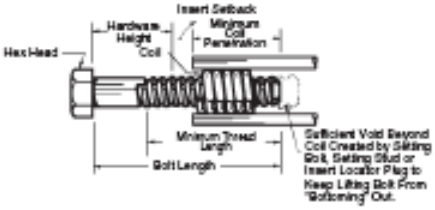

To Order:
Specify: (1) quantity, (2) diameter, (3) name, (4) length of bolt.

Example:
300 pcs., 1" diameter, B-14 Coil Bolts, 6" long.

B-14 Coil Bolts with Integrally Formed Hex Heads (Fabricated from Blanks Meeting ASTM A-307 Grade A)

3/4" Diameter		1" Diameter		1-1/4" Diameter		1-1/2" Diameter	
Forged Hex Head		Forged Hex Head		Forged Hex Head		Forged Hex Head	
Safe Work Load		Safe Work Load		Safe Work Load		Safe Work Load	
Tension	Shear	Tension	Shear	Tension	Shear	Tension	Shear
3,600 lbs.	2,400 lbs.	7,200 lbs.	4,800 lbs.	10,800 lbs.	7,200 lbs.	16,500 lbs.	11,000 lbs.
Minimum Coil Penetration 2-1/4"		Minimum Coil Penetration 2-1/2"		Minimum Coil Penetration 2-1/2"		Minimum Coil Penetration 3"	
Bolt Length	Minimum Thread Length	Bolt Length	Minimum Thread Length	Bolt Length	Minimum Thread Length	Bolt Length	Minimum Thread Length
3"	2-1/4"	3"	2"	3"	2"	–	–
4"	3-1/4"	4"	3"	4"	3"	4"	3"
5"	4-1/4"	5"	4"	5"	4"	5"	4"
6"	5"	6"	5"	6"	5"	6"	5"
Over 6"	5"	Over 6"	5"	Over 6"	5"	Over 6"	5"

Approximate safety factor 5 to 1 for tilt-up hardware.
Note: High strength coil bolts with integrally formed heads are available on special order.
These bolts are fabricated from blanks meeting ASTM A-325 Standards.

B-14 Coil Bolts with Welded Heavy Hex Coil Nut Heads (Fabricated from High Tensile Coil Rod)

3/4" Diameter		1" Diameter		1-1/4" Diameter		1-1/2" Diameter	
Welded Hex Nut Head		Welded Hex Nut Head		Welded Hex Nut Head		Welded Hex Nut Head	
Safe Work Load		Safe Work Load		Safe Work Load		Safe Work Load	
Tension	Shear	Tension	Shear	Tension	Shear	Tension	Shear
7,200 lbs.	4,800 lbs.	15,000 lbs.	10,000 lbs.	22,500 lbs.	15,000 lbs.	27,000 lbs.	18,000 lbs.
Minimum Coil Penetration 2-1/4"		Minimum Coil Penetration 2-1/2"		Minimum Coil Penetration 2-1/2"		Minimum Coil Penetration 3"	

Approximate safety factor 5 to 1 for tilt-up hardware.
Available in any length over 3".

F-53 Thin Slab Coil Insert

The Dayton/Richmond F-53 Thin Slab Coil Insert is designed for lifting thin precast concrete panels from the casting bed and for handling the panels until they are set into their final position. Inserts should be set back 1/2" from the surface of the concrete, maintaining at least 3/4" of concrete below the insert. Minimum spacing between inserts is twice the minimum corner distance. Available in insert heights up to 4".

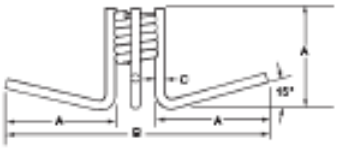

F-53 Thin Slab Coil Insert

To Order:
Specify: (1) quantity, (2) name, (3) bolt diameter, (4) height, (5) finish.

Example:
200, F-53 Thin Slab Coil Inserts, 1" dia. X 4" height, plain finish.

F-53 Thin Slab Coil Insert Selection Chart

Bolt Diameter	Insert Height	Minimum Edge Distance	Minimum Corner Distance	Safe Working Load Tension	Safe Working Load Shear	A	B	C
3/4"	5"	5"	5"	2,000 lbs.	2,000 lbs.	3"	7-1/8"	0.505"
1"	4"	10"	10"	3,000 lbs.	3,000 lbs.	4"	9-3/8"	0.505"
1-1/4"	4"	10"	10"	3,000 lbs.	3,000 lbs.	4"	9-5/8"	0.505"
1-1/2"	4"	10"	10"	3,000 lbs.	3,000 lbs.	4"	9-7/8"	0.505"

Safe Working Load provides a factor of safety of approximately 4 to 1 in 3,000 psi normal weight concrete.

APPENDIX E – MIX DESIGN FOR PANELS AND GIRDERS

Form TL-27 (Rev. 3/05)

VIRGINIA DEPARTMENT OF TRANSPORTATION
MATERIALS DIVISION
STATEMENT OF HYDRAULIC CEMENT CONCRETE MIX DESIGN

SUBMIT one copy to the District Administrator, Virginia Department of Transportation. Approval must be received by the contractor from the Materials Division before work is begun. This mix design is approved for all projects of the Department for the class of concrete shown: Calendar Year 2005. Mix Design No. 5-BC-05.

Producer Bayshore Concrete Products Plant Location Chesapeake Phone (757)549-1630

Type of Mix: Ready Mix Job Mix X Date 10/24/2005

Mix Design – One yd^3 Based on SSD Condition

Class of Concrete A-5 Slump 0-7 in. Air Content 3-7 %

Material			Source	Plant/Quarry Location
Cement 4.8 Bags	451	lbs. Type II	Lafarge	Ravenna, N.Y.
Pozzolans	301	lbs.	Lafarge	Union Bridge, Md.
Sand (1)	1390	lbs.	Vulcan	Puddledock Quarry
No. 67 Stone (1)	1508	lbs.	Vulcan	Richmond Quarry
No. _ Stone (1)		lbs.		
Water (2) 263 lbs.	31.6	gal.	Well	Chesapeake, Va.
Admixture (AE) (3)	6	oz	Sika AEA 14	Lynhurst, N.J.
Admixture (Retarder) (3)	14	oz	Sika Plastiment	Lynhurst, N.J.
Admixture (Other) (3)	40	oz	Sika 6100	Lynhurst, N.J.

NOTES: 2 gallons CNI when required

(1) The quantities of fine and coarse aggregates necessary to conform to specifications in regard to consistency and workability shall be determined by the method described in "Recommended Practice for Selecting Proportions for Normal Weight Concrete" (ACI-211.1) and the actual quantities used shall not deviate more than plus or minus 5 percent from such quantities.

(2) To provide minimum slump permissible in Table II-17 while satisfying placement and finishing requirements. A separate design shall be submitted for each slump desired.

(3) The quantity of admixture will not be approved or disapproved since it varies considerably and must be initially established by trial and error by the producer or contractor with subsequent adjustment during batching to maintain the desired results within the range specified.

Pozzolan–sp.gr.	2.93
Sand–Abs.	.7
Sand–F.M.	2.89
Sand–sp.gr.	2.59
C.A.–Abs.	.6
C.A.–sp.gr.	2.67
C.A.–Unit wt	91.6
Mortar–yd^3	

Contractor Bayshore Concrete Products (Name of Company) By Larry McAllen (Person Preparing Form)

Producer Technician's Certification Number 231-70-8540

DEPARTMENT USE ONLY

Remarks

Copies: State Materials Engineer
District Materials Engineer
Plant Inspector
Sub-Contractor and/or R.M. Producer

Checked by W. B. Stallings

Approved by C. W. Boykin (District Materials Engineer)

Approved tentatively subject to the production of material meeting the requirements of Specifications and Special Provisions.

10/26/05

APPENDIX F– GROUT DATA SHEETS

FIVE STAR® HIGHWAY PATCH

Fast Traffic Area Repair

PRODUCT DESCRIPTION

Five Star Highway Patch is a one component, fast setting hydraulic cement material ideal for horizontal repairs of concrete in traffic areas. Five Star Highway Patch provides resistance to oil, grease, gasoline, salts and other chemicals found in the transportation environment.

ADVANTAGES

- High early strength
- One component/ease of use
- Open to traffic in two hours
- Freeze/thaw resistance
- Adjustable working time
- Resistant to salts
- Cold weather installation
- Coarse aggregate extension

USES

- Highways and bridges
- Parking decks and ramps
- Airport runways and taxiways
- Expansion joint rebuild
- Dowel bar retrofit
- Cold weather repairs

TECHNICAL SUPPORT

Five Star Products maintains the industry's foremost Engineering and Technical Support Group:

- Over 30 years of experience in concrete repair
- Technical Center staffed with experienced engineers available for consultation
- Design-A-Spec™ for engineering specification assistance
- Experienced representatives for field service
- Corporate research laboratory available to customize products for unique applications

PACKAGING AND YIELD

Five Star Highway Patch is packaged in heavy-duty polyethylene lined bags each weighing 50 lb (22.7 kg) yielding approximately 0.40 cubic feet (11.3 liters) and approximately 0.68 cubic feet (19.9 liters) with an 80% coarse aggregate extension. Also available in 3000 lb bulk bags.

SHELF LIFE

One year in original unopened packaging when stored in dry conditions. Higher humidity will reduce shelf life.

TYPICAL PROPERTIES AT 73°F (23°C)

Compressive Strength, ASTM C 109	
2 Hours	2000 psi (13.8 MPa)
3 Hours	3500 psi (24.1 MPa)
1 Day	5100 psi (35.2 MPa)
7 Days	7000 psi (48.3 MPa)
Bond Strength, ASTM C 882	
1 Day	1500 psi (10.4 MPa)
7 Days	2000 psi (13.8 MPa)
Length Change, ASTM C 157	
28 Days Wet	+0.05%
28 Days Dry	-0.05%
Time of Set, ASTM C 266	
Initial	15 minutes
Final	30 minutes
Freeze/Thaw Resistance, ASTM C 666A	
Relative Durability Factor	90%
Flexural Strength, ASTM C 78	
3 Hours	400 psi

The data shown above reflect typical results based on laboratory testing under controlled conditions. Reasonable variations from the data shown above may result. Test methods are modified where applicable.

QUALITY CERTIFIED ISO 9001 FIVE STAR PRODUCTS

PLACEMENT GUIDELINES

1. SURFACE PREPARATION: All surfaces in contact with Five Star Highway Patch shall be free of oil, grease, laitance, and other contaminants. Concrete must be clean, sound and rough to ensure a good bond. Remove all oxidation from exposed reinforcing steel and for additional protection coat reinforcing steel with Five Star® AC Coat. A perimeter edge and minimum depth of one inch (25 mm) should be provided for a durable repair. Featheredging is not desirable. Soak concrete surfaces prior to application with liberal quantities of potable water, leaving the concrete saturated and free of standing water or use Five Star® Bonding Adhesive. Surfaces shall be conditioned to between 35°F and 90°F (2°C and 32°C) at the time of placement.
2. MIXING: Mix Five Star Highway Patch thoroughly for approximately three to five minutes with a mortar mixer or drill and paddle mixer. Adjust consistency if necessary, but do not exceed maximum water content stated on the package or an amount that will cause segregation. Do not mix more material than can be placed in 10 minutes. Addition of coarse aggregate, meeting ASTM C 33, should be used for pours greater than two inches (50 mm) in depth.
3. PLACEMENT PROCEDURES: When bonding adhesive is not used, firmly work Five Star Highway Patch into substrate and place full depth from one side of the repair to the other. Where this is not practical, placement must be continuous to prevent cold joints between pours. Finish as necessary.
   SPECIAL CONDITIONS: For use in cold temperatures, Five Star Highway Patch must be maintained at a temperature of at least 35°F (2°C). Protect from freezing until a compressive strength of at least 1000 psi (6.9 MPa) is obtained. Faster strength gain will occur when the Five Star Highway Patch and mixing water have been conditioned to a higher temperature prior to placement.
   In hot temperatures, Five Star Highway Patch should be kept as cool as possible, but not exceeding 90°F (32°C). Chilled water should be used for mixing to help maintain sufficient working time.
4. POST-PLACEMENT PROCEDURES: Five Star Highway Patch shall be protected until initial set, then immediately coat with an approved curing compound meeting water retention properties of ASTM C 309 or wet cure for a minimum of three days. In-service operation may begin immediately after the required strength has been reached.
   NOTE: PRIOR TO APPLICATION, READ ALL PRODUCT PACKAGING THOROUGHLY. For more detailed placement procedures, call the Five Star Products Engineering and Technical Center at 203-336-7900.

LIMITATIONS

- Never exceed the maximum water content stated on the package or an amount that will cause segregation.
- Temperature of surfaces must be between 35°F and 90°F (2°C and 32°C) at time of placement. For cold and hot weather placement, call the Five Star Products Engineering and Technical Center.
- Substrate shall be free of frost and ice.
- Repair material shall be protected from freezing until it reaches 1000 psi (6.9 MPa).
- Placement shall be continuous to avoid cold joints.

CAUTION

Contains cementitious material and crystalline free silica. International Agency for Research on Cancer has evaluated that there is sufficient evidence for the carcinogenicity of inhaled crystalline silica to humans. Take appropriate measures to avoid breathing dust. Avoid contact with eyes and contact with skin. In case of contact with eyes, immediately flush with plenty of water for at least 15 minutes. Immediately call a physician. Wash skin thoroughly after handling. Keep product out of reach of children. PRIOR TO USE, REFER TO MATERIAL SAFETY DATA SHEET.

For worldwide availability, additional product information and technical support, contact your local Five Star distributor, local sales representative, or you may call Five Star's Engineering and Technical Center at 203-336-7900.

Corporate Offices
Five Star Products, Inc.
425 Stillson Road
Fairfield, CT 06430
Tel: 203-336-7900
Fax: 203-336-7930
www.fivestarproducts.com

American Owned & Operated

APPENDIX G – INITIAL POST-TENSIONING LOSS CALCULATIONS

The procedure for calculating the initial losses is described in Section 4.1.6. The results of the calculations are provided in a series of tables, which show the losses and forces at selected intervals along the length of the lab mockup.

Table G.1 Force Profile in Strands Incorporating the Anchor Losses

A_{ps} =	0.153	in^2	E_{ps} =	28500	ksi	L =	480	in
f'_c =	7.54	ksi	E_c =	4949	ksi			

sequence		11	3	4	12	7	1	2	8	9	5	6	10
strand #		1	2	3	4	5	6	7	8	9	10	11	12
P_J		27.80	27.89	27.80	27.89	27.62	27.92	27.89	27.62	27.89	27.98	28.25	28.16
$P_{D\ for\ K}$		27.45	27.45	27.45	27.45	27.29	27.29	27.29	27.29	26.72	26.72	26.72	26.72
$P_{D\ low}$		24.99	24.99	24.99	24.99	25.46	25.46	25.46	25.46	24.99	24.99	24.99	24.99
ΔP_{ANCH}		1.79	1.42	1.79	2.46	2.10	2.39	2.85	1.21	2.30	2.39	3.04	3.61
Δ_{ANCH}		0.25	0.125	0.25	0.375	0.375	0.25	0.375	0.125	0.125	0.125	0.16667	0.25
P_{max}		26.90	27.18	26.90	26.66	26.57	26.73	26.46	27.01	26.74	26.78	26.73	26.35
l_{max}		1218	769	1218	1331	1556	911	1149	899	474	456	478	604
K (wobble)		0.0003	0.0004	0.0003	0.0004	0.0003	0.0006	0.0005	0.0003	0.0011	0.0011	0.0014	0.0013
	x												
	0	26.01	26.47	26.01	25.43	25.52	25.53	25.04	26.40	25.59	25.59	25.21	24.55
	24	26.03	26.49	26.03	25.45	25.53	25.56	25.07	26.42	25.65	25.65	25.28	24.62
	48	26.04	26.51	26.04	25.48	25.55	25.59	25.10	26.44	25.70	25.72	25.36	24.69
	72	26.06	26.54	26.06	25.50	25.56	25.62	25.13	26.45	25.76	25.78	25.44	24.76
	96	26.08	26.56	26.08	25.52	25.58	25.66	25.16	26.47	25.82	25.84	25.51	24.83
	120	26.10	26.58	26.10	25.54	25.60	25.69	25.19	26.49	25.88	25.90	25.59	24.91
	144	26.11	26.60	26.11	25.56	25.61	25.72	25.22	26.50	25.94	25.97	25.67	24.98
	168	26.13	26.62	26.13	25.59	25.63	25.75	25.25	26.52	26.00	26.03	25.74	25.05
	192	26.15	26.65	26.15	25.61	25.65	25.78	25.28	26.53	26.05	26.09	25.82	25.12

sequence		11	3	4	12	7	1	2	8	9	5	6	10
strand #		1	2	3	4	5	6	7	8	9	10	11	12
	216	26.17	26.67	26.17	25.63	25.66	25.81	25.31	26.55	26.11	26.16	25.90	25.19
	240	26.18	26.69	26.18	25.65	25.68	25.85	25.34	26.57	26.17	26.22	25.97	25.26
	264	26.20	26.71	26.20	25.68	25.69	25.88	25.37	26.58	26.23	26.28	26.05	25.34
	288	26.22	26.74	26.22	25.70	25.71	25.91	25.40	26.60	26.29	26.34	26.12	25.41
	312	26.24	26.76	26.24	25.72	25.73	25.94	25.43	26.61	26.34	26.41	26.20	25.48
	336	26.26	26.78	26.26	25.74	25.74	25.97	25.46	26.63	26.40	26.47	26.28	25.55
	360	26.27	26.80	26.27	25.76	25.76	26.00	25.49	26.65	26.46	26.53	26.35	25.62
	384	26.29	26.82	26.29	25.79	25.78	26.03	25.52	26.66	26.52	26.59	26.43	25.70
	408	26.31	26.85	26.31	25.81	25.79	26.07	25.55	26.68	26.58	26.66	26.51	25.77
	432	26.33	26.87	26.33	25.83	25.81	26.10	25.58	26.70	26.64	26.72	26.58	25.84
	456	26.34	26.89	26.34	25.85	25.82	26.13	25.61	26.71	26.69	26.78	26.66	25.91
	480	26.36	26.91	26.36	25.87	25.84	26.16	25.64	26.73	26.72	26.72	26.72	25.98

Table G.2 Elastic Losses in the Post-Tensioning Tendons

str. #	4	1	12	9	8	5	11	10	3	2	7	6
seq.	12	11	10	9	8	7	6	5	4	3	2	1
0	0.00	0.127	0.257	0.380	0.508	0.640	0.767	0.893	1.021	1.151	1.283	1.409
24	0.00	0.127	0.257	0.380	0.509	0.641	0.768	0.895	1.023	1.153	1.285	1.411
48	0.00	0.127	0.258	0.381	0.509	0.642	0.769	0.896	1.025	1.155	1.287	1.413
72	0.00	0.127	0.258	0.381	0.510	0.642	0.770	0.897	1.026	1.157	1.289	1.415
96	0.00	0.128	0.258	0.382	0.511	0.643	0.771	0.899	1.028	1.158	1.291	1.417
120	0.00	0.128	0.258	0.383	0.512	0.644	0.772	0.900	1.030	1.160	1.293	1.419
144	0.00	0.128	0.258	0.383	0.513	0.645	0.773	0.902	1.031	1.162	1.295	1.421
168	0.00	0.128	0.259	0.384	0.514	0.646	0.774	0.903	1.033	1.164	1.297	1.423
192	0.00	0.128	0.259	0.384	0.515	0.647	0.775	0.904	1.035	1.165	1.299	1.425
216	0.00	0.128	0.259	0.385	0.515	0.648	0.776	0.906	1.036	1.167	1.301	1.427
240	0.00	0.128	0.259	0.385	0.516	0.649	0.777	0.907	1.038	1.169	1.303	1.429
264	0.00	0.128	0.259	0.386	0.517	0.650	0.778	0.909	1.040	1.171	1.304	1.431
288	0.00	0.128	0.260	0.387	0.518	0.651	0.779	0.910	1.042	1.173	1.306	1.433
312	0.00	0.129	0.260	0.387	0.519	0.652	0.780	0.911	1.043	1.174	1.308	1.435
336	0.00	0.129	0.260	0.388	0.520	0.653	0.781	0.913	1.045	1.176	1.310	1.437
360	0.00	0.129	0.260	0.388	0.520	0.654	0.782	0.914	1.047	1.178	1.312	1.439
384	0.00	0.129	0.260	0.389	0.521	0.655	0.783	0.916	1.048	1.180	1.314	1.441
408	0.00	0.129	0.260	0.389	0.522	0.655	0.784	0.917	1.050	1.182	1.316	1.444
432	0.00	0.129	0.261	0.390	0.523	0.656	0.785	0.918	1.052	1.183	1.318	1.446
456	0.00	0.129	0.261	0.390	0.524	0.657	0.786	0.920	1.054	1.185	1.320	1.448
480	0.00	0.129	0.261	0.391	0.525	0.658	0.787	0.921	1.054	1.186	1.321	1.449

Table G.3 Relaxation Losses in the Post-Tensioning Tendons

str. #	4	1	12	9	8	5	11	10	3	2	7	6
seq.	12	11	10	9	8	7	6	5	4	3	2	1
time	0.25	0.25	0.25	0.25	0.25	0.25	2.04	2.04	2.04	2.04	2.04	2.04
0	0.433	0.492	0.340	0.444	0.529	0.432	0.865	0.946	1.037	1.141	0.811	0.915
24	0.436	0.494	0.347	0.450	0.531	0.434	0.882	0.960	1.042	1.147	0.818	0.922
48	0.438	0.496	0.354	0.456	0.533	0.435	0.899	0.975	1.046	1.152	0.824	0.929
72	0.440	0.498	0.361	0.462	0.535	0.437	0.916	0.989	1.050	1.157	0.830	0.936
96	0.443	0.500	0.369	0.468	0.536	0.439	0.933	1.003	1.054	1.162	0.837	0.943
120	0.445	0.502	0.376	0.474	0.538	0.440	0.950	1.018	1.058	1.168	0.843	0.950
144	0.447	0.504	0.383	0.481	0.540	0.442	0.968	1.032	1.062	1.173	0.850	0.957
168	0.450	0.506	0.390	0.487	0.542	0.444	0.985	1.047	1.066	1.178	0.856	0.964
192	0.452	0.508	0.397	0.493	0.543	0.445	1.002	1.061	1.070	1.183	0.863	0.971
216	0.454	0.510	0.405	0.499	0.545	0.447	1.020	1.076	1.074	1.189	0.869	0.978
240	0.457	0.512	0.412	0.506	0.547	0.449	1.038	1.091	1.078	1.194	0.876	0.986
264	0.459	0.513	0.419	0.512	0.549	0.450	1.055	1.105	1.082	1.199	0.882	0.993
288	0.461	0.515	0.427	0.518	0.551	0.452	1.073	1.120	1.086	1.205	0.889	1.000
312	0.464	0.517	0.434	0.525	0.552	0.454	1.091	1.135	1.090	1.210	0.895	1.007
336	0.466	0.519	0.442	0.531	0.554	0.456	1.109	1.150	1.094	1.215	0.902	1.014
360	0.468	0.521	0.449	0.538	0.556	0.457	1.127	1.165	1.098	1.221	0.909	1.022
384	0.471	0.523	0.457	0.544	0.558	0.459	1.145	1.180	1.103	1.226	0.915	1.029
408	0.473	0.525	0.465	0.550	0.560	0.461	1.164	1.195	1.107	1.231	0.922	1.036
432	0.475	0.527	0.472	0.557	0.561	0.462	1.182	1.210	1.111	1.237	0.928	1.043
456	0.478	0.529	0.480	0.563	0.563	0.464	1.200	1.226	1.115	1.242	0.935	1.050
480	0.480	0.531	0.487	0.567	0.565	0.466	1.216	1.211	1.119	1.247	0.942	1.058

Table G.4 Final Forces in the Post-Tensioning Tendons After All Initial Losses

str. #	4	1	12	9	8	5	11	10	3	2	7	6
seq.	12	11	10	9	8	7	6	5	4	3	2	1
0	25.4	25.9	24.5	25.5	26.2	25.4	25.0	25.3	25.7	26.1	24.7	25.2
24	25.4	25.9	24.5	25.5	26.3	25.4	25.0	25.4	25.7	26.1	24.7	25.2
48	25.4	25.9	24.6	25.6	26.3	25.4	25.1	25.4	25.7	26.2	24.8	25.2
72	25.4	26.0	24.7	25.6	26.3	25.4	25.2	25.5	25.7	26.2	24.8	25.3
96	25.5	26.0	24.7	25.7	26.3	25.4	25.3	25.6	25.8	26.2	24.8	25.3
120	25.5	26.0	24.8	25.7	26.3	25.4	25.3	25.6	25.8	26.2	24.9	25.3
144	25.5	26.0	24.9	25.8	26.3	25.4	25.4	25.7	25.8	26.2	24.9	25.4
168	25.5	26.0	25.0	25.9	26.4	25.5	25.5	25.7	25.8	26.3	24.9	25.4
192	25.5	26.1	25.0	25.9	26.4	25.5	25.5	25.8	25.8	26.3	24.9	25.4
216	25.6	26.1	25.1	26.0	26.4	25.5	25.6	25.9	25.8	26.3	25.0	25.4
240	25.6	26.1	25.2	26.0	26.4	25.5	25.7	25.9	25.9	26.3	25.0	25.5
264	25.6	26.1	25.2	26.1	26.4	25.5	25.8	26.0	25.9	26.4	25.0	25.5
288	25.6	26.1	25.3	26.1	26.4	25.5	25.8	26.0	25.9	26.4	25.1	25.5
312	25.6	26.1	25.4	26.2	26.5	25.6	25.9	26.1	25.9	26.4	25.1	25.6
336	25.7	26.2	25.4	26.3	26.5	25.6	26.0	26.2	25.9	26.4	25.1	25.6
360	25.7	26.2	25.5	26.3	26.5	25.6	26.1	26.2	25.9	26.4	25.1	25.6
384	25.7	26.2	25.6	26.4	26.5	25.6	26.1	26.3	26.0	26.5	25.2	25.7
408	25.7	26.2	25.7	26.4	26.5	25.6	26.2	26.3	26.0	26.5	25.2	25.7
432	25.8	26.2	25.7	26.5	26.5	25.6	26.3	26.4	26.0	26.5	25.2	25.7
456	25.8	26.2	25.8	26.5	26.5	25.7	26.4	26.5	26.0	26.5	25.3	25.7
480	25.8	26.3	25.9	26.6	26.6	25.7	26.4	26.4	26.0	26.5	25.3	25.8

APPENDIX H – TIME DEPENDENT RESULTS

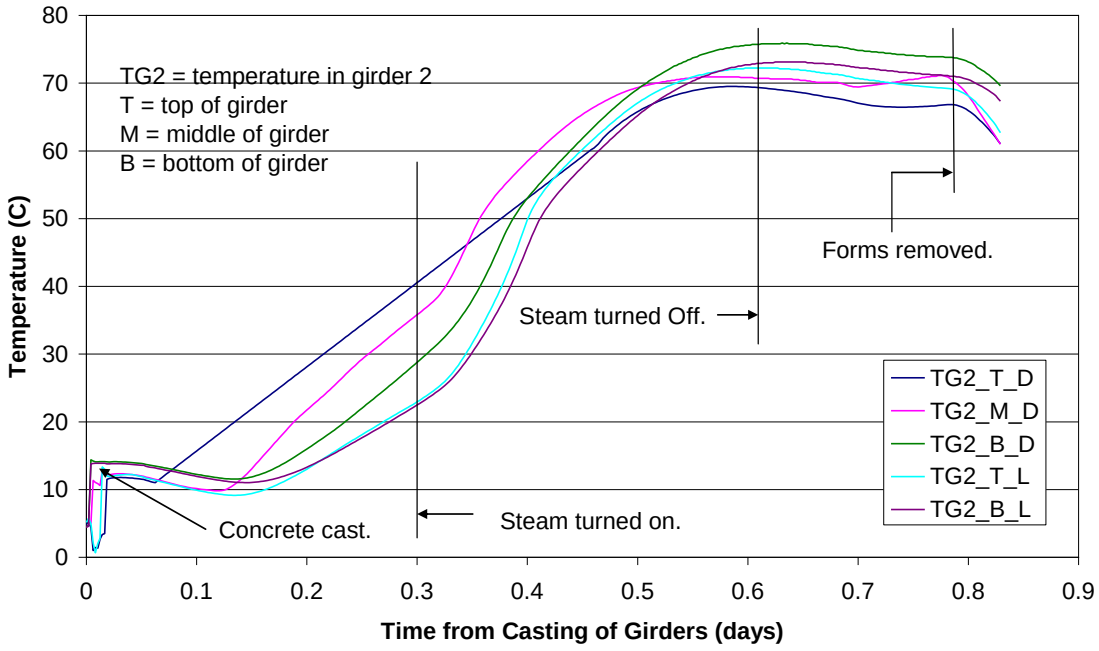

Figure H.1 Variation of Temperature with Time During Casting and Strand Release for Girder 2

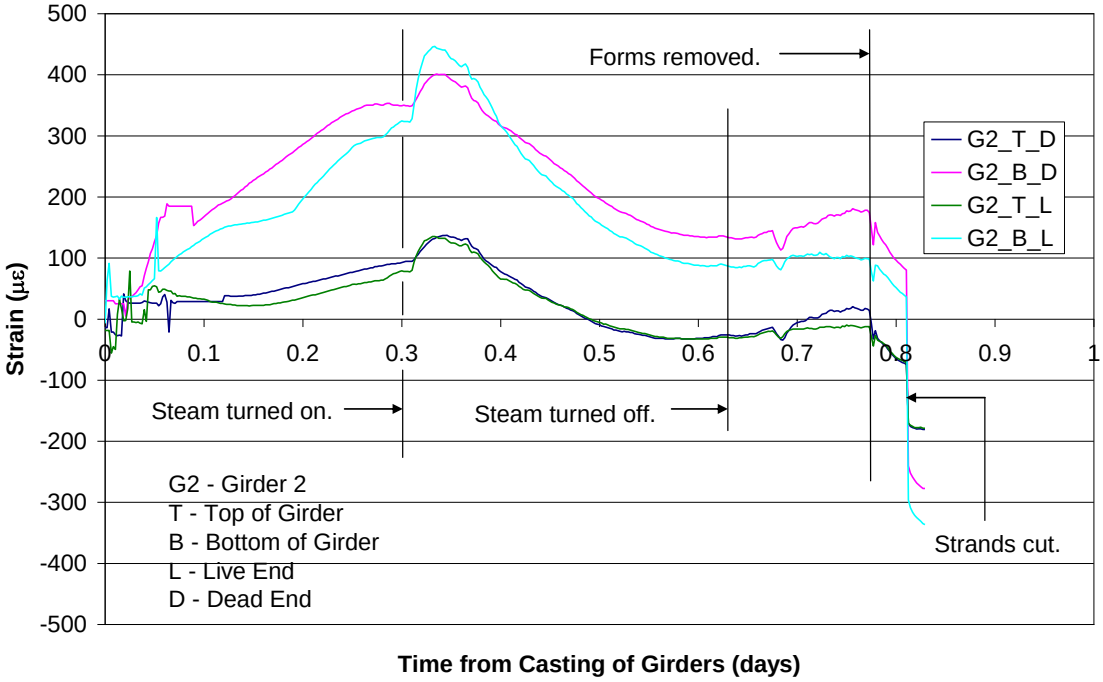

Figure H.2 Variation of Strain with Time During Casting and Strand Release for Girder 2

APPENDIX I – FINITE ELEMENT LIVE LOAD RESULTS

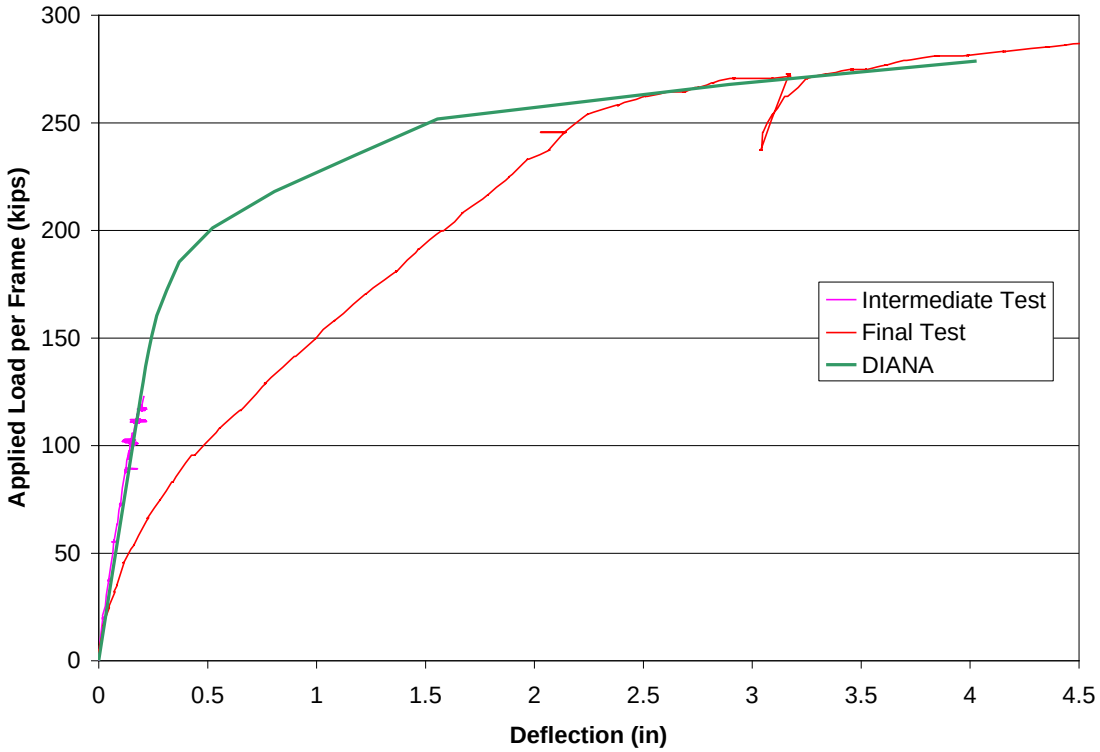

Figure I.1 Deflections in the Finite Element Model for Girder 1 at the Dead End Compared to Experimental Results

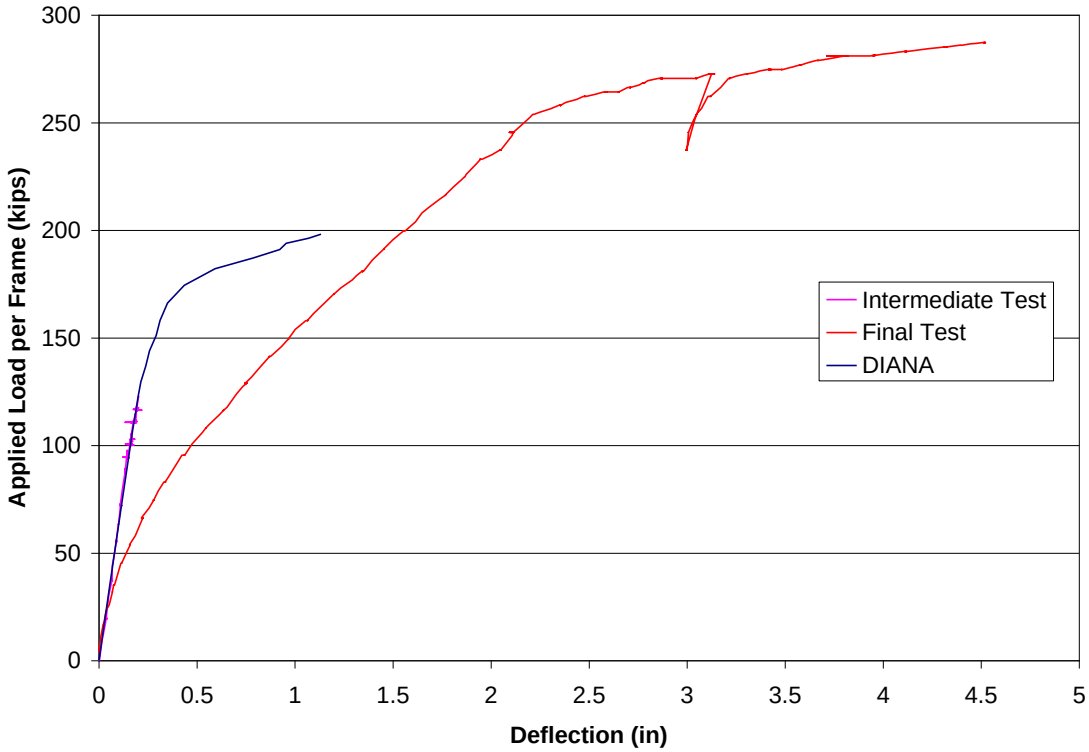

Figure I.2 Deflections in the Finite Element Model for Girder 2 at the Dead End Compared to Experimental Results

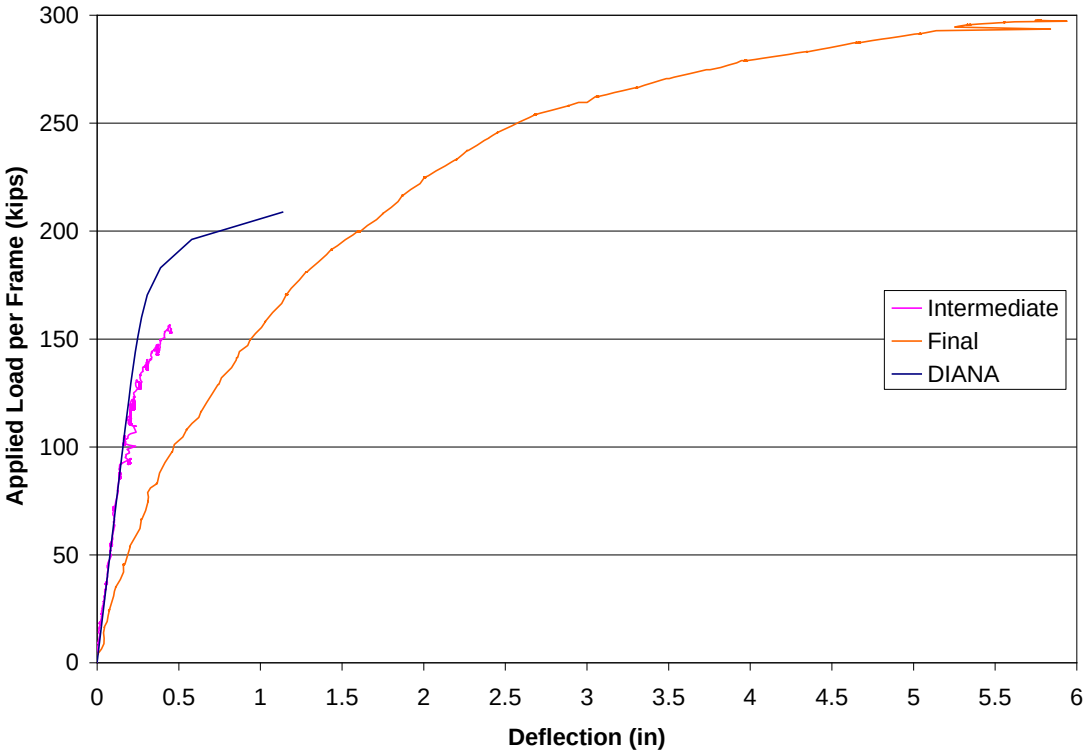

Figure I.3 Deflections in the Finite Element Model for Girder 2 at the Live End Compared to Experimental Results

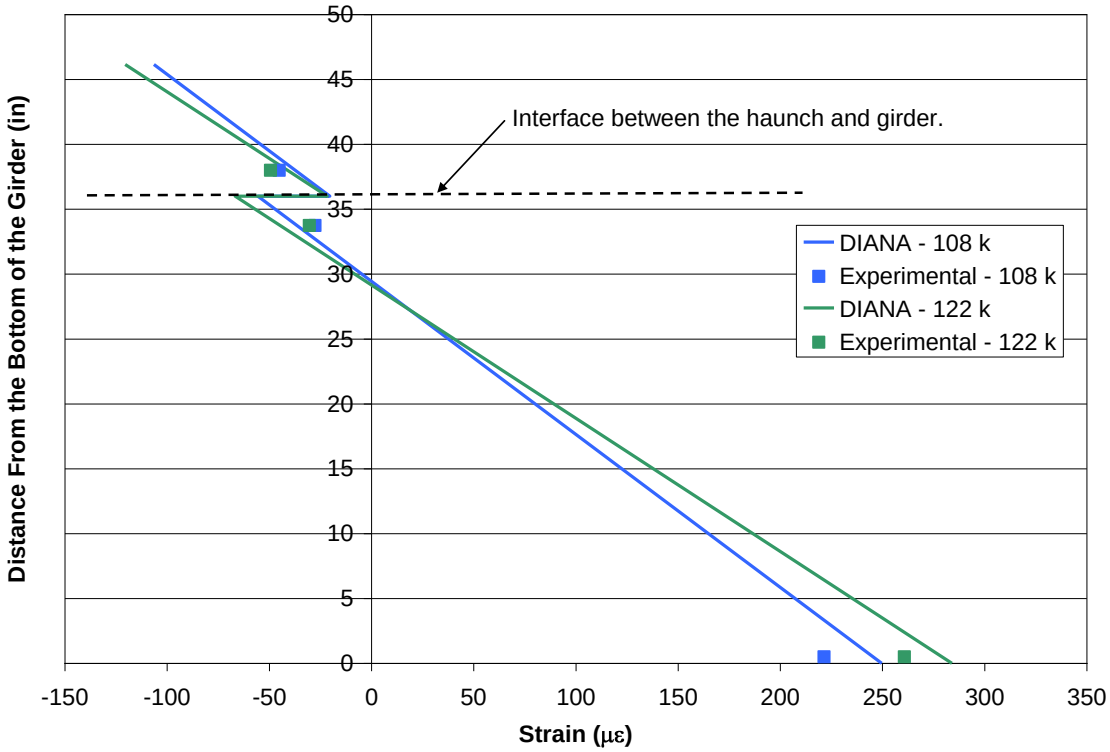

Figure I.4 Strain Profile at the Dead End for Shear Stud Connectors

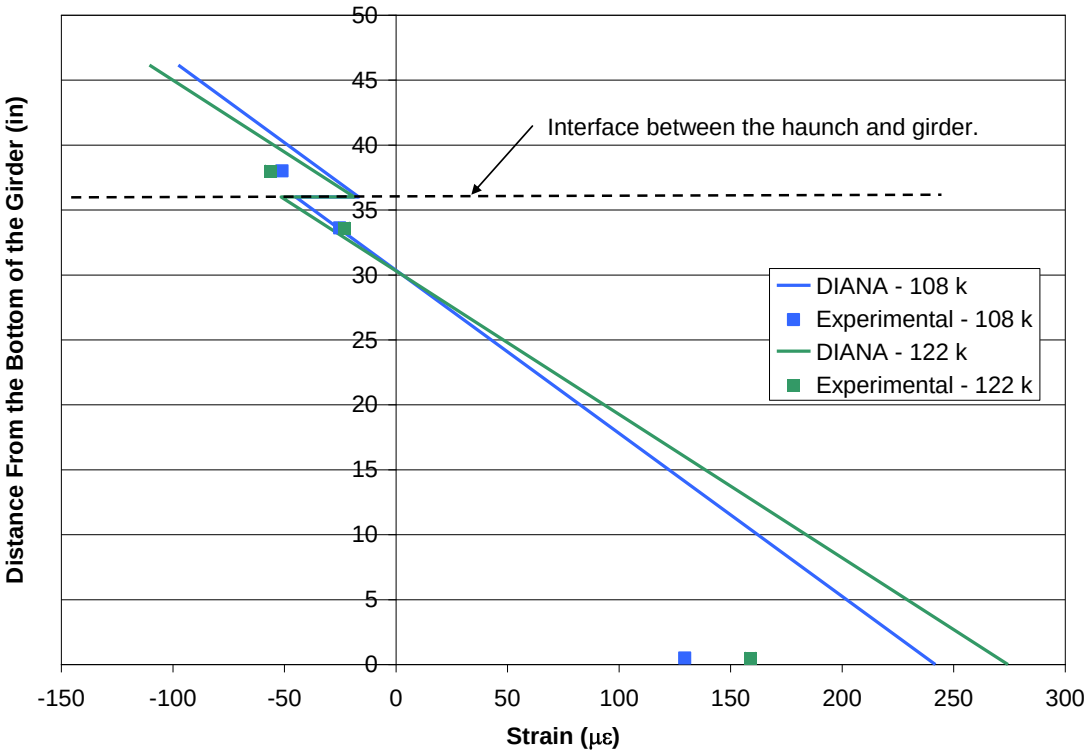

Figure I.5 Strain Profile at the Live End for Hooked Reinforcing Bar Connectors

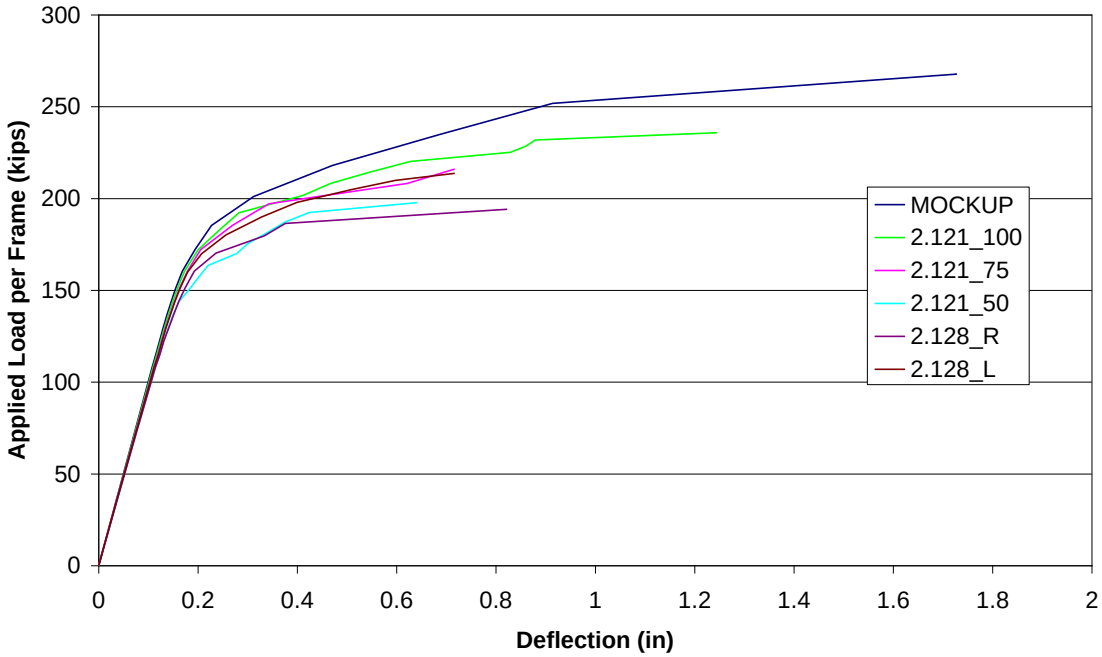

Figure I.6 Comparison of Load vs. Deflection Response for Different Hooked Reinforcing Bar Quantities with 4 ft Pocket Spacing at the Outside Load Point

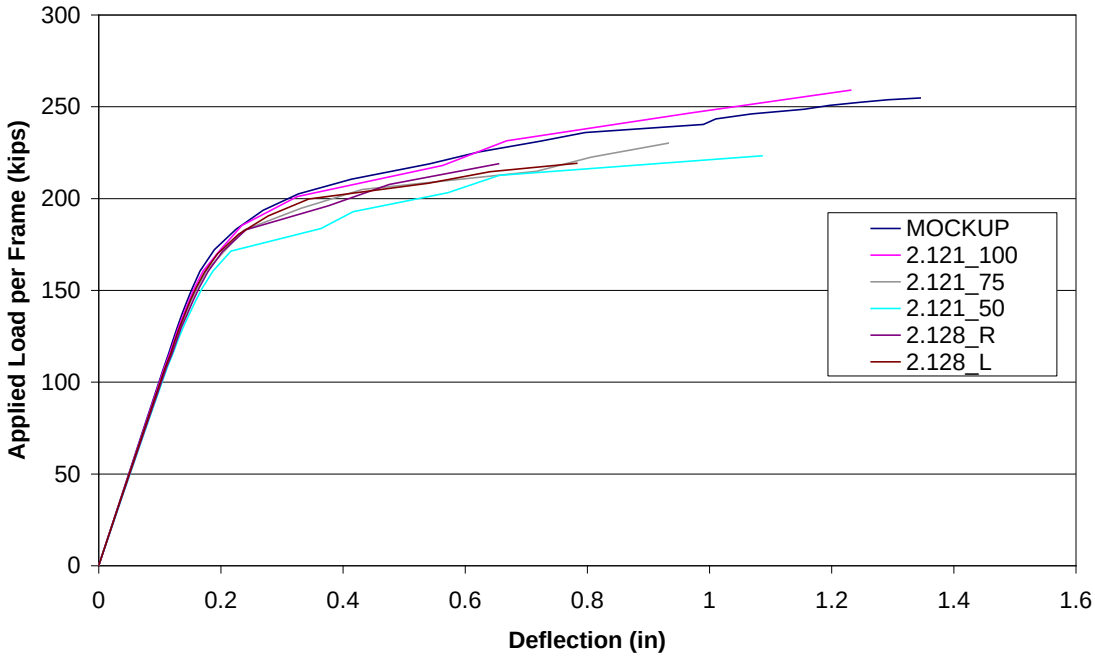

Figure I.7 Comparison of Load vs. Deflection Response for Different Hooked Reinforcing Bar Quantities with 2 ft Pocket Spacing at the Outside Load Point

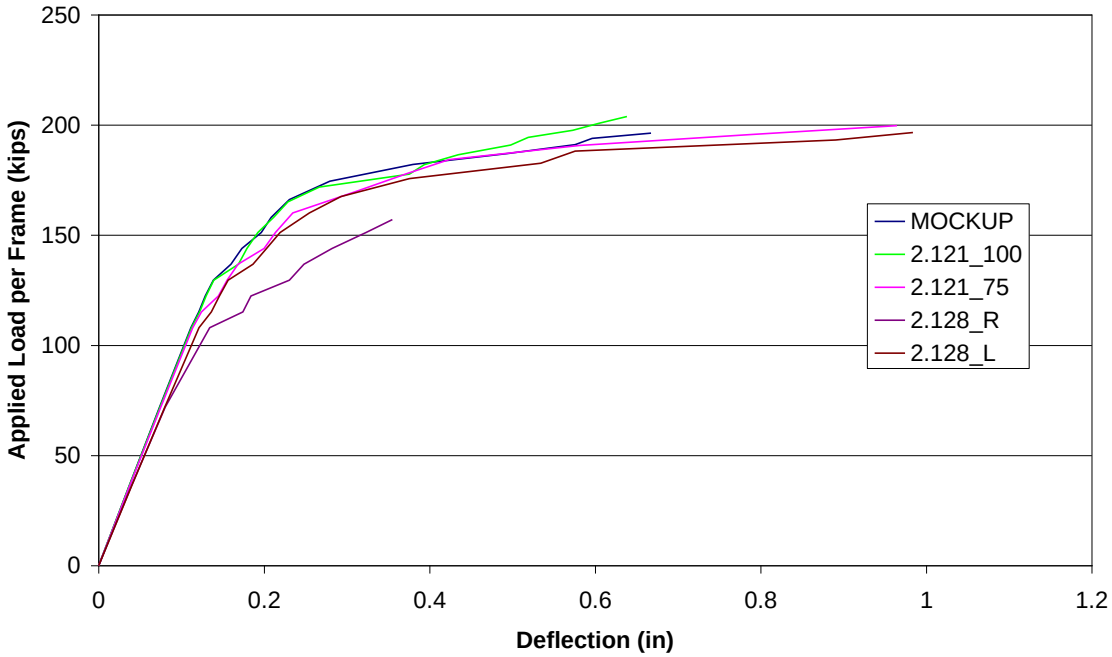

Figure I.8 Comparison of Load vs. Deflection Response for Different Shear Stud Quantities with 4 ft Pocket Spacing at the Outside Load Point

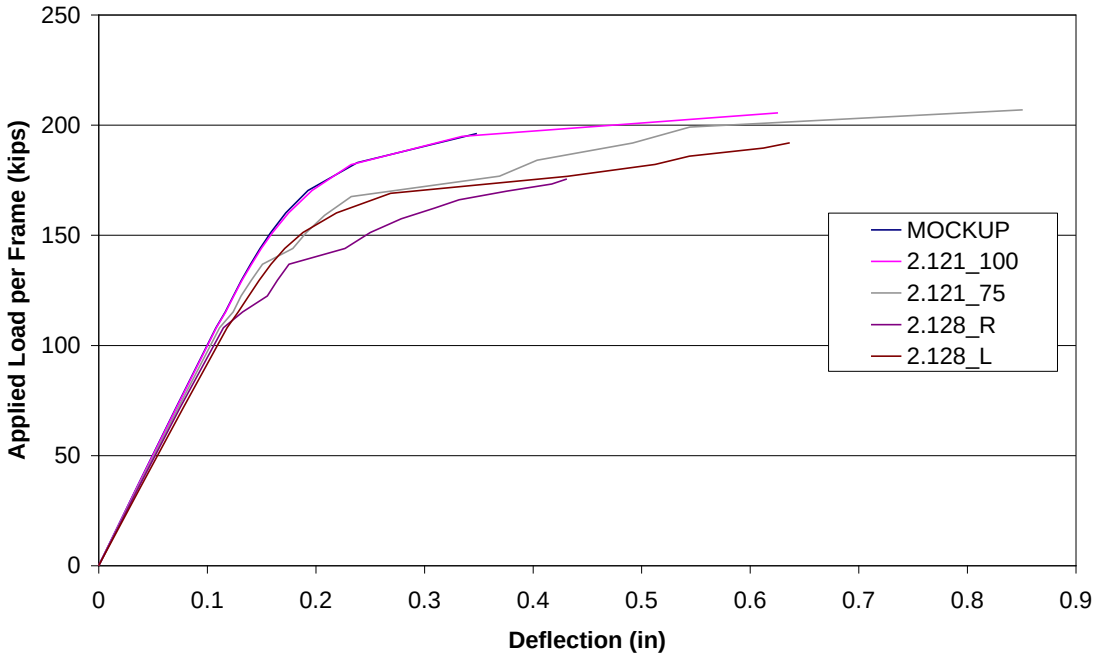

Figure I.9 Comparison of Load vs. Deflection Response for Different Shear Stud Quantities with 2 ft Pocket Spacing at the Outside Load Point

Vita

Sean Robert Sullivan was born on August 11, 1977 in Buffalo, New York. He spent the fist six years of his life in Buffalo, NY. On his 6th birthday, he moved to Toledo, Ohio where he spent the next thirteen years of his life. In September of 1996, Sean started his undergraduate degree at Ohio University. Sean obtained a Bachelor of Science in Civil Engineering from Ohio University in November of 2000. In June of 2003, he obtained a Master of Science from Ohio University. Sean worked for CH2M Hill as a bridge engineer from August of 2003 to July of 2004. In July of 2004, Sean started his Ph.D. at Virginia Polytechnic Institute and State University. He worked for Dr. Carin Roberts-Wollmann on the construction and behavior of precast deck panel systems. Sean successfully defended his dissertation on April 27, 2007.